

AGH University of Science and Technology

The Faculty of Electrical Engineering, Automatics,
Computer Science and Biomedical Engineering



mgr inż. Piotr Oramus

**Researches on Limitation of Electric
Arc in Low Voltage Switches**

*Badania nad ograniczeniem łuku elektrycznego w łącznikach
elektroenergetycznych niskiego napięcia*

Ph. D. Thesis

Under the supervision of:

D.Sc. Ph. D. Eng. Marek Florkowski

Kraków, 2017

STRESZCZENIE

Badania nad ograniczeniem łuku elektrycznego w łącznikach elektroenergetycznych niskiego napięcia

mgr inż. Piotr Oramus

Problematyka pracy doktorskiej dotyczy zagadnień ograniczania łuku elektrycznego w łącznikach elektroenergetycznych wykorzystując elementy półprzewodnikowe. Jest to aktualny problem naukowy w projektowaniu układów łączeniowych nowej generacji o zwiększonej niezawodności.

W pierwszej części przedstawiono podstawy teoretyczne mechanizmu powstawania łuku elektrycznego oraz tworzenia się erozji łukowej w łącznikach niskiego napięcia. Następnie zaprezentowano metody ograniczania energii łuku wraz z przykładami badań przeprowadzonych w tej dziedzinie. W dalszej części pracy, przedstawiono wyniki badań przeprowadzonych przez autora nad ograniczaniem energii łuku w zaprojektowanym i wykonanym układzie pomiarowym.

Dla realizacji celu pracy wykonano program badań eksperymentalnych obejmujący długoczasowe cykle oddziaływania łuku elektrycznego na materiał stykowy łączników dla wybranej metody wspomagającej gaszenie łuku elektrycznego. Dokonano porównania efektywności metod pasywnych oraz metody hybrydowej z zastosowaniem elementów energoelektronicznych ograniczania łuku elektrycznego, przeprowadzono analizę energii łuku dla rozpatrywanych topologii oraz badania morfologiczne powierzchni stykowych. Pomiary ograniczania energii łuku elektrycznego dla różnych metod ograniczających energię wykonano w indukcyjnym obwodzie prądu przemiennego, w celu porównania ich skuteczności dla dwóch różnych napięć zasilających obwód (12 V oraz 230 V). Badania prowadzone były dla następujących konfiguracji: łączenie synchroniczne z precyzyjnie określoną chwilą separacji styków badanego stycznika, dołączanie pasywnych elementów RC oraz nieliniowych elementów napięciowych równolegle do stycznika oraz równolegle dołączanie aktywnych elementów półprzewodnikowych. Zaprezentowano wyniki badań materiałowych dla ograniczania erozji łukowej. Przedstawiono propozycję konfiguracji łączenia hybrydowego, które zostało zidentyfikowane jako metoda dająca najlepsze efekty dla ograniczania energii łuku w rozpatrywanym układzie.

Do oceny skuteczności ograniczania łuku w łączniku wykorzystano zmierzone czasy łukowe oraz obliczone energie łuku elektrycznego dla rozpatrywanych metod. Przeprowadzono także rejestrację dynamiczną układu stykowego badanego stycznika z użyciem szybkiej kamery. W badaniach erozji łukowej wykorzystano styczniki, które wykonały kilkaset tysięcy operacji łączeniowych. W celu oceny stopnia erozji powierzchni badanych styków wykorzystano mikroskop optyczny, profilometr, oraz metodę skaningowej mikroskopii elektronowej sprzężoną z mikroanalizą pozwalającą na identyfikację (powierzchniową i objętościową) pierwiastków chemicznych wchodzących w skład badanego materiału.

Stwierdzono, że zastosowanie elementów pasywnych do ograniczania energii łuku daje różne rezultaty zależne od parametrów rozpatrywanego obwodu. Z tego powodu zastosowanie pasywnych elementów do ograniczania energii łuku powinno być analizowane w indywidualny sposób dla każdego obwodu, w którym istnieje konieczność ograniczania energii łuku. Zastosowanie łączenia synchronicznego daje dobre rezultaty dla ograniczania energii łuku, jednak z praktycznego punktu widzenia powtarzalność uzyskanych efektów może zależeć od czynników zewnętrznych (np. warunków środowiskowych), w których stycznik pracuje.

Efektom pracy uzyskanym w oparciu o program wykonanych badań eksperymentalnych oraz analizy morfologiczne powierzchni materiałów stykowych i analizę energii łuku oraz przebiegów czasowych, jest propozycja układu łącznika hybrydowego, zawierającego programowalny moduł sterujący elementami półprzewodnikowymi.

W pracy wykazano, że łączenie hybrydowe pozwala skutecznie ograniczyć energię łuku niezależnie od parametrów obwodu, dlatego też metoda ta została wybrana do dalszych badań nad ograniczaniem erozji łukowej. Wyniki przeprowadzonych badań pozwalają stwierdzić, że zastosowanie łączenia hybrydowego skutecznie ogranicza erozję łukową. Zostało to potwierdzone zarówno podczas obserwacji mikroskopowych powierzchni styków, jak również w toku analiz profili chropowatości oraz analiz składu chemicznego zewnętrznych warstw badanych powierzchni styków.

Wyniki pracy mogą zostać wykorzystane w projektowaniu nowych generacji łączników hybrydowych niskiego napięcia oraz w badaniach naukowych.

ABSTRACT

Researches on Limitation of Electric Arc in Low Voltage Switches

M.Sc.Eng. Piotr Oramus

Scope of the thesis deals with issues related to limitation of electric arc in low voltage switches through an application of semiconductor components. This is a current scientific problem in the design of a new generation of switching systems with increasing reliability.

In the first part of the thesis, theoretical basics of mechanism of electric arc formation and creation of arc erosion in low voltage switches are discussed. Hereafter, methods for limitation of electric arc energy with examples of researches conducted in this field are presented. In the next part of the thesis, measurement results of researches performed by author on limitation of electric arc energy in designed and prepared laboratory stand are shown.

In order to realize the purpose of this work, a program of experimental researches comprising long-time cycles of electric arc influence on contact material was conducted for selected method supporting limitation of electric arc. Moreover a comparison of effectiveness of passive methods, and hybrid switching with implementation of power electronic elements for limitation of electric arc energy is presented. Additionally, an analysis of electric arc energy for considered topologies and material researches of contact surfaces was performed. Measurements of limitation of electric arc energy were performed for various methods limiting electric arc energy in an inductive alternative current circuit to compare effectiveness of considered methods at two various supply voltages (12 V and 230 V). Researches were conducted for the following configurations: contact separation of the operated switch at precise time slot of current period, connection of passive components RC, nonlinear voltage components and active semiconductor components connected in parallel to the operated switch. Measurement results for limitation of arc erosion are presented and discussed in the thesis. Furthermore, a proposal of hybrid switching system, which was determined as the most effective method for limitation of electric arc energy in considered circuit, is presented.

Measured arcing times and calculated electric arc energies were used to evaluate effectiveness of limitation of electric arc energy for considered methods. Dynamic registration of contact system of tested switch was performed by means of high speed camera. Switches which performed several thousands of switching operations were used to conduct researches on arc erosion. In order to evaluate the degree of arc erosion of contact surfaces, the following devices and methods were used: optical microscope, roughness tester, scanning electron microscopy coupled with energy dispersive spectroscopy (this method enables one to obtain superficial and volumetric identification of the chemical elements of the material tested).

It has been concluded that application of passive components to limit electric arc energy provides different effects which depend on parameters of considered circuit. For this reason, application of passive components in limitation of electric arc energy should be analyzed in an individual way for each considered circuit, in which limitation of electric arc energy is necessary. Application of contact separation of the operated switch at precise time slot of current period provides good effects for limitation of electric arc, however, from practical viewpoint, repeatability of effects obtained may be dependent on external factors (e. g. environment conditions in which the switch works).

The result of this thesis, which was obtained on the basis of the program of experiments performed and morphological analyses of contact surfaces and analyses of limitation of electric arc, is a proposal of the hybrid system with mechanical switch. Proposed solution contains programmable control module which enables the control of semiconductor components.

The thesis demonstrates that the hybrid switching is able to limit efficiently electric arc energy independently of parameters of circuit, therefore, this method was selected to perform further researches on limitation of electric arc erosion. Measurement results lead to the conclusion that application of hybrid switching limits electric arc erosion efficiently. This has been proved both by performed microscope observations of contact surfaces, as well as, in course of analyses of roughness profiles and analyses of chemical composition of external layers of tested contact surfaces.

Measurement results presented in the thesis can be used to design a new generation of hybrid low voltage switches, as well as, in further scientific researches.

I would like to express my thanks to Mr D.Sc. Ph. D. Eng. Marek Florkowski for his supervision of this thesis. I am grateful for all the guidance and suggestions.

I am thankful for assistance and valuable remarks given by my Colleagues from ABB Corporate Research Center in Kraków.

I am also thankful for assistance in performing LV tests given by Scientists from AGH University of Science and Technology.

Table of the Contents

1	LIST OF ABBREVIATIONS AND SYMBOLS.....	8
1.1	ABBREVIATIONS AND SYMBOLS USED THROUGHOUT THE THESIS.....	8
1.2	ABBREVIATIONS USED TO MARK WAVEFORMS.....	9
2	PREFACE	12
2.1	INTRODUCTION.....	12
2.2	LITERATURE RESEARCH – THE STATE OF THE ART	13
2.3	MOTIVATION FOR THE THESIS RESEARCH	15
2.4	THESIS CONTENTS AND STRUCTURE	16
3	ELECTRIC ARC AS THE CONDUCTIVE SUBSTANCE	19
3.1	ELECTRIC ARC IGNITION.....	19
3.2	VOLTAGE-CURRENT CHARACTERISTICS OF THE LV ELECTRIC ARC	23
3.3	INTERRUPTION OF THE ELECTRIC ARC IN LV SWITCHES.....	25
3.3.1	<i>DC Current Interruption</i>	25
3.3.2	<i>AC Current Interruption</i>	26
3.4	MATHEMATICAL MODELS OF THE ELECTRIC ARC	28
4	METHODS FOR QUENCHING THE ELECTRIC ARC AND LIMITING THE ELECTRIC ARC EROSION.....	29
4.1	DESIGN OF THE OPERATED SWITCH.....	29
4.1.1	<i>Types of quenching mediums applied in mechanical switches</i>	32
4.1.2	<i>Design of Contact System</i>	35
4.1.3	<i>Contact Pressure and Contact Material</i>	37
4.2	PERFORMING THE CONTACT SEPARATION AT THE DEFINED ANGLE OF THE CURRENT PERIOD.....	39
4.3	CONNECTION OF THE SUPPRESSORS IN THE INTERRUPTED CIRCUIT	40
4.4	HYBRID SWITCHING.....	44
5	ARC EROSION IN LV SWITCHES.....	48
5.1	ARC EROSION AS A THREAT TO THE NORMAL OPERATION OF THE SWITCH.....	49
5.2	ARC EROSION IN HYBRID SWITCHES.....	54
5.3	CRITERIA FOR THE EVALUATION OF THE ARC EROSION	55
5.3.1	<i>Mass of contacts</i>	56
5.3.2	<i>Contact resistance</i>	57
5.3.3	<i>Observation of the contact surface</i>	57
5.3.4	<i>Roughness profile of contact surface</i>	58
5.3.5	<i>Morphology analysis</i>	60
6	RESEARCH PLAN.....	62
6.1	OVERALL SCOPE OF THE WORK.....	62
6.1.1	<i>Basic Electrical Parameters of the Tested Circuit</i>	62
6.1.2	<i>Researches on the Limitation of the Electric Arc Energy</i>	63
6.1.3	<i>Researches on the Limitation of the Electric Arc Erosion</i>	66
6.1.4	<i>LV Switch Selected as the Tested Object</i>	67
6.2	CONTACT SEPARATION OF THE OPERATED SWITCH AT PRECISE TIME SLOT OF CURRENT PERIOD	67
6.3	CONNECTION OF PASSIVE BRANCHES IN PARALLEL TO THE OPERATED SWITCH	69
6.3.1	<i>Selection of the RC Suppressor Parameters</i>	69
6.3.2	<i>Selection of the Parameters of the Nonlinear Voltage Components: VDR, TVS, ZVL</i>	70
6.3.3	<i>The Parameters of the Passive Parallel Components</i>	71
6.4	HYBRID SWITCHING.....	72

6.5	OBSERVATIONS OF THE ELECTRIC ARC PERFORMED BY THE HIGH SPEED CAMERA	77
6.6	EVALUATION OF THE ELECTRIC ARC EROSION	79
6.6.1	<i>Electrical Setup Used to Perform the Investigations on the Limitation of Electric Arc Erosion</i>	80
6.6.2	<i>Visual Comparison of the Condition of the Analyzed Contacts</i>	80
6.6.3	<i>Roughness Profiles of the Surfaces of the Analyzed Contacts</i>	81
6.6.4	<i>SEM method coupled with the EDS</i>	82
6.7	LABORATORY STAND DEVELOPED TO PERFORM EXPERIMENTS	83
6.7.1	<i>Characteristic of the Laboratory Stand</i>	83
6.7.2	<i>Microcontroller System</i>	86
6.7.3	<i>Detailed Electrical Diagram of the Laboratory Stand</i>	87
6.7.4	<i>Detailed Technical Data of the Operated Switch</i>	89
6.7.5	<i>Detailed Technical Data of the SSR used to the hybrid application</i>	90
7	MEASUREMENT RESULTS FOR THE LIMITATION OF THE ELECTRIC ARC AT 12 V	91
7.1	TIME-CONTROLLED CONTACT SEPARATION AT THE PRECISE TIME SLOT OF THE CURRENT PERIOD....	91
7.1.1	<i>Contact Separation just before the Natural Zero-Crossing of the Current Period</i>	95
7.1.2	<i>Contact Separation at 35° of the Current Period</i>	95
7.1.3	<i>Contact Separation at 90° of the Current Period</i>	96
7.1.4	<i>Contact Separation at 145° of the Current Period</i>	97
7.2	CONNECTION OF THE PASSIVE BRANCHES IN PARALLEL TO THE OPERATED SWITCH.....	97
7.2.1	<i>RC Arc Suppressor</i>	98
7.2.2	<i>Voltage-Dependent Resistor (VDR)</i>	100
7.2.3	<i>Transient Voltage Suppressor (TVS)</i>	101
7.2.4	<i>Zener Voltage Limiter (ZVL)</i>	103
7.3	HYBRID SWITCHING	105
7.4	SUMMARY OF MEASUREMENT RESULTS	107
8	MEASUREMENT RESULTS FOR THE LIMITATION OF THE ELECTRIC ARC AT 230 V ...	113
8.1	TIME-CONTROLLED CONTACT SEPARATION AT THE PRECISE TIME SLOT OF THE CURRENT PERIOD..	113
8.1.1	<i>Separation of the Contacts just before the Natural Zero-Crossing of the Current Period</i>	117
8.1.2	<i>Separation of the Contacts at 35° of the Current Period</i>	118
8.1.3	<i>Separation of the Contacts at 90° of the Current Period</i>	118
8.1.4	<i>Separation of the Contacts at 145° of the Current Period</i>	119
8.2	CONNECTION OF THE PASSIVE BRANCHES IN PARALLEL TO THE OPERATED SWITCH.....	119
8.2.1	<i>RC Arc Suppressor</i>	120
8.2.2	<i>Voltage-Dependent Resistor (VDR)</i>	122
8.2.3	<i>Transient Voltage Suppressor (TVS)</i>	123
8.2.4	<i>Zener Voltage Limiter (ZVL)</i>	124
8.3	HYBRID SWITCHING	126
8.4	SUMMARY OF THE MEASUREMENT RESULTS	129
9	ANALYSIS OF THE EFFECTS OF ELECTRIC ARC LIMITATION.....	135
9.1	MEASUREMENT RESULTS PERFORMED AT 12 V.....	135
9.1.1	<i>Time-Controlled Contact Separation performed at Precise Time Slot of the Current Period</i>	135
9.1.2	<i>Connection of the External Parallel Branches into the Operated Switch</i>	138
9.2	MEASUREMENT RESULTS PERFORMED AT 230 V.....	141
9.2.1	<i>Time-Controlled Contact Separation performed at Precise Time Slot of the Current Period</i>	141
9.2.2	<i>Connection of the External Parallel Branches into the Operated Switch</i>	144
10	OBSERVATIONS OF THE LIMITATION OF THE ELECTRIC ARC PERFORMED BY THE HIGH SPEED CAMERA	148
10.1	REGISTRATION OF THE FORMULATION OF THE ELECTRIC ARC IN THE STANDALONE SWITCH.....	148
10.2	REGISTRATION OF THE FORMATION OF THE ELECTRIC ARC DURING THE HYBRID SWITCHING	150
10.3	COMPARISON OF THE RESULTS	152
11	EVALUATION OF THE ELECTRIC ARC EROSION OF THE ELECTRICAL CONTACTS IN THE TESTED SWITCHES.....	153

11.1	CONDITION OF THE SURFACES OF THE CONTACTS	153
11.2	OBSERVATIONS PERFORMED BY MEANS OF THE OPTICAL MICROSCOPE.....	155
11.2.1	<i>Reference Contact</i>	155
11.2.2	<i>Contact Taken from Standalone Switch after 50 000 the Current Interruptions</i>	156
11.2.3	<i>Contact Taken from the Hybrid Switch after 50 000 the Current Interruptions</i>	156
11.3	ROUGHNESS PROFILES OF THE ANALYZED CONTACTS	157
11.4	MORPHOLOGICAL ANALYSIS	159
11.4.1	<i>Reference Contact</i>	159
11.4.2	<i>Contact Taken from the Standalone Switch after 50 000 Cycles of the Current Interruption</i>	161
11.4.3	<i>Contact Taken from the Hybrid Switch after 50 000 Cycles of the Current Interruption</i>	163
11.4.4	<i>Summary of the Measurement Results</i>	164
12	ANALYSIS OF THE LIMITATION OF THE ELECTRIC ARC EROSION.....	166
13	DISCUSSION AND CONCLUSIONS	169
13.1	SUMMARY	169
13.2	ANALYSIS OF THE EFFECTS OF THE LIMITATION OF THE ELECTRIC ARC ENERGY IN THE TESTED CIRCUIT SUPPLIED BY THE 12 V VOLTAGE SOURCE.....	171
13.3	ANALYSIS OF THE EFFECTS OF THE LIMITATION OF THE ELECTRIC ARC ENERGY IN THE TESTED CIRCUIT SUPPLIED BY THE 230 V VOLTAGE SOURCE.....	172
13.4	ANALYSIS OF THE EFFECTS OF THE LIMITATION OF THE ELECTRIC ARC EROSION	173
13.5	REFERENCE TO THE MAIN THESIS.....	174
13.6	FUTURE RECOMMENDATIONS RELATED TO THE STUDIES ON THE LIMITATION OF THE ELECTRIC ARC IN THE LV SWITCHES	174
14	BIBLIOGRAPHY	176

1 List of Abbreviations and Symbols

1.1 Abbreviations and symbols used throughout the thesis

The following table describes abbreviations and acronyms used throughout the thesis.

Abbreviation	Meaning
AC	Alternative Current
C_s	The capacitance of the RC arc suppressor
DC	Direct Current
E_{arc}	The electric arc energy calculated as the integral from the product of the voltage and the current from the time, when the contacts of the operated switch start to separate up to the time, when the electric arc quenches
E_a	The electric arc energy
E_B	The energy dissipated at the branch connected in parallel to the operated switch
EDS	Energy Dispersion Spectroscopy
FPS	Frame Per Second
HCB	Hybrid Circuit Breaker
h_e	The height of the sphere with the contact material that evaporates during the bridge decay
HV	High Voltage
i_a	The current of the electric arc
i_B	The current of the external branch connected in parallel to the tested switch
i_G	The current of thyristor gate (in practice, it is the current for triggering the SSR)
i_s	The current of the tested switch
i_{SD}	The current of the switch drive
i_T	The current flowing through the thyristor (in practice, it is the current flowing through the SSR)
GTO	Gate Turn-Off thyristor
LV	Low Voltage
MCB	Miniature Circuit Breaker
MOV	Metal-Oxide Varistor
MV	Medium Voltage
p_a	The electric arc power
p_B	The power dissipated at the branch connected in parallel to the operated switch
P_{max}	The maximum value of the power that can be observed in the analyzed waveform
PSD	Particle Sputtering and Deposition
PTC	Positive Temperature Coefficient
R_a	The average roughness of the analyzed contact surface
RCD	Residual Current Device
R_S	The resistance of the RC arc suppressor
R_z	The ten point average roughness of the analyzed contact surface

Abbreviation	Meaning
R_{max}	The maximum roughness height within a length of the analyzed contact surface
R_{WP}	The radius of the isotherm with the temperature TWP in the zone of the bridge decay
SEM	Scanning Electron Microscope
t_{arc}	The time interval between the instant when the electric arc starts to burn, and when the electric arc quenches
t_B	Time, when the contact bridge starts to create
t_0	The time, when the contacts of the operated switch start to separate
t_{0A}	The time, when the electric arc burns in second chamber, and the current starts to commute into semiconductor branch during hybrid switching
t_{0B}	The time, when entire current commutes into an external branch
t_{0D}	The time, when the signal to open the switch is given to switch drive
t_1	The time, when the electric arc is quenched
t_{1B}	The time, when the commutated current into parallel branch stops flowing
t_2	The time, when the steady state voltage appears between the contacts of operated switch after the end of the TRV
t_{zC}	The time, when the control unit detects current zero-crossing
TRV	Transient Recovery Voltage
TRIAC	Triode for Alternating Current
TVS	Transient Voltage Suppressor
SCR	Silicon-Controlled Rectifier
SSR	Solid State Relay
u_a	The arcing voltage
U_{arc_ign}	Arc ignition voltage
U_{arc_quen}	Voltage of quenching arc
U_{arc_max}	The maximum arcing voltage (before quenching the electric arc)
U_{PS}	Voltage of the power source
u_s	The voltage measured across the operated switch
$U_{Threshold}$	The value of the voltage, when the nonlinear voltage-current component starts to conduct
U_{TRV_max}	The maximum value of the Transient Recovery Voltage
U_Z	The Zener Voltage of the Zener diode
VCB	Vacuum Circuit Breaker
VDC	Voltage-Dependent Components
VDR	Voltage-Dependent Resistor
V_s	The volume of the evaporated material from the contact surface during the bridge decay
ZVL	Zener Voltage Limiter

1.2 Abbreviations used to mark waveforms

The following table describes abbreviations used throughout the thesis to mark measured and calculated waveforms presented in the sections 7-8. Due to many combination of the abbreviations, the description was simplified as below. The selected abbreviations of the waveforms were described below the table.

Abbreviation	Meaning
$e_{X_YY_ZZ^\circ}$	<p>Calculated energy: X: type of the calculated energy. A – electric arc energy, B – energy absorbed by a branch connected in parallel to the operated switch.</p> <p>YYY: type of parallel branch connected to the operated switch. RC – RC snubber, VDR – Voltage-Dependent Resistor, TVS – Transient Voltage Suppressor, ZVL – Zener Voltage Limiter, HS – hybrid switching, none – standalone switch</p> <p>ZZ: time, when contacts of the operated switch started to separate: 35°, 90°, 145°, 0° (just before current zero-crossing)</p>
$i_{X_YY_ZZ^\circ}$	<p>Measured current: X: the place, where the current was measured. S – the operated switch, B – parallel branch connected to the mechanical switch.</p> <p>YYY: type of parallel branch connected to the operated switch. RC – RC snubber, VDR – Voltage-Dependent Resistor, TVS – Transient Voltage Suppressor, ZVL – Zener Voltage Limiter, HS – hybrid switching, none – standalone switch</p> <p>ZZ: time, when contacts of the operated switch started to separate: 35°, 90°, 145°, 0° (just before current zero-crossing)</p>
$p_{X_YY_ZZ^\circ}$	<p>Calculated power: X: type of the calculated power. A – electric arc energy, B – power generated at a branch connected in parallel to the operated switch.</p> <p>YYY: type of parallel branch connected to the operated switch. RC – RC snubber, VDR – Voltage-Dependent Resistor, TVS – Transient Voltage Suppressor, ZVL – Zener Voltage Limiter, HS – hybrid switching, none – standalone switch</p> <p>ZZ: time, when contacts of the operated switch started to separate: 35°, 90°, 145°, 0° (just before current zero-crossing)</p>
$r_{X_YY_ZZ^\circ}$	<p>Calculated resistance: X: type of the calculated resistance. A – electric arc resistance, B – resistance of a branch connected in parallel to the operated switch.</p> <p>YYY: type of parallel branch connected to the operated switch. RC – RC snubber, VDR – Voltage-Dependent Resistor, TVS – Transient Voltage Suppressor, ZVL – Zener Voltage Limiter, HS – hybrid switching, none – standalone switch</p> <p>ZZ: time, when contacts of the operated switch started to separate: 35°, 90°, 145°, 0° (just before current zero-crossing)</p>
$u_{S_YY_ZZ^\circ}$	<p>Measured voltage across the operated switch: YYY: type of parallel branch connected to the operated switch. RC – RC snubber, VDR – Voltage-Dependent Resistor, TVS – Transient Voltage Suppressor, ZVL – Zener Voltage Limiter, HS – hybrid switching, none – standalone switch</p> <p>ZZ: time, when contacts of the operated switch started to separate: 35°, 90°, 145°, 0° (just before current zero-crossing)</p>

The selected abbreviations of the waveforms presented in the sections 7-8 were described below as the example according to above table:

$e_{B_HS_90^\circ}$ – Energy absorbed by semiconductor branch connected in parallel to the operated switch, the contacts of the operated switch start to separate at 90° of the current period.

$i_{S_145^\circ}$ – Current of the operated switch, any branch connected in parallel to the operated switch, contacts start to separate at 145° of the current period.

$p_{A_VDR_35^\circ}$ – Calculated power of the electric arc, Voltage-Dependent Resistor was connected in parallel to the operated switch, the contacts of the operated switch start to separate at 35° of the current period.

$u_{S_ZVL_35^\circ}$ – Measured voltage across the operated switch, Zener Voltage Limiter component was connected in parallel to the operated switch, the contacts of the operated switch start to separate at 35° of the current period.

2 Preface

2.1 Introduction

Electrical switches find an application in electric circuits which are being used in each branch of an industry, as well as, in residential installations. The main purpose of these devices is to provide the electric energy to consumers through an energization and a de-energization of electrical circuits. Among all constructions of switching apparatus, the greatest importance lies in mechanical switches, which carry out the switching operation by the movement of mechanical contacts (within each pair of contacts, at least one is a moveable contact). The mechanical switches can be divided by: the type of performing operation, the voltage level, the maximum interrupted current, ability to make appropriate insulating gap due to protection against electric shock, the type of interrupting current, the ability to carry out the switching operation in specific environmental conditions. The following thesis is focused on mechanical LV switches dedicated to indoor application that are able to interrupt nominal AC current.

The proper functioning of switching apparatus depends on surface conditions of electrical contacts, especially under short-circuit conditions. It should be also emphasized that, the electrical contacts are a part of an electrical switch, which is the most responsible for its proper functioning. Moreover, the design of the electrical contacts must be resistant for phenomena such as: a mechanical abrasion, an oxidation and a corrosion, contact welding, heating and a temperature rise, and especially the electric arc erosion of the contacts. It should be highlighted that the greatest influence on the process of formation of the electrical arc erosion lies in a type of the contact material and the construction of the contact system (especially a shape and a size of the electrical contacts, a type of a quenching chamber, etc.).

The limitation of electric arc erosion leads to maintain surface of electrical contacts in good conditions for longer time, which as a consequence causes an increase of the switch lifespan. For this reason, the limitation of the electric arc erosion is important issue to provide a reliability of electricity distribution in electrical power systems. The main method for the limitation of the arc erosion is to reduce the electric arc energy. The electric arc erosion is mainly limited in AC switches by the application of a specified contact system (an appropriate contact material, a shape and of the electrical contacts, a design of the quenching chamber, etc.). However, the electric arc energy can be also limited by means of the electrical methods – as addition of external branches connected in parallel to the operated switch (including also semiconductor hybrid solutions), which leads to limit the arc energy by the commutation of the part of the interrupting current. Another method for limiting the electric arc energy during current interruption in AC circuits can be an application of time-controlled drive switch that is able to provide the possibility of the contact separation at precise time in reference to the current period.

The following thesis covers researches on three methods for the limitation of the electric arc in LV switches leading to limitation of electric arc erosion (an application of time-controlled switching, a connection of external branches in parallel to the operated switch, as well as, the application of the hybrid switching). Presented researches show in which extent the electric arc energy can be limited by application of different methods in inductive electrical circuit with defined parameters. This type of the circuit was selected to the researches, because inductive circuits can be found practically in every electric device, both in solutions dedicated to a domestic usage (such as: household appliances, electro-tools, heating equipment, lightning devices, intelligent home systems, etc.), as well as, in the heavy industry

applications (such as: electric motors, arc furnaces, power electronic inverters, power transformers, special industrial equipment, etc.) Therefore, the presented inhere methods can be used to protect the contacts of the operated switches that can be applied in many industries, which simultaneously can have an influence on increasing a reliability of many electrical circuits. Mechanisms describing formation and maintenance of the electric arc were characterized in this work together with theoretical background for arc erosion formation.

This thesis presents a comprehensive approach to compare the effectiveness of different methods applied in the tested circuit with defined parameters for limiting the electric arc energy. The researches were performed in the tested circuit at two levels of the voltage supply to indicate the influence of the voltage source on the voltage-current characteristics of the electric arc. This approach was applied to show how the voltage-current characteristic impacts on the efficiency of the limitation of the electric arc energy for methods, which are based on the connection of the passive components (RC snubber and nonlinear voltage components) in parallel to the operated switch. Application of passive parallel branch connected to the operated switch may be able to make commuting the current from the operated switch into the external branch during the current interruption possible. In the next stages of the researches, performing time-controlled separation of the contacts of the operated switch, and application of the hybrid switching with connection of the semiconductor branch in parallel to the operated switch were investigated. The hybrid switching was determined as the most effective method to limit the electric arc energy among all considered methods (which was proved by electrical measurement results and registrations of the electric arc formulation that was performed by means of high speed camera). For this reason, this approach was applied to perform researches on the limitation of the electric arc erosion in the tested circuit. For this purpose, 200 000 current interruptions were performed in total by four tested switches (50 000 operations were performed by each tested switch). In course of experiments, the current was being interrupted by two standalone switches, and the current was being interrupted by two switches with applied the hybrid switching. The conditions of the contact surfaces taken from the tested switches were investigated and compared with a new contact surface. For this purpose, the camera, the optical microscope, the roughness tester, as well as, the Scanning Electron Microscope (SEM) coupled with the Energy Dispersive Spectroscopy (EDS) were applied. The application of the hybrid switching caused a reduction in the electric arc erosion significantly in the contacts of the tested switches in comparison to the contacts taken from the tested switch that was being interrupted the current as the standalone one.

Presented methods for the limitation of the electric arc energy can be applied in the design of improved switches having the following features: a longer expected lifespan, an increased expected number of the switching operations, an increased maximum interrupting current rating for an unmodified design of the contact system, an increased permitted switching frequency in defined time, reduced dimensions of the contact system at the same electrical parameters.

2.2 Literature Research – the State of the Art

Researches on the electric arc energy and electric arc erosion were being performed in the past by many researchers under different conditions in various electrical circuits.

Over past decades in Poland, significant contribution in researches on the electric arc was given by researches from Polish Universities. A great influence on the Polish development of switching researches was greatly influenced by scientists of the Łódź University of Technology, who analyzed phenomena related to the electric arc and switching devices in many aspects, such as: electric arc physics [18, 24, 25, 129], contact materials

[23, 38, 137, 138, 140], contact systems [24, 25, 141], simulations of the electric arc [127], reliability of the switches [23, 24, 68], behavior of the electric arc in vacuum [139], and drive systems [128]. Significant contribution in analyses of the electric arc phenomena was also given by scientists from the Warsaw University of Technology, who performed researches focused mainly on switching transients in power systems, the air-insulated and vacuum-insulated power apparatus rated at medium voltage and at high voltage [10-12, 32, 42, 72, 86-88]. Experiments on plasma physics, vacuum switching, and thermal issues of the electrical contacts were performed at the Poznań University of Technology [58-61, 66, 76]. The researches related to arc phenomena and reliability of the low voltage switches, and the vacuum switching technology were also performed at Wrocław University of Science and Technology [66, 146-148]. Other important place on scientific map of Poland is Institute of Power Engineering localized in Warsaw, where many researches on medium and high voltage devices were performed [142, 143]. The analyses of switching transient states dedicated mainly to the insulation coordination purposes, as well as, focused on harmonic distortion were performed at the AGH University of Science and Technology [19, 43, 44, 51, 70]. Issues related to the electric arc were also the object of researches at Częstochowa University of Technology, where the parameters of the electric arc were researched mainly for welding applications [111-113]. Researches on durability of power switches were conducted at Lublin University of Technology [65]. The Gdańsk University of Technology is also the important place on the map of Poland for developing electrical apparatus, where the researches on power switches have been performed for many years [145].

The research on the time-controlled separation of the electric contacts in AC circuit, which is presented in this work as one of the considered methods applied to limit the electric arc were performed and presented in many scientific works in the past. Researches on application of the synchronous switching both in tested circuits with low voltage switches [18], as well as, in MV switches dedicated to rail application [15, 16] were being conducted at Łódź University of Technology. Time-controlled switching in LV switches was being also investigated by other researchers from other countries [136]. The application of synchronous switching is being applied to avoid dangerous transient state especially in HV electrical power systems during breaking and making operation performing by means of circuit breakers [21, 30, 91, 93, 101, 110]. For this purpose, dedicated devices are available commercially on the market, which are being used to control precisely contacts of circuit breakers for limiting the inrush current, as well as, for limiting switching overvoltages [2, 120].

Another considered method that is presented in this thesis to limit the electric arc energy is a connection of a passive branch (that are not required external supply) in parallel into the operated switch. For this purpose, two approaches were investigated – a connection of the RC snubber in parallel to the operated switch, as well as, the connection of the nonlinear voltage-current components in parallel to the operated switch.

The basic idea for connection of the RC snubber in parallel to the operated switch to limit the electric arc is simple – when the contacts of the operated switch just begin to separate and the electric arc starts to create, the load current feeding the arc should be shunted into the parallel capacitor through the series resistance, depriving the arc of some of its energy. As a result, arc duration should be shortened and a loss of the contact material should be also minimized. This approach is commonly used in industrial installations to protect the contacts of the operated switch because of cheapness and simplicity of the method, however, this method is able to limit the electric arc energy only slightly. Moreover, there is no unequivocal method to select the parameters of the RC snubber for different types of the interrupting loads. The manufacturers of the commercially available RC snubbers that are dedicated to limit the electric arc energy present different approaches for calculation of the RC parameters [4, 52, 80, 100, 109, 131]. RC snubbers are also being applied in electrical circuits to protect

the semiconductor components against overvoltages and steepness dU/dt [1, 152], as well as, to limit transient states during switching operations in electric power systems [39, 85].

The application of nonlinear voltage-current components connected in parallel to the operated switch provides a possibility for the current commutation into the branch connected in parallel to the operated switch, if the arcing voltage during the current interruption exceeds the minimal operating voltage of the nonlinear component. This approach is being applied as an alternative or a supplement for the RC snubber connected in parallel to the operated switch [4, 55, 79, 103, 109, 133]. Nonlinear voltage-current components are also applied in electrical circuits to limit the overvoltage during transient states [152].

The last method presented in frame of this thesis, which is being applied to limit the electric arc energy is the hybrid switching. This method is based on a connection of semiconductor components with a mechanical switch. The hybrid switching is a method that was presented in many scientific works [5, 14, 17, 81, 87, 88, 118]. As shown in [119], hybrid switches can be developed with using different components and topologies, also their functionality can be different: limiting short circuit current, a reduction of the arcing time, a limitation of the electric arc, implementation of the soft-start functionality, synchronous switching, support for switching DC currents. In this thesis, hybrid switching was used to limit the electric arc energy in the tested AC circuit. Thus, the interrupting current is able to commute into the parallel semiconductor branch connected to the operated switch, just after the separation of the contacts and stops flowing in the analyzed circuit at its next current zero-crossing.

In course of conducted experiments, the hybrid switching was determined as the most effective method to limitation of the electric arc energy. This method was applied to perform researches on the limitation of the electric arc erosion in the tested circuit. Researches on electric arc erosion were being performed by many researchers [24, 25, 28, 71, 84, 89, 94, 99, 102, 106, 107, 117, 135, 141, 150, 151]. The scope of above-mentioned researches covers a creation of the electric erosion under various conditions – for various values of the interrupting current at various voltages, for various types of the contact systems, for various contact materials, for various number of performed switching operations. In order to evaluate the electric arc erosion, the researchers used the camera, the optical microscope, the SEM method (Scanning Electron Microscope) coupled with EDS (Energy Dispersion Spectroscopy), as well as, measurements of resistance changes and weight changes in function of performed switching operations.

2.3 Motivation for the Thesis Research

The purpose of conducting investigations presented in the following thesis is based on several reasons. As mentioned above, electrical switches are applied in electric circuits being used in each branch of an industry and in residential installations. The limitation of the electric arc erosion leads to maintain the surface of electrical contacts in good conditions for longer time, which as a consequence causes an increase of lifespan of entire switch. For this reason, the limitation of the electric energy and the electric arc erosion is an important issue to provide a high reliability of electricity transmission in electrical power systems.

Although many researches were focused in the past on many aspects related to the limitation of the electric arc and the limitation of the electric arc erosion (as shown in the section 2.2), there is no work comprising a comparison of the effectiveness of considered inhere methods in defined benchmark electric circuit with inductive load at LV with continuous currents.

Interruption of inductive current was selected for researches performed in the frame of this thesis for two main reasons. Firstly, inductive circuits can be found practically in every electric device, both in solutions dedicated to a domestic usage (such as: household

appliances, electro-tools, heating equipment, lightning devices, intelligent home systems, etc.), as well as, in the heavy industry applications (such as: electric motors, arc furnaces, power electronic inverters, power transformers, special industrial equipment, etc.). Secondly, interruption of inductive circuits is especially difficult, which is presented in details in section 3.1. For these reasons, the considered inhere methods can be applied to protect the contacts of the operated switches that can be applied in many industries, which simultaneously can have an influence on increasing a reliability of many electrical circuits.

On the other hand, the scope of this thesis allows to give answer for the question, how the application of cheap solutions based on the passive components that are being commonly used in many electrical circuit to protect the contacts of switches compares to more sophisticated approaches, such as a hybrid switching or performing time-controlled contact separation of the operated switch. Presented measurement results show how the parameters of the tested circuit can influence on voltage-current characteristics of the electric arc, and as a consequence on effectiveness of the passive components connected in parallel to the operated switch applied for limiting the electric arc. For this reason, an application of passive components that are being used to protect the electric contacts against effects of the electric arc should not be performed without analysis of the effectiveness of the considered method, which was proved in this work.

Researches that were performed on hybrid switching seems to be especially important mainly for three reasons. Firstly, this method allows to reduce significantly the electric arc energy, as well as, the electric arc erosion (almost in total independently on parameters of the electric circuit), which causes a significant increase in the lifespan of the switches. Secondly, the huge progress that was made in recent years in development of power electronic components indicates the direction for researches on application of power electronic components in connection with mechanical switches. This combination allows to connect advantages of mechanical switches with semiconductor components to develop improved switching devices. Thirdly, an external semiconductor branch can be integrated inside of the switch (without arcing chamber), which may make a design of a switch with smaller dimension and with higher current and voltage ratings possible.

Moreover, the measurement results obtained in frame of this thesis can be a motivation to start the work on the redesigning of the analyzed mechanical switch. Proposed modifications of the switch could be related among others to minimalize the switch dimensions, as well as, to redesign the shape of and dimensions of the contact system.

A part of measurement results that are presented in this thesis dissertation were published in articles [97, 98]. The author was also involved in researches on switching plasma physics in Medium Voltage circuits [122, 123], and modeling switching transients [33, 34, 95, 96, 126].

2.4 Thesis Contents and Structure

Based on the motivation presented in the section 2.3, and on the performed measurements, the following thesis for this work was prepared:

Limitation of electric arc and electric arc erosion in electric switches is possible by application of external systems to current commutation, as well as, through application of system for controlled-time current interruption. The aim of this research paper is to present qualitative and quantitative influence of various methods for limitation of electric arc burning between contacts of LV electric relay during current interruption process.

Thesis in Polish: *Możliwe jest ograniczenie łuku elektrycznego oraz erozji łukowej w łącznikach elektrycznych poprzez zastosowanie zewnętrznych układów służących do*

komutacji prądowej oraz do synchronicznego wyłączenia prądu. Istotą pracy jest przedstawienie ilościowego i jakościowego wpływu stosowania różnych metod ograniczających łuk elektryczny w przerwie międzystykowej łącznika, podczas operacji przerywania prądu.

Chapter 3 starts with a description of the electric arc ignition between pair of contacts. Arcing phenomena, ionization and deionization processes are explained, a typical arc channel with its typical potential distribution is presented, and limit values of arcing voltages and interrupting current that are necessary to initiate an ignition of the electric arc are presented. Static and dynamic voltage-current characteristics of the electric arc are discussed based on measurement results performed by other researchers. The conditions necessary to quench the electric arc were also presented in this chapter.

The considered methods to limit the electric arc energy are presented in Chapter 4. The influence of a design of the switch (the contact system, the contact material, the arcing chambers) on its capability of quenching arc is discussed in this chapter. Time-controlled separation of the electric contacts to limit the electric arc energy are presented in this chapter as one of the method for limiting the electric arc energy in AC circuits. Another presented method used to limit the electric arc energy is a connection of a passive branch (that are not required external supply) in parallel into the operated switch. Finally, the principle of operation of the hybrid switching dedicated for limiting the electric arc energy is explained.

Chapter 5 describes electric arc erosion of LV switch contacts. The process of the formation of arc erosion is presented and discussed. The influence of the contact material on a creation of the arc erosion is presented based on measured examples. The criteria for an evaluation of the arc erosion are presented – the observation of the contact surface that was performed by the optical microscope, the application of the SEM method coupled with EDS, as well as, the measurements of resistance changes and the weight changes as a function of performed switching operations.

Chapter 6 presents overall research plan, and the detailed description of the laboratory stand used to perform the researches. The description of implementation of considered methods (time-controlled contact separation, connection of the passive components in parallel to the operated switch, hybrid switching sequence), as well as, the description of the selection of the components chosen to perform the researches are presented. Measurement equipment applied to perform the experiments (the high speed camera, roughness tester, device used to EDS and SEM measurements) is characterized briefly. Also, technical data of switches used to perform investigation, as well as, the detailed description of microcontroller system developed to control entire laboratory stand are presented.

Measurement results for the limitation of the electric arc performed in the tested circuit supplied by the 12 V voltage source are presented in chapter 7. Waveforms of interrupted current i_S , voltage measured across the operated switch u_S , electric arc power p_A , as well as, the electric arc energy e_A were presented for time-controlled contact separation of the operated switch at four times of the current period: just before the natural current zero-crossing, at 35°, 90°, and 145° of the current period. In the next part of the chapter, the measurement results are presented for the situation, when the passive branches (RC snubber, Voltage-Dependent Resistor, Transient Voltage Suppressor, Zener Voltage Limiter) were connected to the operated switch. In this case, also waveforms of the electric power dissipated at external branches p_B were presented together with waveforms of the energy absorbed e_B by the external branches. In the last part of the chapter, measurement results were presented for case, when the current was interrupted by the application of the hybrid switching.

Chapter 8 presents measurement results for the limitation of the electric arc performed in the tested circuit that was supplied by the 230 V voltage source. The scope of the presented measurement results coincides with the content of chapter 7.

The analysis of the effects of the limitation of the electric arc was presented in chapter 9. The measurement results presented in chapters 7-8 are discussed in here. The voltage-current characteristics of the electric arc are presented for measurement results performed in the tested circuit supplied both by the 12 V and 230 V voltage source. The voltage-current characteristics of the electric arc are presented for all considered methods limiting the electric arc energy: the time-controlled contact separation, the connection of the passive components in parallel to the operated switch, as well as, for the applied hybrid switching. The voltage-current characteristics of the electric arc show the influence of considered methods on the arcing voltage.

Chapter 10 presents the frames that were obtained for registration of a creation of the electric arc that was performed by the high speed camera. The contact system of the tested switch was observed for two cases – when the current was interrupted by the standalone switch, as well as, when the current was interrupted during the hybrid switching. This approach allowed to indicate the significant differences in a formation of the electric arc between both considered situations.

The evolution of the electric arc erosion of the electrical contacts is presented in chapter 11. The observations of the contact surfaces of the electrical contacts taken from the tested switches (each switch after 50 000 current interruptions) that were performed by means of the camera and the optical microscope are presented in this chapter. Additionally, measurement results from researches that were performed for all analyzed contacts by means of the roughness tester and the SEM coupled with EDS method are presented in this chapter.

Chapter 12 covers the analysis of the limitation of the electric arc erosion performed in frame of this thesis. For this purpose, measurement results obtained from the roughness measurement, as well as, SEM coupled with EDS measurement were discussed.

Chapter 13 contains discussion and conclusions from all performed researches. The differences in measurement results performed in tested circuit supplied by the 12 V and 230 V voltage source are discussed. Effectiveness for limiting the electric arc energy for considered methods are analyzed. Measurement results performed for the limiting electric arc erosion are also discussed. Entire work content was summarized with respect to thesis. Finally, further activities were proposed.

3 Electric Arc as the Conductive Substance

The electric arc is a plasma channel between contacts of the switch that is formed after a gas discharge in the extinguishing medium. During the opening process of the electrical contacts, the magnetic energy stored in the inductances of the electrical circuit forces the flowing current through the quenching medium between electrical contacts of the operated switch. Just before the contact separation, contacts of the switch are connected at a very small surface area, and resulting high current density makes the contact material melt. The melting contact material practically explodes which leads to a gas discharge between electrical contacts as a form of the electric arc, which also causes a rapid increase of the pressure and the temperature in the area around the electrical contacts. The current is able to flow in the interrupting circuit, until the electric arc is quenched. Thus, the electric arc is a complex phenomenon, and processes taking place during the current interruption can be characterized in the electrical, magnetic, mechanical and thermal fields.

Despite of a destructive impact of the electric arc on contact surfaces, presence of the electric arc has also a positive influence on transient states in interrupting electrical circuit. Immediate current interruption with high current steepness di/dt could generate significant overvoltages in interrupted circuit, because of lack of possibility for discharging energy stored in inductive components of circuit. Thus, presence of the electric arc during the current interruption leads to limit Transient Recovery Voltage (TRV). For this reason, there is a need to develop controlled current interruption process with limited arc erosion of electric contacts and limited effect of Transient Recovery Voltage.

This chapter describes the mechanisms leading to the appearance of the electric arc and the processes originated in the switch during the opening process of the electrical contacts, when the current is still able to flow through the circuit. Furthermore, the structure of the electrical arc and its properties were characterized inhere together with factors influencing on the maintenance and the arc extinction.

3.1 Electric Arc Ignition

Plasma is a different material state of aggregation than solid, liquid and gas. Matter changes its state from a solid into a liquid form, while molecular kinetic energy exceeds the combination energy. Similarly, matter changes its state from a liquid state into a gaseous state in the situation, when the Van der Waals forces are overcome, and more energy can be added by an increase in temperature [83].

The most crucial factor leading to the electric arc ignition in the gas environment is the gas ionization. This phenomenon is forced by external factors, such as: voltage between contacts of operated switch or a rapid increase of temperature. Basically, the following phenomena can be observed during the electric arc ignition: an impact ionization, a thermal ionization, thermal emission from cathode, and the photoionization. In contrast to the ionization, there is the deionization, which is a counteractive phenomenon to ionization (gas returns to normal state).

The impact ionization (called also as *the ionization by collision*) is related to the electric field intensity. Free electrons, which are placed in the electric field move in the opposite direction to the electric field vector. The velocity of the movement of electrons depends on the value of the electric field. Electrons are able to obtain the energy that is required to ionize the particle during collision at the specific value of the electric field.

The thermal emission from cathode is related to phenomena which occur during the separation of contacts. The number of contact points between two electric contacts increases with the contact pressure (detailed description of this phenomenon is presented in the section 4.1.3). As soon as contacts start to separate, there is a decrease in the contact pressure. This leads to an increase in the electric resistance of the contacts. Due to the large current density, significant amount of the heat is dissipated in some contact points and that causes entire surface of contacts to heat. Then, the thermal energy is transferred to metal crystals and atoms which lose their valence electrons in favor of the entire crystal. Since these electrons lose the connection with atoms of the crystal, therefore they move freely in entire volume of the crystal. As a result, their behavior is resembling the movement of gas particles inside of the closed vessel (an inert thermal motion) [68].

As it was mentioned above, the ionization can be also achieved by the influence of light waves with specific wavelength (photoionization). Nevertheless, existing sources of ultraviolet rays emit waves with such wavelengths at which the ionization is difficult to attain [68].

The thermal emission can be observed either when a neutral particle of the gas hits another neutral particle, or when an electron hits in a neutral particle. When the gas is placed in a closed vessel the walls of that vessel are hit by moving particles. As a result, a pressure is created that acts on the walls of the vessel. The average length of free paths, the number of collisions at the time unit can be estimated by means of statistical methods [68]. These magnitudes are strongly related to the gas temperature and gas pressure. Thus, the velocity of thermal movements of particles, as well as, the kinetic energy of particles increase together with temperature rise. The energy of particles can be so high that collisions of particles become inelastic, which leads to excitation or ionization. A further rise of temperature provides the particular electrons with so much energy, whereby they are able to dissociate and take a form of separate atoms. In situation, when the energy is increased even further, orbital electrons of the atoms dissociate into free moving electrons, which causes positive ions to remain. This is called the plasma state. Due to presence of the free electrons in plasma channel and the heavier positive ions in the high-temperature, the plasma channel is highly conductive, whereby the current can continue to flow after the contact separation.

As an example, nitrogen (the main component of air) is dissociated into separate atoms ($N_2 \rightarrow 2N$) at about 5000 K and ionizes ($N \rightarrow N^+ + e$) above 8000 K. Likewise, SF_6 dissociates at temperature about 1800 K, and its ionization takes place between 5000 K and 6000 K and as result, its conductivity rapidly increases for higher temperatures. The degree of dissociation and ionization of the medium increases together with temperature, and hence number of charge carriers and the conductivity of the electric arc also increases. This dependence is presented in Figure 3.1 for various metal vapor and atomic gases.

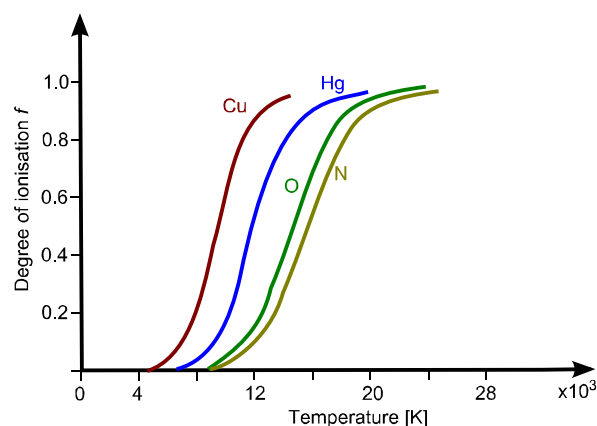


Figure 3.1. Degree of thermal ionization for selected metal vapors and atomic gases [6, 83]

Figure 3.1 shows the dependence between conducting state ($f = 1$) and an insulating state ($f = 0$) of selected metal vapors and atomic gases, for different thermal ionization degrees. As it can be also visible in Figure 3.1, the limitation of the kinetic energy of the moving particles by cooling down with cold gas can be an effective method to change the arc channel from a conducting to non-conducting state, due to steep slope of the function $f(T)$. However, change of the temperature cannot be immediate, so for this reason, a specified amount of time is required before reaching thermal equilibrium after changing from the conducting state to the non-conducting state. This conductivity time constant is dependent on the particle-velocity distribution and the ion-electron recombination speed. Time necessary to achieve a local molecule-atom velocity equilibrium is in the order of 10 ns, while the time required to reach a local electron velocity equilibrium is in the order of 0.1 ns [83]. The time constants of physical mechanisms being key for electro-ion recombination processes are in the order of 10-100 ns [83]. Thus, it can be noticed, that the time required to achieve ionization equilibrium is distinctly shorter than the paces of change in the electrical phenomena from the electrical circuit during current interruption period. Therefore, the electric arc can be considered to be in a thermal-ionization equilibrium for electric switching transient phenomena taking place in the electric power systems. Basically, in the area between separated contacts, three regions of the plasma channel in the electric arc can be distinguished: the cathode, the anode and the column in the middle. The arc channel with typical potential distribution along an arc channel were presented in Figure 3.2. The areas localized nearly contacts are transition regions between the gaseous conductor created by the electric arc column having a variable conductivity and the solid conductor with mostly constant conductivity.

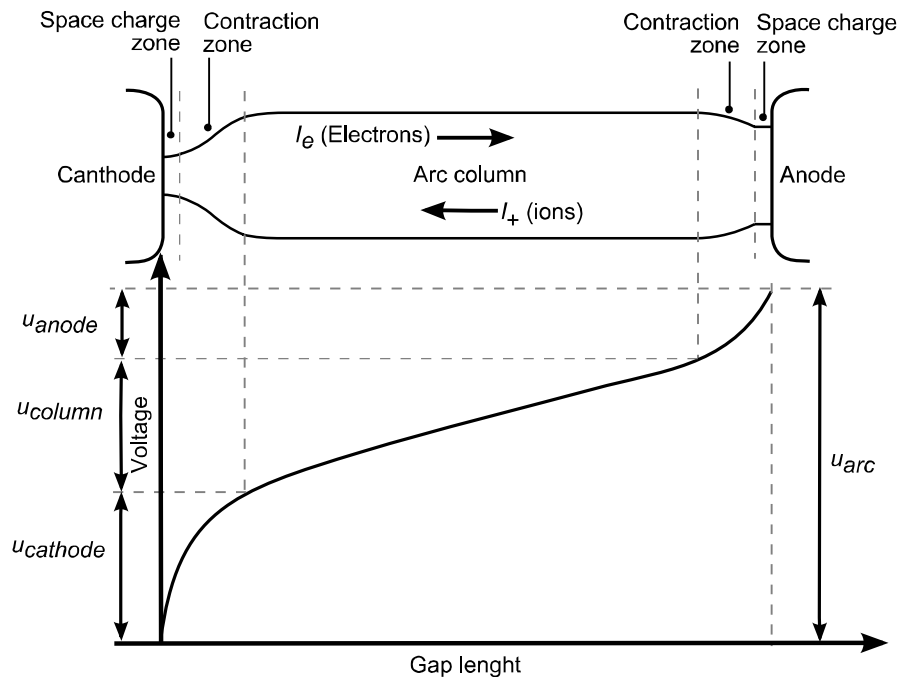


Figure 3.2. The arc channel can be divided into an arc column, a cathode, and an anode region [6, 83]

The potential gradient is a complex function of the physical properties of the arcing medium, the arc current, the pressure, the flow velocity, and the energy exchange between the plasma channel. There are no space charges in the electric arc column, therefore, the current flow is maintained only by electrons, and there is a balance between the electron charges and the positive ion charges. In dependence on the surrounding medium and configuration of quenching chamber, the temperature peak in the arc column can be in the range of 7 000-25 000 K [83].

According to the previous description, the cathode emits the current-carrying electrons into the arc column. In dependence on type of the cathode material, the emission of electrons starts in different conditions. Two types of cathode materials can be distinguished for this process: refractory materials (e. g. molybdenum, tungsten, carbon) and non-refractory material (e. g. such as mercury or copper). Both types of material differ in value of boiling point (low boiling point for refractory materials, and high boiling point for non-refractory materials). When the cathode is made from a refractory material with a high boiling point, the emission of electrons starts as soon as it is heated to temperature below the evaporation temperature (*the thermal ionization*). In this case, current densities that could be obtained are in the order of $10\,000\text{ A/cm}^2$ [83]. The rate of change of Transient Recovery Voltages appearing across the cathode and the anode after arc extinguish is relatively fast in comparison to the cooling down of the heated cathode spot, so the current can be interrupted. Limit values of voltages and current for various contact materials that are necessary to initiate an ignition of the electric arc are listed in Table 3.1.

Table 3.1. Limit values of voltages and current required to initiate electric arc ignitions [88]

Contact material	Limit voltage	Limit current
	[V]	[mA]
Copper	12-13	400
Silver	12	400
Gold	15	300-400
Tungsten	15-16	800-1200
Nickel	14	400-500
Iron	13-15	300-500
Carbon	20	10-20
Platinum	17	700-1100
Palladium	15-16	800-900

As it was mentioned above, the emission of electrons can be also initiated at temperatures lower than thermionic emission due to field emission (*the ionization by collision*). In this case, the ionization is caused by electrons accelerated by an electric field, having much higher velocities than from thermal stimulation. Electrons and ions emanate from individual spots on the cathode surface, depending on the contact material of each cathode spot supplying 15-150 A [83]. Due to very small dimensions of the cathode spot, cooling down of the heated spot is almost immediate when the current reaches zero-crossing. The ionization by collision has a dominant influence when the cathode is made from non-refractory material with a low boiling point (applied mainly in vacuum breakers [121]).

If the distance between contacts is constant when sinusoidal voltage reaches zero-crossing, voltage across contacts decreases, which leads to decrease the electric field. As a consequence, this phenomenon lead to disappearance of the ionization by collision. Near zero-crossing of current sinusoid, the electric arc quenches, and thermal ionization disappears. In simplified case, when the current is in phase with voltage, the reasons of ionization disappear at the time, when voltage and current are near zero-crossing. Just after the time, when the current stops to flow in the circuit, partially ionized gas occurs between contacts (so called *post arc channel*). The velocity of ions and electrons in post arc channel decreases, which causes deionization period to occur. During this time, ions and electrons connect in neutral electric atoms or gas particles, which cases dielectric strength of the post arc channel to increase. Consequently, conductive gas till now, becomes dielectric in the final part of deionization process. The current and voltage waveforms during the current interruption in resistive circuit is presented in Figure 3.3.

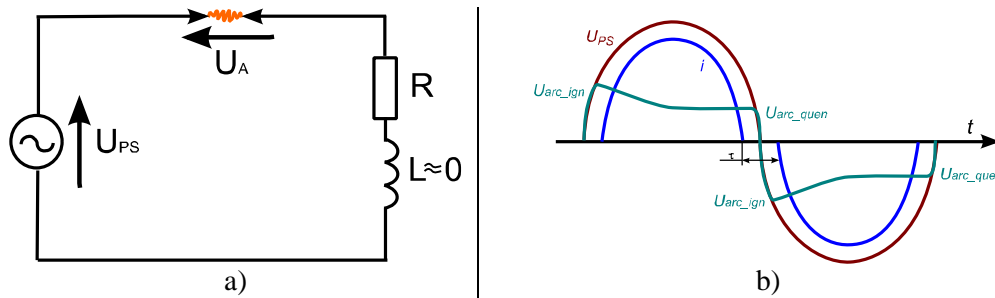


Figure 3.3. Considered resistive circuit (a), waveforms of voltage and current (b): e – supply voltage [V], i – the arc current [A], τ – time, when current does not flow in the circuit [s], U_{arc_ign} – arc ignition voltage [V], U_{arc_quen} – voltage of quenching arc [V] [68]

In inductive circuits, conditions for quenching arc are definitely more difficult. This is due to the most intensive ionization by collision at u_{max} and thermal ionization at i_{min} appear alternately, which makes deionization difficult at the time, when current does not flow in circuit.

Deionization takes place by recombination and diffusion. Recombination can be distinguished as electron recombination and as ion recombination. The significant influence of gas dissociation on deionization process can be observed at high temperature range. Particles of gas move quickly in a disordered way, so their temperature and their motion velocity is sufficient to decay of particles into atoms with simultaneous absorption of heat. Newly formed atoms move into environment, where they are connected as particles, which generates significant amount of heat, taken during dissociation. As a result, dissociation causes an increase of the gas dielectric strength. The avalanche ionization starts at U_{arc_ign} voltage (voltage of arc ignition).

During ionization, two types of anode role can be distinguished: passive and active. In passive mode, anode is a collector for electrons leaving the arc column. In active mode, the anode evaporates, and positive ions are supplied to the arc column when metal vapor is ionized in the anode area. Active anode has significant importance for vacuum arc – when current has high density, anode spots are formed and ions contribute to the plasma. For this reason, these anode spots do not stop to emit ions when current exceeds zero-crossing, and it is an undesirable effect. Heat capacity of anode spots is able to evaporate anode material even if input power is zero, which can lead not to extinguish vacuum arc. With increasing U_{arc_ign} , dielectric strength of arc channel increases.

Just after contact separation time, when the arc starts to ignite, evaporation of contact material is the dominant source of charged particles. In vacuum, when the distance between contacts increases, the evaporation of contact material also becomes the main source of charged particles. The effect of evaporation of contact material is minimal for high-pressure arcs (ignited in air, SF_6 or oil) during opening contacts, whereby the plasma is dependent mainly on the quenching medium.

3.2 Voltage-Current Characteristics of the LV electric arc

The main electrical characteristic of the electric arc is a decreasing voltage-current dependence, completely different from linear voltage-current characteristic of metallic conductors. In contrast to V-I characteristic being a straight cure, arcing voltage decreases when the current increases up to a limit value. This dependence is related to an increase of larger temperature with value of interrupted current, which causes to intensify the ionization. Thereby, the gas conductivity increases, so as a consequence the electric arc voltage decreases.

Static characteristic of the electric arc is a voltage-current dependence for specific pressure value at steady state (when the value of the current and the distance between electrodes are constant). Exemplary measured static voltage-current characteristics of electric arc presented as a function of arc length are shown in Figure 3.4.

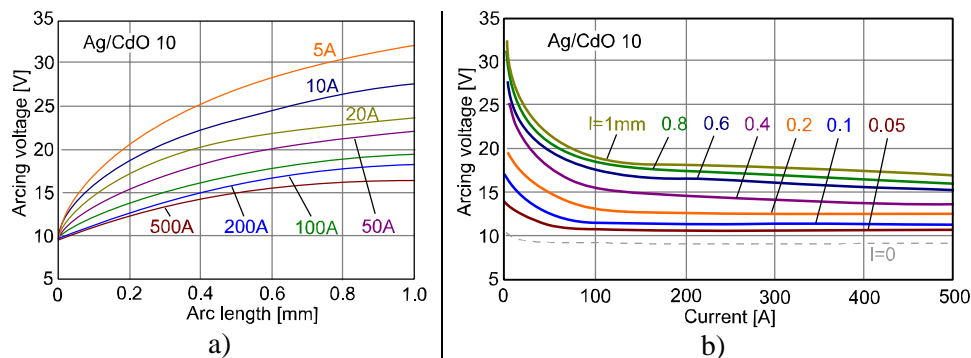


Figure 3.4. Set of static voltage-current characteristics of electric arc for various arc length [141]

Based on performed researches presented in [18], it can be concluded that the greatest of increases of arcing voltage can be observed for small currents and shorter arcing times. During the current interruption of currents larger than 400 A, an influence of the current value on arcing voltage is negligible, which can be also visible in Figure 3.4b. In defined inductive low voltage circuit (lower than 250 V), arcing voltage deforms the current curve and accelerates its descent to zero-crossing value, which also influences on magnitudes characterized by current interruption process, such as: energy and power of the electric arc, electric charge flowing through the electric arc, Joule-Integral, which significantly impacts on electric arc erosion and durability of entire contact system [24]. For this reason, the object of this thesis is focused on inductive small current interruption at low voltage.

During current interruption, the arcing voltage depends on different factors such as: a value of the interrupted current, a length of the electric arc, a shape and dimension of contacts, a contact material and a velocity of the contact separation. Figure 3.5 presents exemplary dynamic characteristic of electric arc that were measured for a single half-wave current at 50 Hz frequency, for constant however different distances between contacts (AgW50, Φ 6 mm, and sinusoidal current peak 2.1 kA).

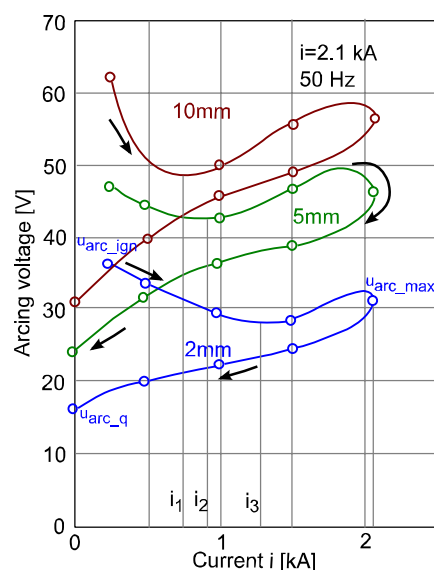


Figure 3.5. Dynamic characteristics of the electric arc for distance between electrodes (constant distance between electrodes) [24]

Characteristics presented in Figure 3.5 describe voltage-current dependences of the electric arc for defined constant distances between electrodes. However, in practice, during current interruption process, separated contacts move, so the distance between operated contacts is lengthened. This phenomenon causes the increase of electric arc resistance, so as a consequence it strongly influences on voltage-current characteristic of the electric arc. Dynamic characteristics of the electric arc that were measured during current interruption for different contact materials are presented in Figure 3.6 [24].

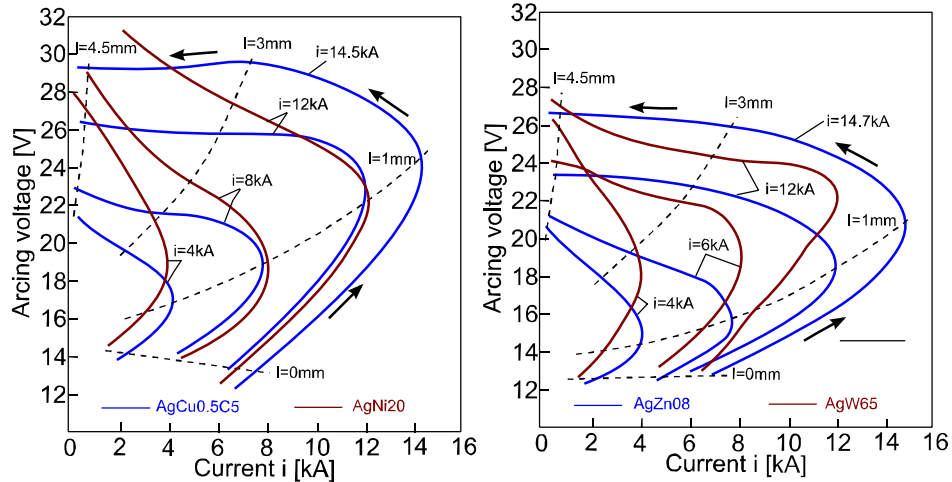


Figure 3.6. Dynamic characteristic of electric arc (distance between electrodes is lengthened) for different contact materials [24]

Thus, arcing voltage depends among others on the value of interrupted current, the distance between contacts, type of the contact material. This dependences can be visible in Figure 3.6.

3.3 Interruption of the Electric Arc in LV switches

This section presents conditions for quenching the electric arc in DC and AC electrical circuits.

3.3.1 DC Current Interruption

In order to analyze conditions for burning and quenching DC electric arc, a simplified circuit diagram including an inductive load is presented in Figure 3.7.

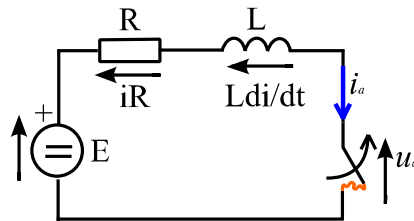


Figure 3.7. Equivalent circuit diagram: E – voltage source [V];
 R – circuit resistance [Ω]; L – circuit inductance [H];
 S – operated switch; u_a – arcing voltage [V]; i_a – arc current [A]

For circuit diagram illustrated in Figure 3.7, the following equation is fulfilled (according to Kirchhoff's second law) [22]:

$$E = i \times R + L \times \frac{di}{dt} + u_a \quad (3.1)$$

Parameters of the electric arc in considered circuit (Figure 3.7) can be analyzed on the based of voltage-current characteristic of electric arc $u_a = f(i)$, according to description presented in

section 3.2 (see Figure 3.4). Thus, based on V-I characteristic of electric arc, the quotient of voltage and current gives information about changes of arc resistance according to Ohm's law (3.2):

$$r_a = \frac{u_a}{i} \quad (3.2)$$

Similarly, the product of arcing voltage and current arc describes the electric arc power, according to formula (3.3):

$$p_a = u_a \times i \quad (3.3)$$

Exemplary static characteristics of DC electric arc continuously burning in considered circuit with characteristic of circuit (Figure 3.7) are shown in Figure 3.8.

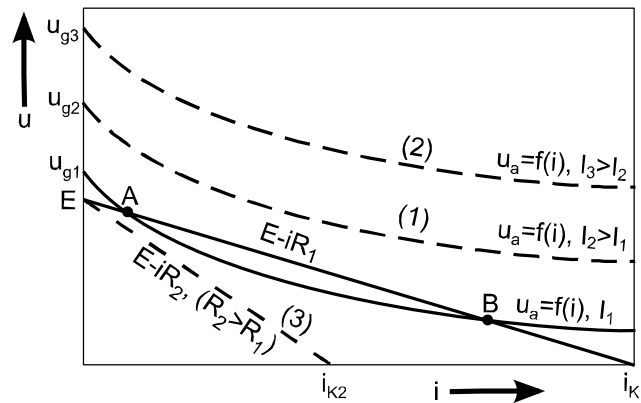


Figure 3.8. Static characteristic of the electric arc

Figure 3.8 is also graphical solution of equation (3.1). As it can be visible, static characteristic of the electric arc has two common points (A and B) with characteristic of considered electric circuit ($E-iR$ line). These points determine area, where quenching stationary electric arc can be stable (below $E-iR$ line). Thus, in order to quench the electric arc in considered circuit, both characteristics should not have common points. Basically, there are two methods to meet this condition:

- moving up the characteristic of the electric arc (respectively curves 1 and 2 in Figure 3.8). In practice, it can be realized by improving conditions for quenching electric arc (such as: lengthening arc, cooling down arc, dividing arc into smaller sections, etc.),
- moving down line $E-iR$ being characterized for considered circuit. In practice, it could be reached by connection of additional resistance into circuit. However, this method is difficult in practical implementation, so is not often applied.

Thus, in practice, in order to quench electric arc in considered circuit, moving up the electric arc characteristic is the most often applied action due to simplicity of the method. Lengthening electric arc can be realized by contact separation for suitable distance, suitable design of contact system or the exhaust of the electric arc. However, with increasing length of the electric arc, arcing voltage also increases, which can be observed in Figure 3.8. This phenomena can be a source of significant switching overvoltages generated during current interruption process in DC circuits. For this reason, it is very important to provide suitable level of overvoltage protection in considered circuit against switching overvoltages.

3.3.2 AC Current Interruption

Quenching electric arc in AC circuits is simplified issue in comparison to DC circuits, due to presence of natural current zero-crossing that occurs twice per each current period. This effect is used to interrupt current without reignition of the arc after current zero-crossing. The

general essence for quenching AC electric arc can be formulated in the following way: channel of the electric arc should be intensively cooled down before current zero-crossing, and when value of the current reaches zero-crossing, conditions for effective deionization process of post arc channel should be fulfilled to obtain fast enough increasing dielectric strength of the Transient Recovery Voltage [87, 88]. Cooling down the electric arc has relevant influence on voltage-current characteristics of the electric arc. Voltage waveforms and current waveforms for different ways of cooling down the electric arc are presented in Figure 3.9.

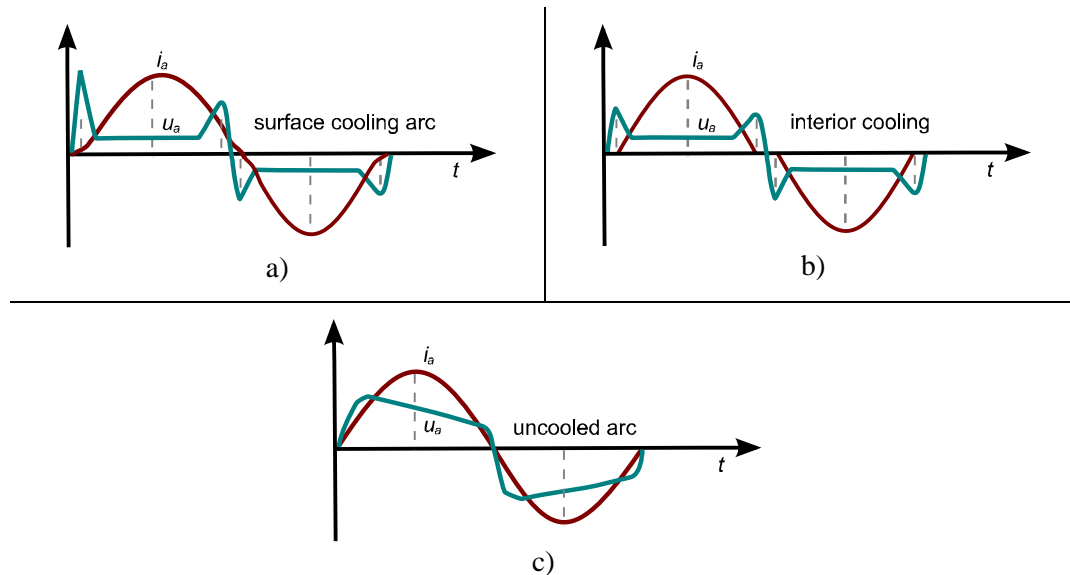


Figure 3.9. Waveforms of arcing voltage and interrupting current: a) cooling down surface of electric arc, b) cooling down internal channel of electric arc, c) uncooled electric arc [68]

Thus, in order to quench the electric arc in AC circuits, contacts of the operated switch should be separated at sufficient distance with large velocity (due to TRV breakdown strength and gas ionization processes). Whereby, the electric arc can be quenched at next natural current zero-crossing.

During quenching LV electric arc in AC circuits, the influence of the arcing voltage can deform the current curve, which is presented in Figure 3.10.

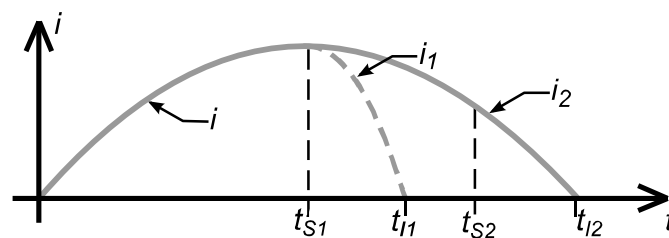


Figure 3.10. A distortion of sinusoidal current during current interruption caused by the influence of the electric arc: t_{S1} – time of contact separation (long arcing time); t_{I1} – zero-crossing time distorted current (long arcing time); t_{S2} – time of contact separation (short arcing time); t_{I2} – zero-crossing time distorted current (short arcing time) [18]

Deformation of current curve impacts on magnitudes characterized by interruption process such as: power of electric arc, energy of electric arc, electric charge flowing through arc, Joule integral. These magnitudes have a direct influence on level of arc erosion of contact system and switching durability of analyzed switch. Deformation of current curve can be especially observed in inductive circuits with voltage source lower than 250 V [24].

Electric arc energy can be calculated as definite integral according to equation (3.4):

$$E = \int_{t_0}^{t_1} (u_a \times i_a) dt \quad (3.4)$$

where: u_a – electric arcing voltage [V]; i_a – arc current [A], t_0 – time, when electric arc starts to burn [s], t_1 – time, when electric arc is quenched [s].

Exemplary voltage-current characteristics of AC electric arc were presented in Figure 3.5 Figure 3.6.

Separation of electric contact causes to occur voltage between contacts so called *Transient Recovery Voltage (TRV)* to occur. This voltage stresses contact gap and has significant influence on effectiveness of quenching arc. As it was mentioned in section 3.1, two contrary processes take place in the post arc channel:

- deionization with increase of electrical resistance of post arc channel,
- ionization caused by increasing TRV between electrical contacts, that can cause increase of gas ionization which as a consequence can lead to generate arc ignition.

Thus, both processes interact with each other in opposition during current interruption process. Effective quenching electric arc (without re-strikes) depends on dominance of deionization over ionization process. Methods for improvement of quenching electric arc process are presented in chapter 4.

3.4 Mathematical models of the electric arc

According to the description presented in this chapter, physical phenomena occurring upon current interruption are very complex that depends on many factors. For this reason, it is still a challenge to use appropriate mathematical arc models that will be able to reflect switching conditions in electrical circuits. The used model should represent non-linear behavior of the electric arc, as well as, the interaction between the switching process and the system components. Moreover, since very small time constants are involved, a correct numerical treatment of the arc-circuit problem is an important aspect as well. Various interrupting mediums with different dielectric strength characteristics are applied in switches depending on particular design, application, price, etc. The dielectric strength determines the maximum electric stress that the dielectric can withstand without breakdown. It is a multi-variable function of the switching process and design of the particular switchgear component.

The general models of the electric arc represent the electric arc behavior in gases, such as Mayr [90] and Cassie [29], are often used in a modified form to reflect the arc voltage condition obtained in the measurement (e.g. the modified Mayr-Cassie equation [7, 13, 57, 108, 114]). The switching process can be measured in synthetic circuit, which allows to reproduce the realistic Transient Recovery Voltage (TRV), arc voltage and post-arc current conditions. The approach proposed by Mayr [90] is well suited for vicinity of current zero crossing. Not only the parameters, but the model itself can be modified according to the measured curves of the arc voltage and post-arc current. The example of the modified Mayr and Cassie equations is the Schwarz-Avdonin model [116].

Mathematical modeling of the electric arc is beyond the scope of this thesis dissertation, so for this reason, more details are not presented in this section. However, Cassie-Mayr model was used to select the parameters of the arc suppressors, which is described in the chapter 6.

The author also was being performed the researches on switching transient states with usage the above-mentioned models [33, 34, 95, 96].

4 Methods for Quenching the Electric Arc and Limiting the Electric Arc Erosion

Basically, the mechanical switch is the electric device that realizes function of conducting current, and switching current (such as: making and interrupting current). In this chapter, methods that are being applied to quenching the electric arc in LV switches are presented. In general, parameters of quenching the electric arc can be improved by increasing the steepness rise of the dielectric strength in the post arc channel. This issue is being taken into consideration during the design of electrical apparatus. In fact, increasing the steepness rise of the dielectric strength in the post arc channel can be realized by [88]:

- decreasing electric field intensity between contacts through contact movement as quickly as possible,
- intensive cooling down the electric arc and the post arc channel,
- increasing gas pressure in environment of the electric arc (thereby free path of electrons decreases, which causes gradient of the arcing voltage to increase),
- removing ionized particles of post arc column mechanically and their replacement by cold gas particles with greater dielectric strength which as consequence leads to increase the thermal time constant of the arc channel,
- lengthening the electric arc through pushing into arcing chamber (e. g. with perforated plates), which can help to divide long electric arc into a few shorter electric arc,
- application of special contact materials with low electron emission coefficient.

Thus, increasing steepness rise of dielectric strength in the post arc channel is an issue related to physics of electric arc phenomena and the design of the considered switch. However, there are also other methods to limit the arcing time that lead as a consequence to reduce the electric arc energy. These methods are focused on external circuits that could cooperate with operated switch, such as:

- external circuits connected to operated switch (RC suppressor, passive semiconductor branches, active systems with power electronic components),
- external systems supporting and controlling drive of the operated switch.

In this chapter, the description of methods that are being applied to quenching the electric arc in LV switches is presented. Application of presented methods inhere influences voltage-current characteristics of electric arc, which impacts on the limitation of the electric arc energy. The scope of this chapter is mainly related to issues connected with interruption of AC currents.

4.1 Design of the Operated Switch

In general, the effectiveness of quenching the electric arc in the LV switch is dependent on features of the design of the switch, such as: the type of applied insulation medium, parameters of the contact systems, the type of the contact material, as well as, the type of the quenching chamber. In this section, the key features of the switch design that strongly influence on the effectiveness of quenching the electric arc are presented and characterized. However, the switch design is strongly related to the intended use of the switch. Basically, LV switches can be divided into the following main groups due to their types of constructions [48]:

1. Contactor

A contactor is a relay with higher current ratings (contractors are designed even for the range of several hundred of Amperes). Contactors are widely applied in many branches of industry to switch circuits consisting of heavy equipment such as: pumps, cranes, etc.

2. Time delay relay

Time delay relay is a type of relay that enables one to perform switching operation with defined time delay. Design of time delay relay can be based on mechanical solution and electronic components.

3. Solid-state relay (SSR)

Design of a solid state relay is based only on electronic components (mainly thyristors, transistor and TRIAC). Lack of moveable component increases reliability of the entire switch. Functionality of the solid state relay is similar to the mechanical contactor, however galvanic insulation between terminals of the relays is not provided in semiconductor solutions (only galvanic separation between control and power circuits can be implemented).

4. Latching relay

A latching relay enables contact position of the relay to be kept in a defined position without power supplied to the coil of the relay. Coil of the latching relay consumes power only for a short time when the relay is being switched, which is an unquestionable advantage in comparison to other constructions.

5. Reed relay

Contacts of reed relay are enclosed in glass tube, which can be evacuated or gas-filled. The contacts of the reed relay are designed of magnetic material. For this reason, they can be closed and open by external magnetic force. Source of the magnetic force can be a solenoid (integral part of the reed relay) or external magnet.

6. Polarized relay

A polarized relay is featured by an increase sensitivity. Design of the polarized relay is based on the armature that is placed between poles of a permanent magnet. Currently, this type of relay is rarely used.

7. Coaxial relay

Type of a coaxial relay is used most often in radio transmitters and receivers. Coaxial relays are usually designed at high voltage range to provide high electric isolation between receiver and transmitter terminals.

8. Buchholz relay

Buchholz relay is applied in protect circuits of power transformers. Contact system of the Buchholz relay is sensitive to an increase of gas that is produced rapidly in the transformer oil, when current flowing through windings of transformer is higher than expected.

9. Overload protection relay

Overload protection relays are applied in electrical circuits to protect devices that are installed in the system against effects of short-circuit currents. Design of overload protection relay is based on heating bimetallic strip that acts on a spring of the relay resulting in operate auxiliary contacts of relays.

10. Vacuum relays

Functionality of vacuum relays is similar to conventional contactors, however vacuum chambers are applied in design of vacuum relays. For this reason, voltage

and current ratings of vacuum relays can be increased with comparable dimensions in comparison to conventional contactors.

11. Safety relays

Safe relays are being designed for realization of safety functions. For this reason, their construction should be featured by increased reliability in comparison to conventional relays.

12. Mercury-wetted relay

Construction of mercury-wetted relay is similar to the reed relay. However, in this case, contacts of the relays are wetted in mercury. Application of mercury inside of a glass tube allows to reduce the contact resistance and contact bouncing. For this reason, mercury-wetted relays are applied mainly to switch low-voltage signals. Due to ecological aspects, usage of mercury-wetted relay is being limited.

13. Mercury relay

In the mercury relay, mercury is applied as the switching component. Relays of this type are used mainly in applications, when contact erosion could be problematic. Similar to mercury-wetted relays, usage of mercury relay is being limited due to toxicity of mercury and ecological aspects.

Listed-above types of switches are being designed to switch AC and DC currents at various voltage and current ratings. Various types of quenching mediums, contact systems, quenching chambers and materials are being applied to develop the switches.

For contactors and starters, the utilization categories as given in Table 4.1 are considered standard [56]. Any other type of utilization shall be based on agreement between manufacturer and user, but information given in the manufacturer's catalogue or tender may constitute such an agreement.

Table 4.1. AC Utilization categories according to IEC standard [56]

Kind of current	Utilization categories	Additional category designation	Typical applications
AC	AC-1	General use	Non-inductive or slightly inductive loads, resistance furnaces
	AC-2		Slip-ring motors: starting, switching off
	AC-3		Squirrel-cage motors: starting, switching off motors during running
	AC-4	Ballast Incandescent	Squirrel-cage motors: starting, plugging, inching
	AC-5a		Switching of electric discharge lamp controls
	AC-5b		Switching of incandescent lamps
	AC-6a		Switching of transformers
	AC-6b		Switching of capacitor banks
	AC-7a		Slightly inductive loads in household appliances and similar applications
	AC-7b		Motor-loads for household applications
	AC-8a		Hermetic refrigerant compressor motor control with manual resetting of overload releases
	AC-8b		Hermetic refrigerant compressor motor control with automatic resetting of overload releases

Technical requirements (such as: making and breaking capacities or conventional operational performance) are specified for all utilization categories in the International Standard [56].

4.1.1 Types of quenching mediums applied in mechanical switches

The most commonly used quenching medium of LV switches is air. Other quenching mediums, like mercury, vacuum or SF₆ are being applied in constructions dedicated to special purposes (e.g. when the switch has to meet its parameters under difficult environmental conditions). Application of air in LV switches as the quenching medium is commonly used due to technical issues (electrical parameters of air are effective enough for interrupting currents at LV, the design of the switch can be simplified in comparison to other quenching mediums), as well as, due to the economical issues (application of air is significantly cheapest in comparison to other quenching mediums). In general, the following types of quenching systems are being applied in constructions of electrical apparatus [88]:

1. Quenching systems with solid materials:
 - gassing materials (such as: organic glass, fiber, polyamide plastic) that are being applied in gas-blast and magnetic-blast switch-disconnectors, and high voltage surge arresters,
 - non-gassing ceramic materials that are being applied in magnetic-blast switch-disconnectors and circuit breakers rated at low and high voltages,
 - low-gassing materials (e. g.: special boron-lead glass that is being applied in active spark gaps).
2. Quenching systems with liquid materials:
 - oil,
 - water.
3. Gas quenching systems:
 - Air
 - SF₆
 - CO₂
4. Vacuum quenching systems.

Quenching systems with solid materials are being designed as close constructions (e.g. in fuses) and open constructions (e. g. in gas-blast and magnetic-blast switch-disconnectors). In construction with applied gassing solid materials, special shapes of channels are designed for gases that are generated during quenching the electric arc. The power is effectively removed from the electric arc in time, when the current still flows in the circuit, and when the electric arc quenches, the heated and partially ionized gases can be blown out. In construction with applied non-gassing ceramic materials, a direct contact of the electric arc channel with the ceramic surface has the key influence. The heat from the electric arc is removed through the conductivity, and some of its amounts is also dissipated for melting the ceramic material, which can be especially observed in elements of fuses [88].

Quenching systems with oil are currently not being developed mainly due to the harmful impact on the environment. Constructions containing water were not effective enough in industrial applications. Oil was applied mainly in MV and HV circuit breakers as the quenching medium, due to its good quenching parameters and insulation properties. Burning the electric arc in oil causes an evaporation and degassing of some its amount, which as a result causes a gas bubble to create around the electric arc channel in the oil that consists of 70-80% of hydrogen, acetylene and methane. Temperature of gases in the bubble reaches a few thousands degrees. In this temperature, hydrogen is featured by very good thermal conductivity, which helps to transfer the heat from external layers of the electric arc channel. Additionally, at higher values of the electric arc current, the electric arc power rapidly

decreases nearly the current zero-crossing, which as a consequence leads to reduce the energy that is transferred into the gas bubble. The pressure inside of the bubble decreases, which causes the evaporation of external layer of the gas bubble to intensify. Vaporous particles take drops of the liquid and introduce it into the electric arc channel with significant velocity, which causes heat to remove intensely. This effect called "expansive" increases with the temperature and the velocity of changes of the pressure near the current zero-crossing.

Gas quenching systems of electrical apparatus are designed mainly with air and SF₆ that can be compressed under high pressure. The higher pressure can be achieved through application of the system to compress the gas (pneumatic and self-compressed), as well as, the pressure of the gas can be increased through the thermal influence of the electric arc. Together with increasing the gas pressure, its dielectric withstand increases (Figure 4.1), while the diameter and the time constants of the electric arc channel decreases. Pneumatic systems are being applied mainly in HV and generator circuit breakers due to their high effectiveness, while self-compressed systems are applied in MV switch-disconnectors. Nitrogen, main component of air is characterized by relative high dissociation energy 9.78 eV [88]. The greater intensity of changes of dissociation and the greater thermal conductive of this gas can be achieved in relative high temperature, about 7500 K. Decreasing the current of the electric arc up to zero causes the temperature of the electric arc channel to decrease below 7500 K. Together with this, electrical conductivity of the plasma decreases, and as a consequence the plasma disappears below 3000 K [88]. For purpose of quenching the electric arc, it is desirable to keep the greater thermal conductivities of the plasma in the temperature range about 3000 K, which takes place in case of SF₆. In SF₆, atoms of fluorine are connected with atom of sulfur through the dissociation energy that is about 22.4 eV [88]. In order to dissociate entire particles of SF₆, six collisions are required, which transfers amplitudes of thermal conductivity of the plasma up to temperature close to 3000 K in this environment. On the other hand, small ionization energy of sulfur causes sufficiently high electrical conductivity of the plasma in SF₆ from 2000 K, which provides relatively smaller values of the arcing voltage gradient, as well as, the power and the energy of the electric arc. Because of the fact that in temperature above 3000 K thermal conductivity of SF₆ is relatively small, transformation of energy is relatively low during quenching the electric arc in SF₆. For this reason, chopping current phenomenon is practically excluded, and that is an additional advantage in comparison to oil, air and vacuum quenching systems. Outstanding dielectric and quenching properties of SF₆ are caused by its capability for binding of free electrons in heavy negative ions (so-called *electronegativity of gas*). After dissociating particles of SF₆, separated atoms of fluorine can create heavy negative ions with electrons ($F + e \rightarrow F^-$). This mechanism provides about 2.5 times increase of dielectric withstand of SF₆ in comparison to air at this same environment conditions.

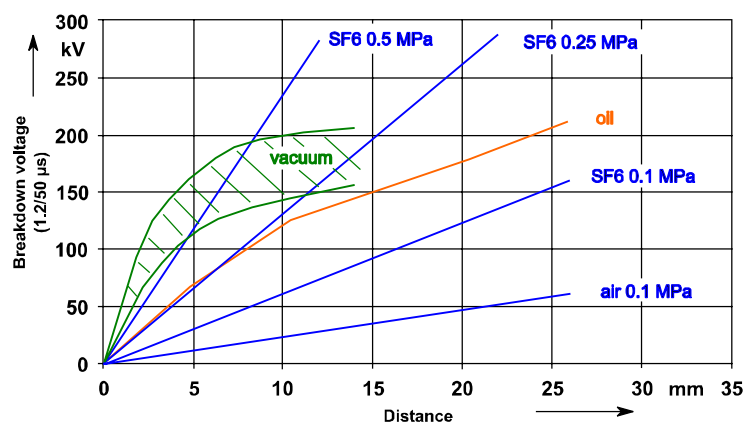


Figure 4.1. Breakdown voltage of various quenching mediums in function of distance between electrodes [3]

As shown in Figure 4.1, breakdown voltage of different quenching mediums (gases, vacuum and oil) in function of distance between electrodes is presented. Although oil was used in the past in power switches as quenching medium, and researches on insulation properties of oil were being performed widely [40, 41], application of oil in switches is being withdrawn due to ecological aspects and increased probability of explosion in comparison to other quenching mediums.

Although SF₆ gas has great properties for quenching the electric arc, it has been recognized as one of the potent greenhouse gases and was indicated to limit the emissions at COP3 at Kyoto in 1997 [134]. In the future, it seems to be necessary to reduce the consumption of SF₆, because its atmospheric life time is observed to be fairly long. Therefore, the amount of SF₆ on the earth will increase, unless amount of SF₆ will be limited. For this reason, many researches are being conducted to analyze possibilities of replacing SF₆ by CO₂. The quenching mediums that are applied in the electric power equipment as environmentally-benign should meet the following requirements: to have no or minimal toxicity, global warming effect, ozone depletion effect and should remain in gaseous form at low temperatures (e.g below -30⁰C). Thus, among all gases only some ones could be applied in electrical devices due to above-mentioned assumptions: air, N₂, O₂, H₂, CO₂, rare gases (He, Ar, etc.) and their mixtures. In practical implementation, adequate insulation and arc-quenching capability, chemical stability, being non-flammable and non-explosive are also required for the applied gas. For this reason, to find potential gas for replacement of SF₆, only air, N₂ and CO₂ could be taken into consideration. A comparison of basic gas properties of SF₆, CO₂, and N₂ is collected in Table 4.2.

Table 4.2. Comparison of basic gas properties of SF₆, CO₂, and N₂ [134]

Gas	Unit	SF ₆	CO ₂	N ₂
Molecular mass	[-]	146.06	44.01	28.01
Density	[kg/m ³]	5.9	1.8	1.1
Global Warming Potential, Integrated period 100 years (IPCC, 1995)	[-]	23900	1	≈ 0
Chemical stability	[-]	Stable	Stable	Stable
Boiling temperature*	[°C]	-51	-78	-198
Dielectric strength**	[%]	100 (-)	34 (-)	25 (+)
Arcing time constant***	[μs]	0.8	15	220

* – At 1 atm

** – 50% breakdown voltage measured by a full scale coaxial cylindrical electrode, Lightning Impulse at 0.9 MPa (the weak polarity vale is shown)

*** – Measured for a free-burning arc at 1 mm

As shown in Table 4.2, CO₂ meets the basic requirements in electrical devices and is environmentally-benign. Moreover, CO₂ is characterized by lower boiling temperature than SF₆. The insulation capability of CO₂ is lower than for SF₆, however, higher than for N₂. Arc-quenching capability is evaluated by arcing time constant as an index for the thermally interrupting capability of a gas. Smaller arcing time constant time suggests better thermal interrupting capability. As shown in Table 4.2, the arcing time constant of CO₂ is higher than for SF₆, but below one tenth of that of N₂.

Thus, it can be concluded that CO₂ is characterized by inferior parameters than SF₆ in insulation and arc-quenching capabilities, however it surpasses N₂ gas. This can suggest that CO₂ is a promising alternative for SF₆, especially for switching apparatuses such as Generator Circuit Breakers.

In vacuum quenching system, under-pressure is maintained $10^{-5} \div 10^{-7}$ Tr (max 10^{-4} Tr), where $1 \text{ Tr} \approx 133.322 \text{ Pa}$. The dielectric strength for these values of under-pressure is presented in Figure 4.1. In this range of the pressure, mean free path is a few meters, thus probability of initialization and maintaining the electric discharge through collisional ionization is very low. Under these conditions, electrons in the electric arc come from thermal emission and ionization of metal vapors in the cathode zone. Electrons that come to the anode are neutralized through positive ions that were created mainly in cathode zone and partially in the anode zone. Unionized metal vapors and particles of the gas that were created from the electrode surfaces settle on the outer shield of the vacuum chamber. Quenching the electric arc provides very high velocity of the diffusion of ions and metal vapors. When the current tends to its zero-crossing, pressure of metal vapors decreases. During intensive deionization, the current is chopped before its natural current zero-crossing. This phenomenon is a characteristic of vacuum switches and can lead to generate significant overvoltages in inductive circuits. The chopping current can be limited in vacuum switches through the application of special contact materials that are characterized by small thermal conductivity and the high pressure of evaporation.

4.1.2 Design of Contact System

The contacts of relays can be divided due to their function into the following way: normally closed contacts, normally open contacts, and change over contacts. Types of contacts in mechanical relays are presented in Figure 4.2.

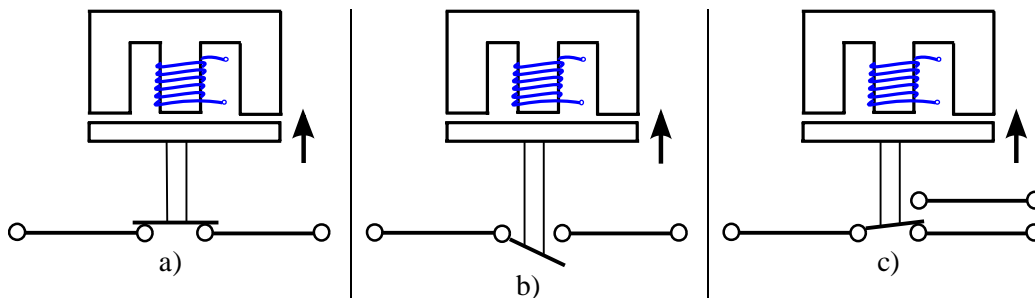


Figure 4.2. Types of contacts in mechanical relays: a) normally closed contacts, b) normally open contacts, c) change over contacts [62]

A contact system is the essential component of any relay. Usually it consists of several elements that are presented in Figure 4.3.

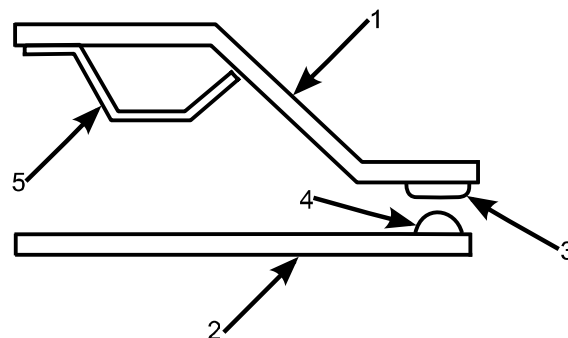


Figure 4.3. Popular types of relay contact systems. 1,2, — current-conducting elements; 3,4 — contact straps; 5 — stop [48]

In Miniature Circuit Breakers (MCBs) a special design of the arc quenching chamber (arc chutes) is being applied to increase the switching capability, which allows to divide the arc into a few smaller arcs [78, 134].

As shown in Figure 4.3, components that conduct the current are usually made of elastic materials (as a rule, bronze, beryllium or phosphor bronze), which are able to obtain the necessary contact pressure. Contact straps are designed by means of materials that are featured by high electric conductivity and resistance to arc erosion (see section 4.1.3). Contact straps are usually made in the form of rivets or pins, and they can be soldered, riveted, or welded on by silver solder to current-conducting springs. Riveted attachment of contact straps are more unreliable than welded attachment, due to the significant increase in transient resistance of a rivet at the point of its joint to the contact spring, caused by heat cycling in course of its maintenance. Contact straps are often bimetallic (two-layer) consist of the contact material (an alloy based on silver) and a copper base [48].

In order to enhance the switching capability of the relay, the contact system can be made in the form of a bridge as double-break contacts (Figure 4.4).

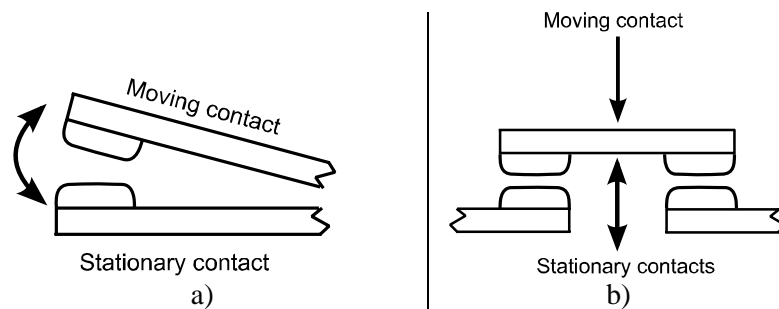


Figure 4.4. Types of contact systems: a) single-break contacts, b) double-break contacts,

As shown in Figure 4.4b, the bridge form of contacts provides better protection against contact welding than single break design. Double-break contacts open the circuit in two places, creating two air gaps. It is analogous to having two contacts in series.

In contrast to contacts fixed on long and flexible console springs, a bridge contact is quite complex. A bridge contact requires additional elements to provide: for compensation of shock during closing, for reliable compression of the movable contact into the stationary contact, as well as, for installation of the bridge in case there are technological variations of sizes, assembling inaccuracies and additional gaps emerging in the course of exploitation of the relay. All of these requirements are in fact met in the simplest constructions by application of a spring abutting from the central part of the bridge [48].

Optimal switching capabilities and easy assembly are features of cylindrical contact rivets that are usually applied as bimetallic, solid or other versions, similarly to the contact parts of miniature relays. The contacts are connected between the flat surface of the fixed contact and the spherical surface of the movable contact (the common contact). Mostly, fixed are bimetallic, and the common contact is a solid one, which is presented in Figure 4.5 [109].

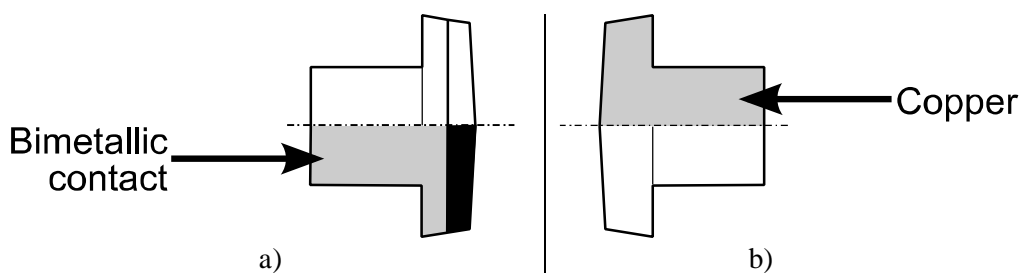


Figure 4.5. Shapes of contact rivets: a) bimetallic contact, b) solid contact [109]

The main part of the central solid contact is produced as a defined form on the one side, and on the other side it is shaped during assembly. The flat-spherical connection between the surfaces of contacts is designed for the limitation of the area of connection and provides an increase of the contact pressure. Moreover, this solution provides the relative surface movement (roll), which helps to achieve enhanced contact performance (Figure 4.6) [109].

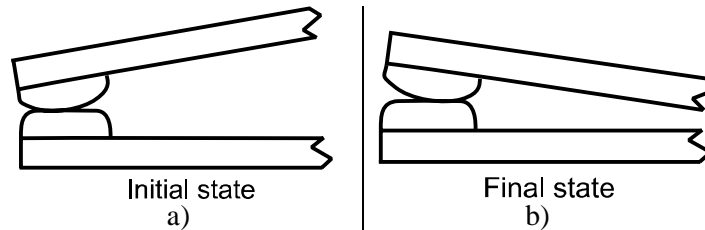


Figure 4.6. Contact movement [109]

Relay contacts can have different forms. The most widespread contacts are of a flat, conical, and semicircular form (Figure 4.7) and can be applied in the same contacting pair in different combinations.

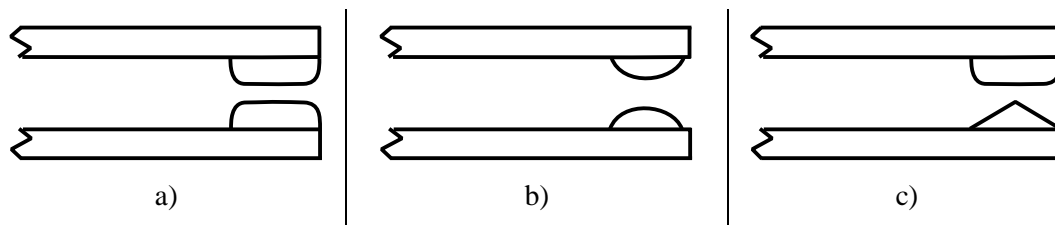


Figure 4.7. Forms of contacts of relays [48]

In order to limit arc erosion and to enhance switching capability of the contacts, the opening and closing velocity of the contacting pairs should be increased as much as possible. On the other hand, high velocity may lead to rebounds, collisions, vibration causing new arcs, and other damages of the contacts. Moreover, oscillations in the switched circuit resulting from contact vibration are undesirable [48].

4.1.3 Contact Pressure and Contact Material

When two contacts come together to close the electrical circuit, they touch each other within the area that depends on the shape of the contacts. The force (N) with which the contacts push against each other as measured on the contact axis, divided by the area of the contact (mm^2) equals the contact pressure (N/mm^2). It is practically impossible to determine the real contact area as it depends also on the roughness of the contact surface. The contact resistance depends on the roughness profile of the contact surface [74]. The contact pressure is determined by the contact force. In order to obtain a large contact area, the contact force must be increased so that the contact area roughness may be deformed. A low force means a few effective contact points and a small area of the contact (i.e. a high contact resistance). On the other hand, a stronger force increases the number of contact points and the total contact area (lower contact resistance). The contact force may be increased only to the limit defined by the mechanical strength of the parts and as much as it is allowed by the supply voltage sensitivity. Manufacturers of relays use different shapes of contacts according to the relay designs and applications.

According to Schaelchlin's theory [27], in place of current flowing from one conductor to another conductor, there is increase of resistance R_p . Value of resistance R_p is related to existence of many micro-contacts on surface between electrical contacts, as shown in Figure 4.8.

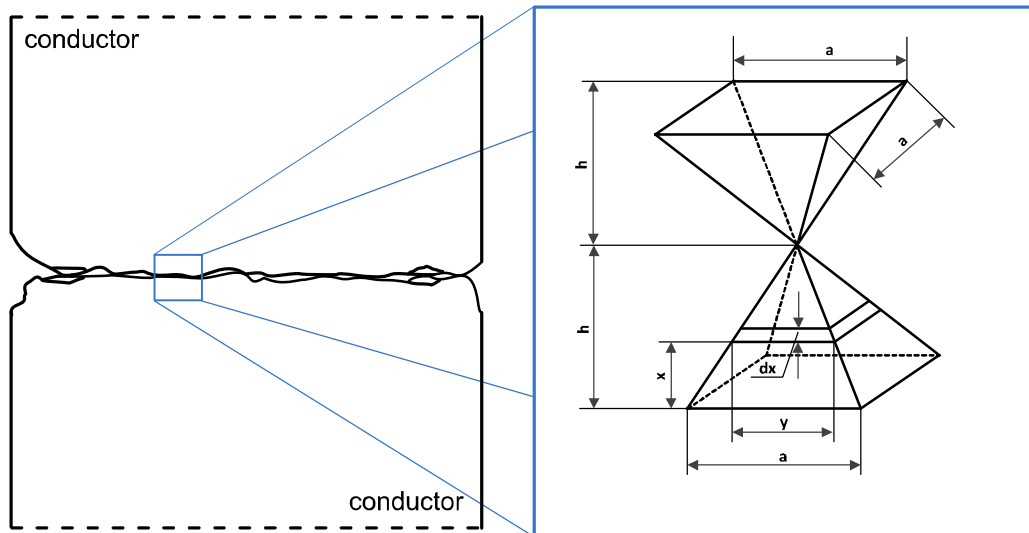


Figure 4.8. Model of micro-contact on surface between electrical contacts

Real surface of single electrical micro-contact (expressed as y in Figure 4.8) is related to contact force between electrical contacts and type of material contacts. Therefore, in practical calculations of contacts resistance, the following formula should be used in order to calculate resistance R_p [27, 62, 88]:

$$R_p = \frac{c \cdot \rho}{(0.15 \times F)^m} \quad (4.1)$$

where: c – coefficient depending on the contact surface condition [$\text{N} \cdot \text{m}/\text{m}$], ρ – resistivity of the contact material [$\Omega \cdot \text{m}^2/\text{m}$], F – force acting on the contact [N], m – coefficient depending on the contact type (surface contact: $m = 1$, linear contact: $m = 0.7$, point (spot) contact: $m = 0.5$).

Value of the product $c \cdot \rho$ can be taken from Table 4.3.

Table 4.3. Values of $c \cdot \rho$ products for different contacts material [88]

Contact material	Value of $c \cdot \rho$ product
	[$\text{m}\Omega \cdot \text{N}^m$]
Copper-Copper	0.08 – 0.23
Copper _{zinc plated} -Copper _{zinc plated}	0.10
Copper-Copper _{zinc plated}	0.07 – 0.10
Silver-Silver	0.06
Brass-Brass	0.67
Brass-Copper	0.38
Steel-Steel	7.60
Steel-Brass	3.04
Steel-Copper	3.10
Aluminum-Aluminum	3.00 – 6.70
Aluminum-Brass	1.90
Aluminum-Steel	4.40

As shown in Table 4.3, value of the product $c \cdot \rho$ is the lowest for contact consisting of two silver conductors. Silver (Ag) is a cheap material that is applied as contact material in electrical switches. Silver is featured by ductility, which helps to form it into various shapes of contacts. This material provides high electrical and thermal conductivity. Main disadvantage of silver is susceptibility to creation of arc erosion, and its low hardness. Silver

reacts easily with sulfur that can be present in air, which as a consequence leads to increase resistance of electric contact. For this reason, application of silver is not recommended in constructions that consist of black rubber, ebony, or wire insulated with rubber, producing sulfuretted hydrogen (hydrogen sulfide) when heated. Silver is used as contact material in devices that are designed at low and medium voltages to switch small and greater currents. In order to increase resistance of silver to erosion, some admixtures can be added, such as platinum, or platinum iridium alloy [48].

Other contact material that is used to design contact systems of power switches is tungsten. This material is featured by high hardness, fire resistance, wear resistance and welding. However, main disadvantage of tungsten is its tendency to form thick oxide surface that results in increased contact resistance. For this reason, application of tungsten as contact material requires application of high contact forces. Resistance of tungsten is relatively high, so this material is applied mainly to design auxiliary (arcing) contacts [48].

As it was mentioned before, alloys of silver with various chemical elements are applied to gain better parameters of contact materials. Silver-tungsten alloy (AgW) is a hard material that is featured by a high melting temperature and a resistance to contact welding. Main disadvantages of AgW is an increased resistance and its susceptibility for oxidation.

Alloy of silver–nickel (AgNi) is resistant on oxidation process and has good properties for arc quenching and resistivity similar to silver. However, this material has tendency for creation of sulfide surface films, and contact resistance of this alloy is greater in comparison to silver [48].

Silver-palladium (AgPd) possesses good contact welding and high corrosion resistance. Contacts made from this material are also resistant on sulfitation process. Disadvantage of AgPd is its tendency to form a polymeric surface film and to absorb organic gases [48].

Alloy of gold-silver (AuAg) stands out by low contact resistance, and its resistance to welding contacts. For this reason, this material is usually applied in measuring circuits with low voltages and currents.

Silver–cadmium oxide (AgCdO) is a ceramic-metal composition. This contact material is prone to welding, has good mechanical wear, and high resistance to influence of electric arc. Disadvantage of AgCdO is its relatively high resistance in comparison to pure silver, and its tendency to form sulfide surface films. This contact material is used to design contacts rated for average and high currents.

Silver–tin oxide (AgSnO) possesses good switching capability for devices that have high inrush currents (e. g. tungsten lamps), where the rated currents are low.

4.2 Performing the Contact Separation at the Defined Angle of the Current Period

On alternating current and at resistive load arc extinction occurs at the moment when the AC sinusoid passes through zero. If the contacts have separated at a distance where the electric strength of the gap between the contacts exceeds voltage restoring on contacts the switching process comes to the end (since repeated break-down of the gap is impossible). If not, another breakdown of the gap between the contacts will occur.

As it was mentioned in section 3, the basic requirement for normal circuit opening is excess of electric strength restoring during the switching process over restoring voltage. Restoring electric strength of a gap between contacts depends on the speed at which the contacts are separating, on the insulating environment of the gap between contacts (air, vacuum, sulfur-

hexafluoride SF₆, oil, etc.), and on the type of switching element (mechanical contact, semiconductor structure, etc.), with all of the above determined by the construction of switching equipment. Restoring voltage in circuit with resistive load equals the resistance of the power source.

Synchronous switching is a method that is being widely applied in AC power systems to avoid switching transient states [47, 54, 73]. There are existing commercially available constructions of synchronous circuit breakers [15, 16], as well as, devices to control high power switches [2, 120] which can be applied to this purpose. In general, controlled switching is being applied to suppress switching transients. In this way, inrush currents, switching overvoltages, and arcing times can be reduced significantly.

Researches on synchronous switching were performed in the past in LV circuits [18]. Application of synchronous switching is able to limit the electric arc energy and arcing time significantly. Basically, this method is based on performing contact separation in AC circuit at defined time just before the current zero-crossing. In this way, it is possible to achieve shortest arcing time which as a consequence also reduce the electric arc energy. Thus, application of synchronous switching leads to limit the arcing erosion.

In order to apply this method in LV circuit, it is necessary to develop the control system that will be able to control contacts of the operated switch. Basic idea of synchronous switching is presented in Figure 4.9.

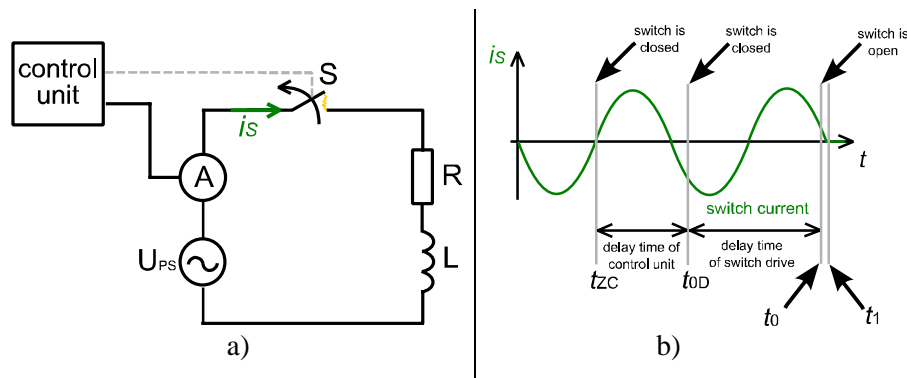


Figure 4.9. A simplified schematic diagram of the circuit (a); simplified waveforms of the current switch and the current of the switch drive during the current interruption (b)

Figure 4.9.b presents the simplified waveforms of the current flowing in the main circuit i_s during the current interruption. According to the description presented above, the control unit is able to separate contacts of the operated switch S just before the current zero-crossing. For this purpose, the control unit detects the current zero-crossing (at t_{zC}) and based on the known values of delay times (time between t_{zC} and t_0) is able to separate the contacts of the operated switch in the defined time. Time delay between t_{zC} and t_{0D} is related to self-delay of the control system, and time delay between t_{0D} and t_0 is related to a mechanical inertia of the operated switch. Because of both values of time delays may be known and repeatable in the operated switch (but only in the same, known environmental conditions), the time of the contact separation can be performed very precisely. For this reason, the contacts of the operated switch can be separated just before the current zero-crossing, which results in limiting the arcing time, as well as, the electric arc energy significantly.

4.3 Connection of the Suppressors in the Interrupted Circuit

In order to suppress switching transient states, passive RC components are being applied in electrical circuits [39, 85]. In general, the main goal of an application of RC snubbers is to

limit dU/dt steepness and values of overvoltages during transient states [53]. This aim can be realized mainly through creating a possibility for discharging an energy stored in inductive components of interrupted circuit. Passive RC components together with nonlinear voltage components are being also applied to protect semiconductor components against voltage transient state [1, 152].

In LV circuit with mechanical switches, passive components are being applied to increase the lifespan of the operated switch through limiting the electric arc energy. Basically, two types of passive components are being applied for this purpose in LV circuits: RC snubbers (comprising of connected in series resistor and inductor) and Voltage-Dependent Components (such as: Voltage-Dependent Resistors, Transient Voltage Suppressors, or Zener Voltage Limiters).

There are existing commercially available RC snubbers to increase lifespan of operated switch [4, 52, 80, 100]. The main role of the snubbers is to absorb the energy that is stored in the load. The most problematic case is interrupting inductive current, because the energy stored in the inductive component endeavors to maintain the current flowing in the circuit during current interruption. This phenomenon can lead to generate significant switching overvoltages that influence on the value of the electric arc. The electric arc erosion is dependent on the value of the electric arc, therefore to keep the contacts in good conditions for long time, it is necessary to limit the electric arc energy. Basically, there are two ways for connecting the RC snubbers as shown in Figure 4.10.

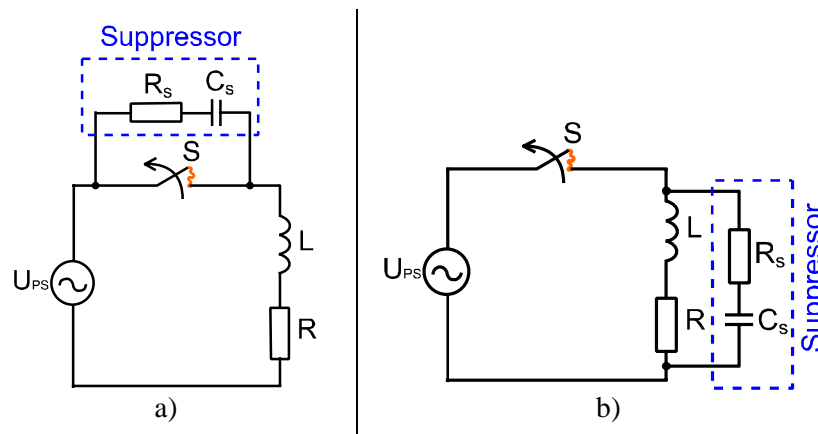


Figure 4.10. A placement of the RC snubber circuit: a) the suppressor connected in parallel to the operated switch, b) the suppressor connected in parallel to the load

As shown in Figure 4.10a, when the snubber is connected in parallel to the operated switch, the current may commute into the RC branch during current interruption and after then the current decays. Because of connection of the snubber in parallel to the operated switch, there is a leakage current that flows through the snubber, when the operated switch is open. To keep this current at acceptable level, a well-designed circuit is required. If the snubber is connected in parallel to the load according to Figure 4.10b, the leakage current appears only, when the operated switch is closed. In this case, the current caused by the transient voltage is not able to flow through the snubber into the voltage source, which leads to improve of the Electro-Magnetic Compatibility (EMC) of the entire circuit. Connecting the snubber in parallel to the load causes also results in keeping galvanic insulation of the operated switch. In considerations if the snubbers should be connected in parallel to the operated switch or to the load, the decisive factor can be the time, when the switch is open and closed. This criterion is important due to limitation of losses generated through the leakage current.

There is no universal formula to design parameters of the RC snubbers. Approaches for sizing parameters of the RC snubbers that can be found in applications notes [52, 80, 100] are based on different empirical equations. For example, according to [80], the value of resistor R_S should be calculated by means of the following formula:

$$R_S = \frac{k \cdot U_{peak}}{I_N} \quad (4.2)$$

where: k – experimental coefficient from range 0.5÷3 [-], U_{peak} – the AC peak voltage [V], I_N – rated current of the operated switch [A].

Lower value of the resistance R_S decreases the contact wear from arcing, while a higher R_S decreases the contact wear from the capacitive inrush current.

Also according to [80], it is recommended to select the value of the capacitor C_S experimentally, starting from 100 nF. According to further recommendations, effectiveness of snubber should be evaluated in course of calculations, simulations or even with usage of the oscilloscope.

Another approach that being used for limiting the electric arc through an application of passive components is connection of Voltage-Dependent Components (such as: Voltage-Dependent Resistors, Transient Voltage Suppressors, or Zener Voltage Limiters) in parallel to the operated switch or in parallel to the load, as shown in Figure 4.11.

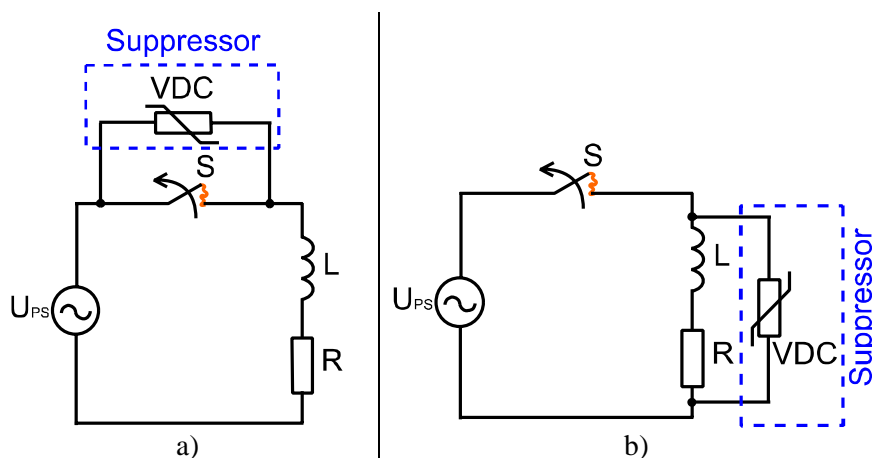


Figure 4.11. A placement of the Voltage-Dependent Components in the circuit

Basically, Voltage-Dependent Components (VDC) conduct the current, when their threshold voltage is exceeded. This feature can be used to limit the electric arc energy, similarly to application of the RC snubber. In fact, VDCs limit the switching overvoltage that is generated above the peak voltage of the interrupting circuit. This helps to discharge the energy stored in load moreover, it could be helpful to limit the electric arc, which as a consequence can lead to limit the electric arc energy.

As shown in Figure 4.11, the connection of nonlinear voltage components in parallel to the operated switch provides a possibility for the current commutation into the snubber branch, if the arcing voltage during the current interruption exceeds the minimal operating voltage of the nonlinear component. Transient voltage waveforms (visible from terminals of the nonlinear voltage components) during current interruption are presented in Figure 4.12.

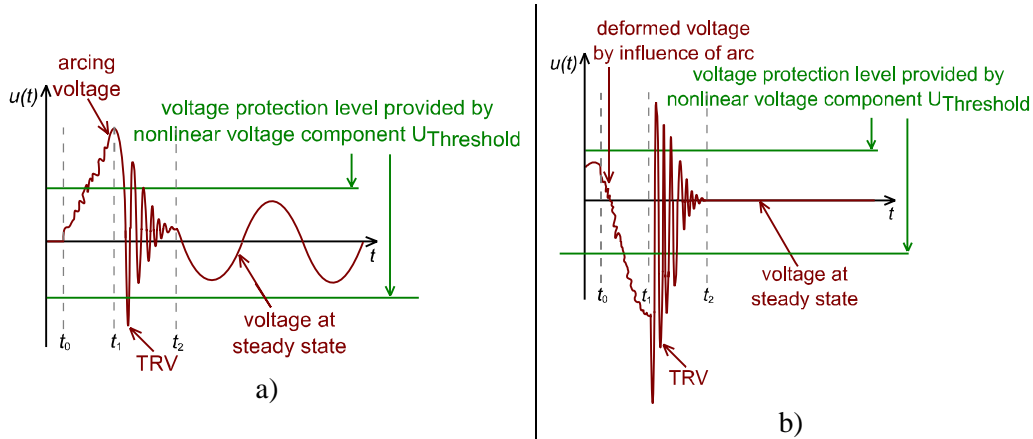


Figure 4.12. Transient voltage waveforms during current interruption:
a) Voltage-Dependent Component is connected in parallel to the operated switch,
b) Voltage-Dependent Component is connected in parallel to the load

As shown in Figure 4.12, the minimal operating voltage $U_{Threshold}$ of the applied nonlinear voltage component cannot be lower than the peak voltage of the supply voltage U_{PS} in the circuit (Figure 4.11). This requirement has to be met, because after opening the operated switch, when the TRV disappears, the entire voltage of the power supply U_{PS} appears across the open contacts of the operated switch S . If the value of the supply voltage U_{PS} could be greater than the minimal voltage of the applied nonlinear voltage component $U_{Threshold}$, then the component VDC starts to conduct, whereby the current starts to flow through the nonlinear voltage component VDC all the time after opening the operated switch S . This situation can lead to a thermal damage of the nonlinear voltage component. For this reason, it is especially important, to select the nonlinear voltage component with its minimal operating voltage $U_{Threshold}$ greater than the voltage peak of supply voltage at the steady state U_{PS} . However, on the other hand, the difference between the voltage peak of the supply voltage at the steady state U_{PS} and the minimal operating voltage $U_{Threshold}$ of the nonlinear voltage component should be as small as possible, because in this case, it is possible to provide the most effective limitation of the electric arc – the sooner nonlinear voltage component starts to conduct, the more electric arc energy could be limited.

In order to determine the influence of the considered suppressor on effectiveness of the electric arc limitation, the electric power generated at external suppressor can be calculated according to formula (4.3):

$$p_B = u_s \times i_B \quad (4.3)$$

where: u_s – voltage measured across the switch [V]; i_B – current of the parallel branch [A].

Electric energy dissipated at the parallel branch can be calculated as a definite integral according to equation (4.4):

$$E_B = \int_{t_0}^{t_1} (u_s \times i_B) dt \quad (4.4)$$

where: u_a – electric arcing voltage [V]; i_a – arc current [A], t_0 – time, when electric arc starts to burn [s], t_1 – time, when electric arc is quenched [s].

In the next part of the thesis, formulas (4.3) and (4.4) were used to determine the capability for limiting the electric arc energy by considered arc suppressors.

4.4 Hybrid Switching

The application of power semiconductors in switches can help to achieve considerable improvement in its performance and possible new capabilities. The connection of mechanical switch with semiconductor components is called as a hybrid switch. In general, semiconductor components combined with mechanical switches are being applied in hybrid solutions for various reasons:

- to reduce electric arc energy and the arc erosion of the contacts, which leads to increase of the lifespan of the switch,
- to suppress switching transients,
- to implement an additional functionality of the switch, such as soft-starter,
- to increase switching capability of the mechanical switch,
- to limit short-circuit currents,
- as a solid-state transfer switch for power-quality (PQ) improvement.

Various types of semiconductors that find the application in typical power electronic devices [104, 105], such as: transistors (mainly: bipolar, unipolar, Insulated Gate Bipolar Transistor), thyristors (mainly: Silicon-Controlled Rectifier SCR, Gate Turn-Off thyristor GTO, Triode for Alternating Current TRIAC) can also be applied in hybrid constructions of switches. The type of the selected semiconductor component that should be applied in the hybrid module depends on the application of the hybrid switch and its functionality. The selected topologies of various hybrid switches with different semiconductor components are presented in this section.

The most common connection of semiconductor components with mechanical switch is presented in Figure 4.13. This kind of combination can be used to interrupt operating currents, as well as, short-circuit currents.

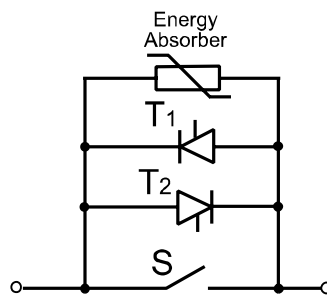


Figure 4.13. AC HCB configuration using thyristors [119]

The topology from Figure 4.13 was presented in the work [119] as a solution to interrupt the short circuit currents. The operating current flows during the steady state through the Miniature Circuit Breaker (MCB) that is presented in Figure 4.13 as the switch S . When a fault occurs, the switch S opens, which causes ignition of the electric arc which forces the current commutation to one of the now turned-on thyristors (depending on the direction of the current). The current can be interrupted by the semiconductor component at the first zero-crossing, and the stored circuit energy can be dissipated at least partially by means of an energy-absorbing device connected in parallel to the operated switch S . This topology can be dedicated also for low frequency currents interruption generated by a wind generator [67]. However, thyristors are characterized by high-power rating but their turned off cannot be controlled, which limits their application in short-circuit applications. For this reason, another construction of the hybrid circuit breaker with GTO components that is based on the topology presented in Figure 4.13 is illustrated in Figure 4.14.

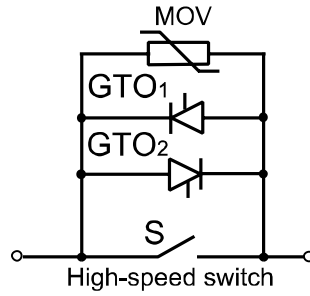


Figure 4.14. GTO-based AC HCB configuration [67]

HCB illustrated in Figure 4.14 was presented in [45, 75], where GTOs, whose turning on and off can be controlled, were used as semiconductor components. The mechanical switch used in this application was a high-speed Vacuum Circuit Breaker (VCB), where an electromagnetic repulsion force was used to open the circuit at high speeds. This helps to limit the short circuit current through GTO components. As soon as a fault is detected, contacts of the VCB open, which results in ignition of the electric arc between contacts of the VCB. The electric arc acts as a counter electromotive force for commutation of the fault current into the GTO components. The overvoltage protection device used in this configuration is a Metal-Oxide Varistor (MOV).

The combination of microelectromechanical switches was presented in [63], its topology is shown in Figure 4.15.

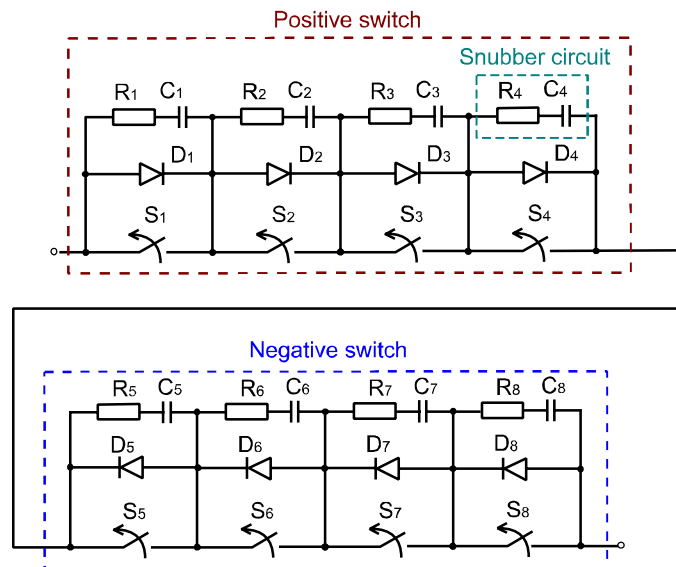


Figure 4.15. AC HCB circuit using microelectromechanical switches [63]

As shown in Figure 4.15, the proposed construction of the hybrid switch consists of a few modules including a diode and a microswitch that are connected in series as a form of a switching string. The proposed HCB is based on the series connection of two such strings (positive and negative switches). For this reason, one string is able to interrupt the positive current and the other string can interrupt the negative current. Suitable voltage rating of the switch can be achieved by the series connection of appropriate number of switching units. Similarly, the current rating of the switch can be increased by the parallel connection of appropriate number of strings. The snubbers connected in parallel to each module are used for ensuring the uniform voltage distribution. The current flows through the microswitches during steady state. When the fault occurs, microswitches open in positive or in negative strings depending on the current polarity. For this reason, the current is able to commute into the diodes. The diodes are able to interrupt the current during its zero-crossing, which

causes the current to interrupt before the end of the first-half cycle. This solution provides small-size and arc-less current interruption.

The conductive polymers are characterized by abilities for limiting current and can be applied in a combination with an MCB to fault current limiting and interrupting [50]. A Positive Temperature Coefficient (PTC) thermistor, composed of conductive polymer material, can be used to limit the current. The temperature of the thermistor increases with the current rise, which leads to an increase of its resistance. The exemplary constructions of HCB including the PTC component is presented in Figure 4.16.

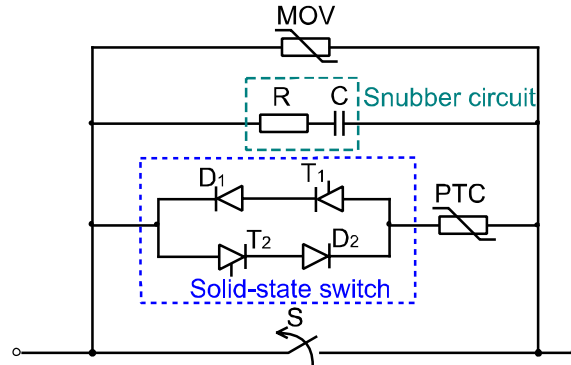


Figure 4.16. Current-limiting HCB using the PTC thermistor [26]

As shown in Figure 4.16, a PTC thermistor was used to limit the current through the semiconductor element in an HCB circuit, which was described in [26]. The switch S represent an MCB was applied to conducting the current in the main path. After receiving a triggering signal, the contacts of the switch S start to separate, which causes ignition of the electric arc which forces the current commutation into the parallel branch. The resistance of the thermistor has to be below the limits for the given current at the time of the contacts separation. This is required to perform the smooth current commutation from the mechanical contacts into the semiconductor component. The current flowing through the thermistor continues to increase after the end of the commutation, thereby the resistance of the thermistor proportionally increases, which leads as a consequence to the limitation of the current. The snubber circuit marked in Figure 4.16 is also applied for limiting the transient voltage during turn-off of the semiconductor element. This topology of the HCB allows to avoid the need of the ultra-high-speed fault detection to limit the current in comparison to the HCB topology presented in Figure 4.14.

Another topology of the current-limiting HCB was shown in Figure 4.17 [149], where a high-speed mechanical switch was applied to conduct the current under normal conditions.

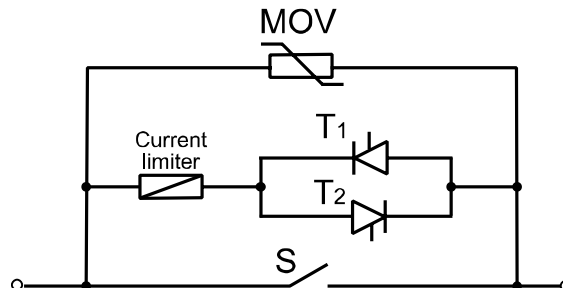


Figure 4.17. A current-limiting HCB [149]

When the short-circuit current is detected, the contacts of the switch S open by means of the electromagnetic repulsion force at a very fast rate, so as a consequence the fault current does not exceed the switching capacity of the circuit breaker current. At the same instant, one of the thyristors T_1 or T_2 is turned-on. The ignition of the electric arc across the contacts of the

switch S forces the commutation of the short-circuit current into thyristor T_1 or T_2 . At this state, the short-circuit current can be limited through the element connected in series with the thyristor that is able to limit the current. After a some delay that is needed to completely open the switch S , the gate signals of thyristors are removed. Thus, the limited short-circuit current is interrupted at the next natural current zero-crossing within only one cycle after the short-circuit occurrence. Similarly to the topologies presented in Figure 4.13, Figure 4.14, Figure 4.16 and Figure 4.16, the MOV component is connected in parallel to ensure the protection of these switches against overvoltages. The current limiter can be based on e.g.: a current-limiting reactor, a saturable reactor, the current-limiting fuses, or a current-limiting resistor. It is obvious that the operating principles of this HCB are similar to those presented in Figure 4.16. However, in this topology, the short-circuit current can achieve high level before the end of the current commutation from the switch S . This could take place due to the application of the current limiter in the semiconductor branch.

An HCB topology that is based on the counter-current injection was proposed in [35]. The schematic of the proposed HCB to limit the current in low voltage AC system is shown in Figure 4.18.

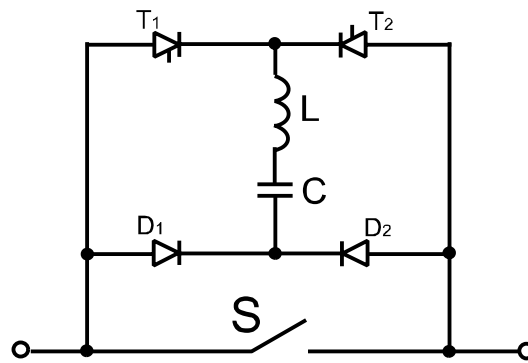


Figure 4.18. A current-limiting HCB using counter-current injection [35]

As shown in Figure 4.18, the switch S represents an MCB that conducts the current under normal conditions. The contacts of the MCB can be opened very fast through the application of an electrodynamic drive. The inductor L and the capacitor C are the passive elements that have selected appropriate sizes for the dedicated application. The capacitor C was applied to pre-charge up to an appropriate voltage level. In order to limit and interrupt the current, thyristor T_1 or T_2 is gated-on firstly (depending on the current polarity at the time of the start of HCB operation). Pre-charged capacitor C provides a counter-current in the opposite direction to the main current and flowing through the switch S in the closed loop of the circuit $T_1(T_2) - L - C - D_2(D_1) - S$. This approach causes the current flowing through the switch S to reduce, since the switch S opens at a fast rate with the limited electric arc. At the next stage, the current commutates into the semiconductor elements that are already turned-on with L and C in the closed loop, according to the above-mention description. The commutation time may depend on the impedances of the two parallel paths and the initial conditions. The current can be finally interrupted in the same way by means of a surge arrester connected in parallel to the switch S , as it is described above with reference to Figure 4.16.

5 Arc Erosion in LV switches

According to the description presented in the chapter 4, in mechanical switches that are being widely applied in electrical circuits, the electric contacts are essential component of any relay. The functions that have to be being realized by each switch can be distinguished as the following way: conducting the current, making the current, and interrupting the current. Proper operation of the entire switch depends mainly on the condition of its electrical contacts. For this reason, it is very important to maintain the electrical contacts in good condition for entire lifespan of the switch.

When the switch is open, its contacts are separated, and for this reason, the current flow in the circuit is not possible. In this state, the voltage source appears between the open contacts of the switch. During making the current, the contacts of the switch close quickly (to avoid many pre-strikes), which can cause the contacts to bounce. If the voltage source is strong high, then the electric arc starts to ignite before touching the contacts, which leads to make the current in the circuit. In this case, the current starts to flow in the circuit before the mechanical touching the contacts. At time, when the contacts start to touch each other, bouncing the contacts can be noticeable. This phenomenon leads to lose the contacts and to ignite of the electric arc. Bouncing of contacts can be caused by the mechanical reflections of contacts, as well as, by electrodynamic forces that are created from making current. For making short-circuit currents, the high energy dissipated in the electric arc during bouncing the contacts can lead to welding contacts as an effect of melting the contact material. This can lead as a consequence to permanent damage of the switch that will not be able to open. If the electric arc energy of making current is negligible, then welding contacts do not occur, however, faster wear of the contacts can be observed. In this case, an excessive evaporation and a spattering contact material on contact surfaces can be noticeable during making current.

When the switch is closed, and the current flows through its contacts, a thermal influence of the current can lead to the damage of contacts. This can be observed, when the current flowing by the contacts significantly exceeds the rated current of the switch, especially under short-circuit conditions. Thus, it is also possible to weld the contacts, when the switch is closed. This may lead to damage of the switch that could not be able to open. Flowing short-circuit current through the switch can also damage the switch due to an influence of the electrodynamic forces.

When the switch interrupts the current, its contacts start to separate, which causes to lose the metallic connection between its contacts, and to ignite the electric arc. In order to quench the electric arc effectively at the next natural current zero-crossing, voltage withstand of the contact gap has to be higher than the value of Transient Recovery Voltage. When the electric arc burns between the contacts of the switch, a considerable amount of the heat is dissipated in the gap between the contacts. This temperature rise leads to create the arc erosion and can influence negatively on entire contact system of the switch. For this reason, it is especially important to reduce the arcing time, as well as, the electric arc energy.

Thus, the contacts of the switch can be damaged in any condition of working the switch: during making, conducting or interrupting the current. However, during switching operating currents, phenomena that are related to quenching the electric arc created from interrupting current play a key role in a creation of damages of contact surface. For this reason, the electric arc erosion created from interrupting current is the subject of this thesis dissertation. A detailed mechanism of a formation of the electric arc erosion, and criteria for its evaluation are described in this chapter.

5.1 Arc Erosion as a Threat to the Normal Operation of the Switch

One of the serious problems during burning the electric arc between the electrodes is a transfer of some amount of the contact material from one contact to another contact, which as a consequence leads to a reduction of the surface of one the contacts. Thus, the transfer of the contact material decreases the lifespan of entire switch. This phenomenon is especially observed in DC switches, where the anode and cathode are constantly oriented due to the polarity of the voltage supply. A good example can be an exploitation of car relays in installations rated at 12 V, where the electric arc does not occur, and the mechanism of transferring the material is related to a formation of a liquid metal bridge. Transferring the material can lead to create bulges and craters on the contact surfaces, which is presented in Figure 5.1.

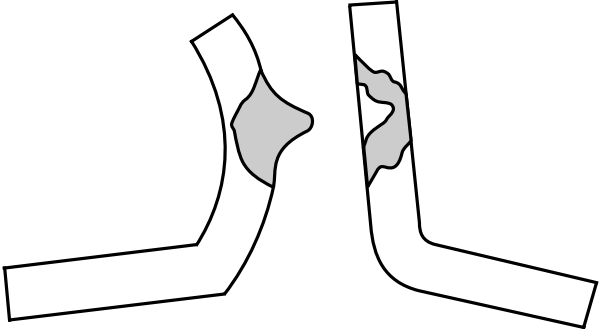


Figure 5.1. *Bulges and craters on contacts caused by electric spark [48]*

Also in AC switches the transfer of the contact material is noticeable. However, in this case, mainly bidirectional transferring of the material can be observed (from the cathode to the anode and vice versa). Material properties of the contact material play a key role in the process of the electric arc creation (especially thermal properties of the contact material and its viscosity, the condition of contact surfaces, etc.). If contacts of the switch were made from different materials, then differences in material properties of both materials could be a reason for unidirectional transferring the contact material. The disproportionate dependence of the arc erosion and transferring the material is caused by an uneven heating of the anode and the cathode.

When the switch interrupts the current without the electric arc ignition, the bridge erosion of the electrical contacts can be observed. A process of the creation of the bridge erosion is presented as a simplified way in Figure 5.2 (the main assumption is that contact surfaces are ideally smooth and clean).

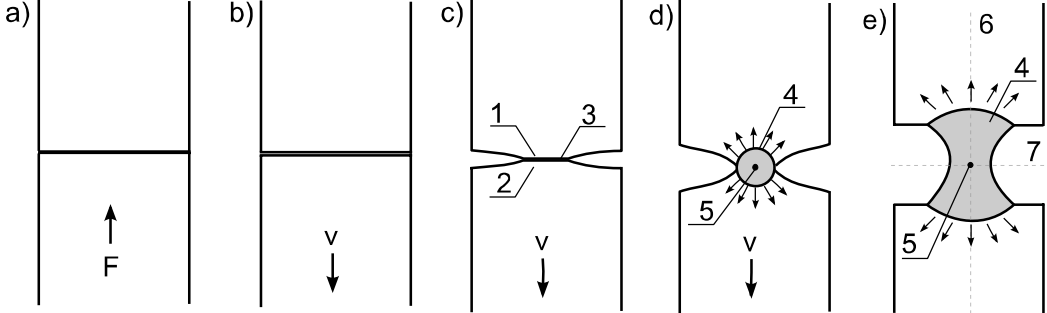


Figure 5.2. *A process of the creation of the bridge erosion [24]: 1, 2 – inequalities that create the bridge, 3 – real contact surface, 4 – melting zone, 5 – temperature hot spot, 6 – axis of symmetry, 7 – surface of symmetry*

As shown in Figure 5.2, when the distance between the contacts starts to increase, the length of the bridge also increases. At the last stage, the bridge is still maintained by forces that come

from wetting the material, and its diameter decreases in the middle zone. A thermal decay of the bridge takes a place, when the temperature in the place where the diameter of the bridge is the smallest reaches the value, at which an internal pressure balances the electrodynamic pressure. The molten metal boils as the overheated liquid in the volume limited by contact surfaces and the side surface of the bridge, and as a consequence evaporates. The discharge process begins when the bridge decays. Independently of the type of the bridge decay, the contact material is removed through the volumetric evaporation. As a result of the bridge decay, contact material evaporates from both contact surfaces in a form of sphere. The volume of the evaporated material can be estimated according to the following formula [24]:

$$V_e = \frac{P \times h_e^2}{3} \times (3 \times R_{WP} - h_e) \quad (5.1)$$

where: h_e – the height of the sphere [m], R_{WP} – the radius of the isotherm with the temperature T_{WP} [m].

According to PSD (Particle Sputtering and Deposition) model [31], during the current interruption with the ignited electric arc, two phases can be distinguished: the metallic phase and the gaseous phase. The process of creating and interrupting the electric arc for small currents is presented in Figure 5.3.

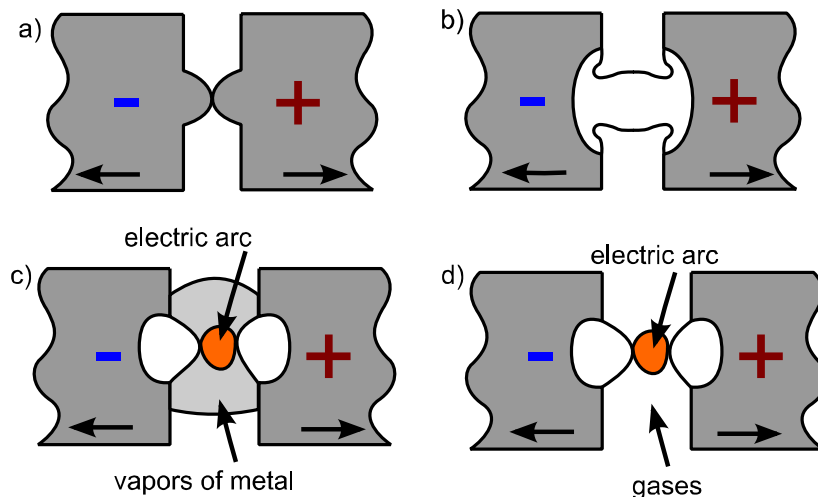


Figure 5.3. Preceding stages of the electric arc creation [24, 31]

According to the description presented in the chapter 3, when contacts of the switch start to separate, the number of contact points on surfaces of contacts decreases rapidly (Figure 5.3a). The current that flows through contact points causes the surface of contacts to heat intensively. This process is caused by an increased resistance of the contacts, and leads as a consequence to melt the contact material. At the next stage, when the distance between contacts increases, a liquid metallic bridge is created between contacts (Figure 5.3b). Together with lengthening the distance between the contacts, the diameter of the bridge decreases. The bridge maintains up to the time, when the temperature rise reaches the boiling point of the contact material. At this time, the bridge is broken off due to an explosion of the melting material. This causes the area between the contacts to fill by vapors of the metal. At this time, the distance between contacts is very small, which influences on significant value of the electric field that can exceed even 10^7 V/cm [24]. Under these conditions, the hot tip of the cathode is a source of thermal and field emission of electrons. As a result of this process, the channel of the electric arc is created. Electrons that are emitted from the tip of cathode are accelerated through the electric field and moved in the direction of the anode. Inelastic collisions during the movement of electrons from the cathode to the anode cause the ionization of the metal vapors. As a consequence, the electron avalanche is created (the number of charged particles rapidly

increases) that moves in direction of the anode. The discharge process begins when the liquid metallic bridge decays (Figure 5.3c). Increasing further the distance between the contacts causes an increase of the importance of the gas ionization that begins to play a main role and causes the phase of the electric arc to change from the metallic phase into the gaseous phase (Figure 5.3d). Increasing further the distance between the contacts helps to create convenient conditions to quench the electric arc.

In LV switches, a length of the electric arc usually does not exceed a few centimeters. For this reason, this type of electric arc is commonly called as the short electric arc. The length of the electric arc is one of the most important factors that influences a creation of the electric arc erosion. A simplified structure of the short electric arc with its characterized zones marked (the electric arc column, cathode and anode zones) is presented in Figure 5.4.

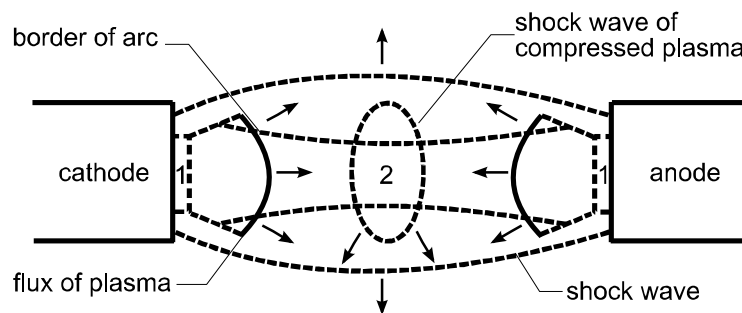


Figure 5.4. A simplified structure of the short electric arc, where:
 1 – cathode and anode zones, 2 – the electric arc column [24]

An illustration of how mass change can occur in arcing contacts is presented in Figure 5.5.

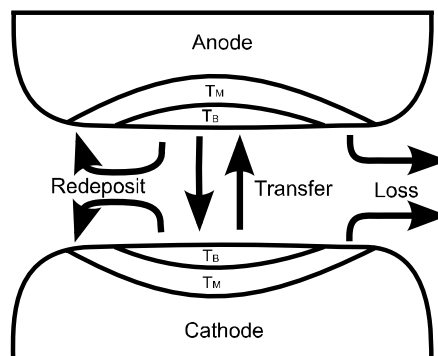


Figure 5.5. An illustration of how mass change can occur in arcing contacts
 (T_m – molten zone, T_b – boiling zone) [24]

The PSD model is being used to explain the process of transferring the contact materials between the cathode and the anode in the metallic phase and in the gaseous phase of the electric discharge.

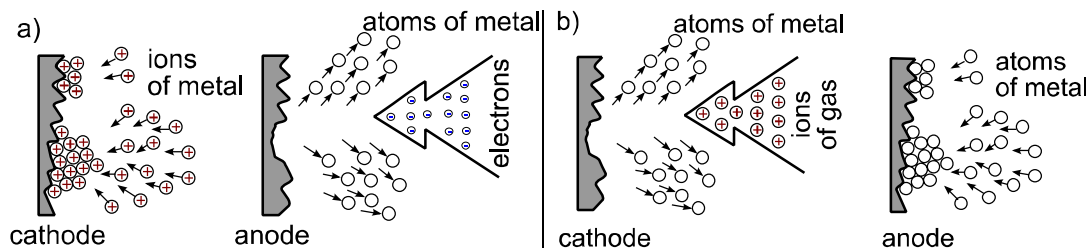


Figure 5.6. Transferring the contact material according to the PSD model [24, 31]:
 a) the metallic phase, b) the gaseous phase

The mechanism of the erosion and transferring the contact material is different in both phases and depends on the emission of ions in the metallic phase and in the gaseous phase. In the

metallic phase, the electric arc ignites in vapors of the metal, and the main moving particles are: electrons coming from the cathode, metallic ions, and metallic atoms. Electrons get the energy in the electric field and move from the cathode to the anode. Metallic ions and electrons are accelerated by the electric field, and reach to the cathode and the anode separately. At the next stage, metallic ions settle on the cathode, and the electrons hit in the anode. During this phase, the direction of transferring the contact material is from the anode to the cathode. In the gaseous phase, the dominant particles are ions, atoms coming from the quenching medium, and metallic atoms from the contact material. When ions hit the cathode, the dispersion of particles takes a place. The particles have the sufficient energy to move from the anode, and can settle on the anode. In this phase, the contact material is being transferred from the cathode into the anode. Both phases are shown can be also observed the voltage waveforms, which is shown in Figure 5.7.

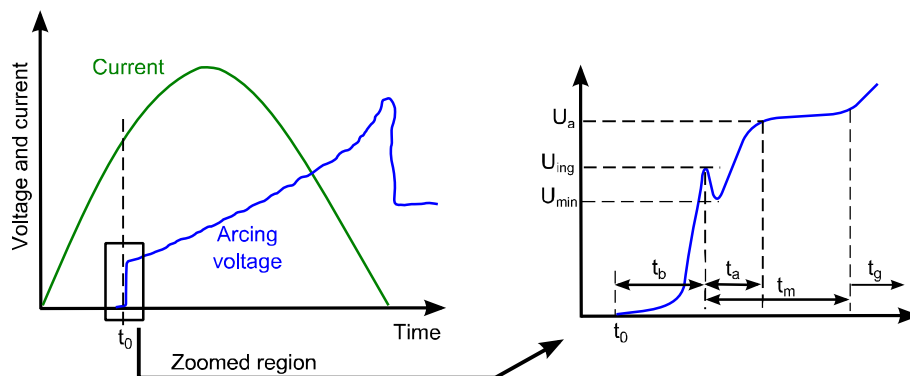


Figure 5.7. A sketch illustrating the various stages of arc formation in contact separation with current flow (t_b – bridge time, t_a – anodic phase, t_m – metallic phase, t_g – gaseous phase) [117]

The times of the phases depend on many factors, such as material properties of the contact material, switching conditions, parameters of the quenching medium, which is presented in Figure 5.8.

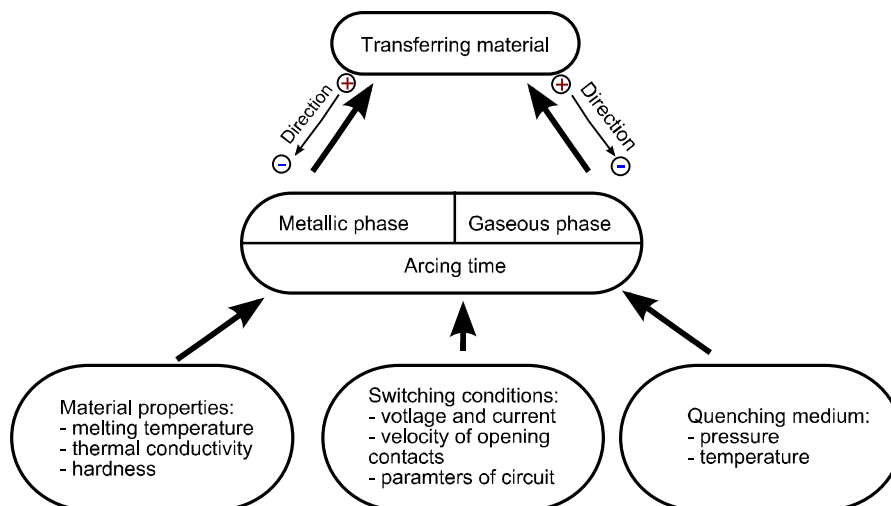


Figure 5.8. An influence of various factors on transferring material in both phases [24, 31]

In principle, a creation of the electric arc erosion in switches is a very complex issue and depends on many factors, such as: parameters of the electric arc, parameters of the quenching system, the design of contacts, switching conditions. Graphic presentation of parameters and factors that influence on creation of the electric arc erosion in switches is presented in Figure 5.9.

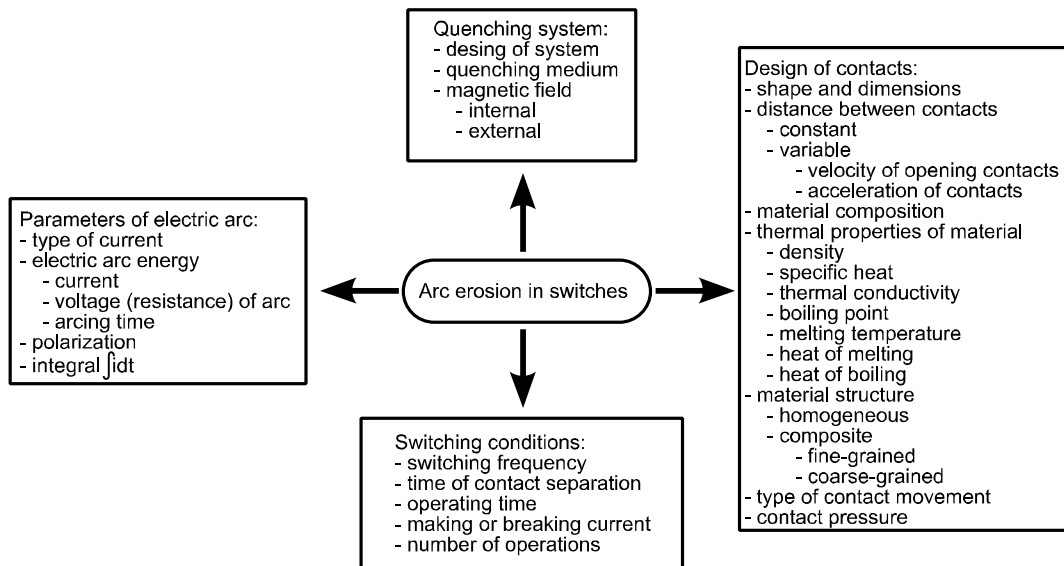


Figure 5.9. *Graphic presentation of parameters and factors that influence on creation of the electric arc erosion in switches [117]*

Thus, as shown in Figure 5.9, researches on the electric arc erosion can be performed in many fields. Selected works related to the electric arc erosion are briefly described below.

An extensive study on the arc erosion is presented in works [24, 25]. The influence of parameters of electric arc, the quenching system, switching conditions, and the design of contacts (according to Figure 5.9) were studied in these works.

Investigations into welding and melting contacts are presented in [71, 135, 137]. The results of investigations of welding behavior of silver and some silver-based composite materials are discussed in [137]. Melting phenomena and arc ignition of breaking relay contacts were described by authors in [135] (breaking contact voltage and current of conventional electromagnetic relays with Ag contacts were measured for two hinge springs, for 12.5-50 V energizing power-supply voltage and for 0.1-20 A contact current). The dependencies of the phenomena on energizing current and residual inductance were confirmed for different contact materials (Ag, Au, Ir, Pd, Pt, Zn) are presented in [71].

Researches on the electric arc erosion created from the electric arc ignited in vacuum are presented in [84, 92]. The objective of article [84] is to investigate the anode erosion pattern caused by the blowing effect in constricted vacuum arcs under an Axial Magnetic Field (AMF). Article [92] presents observations of cross sections of the arc canyon erosion trace and reveals erosion craters covered with a porous columnar film having a diamond structure. Scanning Electron Microscope (SEM) images of this growth structure are presented in this work.

Mathematical approaches that try to describe accompanying phenomena of the arc erosion are presented in [24, 151]. Heat transfer and fluid dynamics in the molten pool in silver contacts are coupled with the gas dynamics in the vicinity of arc spot to determine the evaporation rate due to static arc and they are presented in [151].

Measurements of the electric arc erosion created from switching high currents are presented in the following articles: [59, 77, 94, 99, 106, 117, 141]. Results of experiments which were designed to investigate various aspects of the electrode erosion produced by high current moving arc discharges are presented in [77] together with a simple model for electrode erosion. Two modes of contact material erosion: vaporization and splash erosion are presented in [106]. This model can be used to measure the amount of contact material removed after

one electrical discharge. An experimental study of high current arc erosion on copper electrodes in air is presented in [99], with an evaluation of fraction lost by gross melting and vaporization. The paper [141] presents the problem of using extensive experimental results on the erosion behavior of the high current contacts and various contact materials for computer aided designing CAD of low voltage switching devices and for computer modelling switching phenomena in these devices. The purpose of study [94] was to develop scaling relations for material erosion with respect to electrical current for aluminum and titanium. In the article [59], the researches and the analyses of the conditions of the anode spot formation are shown. The heating processes were examined in the case of constant and variable heat flux transmitted to anode, and the analyses are based on the photographic studies of the arc. In the paper [117], contact break arc erosion fundamentals applicable to high power switching devices in air (e.g. air magnetic circuit breakers and contactors) are reviewed along with recent results showing dominant factors that affect contact erosion in the range of 3kAp to 22kAp.

Researches on the influence of contact materials on the creation of the electric arc erosion are presented in the following works: [28, 64, 82, 107, 140, 150]. Experimental study of Ag-W-Re composite materials under high-current conditions is presented in the work [140] (the results of testing the properties of the new contact material silver-tungsten-rhenium under high current conditions are presented, arc erosion, contact resistance, and statical welding characteristics have been investigated). An experimental study of the dependence on the current intensity of the erosion of thoriated tungsten cathodes in plasma arcs is presented in [28] (the erosion occurring in thoriated tungsten cathodes used in transferred plasma torches operating with current intensities ranging from 30-210 A has been experimentally investigated). The objective of [150] is to investigate vacuum arc erosion characteristics of a nanocrystalline CuCr (Cr 50 wt%) contact material. Influence of Contact Materials on Phenomena in a Short Electrical Arc is presented in work [64] (special experiments with two contacts materials, AgCdO and AgSnO₂ have been carried to verify the mathematical model). The arc erosion behavior of Cu-15%Nb and Cu-15Cr composites was studied for both low-energy make-and-break contact and a high-energy stationary arcing gap configuration is presented in [82]. Experiments and modeling towards the design of an AgCdO substitute of electrical contact arc erosion is presented in [107].

Electric-arc erosion of deion plates of arc suppressors of automatic circuit breakers during at switch-off of extreme commutation currents is investigated. The proposed technique is used to evaluate the effect of electrodynamic forces of the electric switch-off arc in the limiting short-circuit regimes and is presented in [89].

Issues related to an analysis of the reliability of the switch were discussed in literature [32, 146-148]. Multi-parameter simulating model for forecasting with current production the durability of contacts of electromagnetic contactors was presented and described in [146-148]. Paper [32] presented proposed methods for examining the status of the vacuum in vacuum circuit breaker by measuring the chopping current. This phenomenon was studied in a chamber with a pressure control where chopped AC and DC currents were measured, and the results give rise to a continuation of its practical application.

5.2 Arc Erosion in Hybrid Switches

In the past, researches on limitation of the electric arc erosion were being conducted. Selected studies are listed and described briefly in this section.

A low-current (5 A_{RMS}) push-button hybrid switch was presented in work [69]. The switch is rated at 120 V, and its hybrid module is based on a silicon-controlled rectifier (SCR) within a diode bridge that was applied for AC operation. A bipolar transistor, along with resistors

and capacitors, was used to obtain zero-voltage turn on of the SCR (i.e. lower than 20 V) for both resistive and inductive loads. Life tests (1 000 000 operations in total) were performed using a 120 V 5 A resistive load for closing and opening. Application of the hybrid module influences on condition of contact switch, which is observed as a significant reduction of contact damage.

Basic investigations of the commutation and switching mechanisms between contacts and parallel thyristors and on results of erosion measurements at currents up to 500 A, 220 V, 50 Hz are presented in [46]. Authors presented measurement of commutation parameters for different contact material and photographs of the fixed and moving contacts after life tests with 150 000 breakings.

An experimental DC hybrid switching device that minimizes arcing for 42 V applications was presented in [125]. The characteristics of micro-arcing are investigated to determine the factors which influence the duration of micro-arcs. Surface profiling techniques are used to determine low level contact erosion. The magnitude of contact erosion is related to the micro-arcing.

A method for reducing arc erosion was developed consisting of injecting an additional electrical current flowing parallel to the contact surface and was shown in [102]. This method was examined in three arc environments using the additional electrical current with a density lower than 1 A/mm²: (1) Automobile ignition contacts; (2) Pulsed air arc; (3) Low pressure arc in Nitrogen. SEM and X-ray examination showed that application of a transverse current in a contact during arcing changed the phase composition and micro structure of the contact surface. Under optimal conditions the micro structure which is formed is significantly more erosion resistant than without the transverse current injection.

Paper [37] presents a case study of an event that occurred in an industrial facility that resulted in an outage without extensive damage and no harm to employees due to proper use of arc flash reduction products and a safety program. The case in point will illustrate a design of a power distribution system that was approached with safety in mind, as well as, the safety program that complimented the design resulting in a much less severe event. Arc flash reduction solutions and techniques will be discussed, especially those that were used in this example. The safety program implemented at this facility will also be reviewed to illustrate the proper recipe for safety. This case illustrates how even working de-energized can present opportunities for accidents to occur that should be addressed through proper use of installed safety equipment coupled with the successful implementation of a safety program

5.3 Criteria for the Evaluation of the Arc Erosion

In order to evaluate the electric arc erosion in electric switches, the following methods are being commonly used by researchers:

- a change of a weight of contacts,
- a change of the resistance between contacts,
- observations of a microstructure of the contact surface performed by a microscope and Scanning Electron Microscope (SEM),
- measurements of the roughness profile of the contact surface,
- a morphology analysis that can be performed e. g. by Scanning Electron Microscope (SEM) coupled with an Energy Dispersive Spectroscopy (EDS).

Above-mentioned methods are described in the next part of this chapter. Selected research results from measurements performed by other researches are presented in this chapter.

5.3.1 Mass of contacts

Changes of a weight of contacts are caused by transferring the contact materials between the electrodes. The mechanism of this phenomena was described in the chapter 5.1. The change of a weight of contacts can be observed as the function of switching operations especially during breaking large currents (above a few kA). An amount of the transferred material depends on many factors that are presented in Figure 5.9. An amount of the transferred material is usually small and can be measured in milligrams [25, 138]. Selected measurement results of researches that were performed for changes of the weight of contacts are described in detailed in [46, 64, 81, 85, 99, 117] and presented in Figure 5.10.

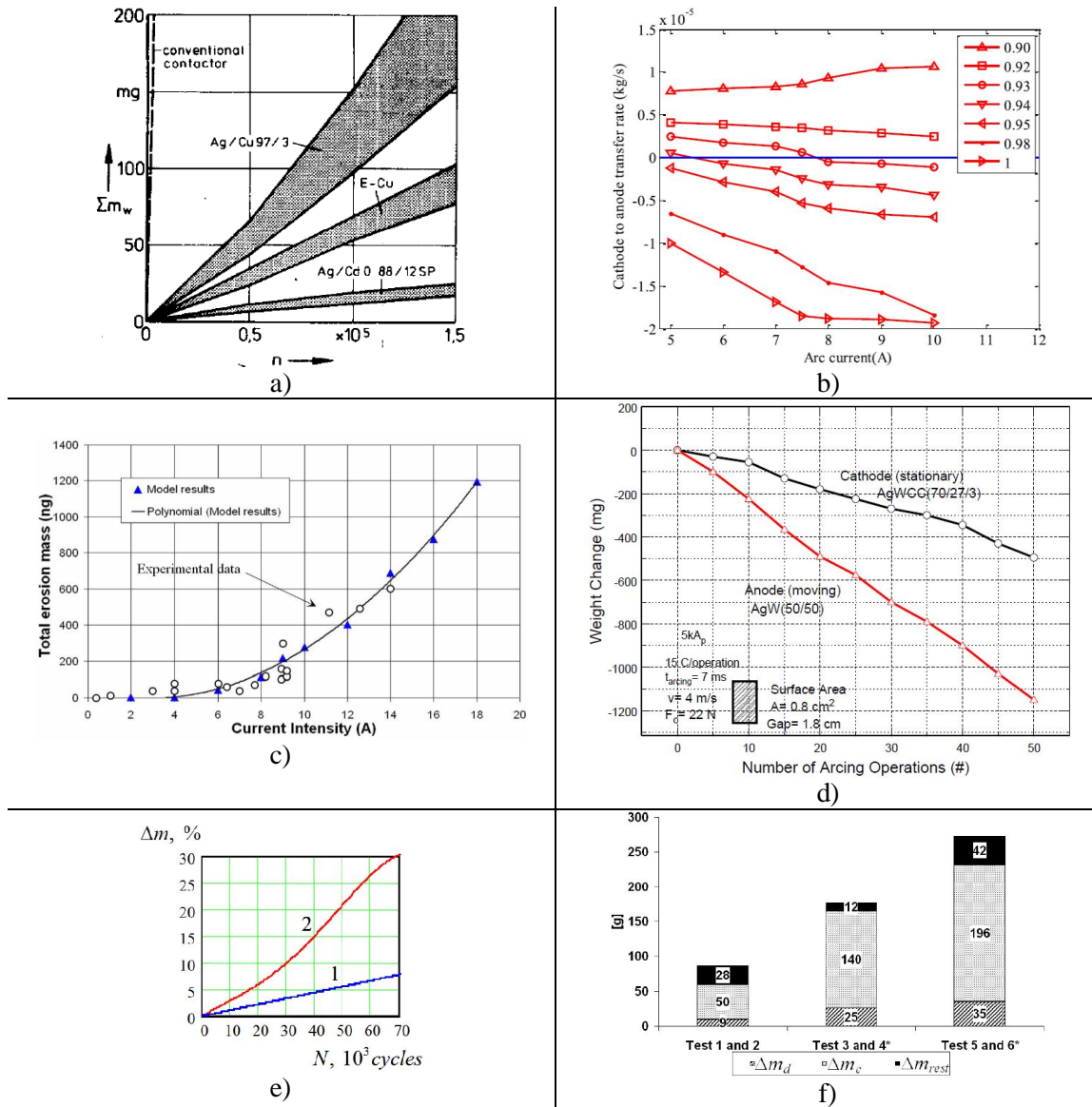


Figure 5.10. Measurements of material losses: a) total erosion loss Σm_w at breaking for different contact materials versus number of operations at $I = 500 A_{RMS}$ [46]; b) material transfer rate under different arc currents (legend represents kq) [78], c) Experimental data and model results of AgCdO cathode arc erosion [82]; d) Asymmetric contact pair shows constant erosion rate with increasing number of arcing operations [117]; e) Wear intensity of contact mass Δm for Ag (1) and for Ag-NbSe2 (2) [64]; f) Total mass loss from the electrodes Δm_e reconstructed as the mass collected on the discs Δm_d and cylinder Δm_c and a residual mass loss Δm_{rest} for test 1 to 6 [99]

As it was mentioned above, changes of weight in contacts can be observed especially, when significant values of current are interrupted. For this reason, this method was not used in researches that are presented in this thesis (measurements results presented in here are related to operating currents, thus, changes in weight of analyzed contacts are relatively insignificant for number of performed operations).

5.3.2 Contact resistance

An increase of the contact resistance is related to changes of the material properties that are caused mainly by the thermal influence of the electric arc. The creation of oxides on the contact surface leads to increase in the contact resistance. When the switch is closed and the current flows through its contacts, the thermal influence of the current can impact the contact resistance by burning oxides. This process can have a nonlinear character, which hinders the measurement of the contact resistance. For this reason it is very important to apply appropriate current during measurements of the contact resistance. On the other hand, the number of contact points between two materials (Figure 4.8) depends on many factors, such as the contact pressure, the velocity of closing contacts, a shape and dimensions of the contacts, a type of the contact material. For this reason, measurements of the contact resistance are characterized by a large dispersion. Exemplary values of the contact resistance presented as a function of contacting cycles are presented in Figure 5.11.

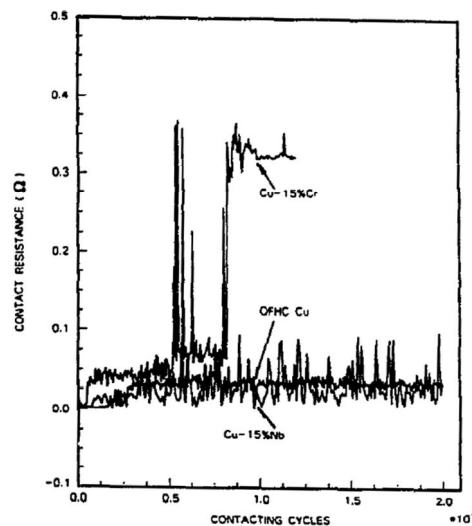


Figure 5.11. Variation of contact resistance with contacting cycles: test conditions 210 V, 14.6 A, contact head diameter 6.35 mm [82]

Measurement results that are presented in Figure 5.11 were performed for the cold rolled oxygen-free high conductivity copper applied as the contact material. As it can be observed, the contact resistance in the initial stage of operation (up to 5000 operations) for each of the three materials was fairly low [82]. However, relatively great dispersion of the measurements can be observed, which is caused by different number of contact points (Figure 4.8) between two movable contacts that contact each other during each contacting cycle. This phenomenon is related to a kinematical dispersion of mechanical movement of the contacts. Due to significant dispersion of measurement results, this method was not used in researches that are presented in this work.

5.3.3 Observation of the contact surface

In order to observe a thermal influence of the electric arc, surfaces of contacts can be observed by means of the optical microscope. This method allows to indicate changes in the microstructure of the observed surface, which is very helpful especially in an evaluation of

the electric arc erosion for composite materials that consist of a few chemical elements with different material properties. Observations performed by means of the optical microscope can provide information related to the temperature distribution during breaking current based on the colors and deformations of the analyzed surface (micro-cracks, micro-craters, melted layers, etc). This approach provides qualitative results for the observed surface. Exemplary photographs that illustrate performed researches on the arc erosion in the past are presented in Figure 5.12.

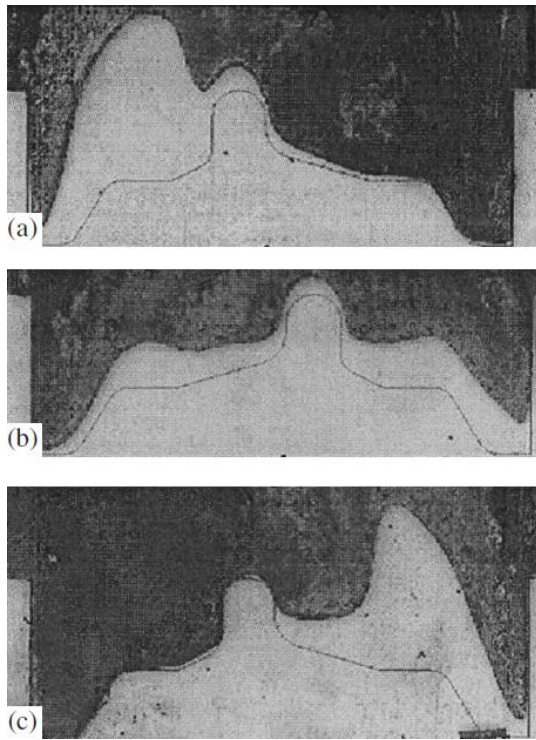


Figure 6. Droplets melted on the Cu collectors observed after test 1.

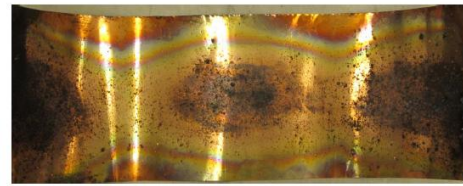


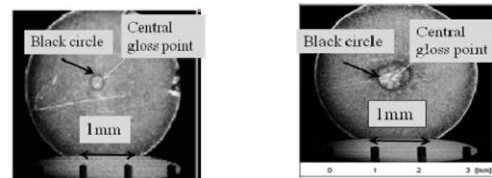
Figure 7. Dissipation of droplets on the outstretched copper plate after test showing clearly two areas (top and bottom) with higher density of molten droplets.



Figure 8. Left: Shape of the electrode fingers with a moving arc after test Right: Shape of cylindrical rod after a test with a stationary arc .



c)



(a) Hemisphere radius:0.25mm (b) Hemisphere radius:2.0mm

d)

Figure 5.12. a) Electric arc erosion of arc chute metal plates at commutation of current with amplitude 105-120 kA 1 – phase A, 2 – phase B, 3 – phase C [89]; b) [99]; c) Impacted surface layer after ten electrical arcs (25x) [107]; Contact surfaces after one time arc ignition for 50 V/1A breaking operation [135]

Detailed descriptions of performed researches, whose measurement results are presented in Figure 5.12 were published in [89, 99, 107, 135].

Observations of contact surface were also performed in the frame of researches presented in this thesis. For this purpose, tested contacts were photographed and their surfaces were observed by means of the optical microscope.

5.3.4 Roughness profile of contact surface

Changes in the microstructure of the contact surface created from the electric arc influence cause a deformation of the roughness profile of the contact material. For this reason,

roughness profile of analyzed contacts can be a measure of the electric arc erosion. A roughness profile can be measured by means of the roughness tester. According to international standards, roughness is characterized by defined parameters. Selected roughness parameters that were used to perform researches presented in this work (R_a , R_z , R_{max}) are described briefly below and shown in Figure 5.13.

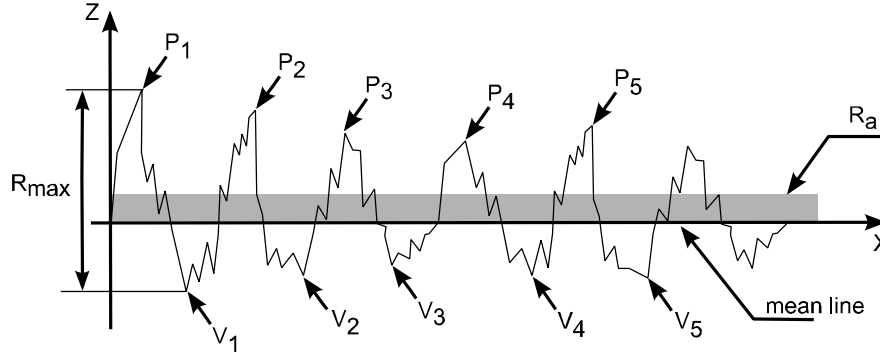


Figure 5.13. Roughness profile with marked parameters R_a , R_z , R_{max}

The area between the roughness profile and its mean line is defined as the average roughness R_a . This magnitude can be calculated as the integral of the absolute value of the roughness profile height over the evaluation length, according to the formula (5.2) [132]:

$$R_a = \frac{1}{L} \int_0^L |r(x)| dx \quad (5.2)$$

where: L – the length of the profile [m], $r(x)$ – a roughness profile height as the function of distance x [m].

Formula (5.2) can be also approximated by a trapezoidal rule, when evaluated data are digitalized according to the formula (5.3).

$$R_a = \frac{1}{N} \sum_{n=1}^N |r_n| \quad (5.3)$$

where: N – the number of measured points [-], r_n – a measured height of the roughness profile at the point n [m].

R_z is the ten point average roughness that is calculated as averages of the five highest peaks plus the depth of the five deepest valleys over the evaluation length (which is presented according to marks p_1 - p_5 and v_1 - v_5 in Figure 5.13) [132]:

$$R_z = \frac{|p_1 + p_2 + p_3 + p_4 + p_5| + |v_1 + v_2 + v_3 + v_4 + v_5|}{5} \quad (5.4)$$

R_{max} (marked also as R_y) is the maximum peak to lowest valley vertical distance within a single sample length [132].

Researches on roughness profiles of contacts were being performed in the past [94, 102, 125]. Selected measurement results (3-D profile of hybrid switch contacts, example of an arc erosion scan, as well as, measured surface roughness as a function of transverse current density) are presented in Figure 5.14.

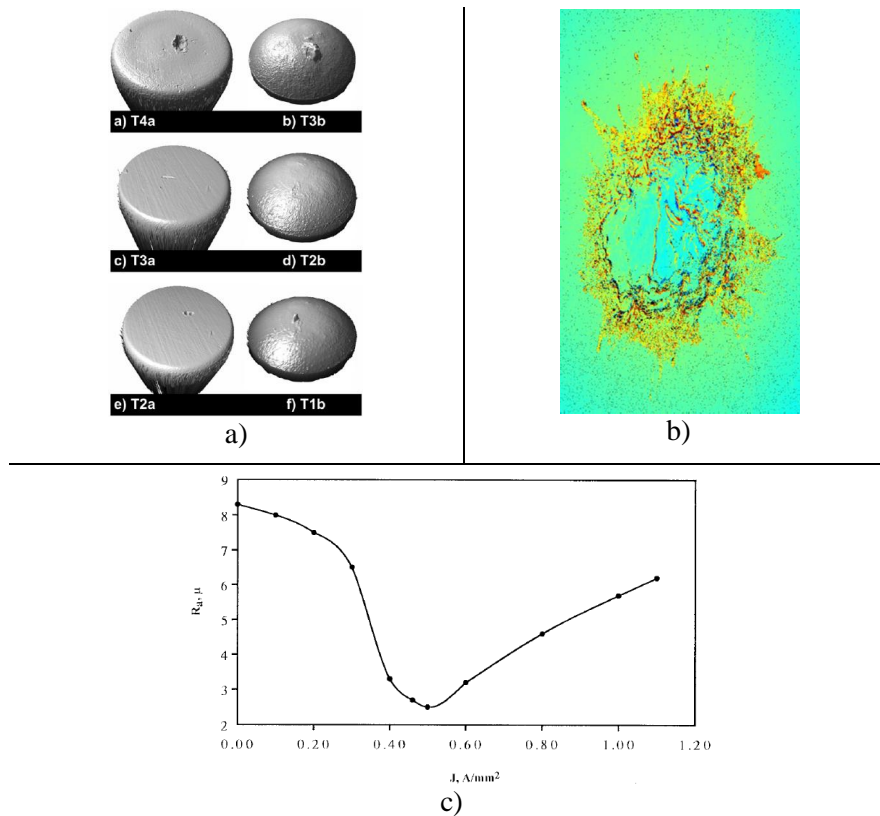


Figure 5.14. a) 3-D profile of hybrid switch contacts after 2000 op at 8 A [125];
 b) Example of an arc erosion scan, false color represents the height [94];
 c) Surface roughness R_a as a function of transverse current density
 (low pressure arc in nitrogen) [102]

Thus, researches on roughness of contact profiles can be helpful especially to determine an amount of transferring contact material between contacts and between contact area. For this reason, this method was selected to perform evaluation of arc erosion for presented experiments in the frame of this work.

5.3.5 Morphology analysis

Optical observations of contact surfaces (presented in section 5.3.3) allow to indicate changes in microstructure of analyzed contacts (these methods allow to observe microstructures of the contacts with magnification of 200-2000 times). Unfortunately, optical observations cannot provide information related to chemical composition of analyzed samples. For this reason, connection of optical observations with morphological analysis is necessary. For this purpose, different spectrographic methods which enable to the analysis of the chemical composition of external layers of analyzed contacts can be used (such as: Auger Electron Spectroscopy, Secondary Ion Mass Spectroscopy, Secondary Neutrals Mass Spectroscopy, Electron Spectroscopy for Chemical Analysis, Rutherford Back Scattering, Inductively Coupled Plasma Atomic Emission Spectrometry, Glow Discharge Optical Emission Spectroscopy or Glow Discharge Mass Spectroscopy). Spectrographic methods allow to analyze chemical composition of samples through acting flux of particles (electrons, ions, photons) on analyzed surface. In this way, excited particles from analyzed surfaces are detected and analyzed. As a result, intensity of emitted particles from observed surfaces is obtained, and chemical composition of tested samples can be determined based on this information [25].

The chemical composition of the contact material can change as a result of the thermal influence of the electric arc. In order to analyze chemical composition of contacts, spectrographic methods can be used. Scanning Electron Microscope (SEM) coupled with an

Energy Dispersive Spectroscopy (EDS) is one of the most commonly used methods to analyze surfaces of electrical contacts [25] and for this reason this method was applied to evaluate the electric arc erosion in frame experiments that are presented in this work.

Scanning Electron Microscope (SEM) coupled with an Energy Dispersive Spectroscopy (EDS) is an analytical technique used for the elemental analysis or chemical characterization of a sample. It is based on an interaction of some source of X-ray excitation and a sample. Its characterization capabilities are due in large part to the fundamental principle that each element has a unique atomic structure allowing a unique set of peaks on its electromagnetic emission spectrum (which is the main principle of spectroscopy).

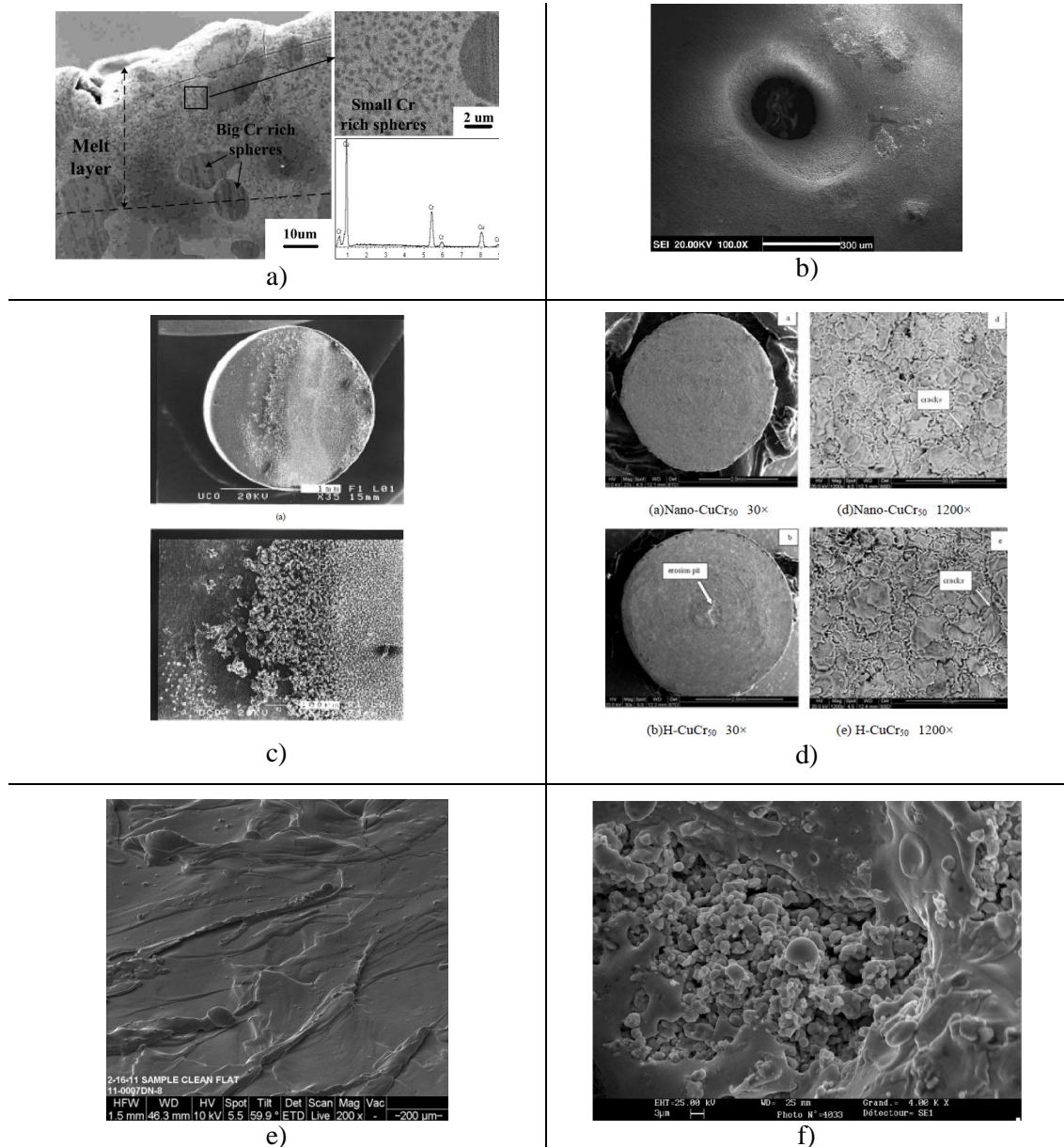


Figure 5.15. a) Cross-sectional microstructures and the composition of the melt layer of Erosion Region [84]; b) Degradation on the contact surface [151]; c) SEM photos of cathode surface after arcing with an arc current of 170 A. 1 Surface of the cathode tip cross-section. 2. Detail of central zone of the cathode tip surface [150] d) SEM micrographs of CuCr cathode contact materials eroded by arc after switching 5000 times 10 A current; e) Photo obtained using SEM on an aluminum sample [94]; f) SEM picture of a cavity full of granules (anode) [107]

6 Research Plan

The main goal of electrical measurements presented in the thesis was to perform researches on a limitation of an electric arc energy and an electric arc erosion. The researches on the electric arc mitigation were performed in a tested circuit by means of different considered methods. The measurements were conducted in the tested circuit for two scenarios of a supply voltage: 12 V and 230 V. These studies were necessary to indicate the most effective method for the limitation of the arc energy that could be used to a next step of researches, which was focused on an investigation into a limitation of an electric arc erosion in tested LV switches. The researches on the mitigation of the electric arc energy and the electric arc erosion were performed in the tested circuit with the same electrical parameters.

The method giving the best results for the limitation of the electric arc energy (hybrid switching) was determined based on the electrical measurement results. This method was used to perform the researches on the limitation of the arc erosion in the tested switches. For this purpose, 200 000 cycles of a current interruption in the tested circuit were performed by means of four switches in total.

A detailed research plan of the performed researches is presented in the section 6.1.

6.1 Overall Scope of the Work

All researches performed in the frame of the thesis can be divided into two main groups:

- a) the researches performed on the mitigation of the electric arc energy,
- b) the researches performed on the mitigation of the electric arc erosion.

Detailed research plans are presented respectively in the section 6.1.2 and in the section 6.1.3. The researches were performed in the inductive tested circuit for a selected type of an operated switch. The basic electrical parameters of the tested circuit are presented in the section 6.1.1, and a description of the type of the operated switch, which was used to perform the researches is presented in the section 6.1.4.

6.1.1 Basic Electrical Parameters of the Tested Circuit

The researches on the mitigation of the electric arc energy and the electric arc erosion were performed in the same, almost quite pure inductive circuit – for this purpose, an air-core coil ($L = 29.8$ mH) with slight resistance of winding was used ($R = 1.2$ Ω). This type of the load was selected to perform the researches for two main reasons.

Firstly, the inductive load is especially difficult due to conditions for quenching the electric arc (according to the description presented in the section 3.1). For this reason, measurement results presented in this thesis can be treated as the worst case: a power factor of the tested circuit is more problematic than the conditions specified for example in the IEC standard [56]. This document defines AC categories that have to be met for an each LV switch available commercially. According to the AC-3 utilization category [56], the switch has to provide breaking capability in an electrical circuit with $\cos \varphi = 0.45$ (for the interrupted current lower than 100 A). The nominal current of the tested switch at 230 V is 33 A for the AC-3 utilization category (see the section 6.7.3 for details). The RL parameters of the tested circuit give $\cos \varphi \approx 0.13$, and respectively about 1.3 A_{RMS} at 12 V and about 24.3 A_{RMS} at 230 V. Thus, the value of the power factor in the tested circuit is much worse from viewpoint of the breaking capability of the tested switch. According to the AC-3 utilization category [56], the switch has to provide breaking capability in an electrical for at least 6 000 operating cycles.

The researches on limitation on the electric arc erosion presented in thesis dissertation were performed for 50 000 operating cycles performed by each tested switch. Thus, the exceptionally hard conditions selected to perform the experiments guarantee that the method limiting the electric arc determined as the most effective can give comparably good results practically in an each considered inductive electric circuit.

Secondly, almost an each existing electrical circuit is characterized by an inductive character at least partially. Thus, the inductive circuits can be found practically in an each electric device, both in solutions dedicated to a domestic usage (such as: household appliances, electro-tools, heating equipment, lightning devices, etc.), as well as, in the heavy industry applications (such as: electric motors, arc furnaces, power electronic inverters, power transformers, special industrial equipment, etc.) Therefore, the presented inhere methods can be applied to protect the contacts of the operated switches that can be used in many industries, which simultaneously can influence on increasing a reliability of many electrical circuits.

In general, the tested circuit consists of the air-core coil ($L = 29.8 \text{ mH}$) with its slight resistance of a winding ($R = 1.2 \Omega$), which was used as a load, an operated switch, and a voltage source. A general diagram of the tested circuit is presented in Figure 6.1.

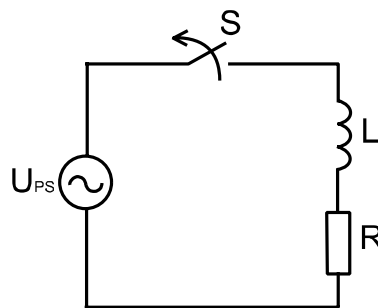


Figure 6.1. A general diagram of the tested circuit.
 $U_{PS} = 12 \text{ V or } 230 \text{ V}, R = 1.2 \Omega, L = 29.8 \text{ mH}$

As shown in Figure 6.1, the current flowing in the tested circuit is interrupted by the operated switch S . The researches presented in the thesis are focused on the limitation of the electric arc energy generated between the contacts of the operated switch S during the current interruption. The researches were performed in the single-phase circuit.

Detailed research plans are presented respectively in the section 6.1.2 and in the section 6.1.3. A description of the type of the operated switch, which was used to perform the researches is presented in the section 6.1.4. A detailed description of the laboratory stand consists of the tested circuit a measurement equipment, a microcontroller system to control the entire switching operation, and additional protections to provide the safety of the use was presented in the next part of the thesis.

6.1.2 Researches on the Limitation of the Electric Arc Energy

In this section, the detailed research plan for the mitigation of the electric arc energy performed in the tested circuit was presented.

The investigations on the limitation of the electric arc energy during the current interruption were conducted in the tested circuit for the following scenarios (the experiments were performed both at 12 V, as well as, at 230 V of the supply voltage, and measurements results were presented in two separated chapters in next part of the thesis):

1. Performing the contact separation of the operated switch at four defined phase angles of the current period: just before a current zero-crossing, at 35° , at 90° , at 145° . A detailed description is presented in the section 6.2.

2. Performing the contact separation of the operated switch at the defined phase angle of the current period in the tested circuit (respectively: at 35° for the 230 V supply voltage, and at 90° for the 12 V supply voltage, these conditions were selected due to expected the largest electric arc energy) with a connection of various passive external branches in parallel to the operated switch, such as: a RC arc suppressor, a Voltage-Dependent Resistor (VDR), a Transient Voltage Suppressor (TVS), a Zener Voltage Limiter (ZVL). A detailed description of this method is presented in the section 6.3.
3. Performing the contact separation of the operated switch at the defined phase angle of the current period in the tested circuit (similarly to the point 2: at 35° of the current period for the 230 V supply voltage, and at 90° of the current period for the 12 V supply voltage) with the application of a hybrid switching system. This method is based on the connection of a semiconductor branch in parallel to the operated switch. For this reason, the current commutation into the semiconductor branch is possible during the current interruption. A detailed description of this method is presented in the section 6.4.

The following signals were measured during the researches:

- a voltage u_S between the contacts of the operated switch S ,
- a current i_S of the operated switch S ,
- a current i_B of an external branch connected in parallel to the operated switch S .

The researches were conducted at the two different voltage levels (at 12 V and at 230 V) in the tested circuit. Another electrical parameters of the tested circuit are the same in both variants of the voltage supply. This approach was applied to point out the influence of the voltage supply on the effectiveness of the application of the considered method applied to limit the electric arc in the tested circuit. The researches were repeated at least 10 times for each investigated method to ensure that the obtained measurement results are repeatable. Slight differences could be observed in the registered waveforms for the each considered method that were caused by random phenomena taking part in a physical process of the electric arc formulation. In this thesis, the registered waveforms from single selected representative experiment were presented for the each considered method.

Based on the measured data, the following waveforms were calculated and presented in the next part of the thesis (respectively in the chapter 7 and in the chapter 8):

- a power of the electric arc p_A – calculated as a product of the current interrupted by the operated switch S and the voltage measured between the contacts of operated switch, according to the dependence (3.3),
- a power generated at the external branch connected in parallel to the operated switch p_B – calculated as a product of the current commuted into the external branch connected in parallel to the operated switch and the voltage measured between the contacts of operated switch, according to the dependence (4.3),
- an energy of the electric arc e_A – calculated as a definite integral for the power of the electric arc according to the dependence (3.4), for the time between the contact separation of the operated switch and the time, when the electric arc quenches,
- an energy absorbed by the external branch connected in parallel to the operated switch e_B – calculated as a definite integral calculated for the power generated at the external branch according to dependence (4.4), for the time between the contact separation of the operated switch and the time, when the electric arc quenches.

A theoretical waveforms of the measured voltage across the operated switch and the measured interrupted current with theoretical waveforms of the calculated electric arc power and the calculated electric arc energy together with marked the key instants during the current interruption process are presented in Figure 6.2.

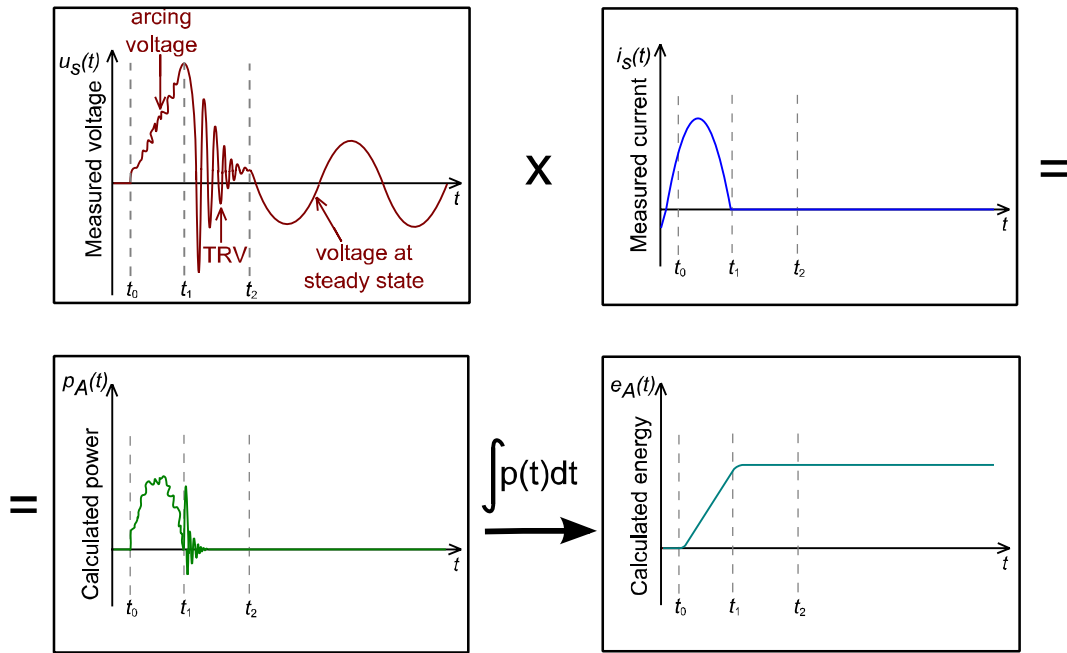


Figure 6.2. A theoretical waveforms of the measured voltage and current with theoretical waveforms of the calculated power and energy; t_0 – the time, when the contacts of the operated switch start to separate, t_1 – the time, when the electric arc was quenched, t_2 – the time, when the steady state voltage appears between the contacts of operated switch after the end of the TRV

As shown in Figure 6.2, the electric arc energy e_A was calculated as a definite integral from the product of the measured voltage across the operated switch u_S and the interrupted current i_S . The electric arc energy starts to increase from the time t_0 , when the contacts of the operated switch start to separate, and the arcing voltage starts to increase. The electric arc quenches at time t_1 , and just after that oscillations can be observed in the electric arc power p_A . This phenomenon is observed only during measurement a small current in the tested circuit supplied by 12 V voltage source (during experiments performed for larger current in the tested circuit supplied by the 230 V voltage source, similar oscillations were not observed). Thus, these oscillations are caused by measured negligible oscillations of the small current i_S that appear after the current zero-crossing (it is not the post arc current, this phenomenon is caused by an inaccuracy of the measurement realized by the current probe). The oscillations negligibly influences on the calculated final value of the electric arc energy e_A (after t_1). However, in course of the following analyses, the electric arc energy e_A was always read out precisely at time t_1 . For this reason, the values of the electric arc energy e_A presented in the next part of this thesis are related to only the time, when the electric arc burns (between t_0 and t_1). The same approach was applied to calculate the energy absorbed by the external branch e_B connected in parallel to the operated switch.

The studies of the above-mentioned signals allow to perform both the quantitative, as well as, the qualitative analysis of the limitation of the electric arc energy for the different considered methods. Based on the measurement results, the application of the hybrid switching was determined as the most effective method for the limitation of the electric arc energy.

In order to highlight physical differences in the formation of the electric arc created between the contacts of the operated switch during the application of the hybrid switching, a registration of the contact system was performed by means of the High Speed Camera dedicated to register slow-motion observations. The registrations of a formulation of the electric arc were conducted in the situation, when the contacts of the operated switch start to separate at 35° of the current period, and the tested circuit was supplied by the 230 V voltage

source. These conditions were selected due to expected greater electric arc energy. Registered frames are presented in the chapter 10, for the two analyzed situations: both for the current interrupted by the standalone switch, as well as, for the same switch equipped with the hybrid switching.

6.1.3 Researches on the Limitation of the Electric Arc Erosion

In this section, the detailed research plan for the limitation of the electric arc erosion is presented. As it was mentioned in the section 6.1.2, the application of the hybrid switching was determined as the most effective method for the limitation of the electric arc energy among all considered methods. The researches on the influence of the selected method on the limitation of the electric erosion created in the contact surfaces of the operated switch were performed in the function of the switching operations. The measurements were performed for four switches of the same type. For this purpose, 200 000 cycles of the current interruptions were conducted in total. The researches were performed according to the following plan:

1. 100 000 cycles of the current interruption were performed by the two standalone switches (50 000 cycles of the current interruption were performed by the each analyzed switch).
2. 100 000 cycles of the current interruption were performed by the two switches installed in the tested circuit with the hybrid switching method applied (in this case, also 50 000 cycles of the current interruption were performed by each analyzed switch).

The researches were performed for two switches for the each analyzed method, to verify a similarity of the arc erosion degree in the both investigated switches. Because of higher electric arc energy during the current interruption, the researches were performed in the tested circuit supplied by the 230 V voltage source, when the contacts of operated switch start to separate at 35° of the current period. These parameters provide the difficult conditions for quenching the electric arc, so for this reason, they were selected to highlight the effectiveness of the application of the hybrid switching in the tested circuit. A comparison of surface conditions of the analyzed contacts taken from the new switch and the tested switches was performed by means of the following devices:

- a photo camera,
- an optical microscope,
- a roughness tester,
- a Scanning Electron Microscope (SEM) coupled with an Energy Dispersive Spectroscopy (EDS).

The researches performed by means of the photo camera and the optical microscope allow to compare visual conditions of the contact surfaces dismantled from the analyzed switches after the experiments. The roughness tester was applied to measure roughness profiles of the contact surfaces taken from the operated switches after the tests. The Scanning Electron Microscope (SEM) coupled with the Energy Dispersive Spectroscopy (EDS) was applied to perform the more accurate observations of the surface microstructures of the analyzed contacts together with the analysis of their chemical composition.

The application of the above-mentioned methods allows to perform both the quantitative, as well as, the qualitative analysis of the electric arc erosion degree. A detailed description of the research program on the limitation of the electric arc erosion is presented in the section 6.5, and a detailed description of the methods applied to determine the degree of the electric arc erosion is presented in the section 6.6.

6.1.4 LV Switch Selected as the Tested Object

In order to perform the researches, the three-phases low voltage (LV) switch with the double-break contact system (Figure 4.5b) was chosen as the tested object. This type of the switch was applied to perform the experiments due to its specified design. A distribution of the electric arc into two smaller arcs in the both quenching chambers during the current interruption improve conditions for cooling of the arc channel. According to the description presented in the section (3.3.2), changing the conditions for cooling down the electric arc impacts on its voltage-current characteristic. For this reason, existence of the two arc quenching chambers, in which the electric arc burns during the current interruption process causes to increase the total arc resistance across the entire switch, which also causes creation of the greater voltage drop across the entire switch (created from the arcing voltage). The creation of the greater arcing voltage can give better results (for the some parameters of the tested circuit) to limit the electric arc energy through the application of external passive branches connected in parallel to the operated switch. This mechanism is described in detail in the section 6.3.2.

Thus, the applied switch equipped with the double arc-quenching chambers was used as the tested object to perform the experiments. The simplified schematic of the single-pole contact system of the analyzed switch is presented in Figure 6.3.

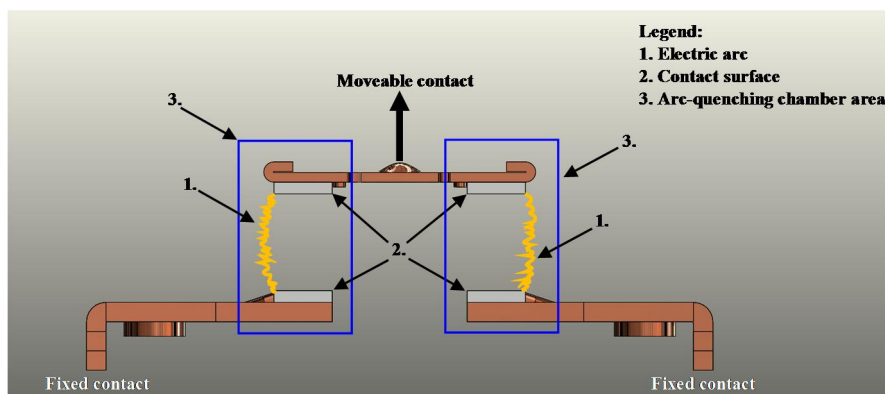


Figure 6.3. The simplified diagram of the single-pole contact system of the operated switch

As shown in Figure 6.3, the single-pole contact system of the analyzed switch consists of the two fixed contacts and the one moveable contact. During the current interruption, the electric arc burns between the separated contacts in the both arc-quenching chambers (arc-quenching chambers are marked in the simplified way as the blue frames in Figure 6.3).

Applied contractors are typical three-phases switches, which can be used for controlling power circuits up to 690 V_{AC} and 220 V_{DC}. The contractors include an electronic coil interface providing reduced pull-in and holding consumption, particularly for AC control circuits. The manufacturer offers various parameters of drive coil that is applied in this type of relay – the selected type of contactor is equipped with a coil that could be supplied by 24-60 V_{50/60 Hz}, as well as, 20-60 V_{DC}, which allowed its easy application in the tested circuit. Silver and tin oxide mixture with dopants was applied as the contact material in the analyzed switch. Detailed electrical parameters of the contractor are presented in the section 6.7.4.

6.2 Contact Separation of the Operated Switch at Precise Time Slot of Current Period

According to the description presented in the section 4.2, performing the contact separation of the operated switch at the defined phase angle of the current period can influence the electric arc energy during the current interruption in the AC systems. For this reason, detailed

measurements were conducted in the thesis to investigate this dependence in the tested electrical circuit. For this purpose, four different phase angles of the current period were chosen to perform the contact separation: 35° , 90° , 145° and the time just before the natural current zero-crossing. In order to indicate the differences in values of the electric arc energies during the current interruption, the researches were performed in the tested circuit for two voltage levels of the supply voltage (both at 12 V, as well as, 230 V).

In order to perform the measurements, a microcontroller system with implemented special algorithm was developed. The microcontroller unit was used to control the operated switch in the tested circuit. A simplified schematic diagram of the tested circuit with the applied microcontroller system to separate contacts of the operated switch at defined time, as well as, simplified waveforms illustrating the current switch drive during the current interruption process are presented in Figure 6.4.

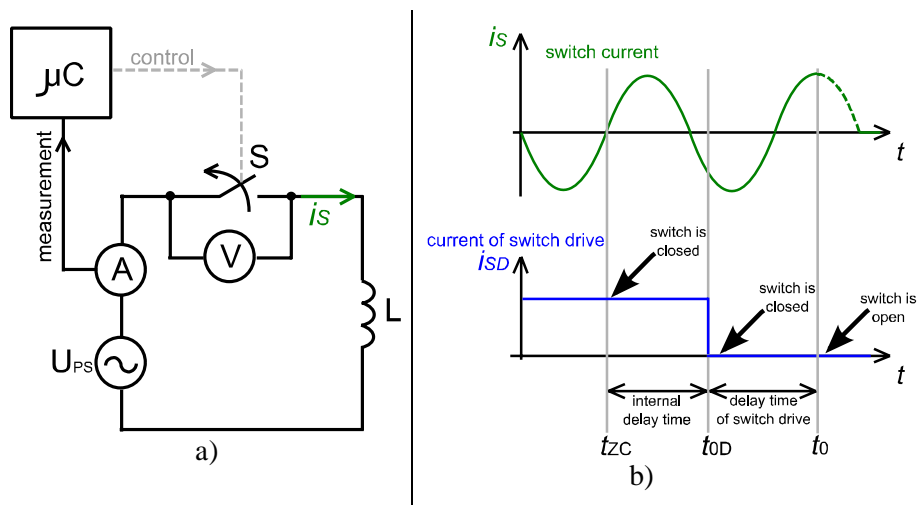


Figure 6.4. A simplified schematic diagram of the tested circuit (a); simplified waveforms of the current switch and the current of the switch drive during the current interruption (b): t_{ZC} – the detection of the current zero-crossing; t_{OD} – giving the signal to open the switch; t_0 – the time of the contact separation

As shown in Figure 6.4a, the switching sequence of the operated switch S is controlled through the microcontroller system, which takes into account known values of delay times (being composed of a self-delay time of the control system, as well as, a delay time of the switch drive response). The microprocessor unit measures continuously the instantaneous value of the current flowing in the tested circuit. Therefore, the microprocessor system is able to make a decision about the time to give a triggering signal to open the contacts of the operated switch (through the control of the current of the switch drive i_{SD}) precisely in the defined phase angle of the current period.

Figure 6.4b presents the simplified waveforms of the current flowing in the main circuit i_S and the current of switch drive during the current interruption i_{SD} . According to the description presented above, the microcontroller system detects the current zero-crossing (at t_{ZC}) and based on the known values of delay times (time between t_{ZC} and t_0) is able to separate the contacts of the operated switch in the defined time. Because of the values of internal time delays are known and repeatable in the operated switch (but only for the same, known environmental conditions), the time of the contact separation can be determined very precisely (in practice, a inaccuracy of the time contact separation is shorter than 1 ms due to a dispersion caused by a mechanical delay of the operated switch). A flowchart of a developed algorithm implemented into the microprocessor unit controlling the entire switching process is presented in Figure 6.5.

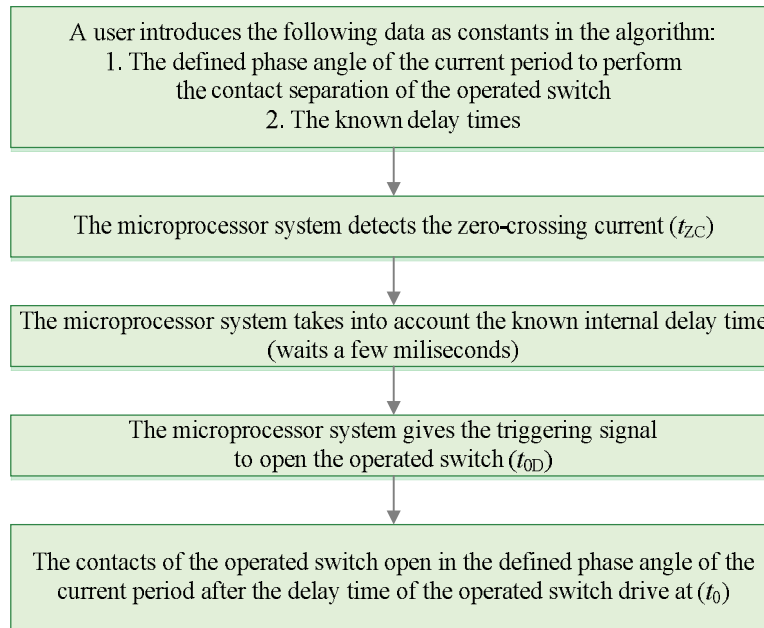


Figure 6.5. A flowchart of the developed algorithm to control the operated switch (the remarks are consistent to Figure 6.4)

The self-delay time of the developed system and the time delay of the switch drive were determined in the course of the measurements. These values together with the defined times to the contacts separation are introduced into algorithm as the constants manually by the user (see the section 6.7 for details).

6.3 Connection of Passive Branches in Parallel to the Operated Switch

In order to determine the influence of the components connected in parallel to the operated switch on the electric arc energy, the detailed measurements were performed in the following conditions:

- the RC arc suppressor,
- the Voltage-Dependent Resistor (VDR),
- the Transient Voltage Suppressor (TVS),
- the Zener Voltage Limiter (ZVL),
- the Solid State Relay (SSR) applied as a bypass of the operated switch in application of the hybrid switching method.

The parameters selection of the applied components used to perform the researches are presented in this section.

6.3.1 Selection of the RC Suppressor Parameters

According to description presented in section 4.3, an impedance of the RC suppressor connected in parallel to the operated switch (according to the row 1 in Table 6.1) cannot be too low, due to the expected large value of a leakage current in the time, when the contacts of the operated switch are opened. Specialized simulations of the current interruption were performed with the various resistances and the capacitance of the RC suppressor to find the most appropriate RC parameters to perform the experiments. Calculations were performed by means of the mathematical model of the electric arc behavior implemented into EMTP-ATP software by author, that was also used in [8, 20, 29, 33, 34, 49, 90, 95, 96, 115]. However, in the course of the performed simulations, no significant influence of the parameter changes of the RC suppressor on the commutation process was observed for both levels of the supply

voltages. For this reason, the parameters of the RC suppressor ($R_S = 47 \Omega$; $C_S = 0.1 \mu\text{F}$) were selected to the experiments based on widely available commercial arc suppressors applied to protect the electric contacts against the effects of the electric arc.

6.3.2 Selection of the Parameters of the Nonlinear Voltage Components: VDR, TVS, ZVL

According to the description presented in section 4.3, the application of nonlinear voltage components (such as: the VDR, the TVS, the ZVL) connected in parallel to the operated switch provides a possibility for the current commutation into the branch connected in parallel to the operated switch, if the arcing voltage during the current interruption exceeds the minimal operating voltage of the nonlinear component. A simplified tested circuit diagram including the nonlinear voltage component R connected in parallel to the operated switch S , as well as, a simplified waveform of the voltage across the operated switch u_S during interruption of the current i_S , together with marked voltage protection level provided by the parallel component $U_{Threshold}$ are presented in Figure 6.6.

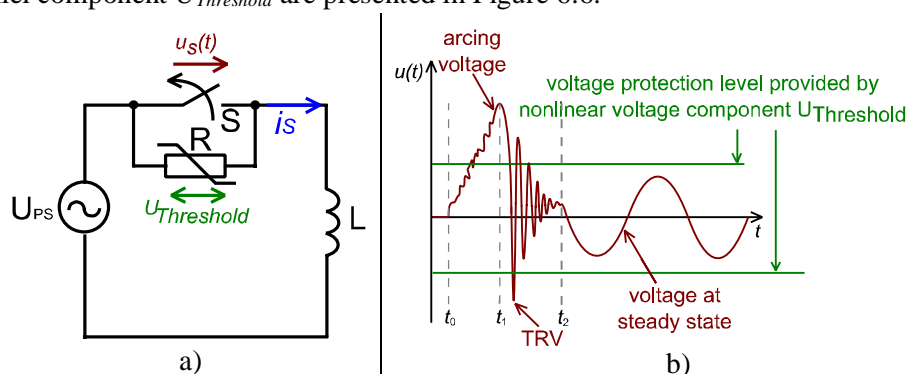


Figure 6.6. A simplified tested circuit with connected parallel nonlinear voltage component to the operated switch (a); a simplified waveform of voltage across the operated switch (b); t_0 – the time, when the contacts start to separate, and the electric arc starts to burn, t_1 – the time, when the electric arc quenches, and the TRV appears at the terminals of the operated switch, t_2 – the time, when the TRV disappears, and the voltage achieves steady state, U_{PS} – the power supply, R – the nonlinear voltage component, S – the operated switch, L – the electrical load; $u_S(t)$ – the voltage across the switch

As shown in Figure 6.6, the minimal operating voltage $U_{Threshold}$ of the applied nonlinear voltage component cannot be lower than the peak voltage of the supply voltage U_{PS} in the tested circuit. This condition has to be met, because after opening the operated switch, when the TRV disappears, the entire voltage of the power supply U_{PS} appears across the open contacts of the operated switch S . If the value of the supply voltage U_{PS} could be greater than the minimal voltage of the applied nonlinear voltage component $U_{Threshold}$, then the component R starts to conduct, whereby the current starts to flow through the nonlinear voltage component R all the time after opening the operated switch S . This situation can lead to a thermal damage of the nonlinear voltage component. For this reason, it is especially important, to select the nonlinear voltage component with its minimal operating voltage $U_{Threshold}$ greater than the voltage peak of supply voltage at the steady state U_{PS} . However, on the other hand, the difference between the voltage peak of the supply voltage at the steady state U_{PS} and the minimal operating voltage $U_{Threshold}$ of the nonlinear voltage component should be as small as possible, because in this case, it is possible to provide the most effective limitation of the electric arc – the sooner nonlinear voltage component starts to conduct, the more electric arc energy could be limited.

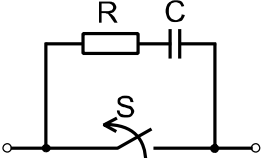
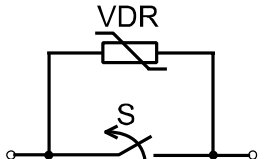
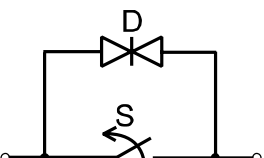
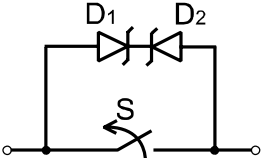
Thus, the parameters of the nonlinear voltage components (VDR, TVS, ZVL) connected in parallel to the operated switch were selected to meet the assumptions presented above, both

in the tested circuit supplied by the 12 V, as well as, the 230 V voltage source. For this purpose, the components with the typical voltage values, which can be find in a commercial application were selected. The detailed parameters of the applied components are presented in the section 6.3.3.

6.3.3 The Parameters of the Passive Parallel Components

The parameters of the passive components connected in parallel to the operated switch for limiting the electric arc energy were selected according to the description presented in the chapters 6.3.1-6.3.2. The parameters of the passive components connected are presented in Table 6.1.

Table 6.1. The considered passive methods to limit the electric arc energy [36, 124, 130]

Snubber	Schema	Basic electrical parameters		
		The 12 V supply voltage		The 230 V supply voltage
1. RC snubber		$R = 47 \Omega$ $C = 0.1 \mu\text{F}$		
2. VDR		Type:		
		B72214S0200K101	B72220S0231K101	
		Voltage Rating AC:		
		20 V	230 V	
		The voltage between two terminals with the 1 mA current applied:		
		33 V	360 V	
		Nominal surge current 8/20 μs :		
		1000 A	8000 A	
Nominal Peak Energy 10/1000 μs :				
6 J	130 J			
3. TVS		Type:		
		1.5KE24CA	1.5KE400CA	
		Peak power pulse (10/1000 μs):		
		1.5 kW		
		Stand-off voltage:		
		20.5V	342 V	
		Nominal Breakdown Voltage:		
		24 V	400 V	
4. ZVL		Type:		
		1N5357B	1N5386B	1N5388B
		Zener Voltage:		
		20 V	180 V	200 V
		Reverse voltage:		
		> 15.2 V	> 137 V	> 152 V
		Zener Current:		
		238 mA	26 mA	24 mA
		Non repetitive peak power dissipation, $t < 10 \text{ ms}$:		
		80 W		

As shown in the row 4 of Table 6.1, two Zener diodes were connected in series with common cathodes in the parallel branch connected to the operated switch. This way of the connection allows to provide the possibility of the current commutation independently on the polarization of the voltage across switch. This issue does not matter during the application of the VDR and bidirectional TVS – both components are not sensitive to the sign of the voltage connected to their terminals, so the current commutation can be performed independently on the polarization of the voltage appearing across the operated switch.

As shown in the row 4 of Table 6.1, two types of Zener diodes were applied in the tested circuit supplied by the 230 V voltage source (with the Zener Voltage respectively: 180 V and 200 V). In order to achieve required voltage level, two Zener diodes (with Zener voltage 200 V and 180 V) were connected in series to obtain the highest summary Zener Voltage in total ($180\text{ V} + 200\text{ V} = 380\text{ V}$), which is presented in Figure 6.7.

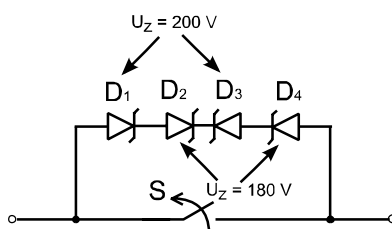


Figure 6.7. A way of the connection of the Zener diodes to achieve higher Zener Voltage (U_Z)

Thus, based on the data listed in Table 6.1, the threshold voltages $U_{Threshold}$ collected for the considered passive nonlinear voltage components are listed in Table 6.2.

Table 6.2. Threshold voltages collected for considered passive voltage components

Voltage source in the tested circuit	Threshold voltage $U_{Threshold}$ of the considered nonlinear voltage components		
	VDR	TVS	ZVL
12 V	33 V	24 V	20 V
230 V	360 V	400 V	$180 + 200 = 380\text{ V}$

Thus, as shown in Table 6.2, in the tested circuit supplied by the 12 V voltage source, the ZVL has the lowest threshold voltage, while the VDR has the highest threshold voltage. In the tested circuit supplied by the 230 V voltage source, the VDR has the lowest threshold voltage, while the TVS has the highest threshold voltage. The parameters of the nonlinear voltage components (VDR, TVS, ZVL) connected in parallel to the operated switch were selected to meet the assumptions presented in the section 6.3.2, both in the tested circuit supplied by the 12 V, as well as, the 230 V voltage source.

6.4 Hybrid Switching

In this section, a detailed description of the hybrid switching is presented.

The method presented inhere is based on the connection of the semiconductor branch in parallel to the operated switch. The semiconductor branch is controlled by the microcontroller unit during the entire switching sequence. The control of the semiconductor branch is realized to provide the following switching sequence:

1. The semiconductor branch does not conduct the current when the operated switch is closed – entire current i_S flows by the contacts of the operated switch S .
2. The semiconductor branch should start to commute the current i_S (into the semiconductor branch as the current i_B) simultaneously, when the contacts of the operated switch start to separate. After opening the contacts of the operated switch S ,

the entire current i_B flows only through the semiconductor branch up to the nearest natural zero-crossing of the interrupted current i_B .

3. The current i_B stops flowing in the tested circuit as close as possible its natural zero-crossing (in the practice, the current i_B stops flowing below the minimal holding current that is one of the parameters of the semiconductor component. The minimal holding current is negligible in comparison to the interrupted current i_B).

In order to present the switching sequence presented above, a simplified circuit diagram with the switching sequence during the current interruption is shown in Table 6.3.

Table 6.3. *The hybrid switching sequence*

The sequence number	The circuit diagram with the marked currents	The waveforms
1.		
2.		
3.		

Thus, as shown in Table 6.3, the following key steps can be distinguished during the hybrid switching:

1. a steady state occurs in the tested circuit, the operated switch S is closed, entire current i_S flows through the contacts of the operated switch S ,
2. a triggering signal is given to the operated switch S to open its contacts in the defined phase angle of the current period. For this purpose, the microcontroller unit takes into account the known values of the delay times (being composed of the self-delay time of the control system, as well as, the delay time of the switch drive response, according to the description presented in the section 6.2). In the next step, a short trigger signal i_G is given to the semiconductor component to ensure possibility for performing the current commutation to the thyristor branch as soon as possible. The microprocessor unit is able to send this signal just before the contact separation of the operated switch, taking into account the known delay times of the operated switch. This is possible, because the response time of the semiconductor branch is significantly shorter in comparison to the delay time of the operated switch. Just after the contact separation, the arcing voltage u_S across the switch increases (see Figure 6.9 for the details), and when its value exceeds the minimal rated operational voltage of the semiconductor branch, the entire current commutes into the semiconductor branch from the operated switch S . The semiconductor branch stops conducting the current i_B , when the value of the current i_B is lower than the minimal holding current value of the semiconductor branch,
3. the contacts of the operated switch S are open, the semiconductor branch does not conduct, the current does not flow in the circuit.

As shown in Table 6.3, the branch including the thyristor connected in parallel to the operated switch was presented in the simplified way to clarify the Figure. In practice, the function of the thyristor T shown in Table 6.3 is realized by an opto-isolated Solid State Relay (SSR) composed of the connected two anti-parallel thyristors, however, the control of the SSR is realized in the same way in the both cases. A simplified circuit diagram of the hybrid system used in the tests with the detailed topology of the applied SSR is presented in Figure 6.8.

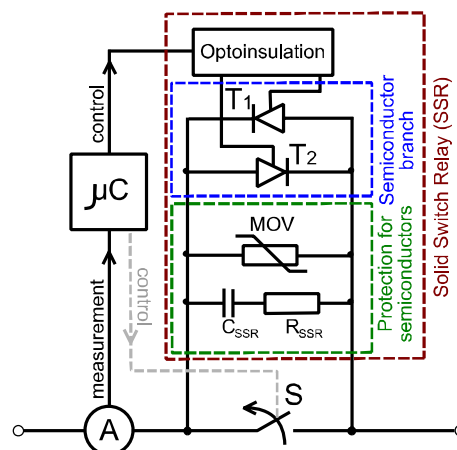


Figure 6.8. A simplified circuit diagram of the hybrid system used in the tests with the detailed topology of the applied SSR

The application of the SSR allows to perform the current interruption both in positive, as well as, negative the half-wave of the current. As shown in Figure 6.8, the SSR consists of an opto-insulated module, two anti-parallel connected thyristors, a MOV component, as well as, a RC suppressor. The application of the opto-insulated module provides a full galvanic isolation between the main circuit and the control circuit, which prevents damages of the microcontroller system, which is responsible for the control of the entire system. The

arcing voltage u_S up to about 20 V. Thus, the two-step voltage rise in the arcing voltage u_S is caused by the non simultaneous movement of the moveable contact in the both arc-quenching chambers.

As shown in Figure 6.9a and in Figure 6.9b, during the current interruption performed by the standalone operated switch, the arcing voltage u_S appears before 1st ms, and starts to increase from about 12 V to 120 V just before the current zero-crossing i_S (at about 8th millisecond), which takes over 7 ms. Such a long the arcing time has the negative influence on the condition of the contact surfaces. The significant reduction of the arcing time is provided during the hybrid switching, which can be observed in Figure 6.9c and in Figure 6.9d. Similarly to the situation shown in Figure 6.9a and in Figure 6.9b, the electric arc starts to burn before 820th μ s. When the value of the arcing voltage u_S exceeds 18 V, the current i_S starts to commute into the semiconductor branch, which causes the electric arc to quench totally. Thus, as a consequence, the voltage measured across the entire switch u_S decreases to the value of the on-state voltage of the SSR occurring across the entire switch, when the current i_B flows through the SSR. As it can be observed in Figure 6.9c, at about 9th ms, the current reaches the minimal holding current of the applied SSR, so as a consequence, the current i_B stops flowing in the tested electric circuit. As shown in Figure 6.9a, the current i_B achieves its zero-crossing earlier about 1 ms in comparison to the situation presented in Figure 6.9c. This is caused by an existence of the electric arc resistance in the interrupted circuit. The electric arc resistance is higher in comparison to the resistance of the SSR, moreover, the electric arc resistance tends to the infinity faster, which is also reflected in shorter arcing time. The detailed analyses of the electric arc resistance, as well as, the resistance of the SSR during current interruption processes are presented respectively in the section 7.4 and in the section 8.4 for the tested circuit supplied by the 12 V and by the 230 V voltage source.

The zoomed waveforms of the arcing voltage u_S and the measured currents during the hybrid switching, when the current i_S is commutated into the external branch as the current i_B are presented in Figure 6.10.

– The current of the operated switch – The commutated current
– The voltage across switch

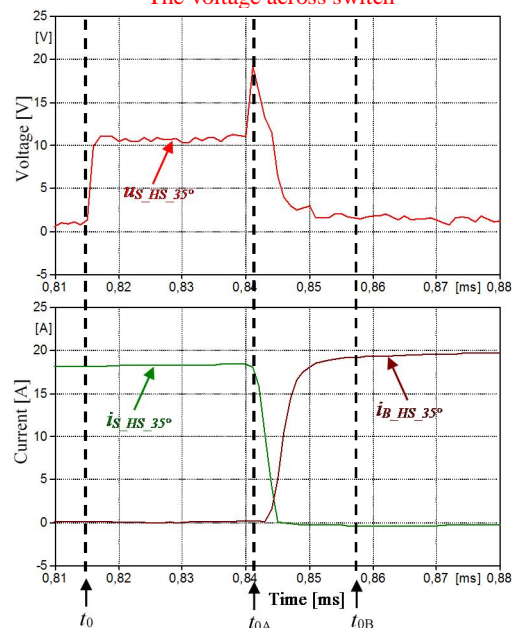


Figure 6.10. Waveforms measured during the current commutation (the contact separation was performed at 35° of the current period): $i_{S_HS_35^\circ}$ – the current of the operated switch; $i_{B_HS_35^\circ}$ – the current of the semiconductor branch; $u_{S_HS_35^\circ}$ – the voltage measured across the entire switch

As shown in Figure 6.10, the two main stages of the commutation process can be distinguished. The contacts of the operated switch S open at the time t_0 , whereby the electric arc starts to burn between the contacts. The arcing voltage u_S reaches initially about 10 V, however, this value is lower than the minimal operational voltage of the applied SSR, whereby the current commutation into the semiconductor branch is not yet possible. After the next 25 μs , the arcing voltage u_S increases rapidly at the time t_{0A} up to the minimal operational voltage of the applied SSR ($\approx 20\text{ V}$), so as a consequence, the current i_S starts to commute into the parallel branch as the current i_B and the arcing voltage u_S decreases.

From the time t_{0A} , the current i_S starts to commute into the semiconductor branch just as the current i_B (the current of the switch decreases, and the current of the semiconductor increases). This process takes about 20 μs , up to the time t_{0B} , when the semiconductor branch takes over the entire interrupting current. From the time t_{0B} , the voltage u_S between the contacts of the operated switch S achieves the on-state voltage of the semiconductor branch, and the entire current flows only through the semiconductor branch. The current i_B stops flowing in the semiconductor branch, when its value reaches the minimal holding current of the semiconductor branch, near the natural current zero-crossing.

In order to perform the investigations on the hybrid switching, the Solid State Relay (SSR) was applied as the semiconductor branch connected in parallel to the operated switch for the following reasons:

- the SSR allows to perform the current interruption both in positive, as well as, negative the half-wave of the current,
- the SSR provides a full galvanic isolation between the main circuit and the control circuit, which prevents possible damages of the microcontroller system due to overvoltages in the tested circuit,
- the SSR provides also switching overvoltage protection in the form of the application of the additional RC suppressor and the MOV elements integrated inside of the SSR.

The basic criteria for selecting SSR to perform researches on limitation of electric arc energy in hybrid switch, were based on the voltage and the current ratings. Thus, the SSR should meet the requirements comparable to the ratings of the operated switch. The electrical parameters of the SSR that was selected to perform experiments are listed in the section 6.7.4.

6.5 Observations of the Electric Arc Performed by the High Speed Camera

In order to investigate electric arc formulation in examined LV switch, registration of contact system of the operated switch during current interruption was conducted by means of the High Speed Camera. The registrations of a formulation of the electric arc were conducted in the situation, when the contacts of the operated switch start to separate at 35° of the current period, and the tested circuit was supplied by the 230 V voltage source. These conditions were selected in order to expect the greater electric arc energy.

Registered frames are presented in the chapter 10, for the two analyzed situations: both for the current interrupted by the standalone switch, as well as, for the same switch equipped with the hybrid switching.

The contact system of the operated switch was registered during the current interruption process. For this purpose, High Speed Camera AOS Technologies, type AG Q-MIZE was used.

The key features of the used camera are listed below [9]:

- 1300x1060 Pixel image resolution up to 1000 fps,

- 900x700 Pixel image resolution up to 2000 fps,
- 3 MPixel image resolution up to 500 fps,
- Super-compact, fits into tight spaces,
- Re-chargeable battery built in for true mobile applications and data backup,
- Gigabit Ethernet interface,
- Auto Exposure control.

Electric arc observation was performed with 400x296 resolution, velocity registration was 250 fps (frames were registered with resolution of 250 μ s).

To perform the researches, a sidewall of the housing of the operated switch was removed. For this reason, the contact system of the operated switch could be visible. In order to ensure the safety during the experiments, the removed sidewall was replaced by a piece of transparent plexiglass. The view of the switch used for the experiments was presented in Figure 6.11.

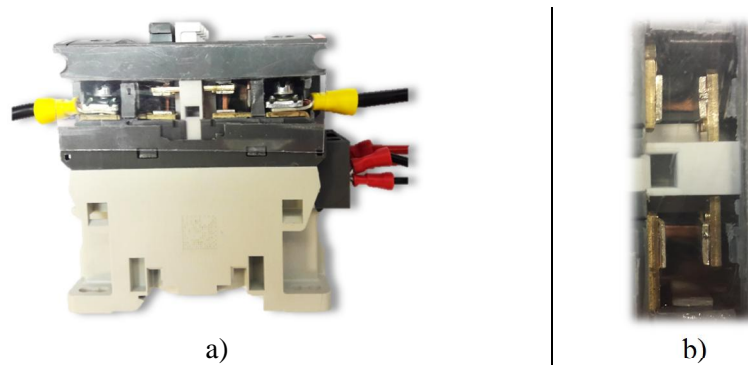


Figure 6.11. The modification of the switch introduced to perform the observations of the electric arc formulation (a); the contact system of the operated switch (b)

A simplified circuit diagram showing the control of the High Speed Camera during the researches is presented in Figure 6.12.

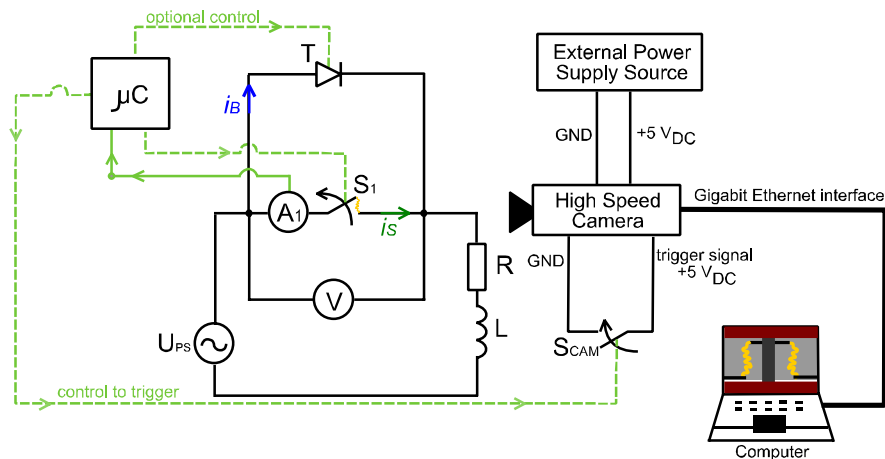


Figure 6.12. A simplified circuit diagram showing the control of the High Speed Camera during the researches

As shown in Figure 6.12, the High Speed Camera was triggered to record by means of the additional switch S_{CAM} , which was closed just before the current interruption (the camera was triggered to record by the falling slope). The switch S_{CAM} was controlled by the microcontroller device, as shown in Figure 6.12. The High Speed Camera was connected to the computer by the Gigabit Ethernet interface.

6.6 Evaluation of the Electric Arc Erosion

The overall plan of the researches performed on the limitation of the electric arc erosion is presented in the section 6.1.3. According to this, the application of the hybrid switching was determined as the most effective method for the limitation of the electric arc energy among all of the considered methods.

The researches on the influence of the selected method on the limitation of the electric erosion created in the surfaces of the contacts of the operated switch were performed as a function of the current interruptions. The measurements were performed for the four different switches of this same type. For this purpose, 200 000 cycles of current interruptions were conducted in the tested circuit totally. The researches were performed according to the following plan:

1. 100 000 cycles of the current interruptions were performed by the two standalone switches (50 000 cycles of the current interruptions were performed by the each analyzed switch).
2. 100 000 cycles of the current interruptions were performed by the two switches installed in the tested circuit with the hybrid switching method applied (in this case, also 50 000 cycles of the current interruptions were performed by the each analyzed switch).

In both analyzed cases, the switching operations were performed every 3 s. The experiments were performed at the High Voltage Laboratory localized at the AGH University of the Science and Technology in the similar environment conditions during all of the tests. The switching cycles were conducted for a few hours per each day, up to the time, when the operated switch performed 50 000 cycles of the current interruptions in total.

The researches were performed for two switches in both analyzed cases, to verify a similarity of the degree of the arc erosion in both investigated switches. The simplified contact system with donated investigated contacts is illustrated in Figure 6.13 (based on Figure 6.3, respectively, the fixed contacts are marked as #1 and #3, and the moveable contact as #2).

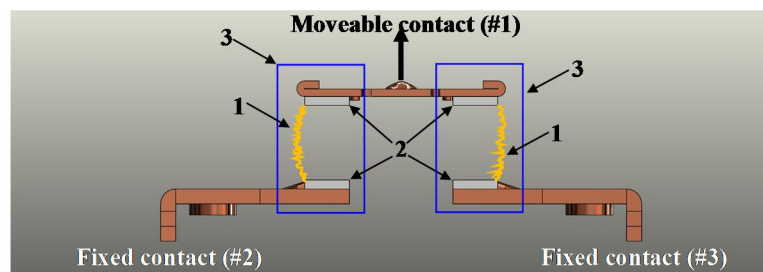


Figure 6.13. *The simplified contact system of the operated switch: 1. The electric arc; 2. The electrical contacts; 3. The area of the arc-quenching chambers. The fixed contacts are marked respectively as #2 (the cathode) and #3 (the anode), and the moveable contact as #1.*

According to the description presented in the section 6.1.3, the researches were performed for two switches in the both analyzed cases, to verify a similarity of the degree of the arc erosion in the both analyzed switches. Because of higher electric arc energy value, the researches were performed in the tested circuit supplied by the 230 V the voltage source to highlight the effectiveness of the applied method for the limitation of the electric arc. During the performed measurements, the contacts of the operated switches were separated at 35° of the current period, in order to expect the largest electric arc energy in comparison to later time slots.

The contact separation was being performed always at 35° of the current period at the positive half-wave, which allows to perform the current interruption for the oriented anode (the fixed contact #2) and the cathode (the fixed contact #3) constantly.

A comparison of the surface conditions of the analyzed contacts taken from the new switch and the tested switch was performed by means of the following devices:

- a photo camera,
- an optical microscope,
- a roughness tester,
- a Scanning Electron Microscope (SEM) coupled with an Energy Dispersive Spectroscopy (EDS).

A detailed description of the performed researches on the limitation of the electric arc erosion is presented in the sections 6.6.1-6.6.4.

6.6.1 Electrical Setup Used to Perform the Investigations on the Limitation of Electric Arc Erosion

The researches on the limitation of electric arc erosion were performed in the tested circuit, its simplified electrical circuit diagram presented in Figure 6.14.

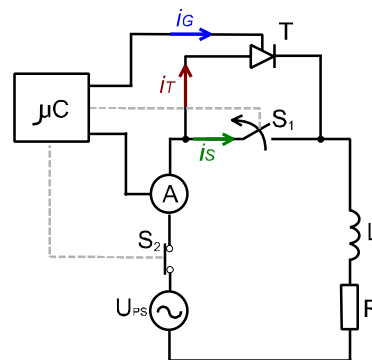


Figure 6.14. A simplified electrical circuit diagram of the tested circuit with the marked currents

According to Figure 6.14, the switch S_1 is the tested object, so the current interruption in the tested circuit is realized only through the switch S_1 . At this time, the switch S_2 is always closed, and its function is only making the current i_S in the tested circuit, when the switch S_1 is closed. The switch S_2 was applied only to the total elimination of the electric arc created from bouncing the contacts during closing the switch S_1 . For this reason, the contacts of the tested switch S_1 close always in dry-contact conditions. The created arc erosion in the surfaces of the analyzed contacts is related only to formulating the electric arc during the current interruption. The current is interrupted in the tested circuit according to the hybrid switching sequence described in the section 6.5. Similarly to the previous description, the thyristor T presented in Figure 6.14 was shown only to simplify the Figure, and its function is realized by the applied SSR in practice. The detailed sequence of the hybrid switching is presented in the section 6.5.

The researches on the limitation of the electric arc erosion were performed for the both analyzed approaches: both for the current interrupted by the standalone switch, as well as, for the same switch equipped with the hybrid switching.

6.6.2 Visual Comparison of the Condition of the Analyzed Contacts

In order to compare a visual condition of the analyzed contacts, entire surfaces of the electrical contacts were photographed by means of the photo camera. Pictures of the new contact taken from the new switch were also presented to compare the differences in the condition of the analyzed contact surfaces taken from the switches after the tests (when the current was interrupted by the standalone switch, as well as, when the current was interrupted by the switch with the hybrid method implemented). All contacts taken from all of the tested

switches were investigated according to Figure 6.13 (respectively, the fixed contacts are marked as #1 and #3, and the moveable contact as #2). The sets of the taken pictures are presented in the section 11.1.

In order to perform more accurate observations of the contact surfaces (to show cracking microstructure, deformations, and discoloration of surfaces), the microstructure of the contact surfaces was also observed by means of the optical microscope. For this purpose, areas localized close to a left edge of the contacts were selected to the analysis (marked in Figure 6.15 as the white circle).

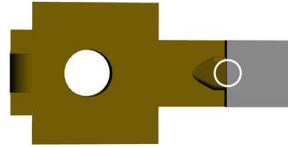


Figure 6.15. *The selected area to perform the detailed observations of the microstructure of the contact surface marked as the white circle*

The selected part of the contact surface (according to Figure 6.15), was chosen to perform the observations due to noticeably greater damages in comparison to the other part of observed contact surface. The microscope observations were performed for the new contact, the contact taken from the standalone switch, as well as, for the contact taken from the switch interrupting the current in the hybrid switching system. The observation results are presented in the section 11.2.

6.6.3 Roughness Profiles of the Surfaces of the Analyzed Contacts

In order to compare the condition of the analyzed contacts, roughness profiles of the surface of the analyzed contacts were measured. Measurements were performed for all of the tested contacts, however, only three selected roughness profiles were presented in the thesis, due to a good repeatability of the measurement results. The following selected parameters describing the roughness profile were selected to analyze:

- the average roughness R_a ,
- the ten point average roughness R_z ,
- the maximum roughness height within a sample length R_{max} .

Detailed description of parameters describing roughness profile is presented in the section 5. Measured parameters were presented and compared to indicate differences in the condition of the observed surfaces of the analyzed contacts.

The measurements were performed by means of the ESA RUGOSURF Roughness Tester 90G.

The key features of the used Roughness Tester are listed below [144]:

- measures roughness parameters according to ISO 4287, 12085 (CNOMO), 13565, DIN 4776, JIS B0601:2001 and ASME B46-2002,
- tactile TFT color display with size to 3,5",
- three function keys,
- graphical interface,
- direct displaying of all measured values and computed profiles,
- measuring span to 50 mm/2 in (X-axis) or 1000 μm /39370 μ in (Z-axis),
- interchangeable probe, with or without contact skid,
- possible input of tolerances,
- USB digital output for data transfer to a PC running TESA Measurement Studio (this software is available as an option),

- measures up to 90 mm vertically without the need for a special support,
- profile measurement up to 2 mm (optional accessory).

The roughness profiles were measured across a coaxial line of the contacts (for a distance of 3 mm), with an initial point as close as possible to the left edge of the analyzed contact, according to Figure 6.16.

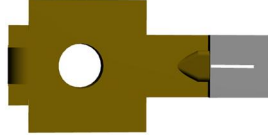


Figure 6.16. *The white line of the contacts that was selected to perform the researches on roughness profiles of the contacts surfaces*

Similarly to the visual observations, the localization of the axial line across the contact surface was selected to the observations due to noticeably greater damages in comparison to the other part of contact surface. The roughness profiles with their parameters were measured for the selected new contact, the contact taken from the standalone switch, as well as, for the contact taken from the switch interrupting current in the hybrid switching system. The observation results are presented in section 11.3.

6.6.4 SEM method coupled with the EDS

The Scanning Electron Microscope (SEM) coupled with the Energy Dispersive Spectroscopy (EDS) was applied to perform the more accurate observations of the microstructure of surfaces of the analyzed contacts together with the analysis of their chemical composition. The measurements were performed at the AGH University of Science and Technology (Faculty of Materials Science and Ceramics, Department of Silicate Chemistry and Macromolecular Compounds).

The SEM method was applied with a greater magnification in comparison to the observations performed by means of the optical microscope. This was applied to perform more accurate researches on the conditions of analyzed surfaces.

The EDS technique is able to provide information about a quantitative atomic concentration in a damaged metal part. Therefore, the application of this method allowed to determine a percentage share of chemical elements on the tested surfaces, which is helpful to indicate the quantitative influence of the hybrid switching on the improving the condition of the investigated contact surfaces.

Thus, the application of the Scanning Electron Microscope (SEM) coupled with the Energy Dispersive Spectroscopy (EDS) allows to perform both the quantitative, as well as, the qualitative analysis of the degree of the electric arc erosion. Similarly to methods presented previously in the sections 6.6.1-6.6.3, the measurements were performed for all of the tested contacts. However, only three selected roughness profiles were presented in the thesis, due to a good repeatability of the measurement results.

In order to perform the researches, the Nova NanoSEM 200 device was used. The following parameters of the device were set during the measurements:

- the accelerating voltage: 18 kV
- the working distance (the distance the underside of the objective lens to the specimen surface): 7.3 mm
- the magnitude: 350x
- the used detector: Low Vacuum Detector
- the probe current (the total amount of current to be irradiated on the specimen): 4.0 A

- the sample surface that is observed in the image (HFW): 568 μm

The detailed description of the SEM method coupled with the EDS method is presented in the section 5. The measurement results are presented in the section 11.4.

6.7 Laboratory Stand Developed to Perform Experiments

The technical details and the description of the laboratory stand used to perform the researches in frame of the thesis is presented in this section.

6.7.1 Characteristic of the Laboratory Stand

The developed laboratory stand provides the possibility to perform the researches on the limitation of the electric arc, as well as, the limitation of the electric arc erosion in LV switches, according to the description presented in the previous part of this chapter. In order to perform the researches, the following requirements for the functionality of the laboratory stand have to be met:

- performing the contact separation of the operated switch at the defined angle of the current period,
- the possibility of the connection of the additional branches in parallel to the operated switch,
- the possibility for the implementation of the hybrid switching sequence into the operated switch, according to the description presented in the section 6.4,
- the possibility to measure the current and the voltage waveforms during the transient states to determine the electric arc energy, as well as, the energy absorbed by the connected parallel branch into the operated switch,
- the safe interface for the user,
- additional protections to interrupt the researches immediately, when the welding contacts of the operated switch is detected, or when the temperature rise in the inductive load is close the dangerous value.

The listed above-mentioned assumptions were defined based on the description of the researches presented in the sections 6.1-6.6. A general circuit diagram of the developed laboratory stand including the entire required equipment is presented in Figure 6.17 in a simplified form (see the section 6.7.2 for more details).

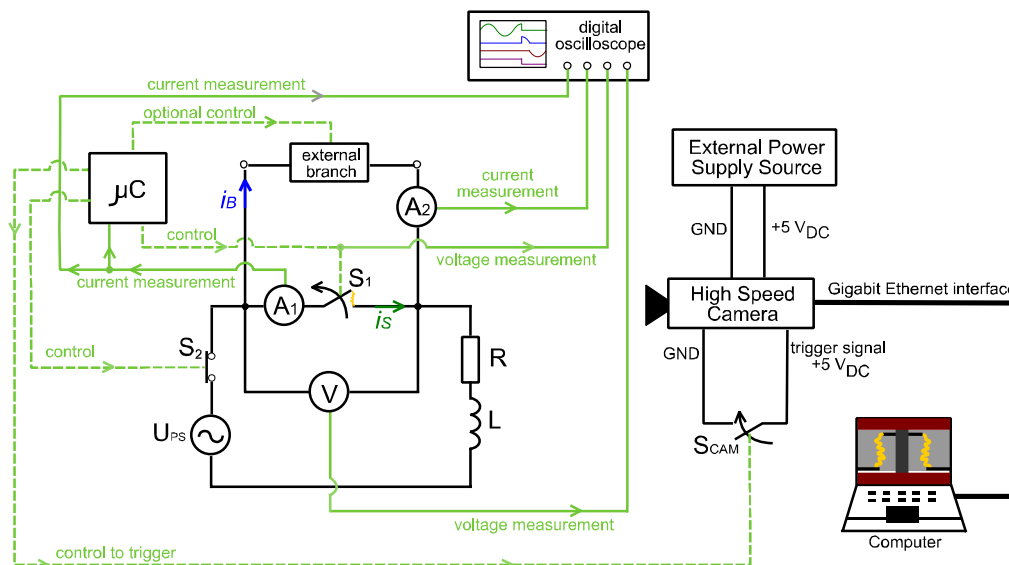


Figure 6.17. The general circuit diagram of the laboratory stand.
The basic electrical parameters: $U_s = 12 \text{ V or } 230 \text{ V}$, $R = 1.2 \Omega$, $L = 29.8 \text{ mH}$

All components installed in the laboratory stand are listed and described below (according to the remarks presented in Figure 6.17):

- the microcontroller system (μC) applied to the precise control of the switching sequence in the tested circuit during the current interruption. The detailed parameters of the cycles of the current interruption (such as: the number of the switching operations to performing, the time of the contact separation, the time to give triggering pulse to the semiconductor branch, the duration time of the pulse, the time duration for the open-state and the close-state of the operated switch, etc.) could be introduced into the device by means a special user interface with a LCD display (see Figure 6.18d). The detailed description of the microcontroller system is presented in the section 6.7.2.
- the operated switch S applied as the tested object with the drive controlled by the microcontroller system (the detailed technical ratings of the operated switch used to perform the tests is presented in the section 6.7.3),
- the inductive air-core coil ($L = 29.8 \text{ mH}$) with the slight winding resistance ($R = 1.2 \Omega$) used in the tested circuit as the load,
- the voltage source U_{PS} ($12 V_{\text{RMS}}$ or $230 V_{\text{RMS}}$) supplied the tested circuit. The maximum value current is limited by the additional protection up to $32 A_{\text{RMS}}$ due to the safety reasons. During the measurements performed at 230 V of the supply voltage, the tested circuit was supplied directly from the electrical network 230 V . In order to transform the voltage at 12 V , a small toroidal transformer was used. The inductance of the secondary winding of the applied toroidal transformer was measured (it is about $14 \mu\text{H}$). Due to the small value of the measured inductance (significantly less in comparison to the inductance of the applied coil as the load), its value was omitted in the specification of the electrical parameters of the tested circuit supplied by the 12 V voltage source,
- the different optional branches that could be connected in parallel to the operated switch. The detailed description is presented in the previous part of this chapter,
- the current probes A_1 and A_2 applied to measure respectively: the current i_S of the operated switch S and the current i_B of the branch connected in parallel to the operated switch. The measurements were performed by means the Tektronix TCP 0150 current probes,
- the voltage probe V applied to measure the entire voltage across the operated switch during the current interruption. The measurements were realized by the Tektronix P5210A differential voltage probe,
- the digital oscilloscope used to the acquisition of measured data. For this purpose, the Tektronix DPO 4054 was used,
- the additional switch used to trigger the High Speed Camera for the registration of the contact system of the operated switch in slow-motion. The switch is also controlled by means of the microcontroller system.

To provide the safe environment during the tests, the laboratory stand was equipped with the following protections and additional equipment:

- the Residual Current Device (RCD) $\Delta I = 30 \text{ mA}$,
- the overcurrent protections (the protection with the C40 characteristic was applied in the power circuit and the protection with the B6 characteristic was applied in the control circuit),
- the thermal protection (the current is interrupted by the additional safety switch, when the temperature rise inside of the inductive air-coil is greater than 180°C),

- the protection against welding the contacts (the current is interrupted by the additional safety switch, when the current flows continuously in the tested circuit longer than 15 s),
- the fan forcing the air flow inside of the winding of the coil in the case, when an increase of the temperature could achieve the dangerous value,
- the grounded electromagnetic shield placed around the air-core coil, that provides the protection for the user against the influence of the electromagnetic field generated around the air-core coil,
- the overvoltage protections installed in the control circuit, as well as, in the power circuit to protect the entire electrical equipment installed in the laboratory stand against the voltage surge.

The overall view of the laboratory stand, the view of the control panel, as well as, the view of the panel with the operated switch are presented in Figure 6.18.



Figure 6.18. The laboratory stand: a) the overall view; b) the control panel; c) the panel with the operated switch (marked as P19); d) the LCD user interface with buttons

The inductive air-core used as load to perform researches is presented in Figure 6.19.



Figure 6.19. *The inductive air-core load used to perform the researches*

As shown in Figure 6.19, the inductive air-core is equipped with six taps of the winding to provide a six values of inductance, however, in presented researches, only 1 tap was used ($L = 29.8 \text{ mH}$, $R = 1.2 \Omega$).

6.7.2 Microcontroller System

The microcontroller system (μC) was applied to the precise control of the switching sequence in the tested circuit during the current interruption. The system is based on the ATmega1284-AU microcontroller. The microcontroller system uses a 1 analogous input channel to measure the current flowing in the analyzed circuit and 4 output channels dedicated to control the operated switch, as well as, to control the optional equipment that could be used to extend the functionality of the measurement stand (such as: the applied SSR in the hybrid switch, the additional switch S_2 presented in Figure 6.14 and the switch S_2 used to trigger the High Speed Camera, according to Figure 6.17). The detailed parameters of the cycles of the current interruption (such as: the number of the switching operations to performing, the time of the contact separation, the time to give triggering pulse to the semiconductor branch, the duration time of the pulse, the time duration for the open-state and the close-state of the operated switch, etc.) could be introduced into the device by means of a special user interface with a LCD display (see Figure 6.18b). The general block diagram of the microcontroller device is presented in Figure 6.20.

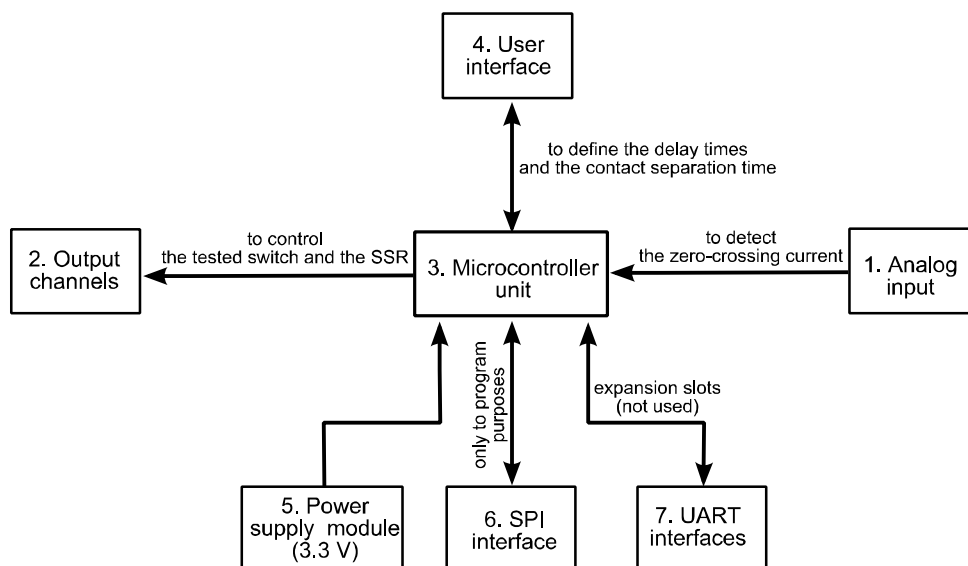


Figure 6.20. *The general block diagram of the microcontroller device*

As show in Figure 6.20, the device consists of the following major components:

1. the analog voltage terminal, which is connected to the internal A-D converter of the microprocessor. The terminal was used to measure voltage signal provided by the current probe, which was applied to measure the instantaneous value of the current flowing in the circuit. Based on this information, the algorithm implemented into the microcontroller is able to detect the current zero-crossing in the tested circuit,
2. the four output channels applied to control external switches. The applied power transistors allow to control external circuit up to 500 V and 21 A (in practice, these channels control the coils of the operated switches at 24 V),
3. the microprocessor unit (ATmega1284-AU),
4. the two terminals applied to control the user interface (the LCD and the buttons, see Figure 6.18b),
5. the power supply module, which allows to supply the device both by the 24 V power supply, as well as, by the 9 V battery,
6. the SPI interface (used only to program the microprocessor),
7. the two UART interfaces, which finally were not used during the researches. These slots were predicted for extension of the device functionality (e.g. to apply the wireless control or to connect the additional sensors).

A view of the microcontroller device used to perform the researches with the major components marked was presented in Figure 6.21.

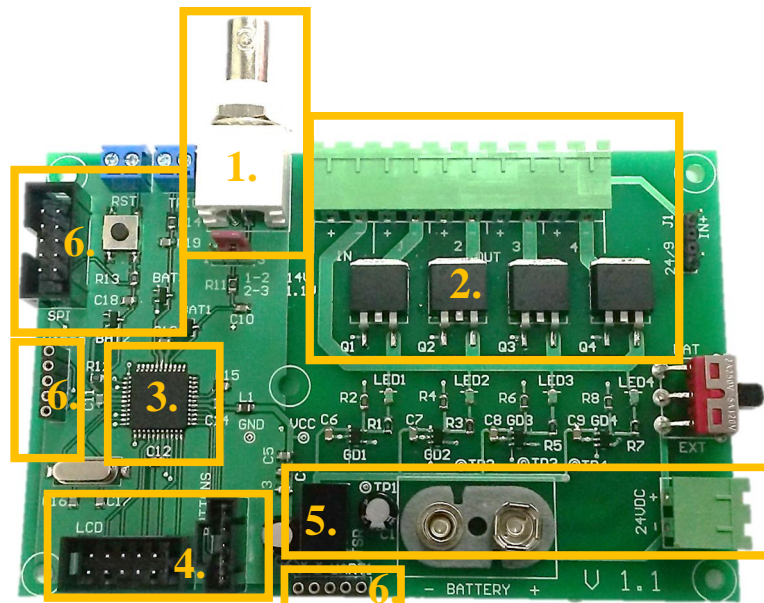


Figure 6.21. The view of the microcontroller device used to perform the researches. The marks were introduced according to Figure 6.20 and the previous description

The detailed electrical diagram showing the connections between the device and other components of the laboratory stand was presented in the section 6.7.3.

6.7.3 Detailed Electrical Diagram of the Laboratory Stand

The detailed electrical schema of the developed laboratory stand used to the performed research is presented in Figure 6.22.

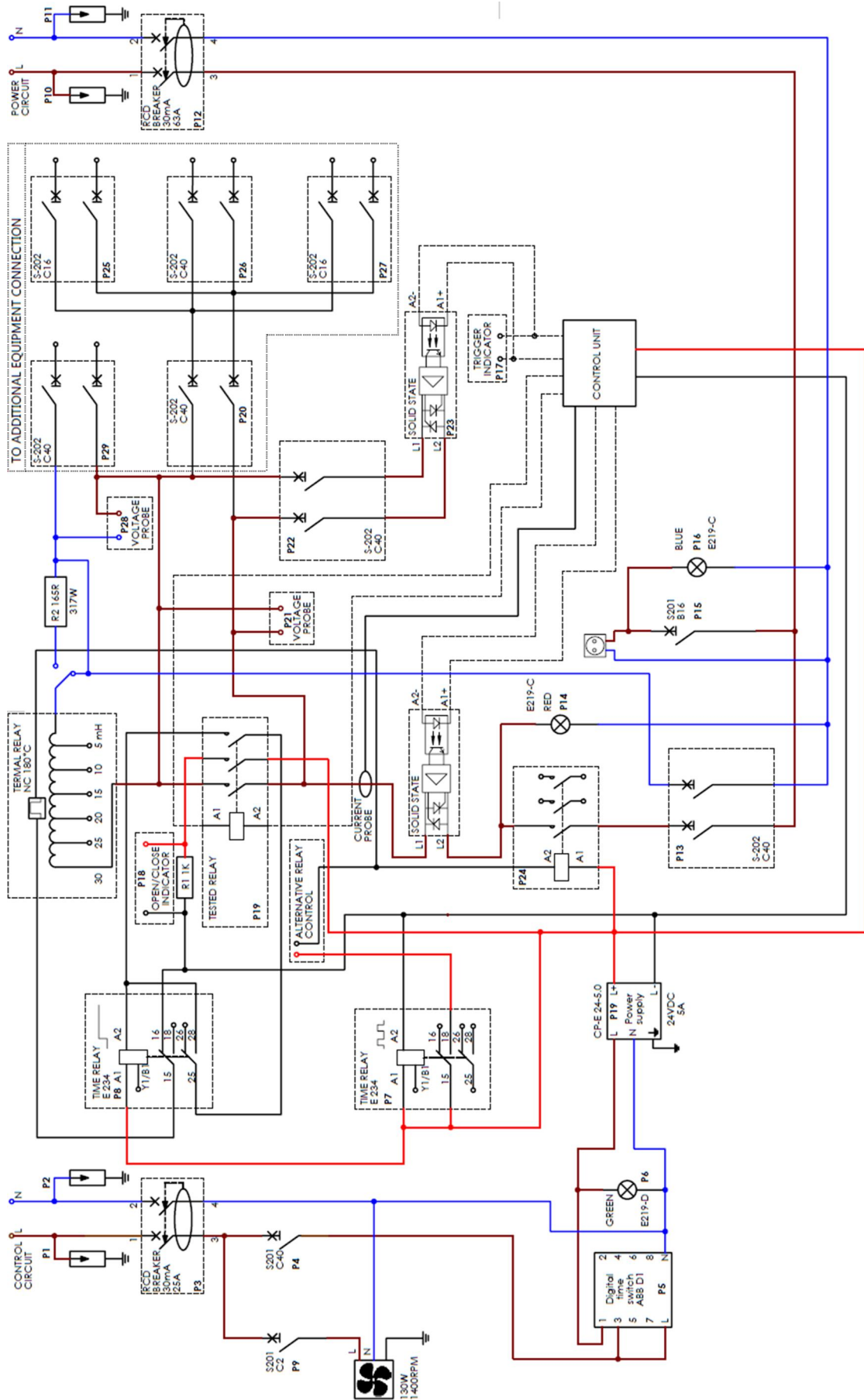


Figure 6.22. The detailed circuit diagram of the laboratory stand

6.7.4 Detailed Technical Data of the Operated Switch

Detailed parameters and utilization characteristics of the switch used to perform researches as the operated switch are listed in Table 6.4.

Table 6.4. *The characteristic of the switch according to the IEC 60947-1 standard*

Rated operational voltage	690 V	
Rated frequency limits	25-400 Hz	
Conventional free-air thermal current I_{th} according to IEC 60947-4-1, open contactors, $\theta \leq 40^\circ\text{C}$ with conductor cross-sectional area	50 A	
	10 mm ²	
AC-1 Utilization category for air temperature close to contactor		
Ie/AC-1 rated operational current Ue max. ≤ 690 V; 50/60 Hz with conductor cross-sectional area	$\theta \leq 40^\circ\text{C}$	50 A
	$\theta \leq 60^\circ\text{C}$	42 A
	$\theta \leq 70^\circ\text{C}$	37 A
	10 mm ²	
AC-3 Utilization category for air temperature close to contactor $\theta \leq 60^\circ\text{C}$ (for 150 r.p.m., 50 Hz or 1800 r.p.m., 60 Hz, 3-phase motors)		
Ie/AC-3 max. rated operational current 3-phase motor	220-240 V	33 A
	380-400 V	32 A
	440 V	32 A
	690 V	21 A
Ie/AC-3 max. rated operational current 1500 r.p.m. 50 Hz 1800 r.p.m. 60 Hz 3-phase motor	220-240 V	9 kW
	380-400 V	15 kW
	415 V	15 kW
	440 V	18.5 kW
	500 V	18.5 kW
	690 V	18.5 kW
Rated making capacity AC-3	10 x Ie AC-33 according to IEC 60947-4-1	
Rated breaking capacity AC-3	8 x Ie AC-33 according to IEC 60947-4-1	
AC-8a utilization category (without thermal overload relay – Ue = 400 V; $\theta \leq 40^\circ\text{C}$)		
Ie/AC-8a rated operational current	40 A	
AC-8a rated operational current	20 kW	
Short-circuit protection for contractors without thermal O/L relay – motor protection excluded Ue ≤ 500 V AC – gG type fuse	63 A	
Rated short-time withstand current Icw At 40°C ambient temperature, in free air from a cold state	1 s	700 A
	10 s	350 A
	30 s	225 A
	1 min	150 A
	15 min	50 A
Maximum breaking capacity cos $\phi = 0.45$	at 440 V	500 A
	at 690 V	200 A
Heat dissipation per pole	Ie/AC-1	2.4 W
	Ie/AC-3	0.9 W
Max. electrical switching frequency	AC-1	600 cycles/h
	AC-3	1200 cycles/h
	AC-2	150 cycles/h
	AC-4	

Detailed dimensions of the analyzed contacts of the operated switch are presented in Figure 6.23.

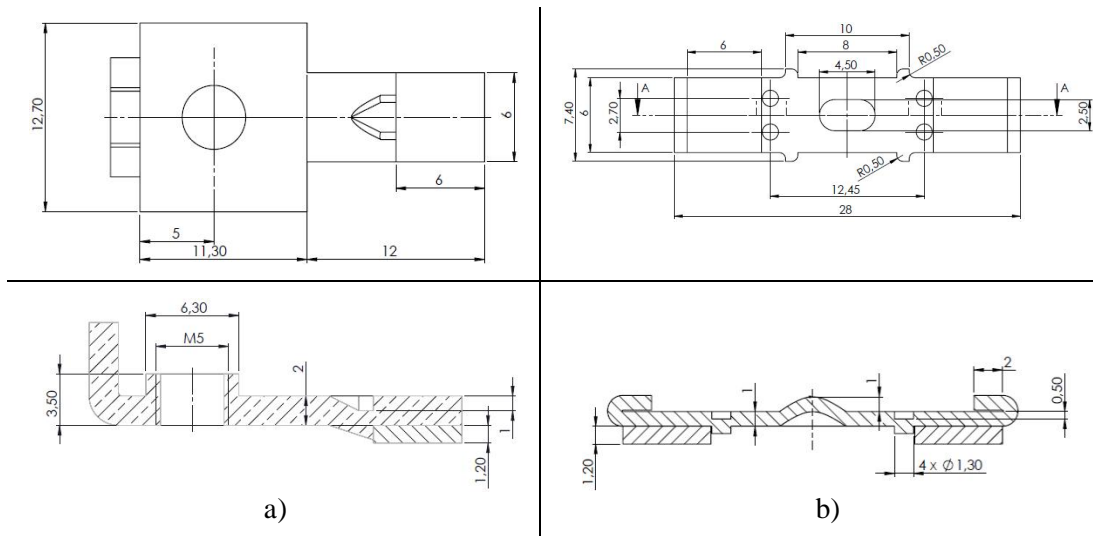


Figure 6.23. The detailed dimensions of the analyzed contacts

6.7.5 Detailed Technical Data of the SSR used to the hybrid application

The electrical parameters of the Solid State Relay, which was used to the researches on the hybrid switching are listed in Table 6.5.

Table 6.5. Electrical parameters of the semiconductor contactor

Output circuit		
Switching element	thyristor	
Rated operation voltage V_e	44-660 V AC	
Period peak inverse voltage (V_{peak})	1200 V _{pp}	
Rated operation current at $T_a = 25^\circ\text{C}$	AC-51	30 A AC
	AC-53a	15 A AC
Operating frequency	45-65 Hz	
Max. off-state leakage current (at V_{max} and $T = 25^\circ\text{C}$)	< 3 mA _{RMS}	
Minimum load current	150 mA	
Max. surge current I_{TSM} ($t = 10$ ms)	400 A	
Max. overcurrent ($t = 1$ s)	< 125 A AC	
Max. load integral $\int i^2 dt$ ($t = 10$ ms)	1800 A ² s	
Conducting state voltage at I_{max} and $T = 25^\circ\text{C}$ (V_{peak})	1.6 A	
Critical gradient di/dt	$\geq 100\text{A}/\mu\text{s}$	
Permissible commutating voltage gradient du/dt	500 V/ μs	
Permissible static voltage gradient du/dt	500 V/ μs	
Input circuit		
Rated control circuit voltage	4-32 V DC	
Make voltage	4.25 V DC	
Inverse voltage	32 V DC	
Break voltage	1 V DC	
Input current (at V_{max})	15 mA	
Turn-on time (max.)	1 period	
Turn-off time (max)	1 period	

7 Measurement Results for the Limitation of the Electric Arc at 12 V

This chapter presents the measurement results of the performed researches on the limitation of the electric arc. The experiments were performed in the tested circuit supplied by the 12 V voltage source. The measurements presented in here were performed according to the detailed description presented in the section 6, for the following scenarios of the researches:

- performing the contact separation of the operated switch at the defined angle of the current period (the detailed description is presented in the section 6.2),
- the connection of the external passive branches in parallel to the operated switch (the detailed description is presented in the section 6.3),
- the application of the hybrid switching (the detailed description is presented in the section 6.4).

The measurement results for the above-mentioned cases are presented respectively in the sections 7.1-7.3. The waveforms of the following magnitudes are presented in this chapter: the measured current, the measured voltage across the entire switch, the calculated electric arc powers, the calculated electric arc energies, the calculated powers generated at external branches connected in parallel to the operated switch, as well as, the calculated energies absorbed by the external branches. The calculations of the electric powers and the energies were performed according to the description presented in the section 6.1.

7.1 Time-Controlled Contact Separation at the Precise Time Slot of the Current Period

The results of the researches on the limitation of the electric arc energy performed by the application of the time-controlled contact separation are presented in this section. The measurements were conducted according to the description presented in the section 6.2. In order to perform the researches, the contact separation was performed at four different angles of the current period, respectively: at 35°, at 90° and at 145°, as well as, just before the natural current zero-crossing (as close as possible due to the dispersion of the mechanical inertia of the switch drive – in practice, the contacts of the operated switch were separated tens of microseconds before the expected current zero-crossing).

The following magnitudes summarizing the measurements are listed in Table 7.1:

- the electric arc times t_{arc} ,
- the maximum observed value of the TRV during the current interruption U_{TRV_max} ,
- the maximum arcing voltage value U_{arc_max} ,
- the maximum value of the power of the electric arc P_{max} (calculated according to the description presented in the section 6.1),
- the maximum value of the electric arc energy E_{arc} (calculated according to the description presented in the section 6.1).

Table 7.1. The measurement results for the considered times of the contact separation – the tested circuit supplied by the 12 V voltage source

The time of the contact separation	t_{arc}	U_{TRV_max}	U_{arc_max}	P_{max}	E_{arc}
[degrees]	[μ s]	[V]	[W]	[mJ]	
Just before 0	53	293	15	1.1	0.1
35	839	571	100	40	25
90	1080	848	130	64	51
145	575	714	30	34	15

As shown in Table 7.1, the electric arc energy is the smallest (even less than 1 mJ) when the contacts of the operated switch start to separate just before the current zero-crossing, whereas the higher value of energy (51 mJ) is observed in the situation, when the contacts are separated at the current extreme. The electric arc energy are comparable when the contacts of the operated switch start to separate at 35° of the current period, as well as, at 145° of the current period (respectively, the electric arc energy is equal 25 mJ and 15 mJ).

The similar trend is also observed for the measured arcing times that are also listed in Table 7.1. The shortest arcing time is observed when the contacts of the operated switch start to separate just before the natural current zero-crossing, whereas, the longest arcing time is noticeable in the situation, when the contacts open during the current extreme.

The measured voltages across the operated switch u_S during the contact separation performed at the considered times are presented in Figure 7.1. The zoomed waveforms of the arcing voltage are presented respectively in Figure 7.5a – Figure 7.8a.

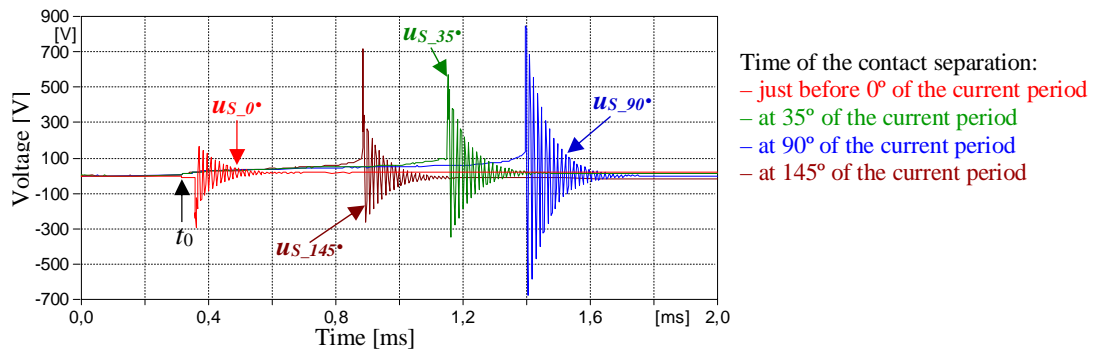


Figure 7.1. The voltages measured across the operated switch for the different times of the contact separation (t_0 – the contact separation time)

As shown in Figure 7.1, as well as, in the zoomed waveforms presented respectively in Figure 7.5a – Figure 7.8a, the maximum values of the arcing voltage depends on the considered time of the contact separation (see also Table 7.1 for details).

In the case, when the contacts of the operated switch start to separate just before the natural current zero-crossing, the arcing voltage $u_{S_0^\circ}$ does not exceed even 20 V. In opposite to this situation, when the contacts are separated at the current extremum, the arcing voltage $u_{S_90^\circ}$ reaches over 130 V (the arcing voltage is over 8 times greater than the maximum peak of the supply voltage during the steady state).

In the cases, when the contacts of the operated switch are separated at 35° of the current period, the electric arc voltage $u_{S_35^\circ}$ achieves 100 V, whereas when the contacts of the operated switch are separated at 145° of the current period, the electric arc voltage $u_{S_145^\circ}$ achieves 30 V.

Significant values of the overvoltages are also observed in the TRV waveform. The maximum registered peak of the TRV exceeds 840 V, which is the value almost 50 times greater in comparison to the maximum peak voltage of the supply voltage at the steady state. Such high values of the observed TRV are caused by the high steepness of the current tending its zero-crossing, which is described in the next part of this section. The frequency of the TRV oscillations is related to the electrical parameters of the tested circuit. Thus, the time of the performed contact separation in relation to the current period does not influence the frequency of the TRV oscillations.

The measured waveforms of the interrupted current i_s during the contact separation performed at the considered times are presented in Figure 7.2. The zoomed current waveforms are presented respectively in Figure 7.5b – Figure 7.8b.

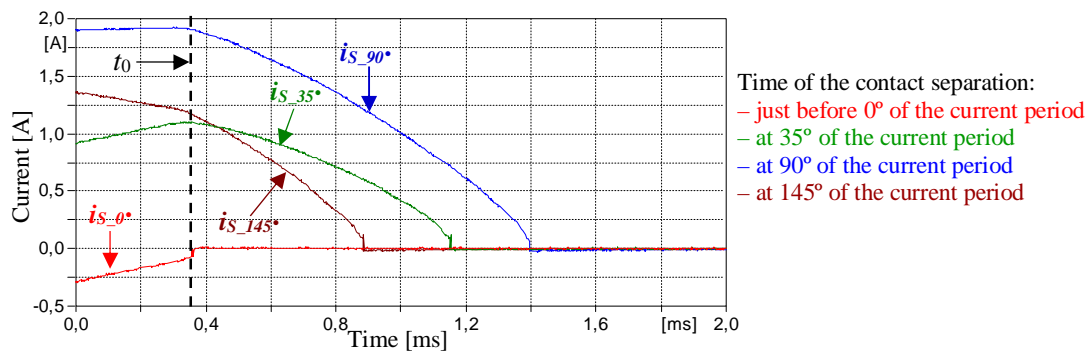


Figure 7.2. The measured currents of the operated switch for the different times of the contact separation (t_0 – the contact separation time)

As shown in Figure 7.2, as well as, in the zoomed waveforms of the interrupted current i_s presented respectively in Figure 7.5b – Figure 7.8b, all curves of the measured currents are strongly deformed and tend to the current zero-crossing very fast (shorter than 1 ms), just after the contact separation time. As it can be observed in the measured waveforms, a strong steepness of the current i_s (over 40 A/ms) appears between the time of the contacts separation and before the current zero-crossing. Such a high the di_s/dt steepness causes significant switching overvoltages to generate, which can be observed in the arcing voltage, as well as, in the TRV peaks in Figure 7.1. This phenomenon is related to the weak ionization conditions of the gas localized between the separated contacts of the operated switch: the relatively small value of the electric field, as well as, the small instantaneous value of the interrupting current i_s , insufficient to achieve the significant temperature rise between the contact surface, which is necessary to obtain the powerful gas ionization (according to the description presented in the chapter 3). As a consequence, it leads to create the significant electric arc resistance that influences the high arcing voltage.

As it can be observed in Figure 7.2, the electric arc is quenched almost immediately when the contacts of the operated switch are separated just before the natural current zero-crossing. In opposite to this situation, the electric arc burns the longest, when the contacts start to separate at the current extremum. The difference in the measured arcing times, for the situations when the contacts are separated at 35° and at 145° of the current period is less than 300 μ s. However, the arcing time takes longer while the contacts open at the time, when the current increases just before the contact separation (at 35° of the current period).

The waveforms of the electric arc power calculated for the considered times of the contact separation are presented in Figure 7.3. The calculations were performed according to the description presented in the section 6.1.2. The zoomed waveforms of the electric arc power are presented respectively in Figure 7.5c – Figure 7.8c.

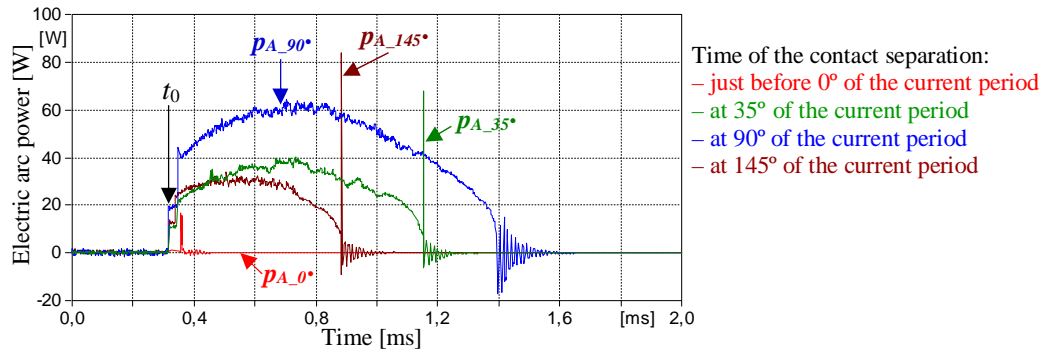


Figure 7.3. The calculated electric arc powers for the different times of the contact separation (t_0 – the contact separation time)

As shown in Figure 7.3, as well as, in the zoomed waveforms of the electric arc power p_A presented respectively in Figure 7.5c – Figure 7.8c, the electric arc power $p_{A_0^\circ}$ appears only for the short time (less than 60 μ s) when the contacts are separated just before the current zero-crossing. In this case, the power curve is similar in the shape to a single peak whose value is below 20 W. For other considered cases, the waveforms of the power curves are very similar in the shape. The greater values of the electric arc power are observed for the cases when the contacts start to separate respectively at 90°, 35°, 145°, and just before 0° of the current period. In the calculated waveforms of the electric powers, the oscillations caused by the TRV can be observed just after the current zero-crossing due the measured negligible values of the current i_s , which were caused by the measurement inaccuracy of the applied current probe.

The waveforms of the electric arc energy calculated for the considered times of the contact separation are presented in Figure 7.4. The calculations were performed according to the description presented in the section 6.1.2. The zoomed waveforms of the electric arc energy e_A are presented respectively in Figure 7.5d – Figure 7.8d.

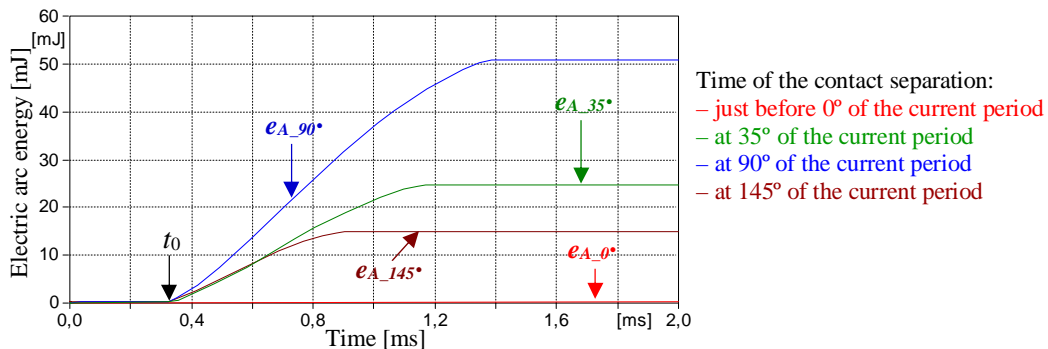


Figure 7.4. The electric arc energies calculated for the different times of the contact separation

As shown in Figure 7.4, as well as, in the zoomed waveforms of the electric arc energy presented respectively in Figure 7.5d – Figure 7.8d, the greater values of the electric arc power were calculated for the situations when contacts are separated respectively at 90°, at 35°, at 145°, and just before the zero-crossing of the current period.

Thus, it can be concluded that the most favorable conditions for the current interruption occur in the tested circuit supplied by the 12 V voltage source, when the contacts of the operated switch start to separate just before the current zero-crossing. Only in this situation, the electric arc energy is negligible, which can have only slightly influence on creating the arc erosion in the contact surfaces. The best conditions for the current interruption are precisely at the current zero-crossing. However, due to the dispersion of the mechanical inertia of the operated

switch, this situation is very difficult to achieve in the practice. The electric arc energy is the greatest, when the contacts of the operated switch open during the current extreme of the interrupted current. In this situation, the electric arc energy is generated in the considerable amount, which can influence on the significant creation of the electric arc erosion.

The zoomed waveforms of the voltage measured across the switch, the interrupted current, the electric arc power and the electric arc energy for considered times of the contact separation are presented in the sections 7.1.1 – 7.1.4. The key instants were marked in waveforms:

- t_0 – the time, when the contacts of the operated switch start to separate,
- t_1 – the time, when the electric arc was quenched,
- t_2 – the time, when the steady state voltage appears between the contacts of operated switch after the end of the TRV.

7.1.1 Contact Separation just before the Natural Zero-Crossing of the Current Period

In this section, the detailed waveforms are presented for the situation, when the contacts of the operated switch start to separate just before the natural zero-crossing of the current period. The detailed waveforms of the measured voltage across the operated switch $u_{S,0^\circ}$, the interrupted current $i_{S,0^\circ}$, the electric arc power $p_{A,0^\circ}$, as well as, the electric arc energy $e_{A,0^\circ}$ during the contact separation performed just before the natural current zero-crossing of the current period are presented in Figure 7.5.

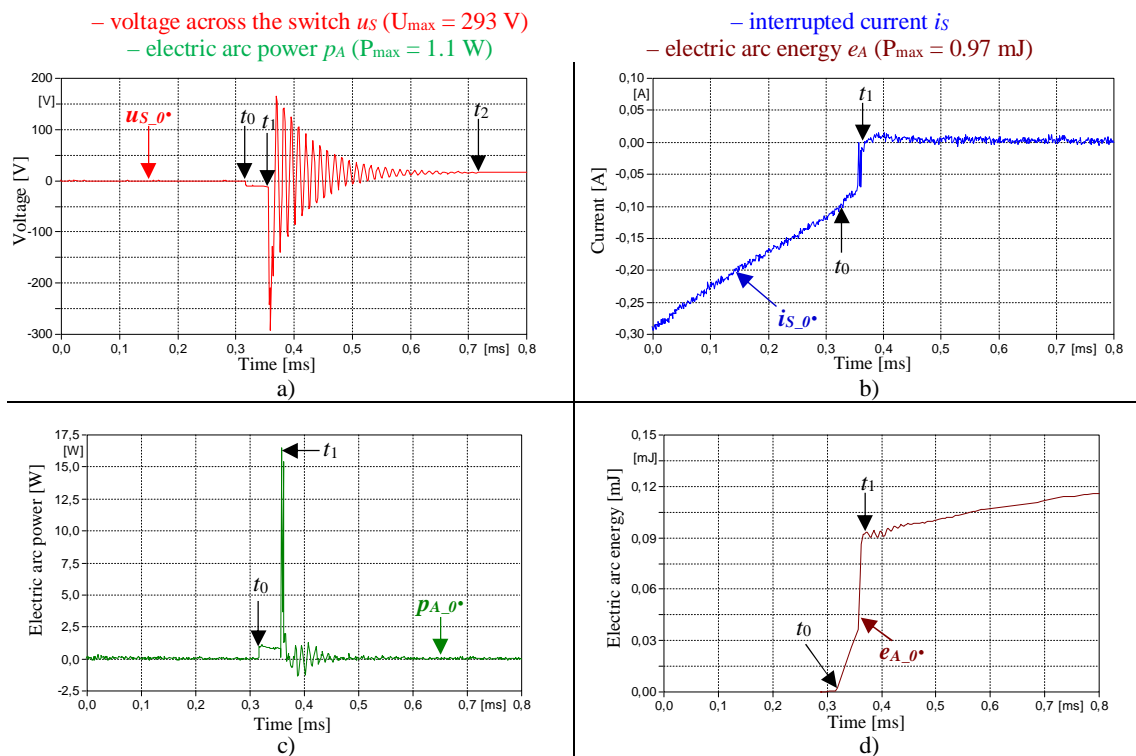


Figure 7.5. Contact separation just before the natural current zero-crossing : the measured voltage across the operated switch (a), the current of the operated switch (b), the calculated electric arc power (c), the electric arc energy (d)

7.1.2 Contact Separation at 35° of the Current Period

The detailed waveforms of the measured voltage across the operated switch $u_{S,35^\circ}$, the interrupted current $i_{S,35^\circ}$, the electric arc power $p_{A,35^\circ}$, as well as, the electric arc energy $e_{A,35^\circ}$, when the contacts of the operated switch start to separate at 35° of the current period are presented in Figure 7.6.

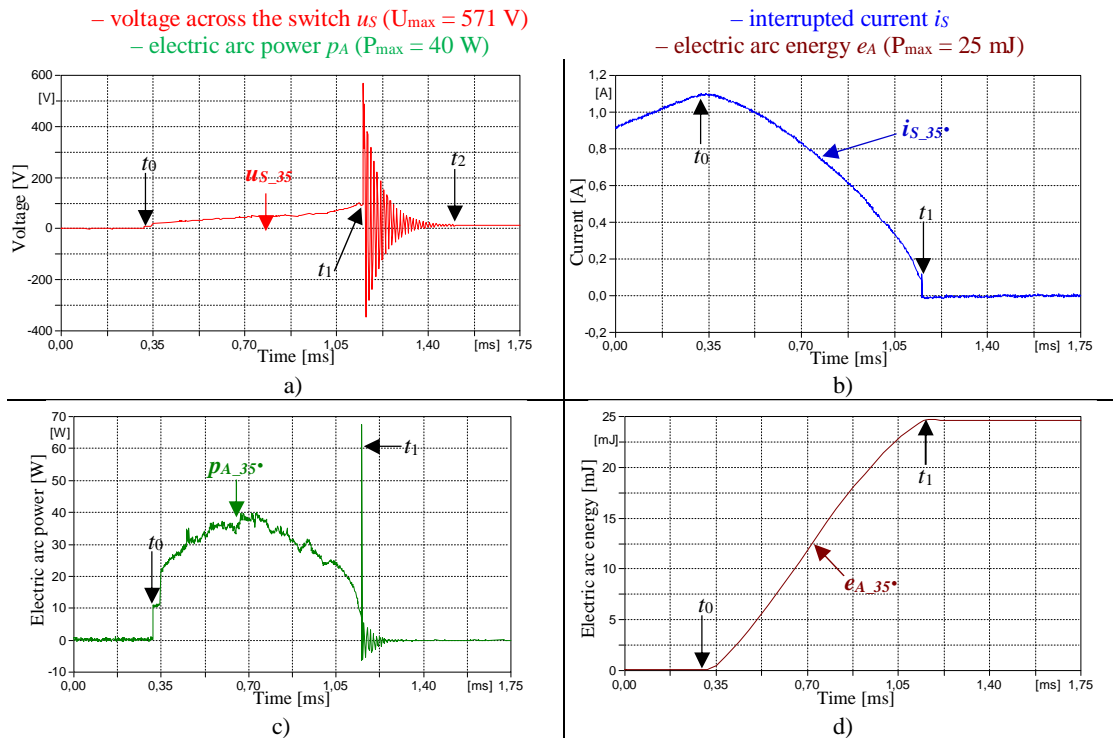


Figure 7.6. Contact separation at 35° of the current period: the measured voltage across the operated switch (a), the current of the operated switch (b), the calculated electric arc power (c), the electric arc energy (d)

7.1.3 Contact Separation at 90° of the Current Period

The detailed waveforms for the situation, when the contacts of the operated switch start to separate at 90° of the current period are presented in Figure 7.7.

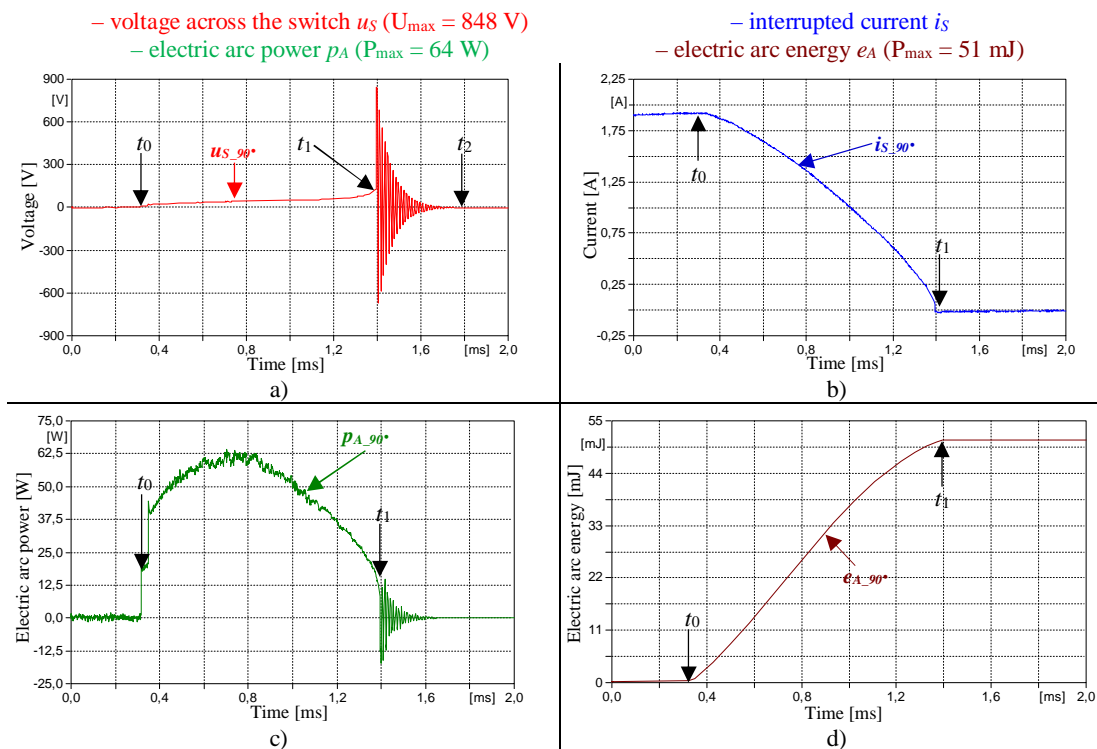


Figure 7.7. Contact separation at 90° of the current period: the measured voltage across the operated switch (a), the current of the operated switch (b), the calculated electric arc power (c), the electric arc energy (d)

7.1.4 Contact Separation at 145° of the Current Period

The detailed waveforms of the measured voltage across the operated switch $u_{S_{145^\circ}}$, the interrupted current $i_{S_{145^\circ}}$, the electric arc power $p_{A_{145^\circ}}$, as well as, the electric arc energy $e_{A_{145^\circ}}$, when the contacts of the operated switch start to separate at 145° of the current period are presented in Figure 7.8.

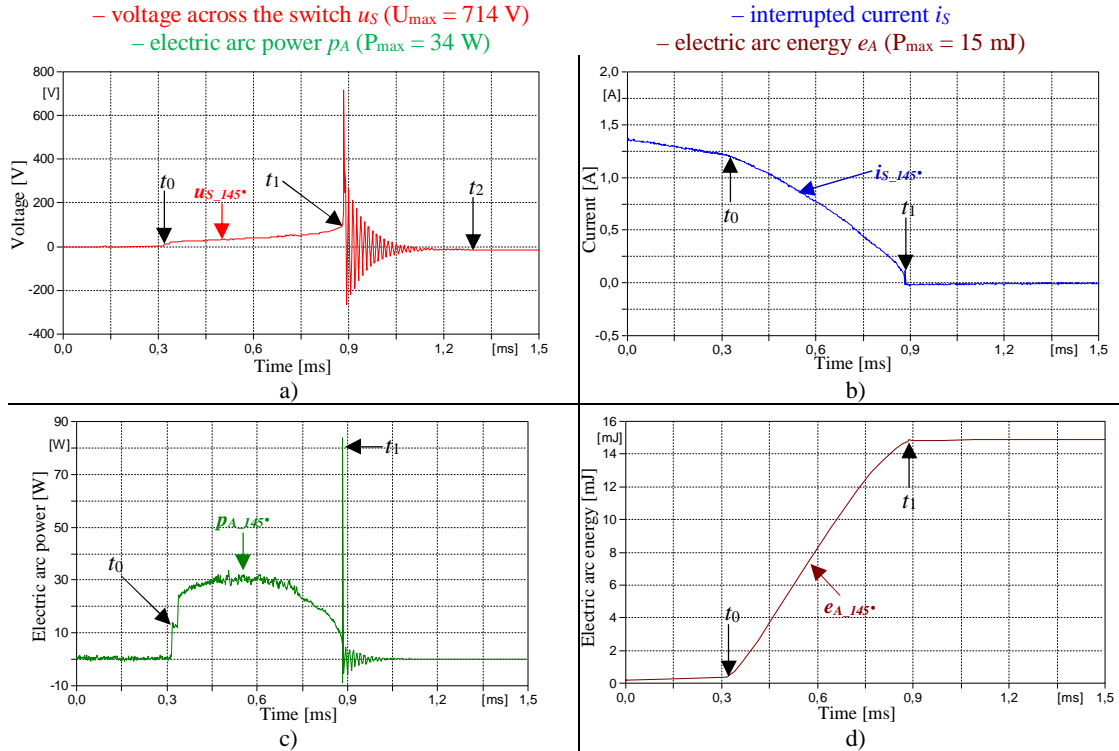


Figure 7.8. Contact separation at 145° of the current period: the measured voltage across the operated switch (a), the current of the operated switch (b), the calculated electric arc power (c), the electric arc energy (d)

7.2 Connection of the Passive Branches in Parallel to the Operated Switch

In this section, the measurement results are presented for limiting the electric arc energy by means of the connection of the different passive branches in parallel to the operated switch. In order to perform the researches, the following branches were connected in parallel to the operated switch:

- RC arc suppressor,
- Voltage-Dependent Resistor (VDR),
- Transient Voltage Suppressor (TVS),
- Zener Voltage Limiter (ZVL).

The researches were performed in the tested circuit supplied by the 12 V voltage source for the situation, when the contacts of the operated switch start to separate at 90° of the current period. This case was chosen to the researches due to the greater value of the electric arc energy, based on the measurement results presented in the section 7.1.

Thus, the effectiveness of the limitation of the electric arc was investigated in the tested circuit for the different external branches connected in parallel to the operated switch. The detailed description of the research plan was presented in the section 6.2.

In the course of the measurements, the following magnitudes were measured: the voltage across the operated switch u_S , the current of the operated switch i_S and the current commuted into the external branch during the current interruption i_B . Based on these magnitudes, the following waveforms were calculated and presented in this section: the electric arc power e_A , the electric arc energy e_B , the power generated at the parallel branches p_B and the energy absorbed by the parallel branches e_B . The above-mentioned waveforms are presented in this section for each considered method limiting the electric arc.

The key instants were marked in all presented waveforms in this section:

- t_0 – the time, when the contacts of the operated switch start to separate and the electric arc starts to burn,
- t_1 – the time, when the electric arc was quenched,
- t_2 – the time, when the steady state voltage appears between the contacts of operated switch after the end of the TRV.

7.2.1 RC Arc Suppressor

In order to determine the influence of the RC suppressor connected in parallel to the operated switch on the level of the electric arc energy, the researches were performed. For this purpose, the RC suppressor was connected in parallel to the operated switch according to Figure presented in Table 6.1 (row 1). The parameters of the RC suppressor are also listed in Table 6.1 (row 1).

A waveform of the current flowing through the operated switch $i_{S_RC_90^\circ}$, a waveform of the current commuted into the parallel branch with the RC suppressor $i_{B_RC_90^\circ}$, as well as, a waveform of the measured voltage across the operated switch during the current interruption $u_{S_RC_90^\circ}$ are presented in Figure 7.9.

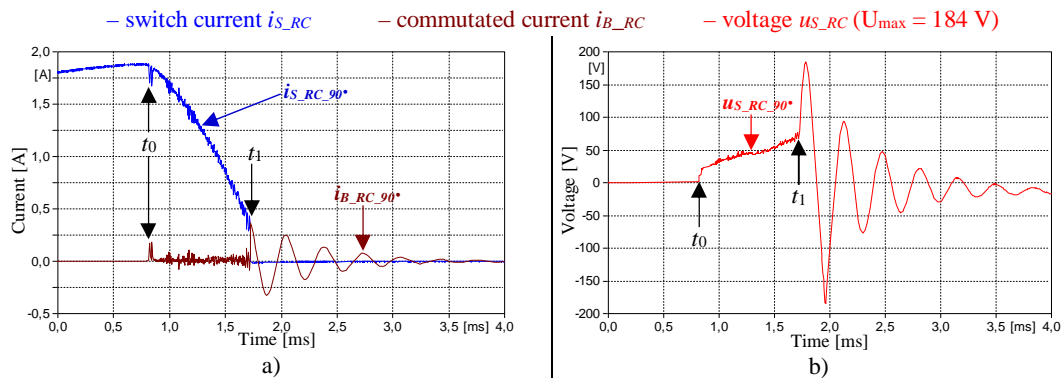


Figure 7.9. The measured currents (a), the measured voltage across the operated switch (b).
The RC suppressor is connected in parallel to the operated switch

As shown in Figure 7.9, the application of the RC suppressor limits the arcing voltage, the arcing time, as well as, the overvoltages of the TRV in comparison to the situation, when the current was interrupted by the standalone switch (Figure 7.7). The measured differences in the waveforms can be observed in Figure 7.10, where the waveforms of the currents and the voltages are presented for both analyzed cases.

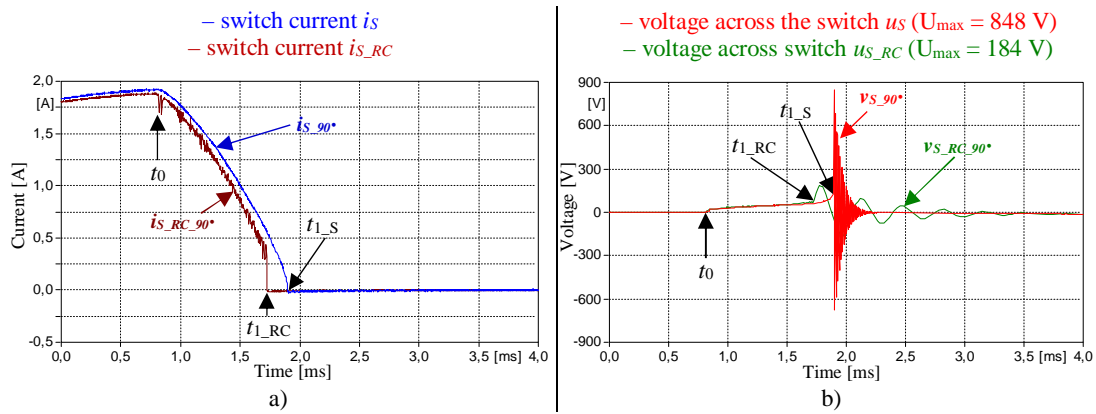


Figure 7.10. The measured current waveforms (a) and measured voltages across the operated switch (b) when the operated switch interrupts current as the standalone one, as well as, when the RC suppressor is connected in parallel to the operated switch

As shown in Figure 7.10a, the connection of the RC suppressor in parallel to the operated switch changes the shape of the current $i_{S_90^\circ}$ waveform. The small oscillations related to arcing voltage are reflected in the interrupting current $i_{S_RC_90^\circ}$, and the current of the operated switch $i_{S_RC_90^\circ}$ is chopped just before its current zero-crossing. When the operated switch interrupts the current $i_{S_90^\circ}$ as the standalone one, the maximum arcing voltage reaches over 130 V. The connection of the parallel RC suppressor causes limitation of the electric arc voltage up to about 75 V (about 42%), and the peak value of the TRV is also limited (from 848 V to 184 V, thus over 4 times), which can be observed in Figure 7.10b. Connecting the RC suppressor in parallel to the operated switch causes also a decrease of the frequency of the TRV oscillations. This is caused by the presence of the additional capacitance connected between the contacts of the operated switch. The arcing time is shorter in the situation, when the RC suppressor is connected to the operated switch (the decrease from 1080 μ s to 912 μ s was observed).

In order to determine the influence of the connection of the RC suppressor in parallel to the operated switch on the limitation of the electric arc, the following waveforms were calculated: the electric arc power $p_{A_RC_90^\circ}$, the electric arc energy $e_{A_RC_90^\circ}$, the power generated at the RC suppressor $p_{B_RC_90^\circ}$, as well as, the energy absorbed by the RC suppressor $e_{B_RC_90^\circ}$. The waveforms of the above-mentioned magnitudes are presented in Figure 7.11. The calculations were performed according to the description presented in the section 6.1.2.

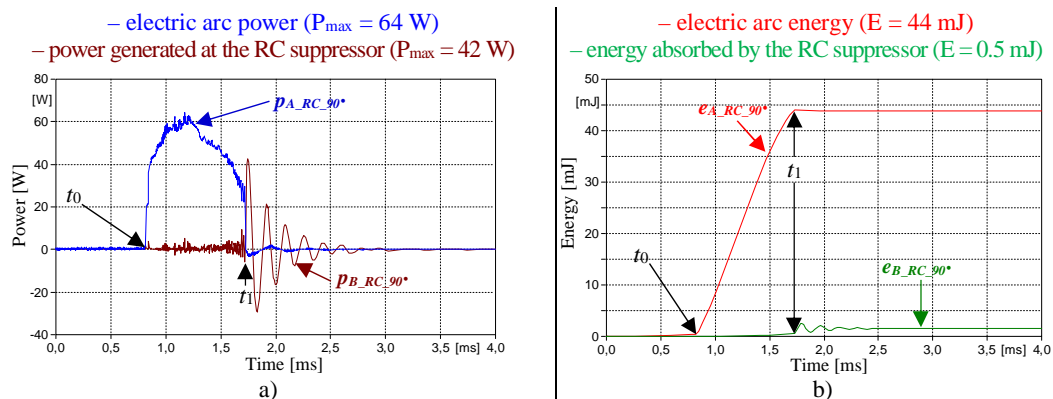


Figure 7.11. The calculated waveforms of the electric arc power, and the power generated at the RC suppressor (a), the calculated waveforms of the arc energy and the energy absorbed by the RC suppressor (b) during the current interruption process

As shown in Figure 7.11, connecting the RC suppressor to the operated switch does not influence peak of the electric arc power $p_{A_RC_90^\circ}$ (in the base case it is also 64 W). However,

the application of the RC suppressor impacts the increase of the steepness of the electric arc power $p_{A_RC_90^\circ}$ that tends faster to its zero-crossing. The application of the considered method impacts the limitation of the electric arc energy $e_{A_RC_90^\circ}$ (the reduction from 51 mJ to 44 mJ, about 14%).

7.2.2 Voltage-Dependent Resistor (VDR)

The next examined method applied to the passive limitation of the electric arc is based on the connection of the Voltage-Dependent Resistor (VDR) in parallel to the operated switch, according to Figure presented in Table 6.1 (row 2). The parameters of the applied VDR are also listed in Table 6.1.

A waveform of the current flowing through the operated switch $i_{S_VDR_90^\circ}$, a waveform of the current commuted into the parallel VDR $i_{B_VDR_90^\circ}$, as well as, a waveform of the measured voltage across the operated switch during the current interruption $u_{S_VDR_90^\circ}$ are presented in Figure 7.12

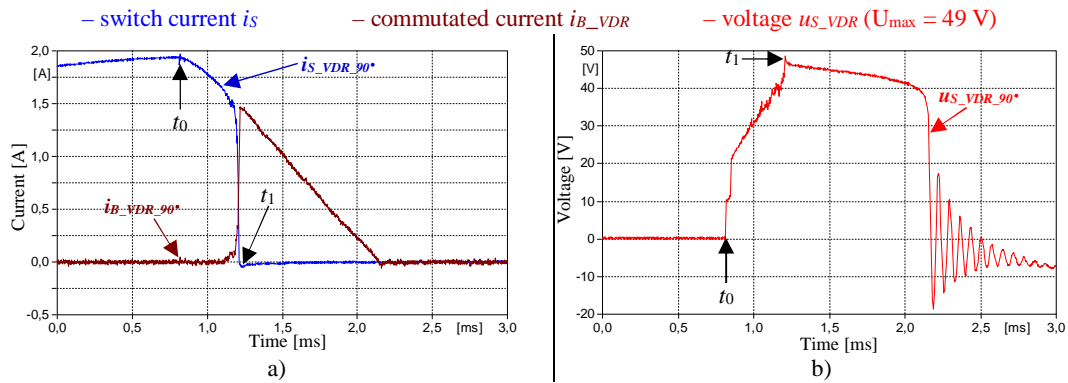


Figure 7.12. The measured currents (a), the measured voltage across the operated switch (b), the VDR is connected in parallel to the operated switch

As shown in Figure 7.12, the application of the VDR limits the arcing voltage, the arcing time, as well as, the overvoltages of the TRV in comparison to the situation, when the current was interrupted by the standalone switch (Figure 7.7). The measured differences in the waveforms can be observed in Figure 7.13, where the waveforms of the currents and the voltages are presented for both analyzed cases.

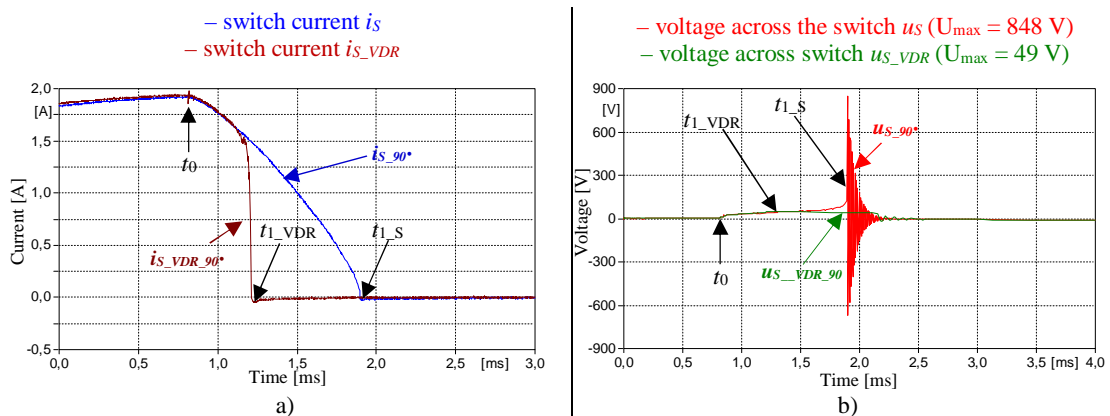


Figure 7.13. The measured current waveforms (a) and measured voltages across the operated switch (b) when the operated switch interrupts current as standalone one, as well as, when the VDR is connected in parallel to the operated switch

As shown in Figure 7.13a, the connection of the VDR in parallel to the operated switch changes the shape of the current $i_{S_VDR_90^\circ}$ waveform significantly. As it can be visible in the current waveform $i_{S_VDR_90^\circ}$, the current of the operated switch tends to the zero-crossing with

a high steepness below of the value 1.5 A of the interrupted current. When the operated switch interrupts the current $i_{S_90^\circ}$ as the standalone one, the arcing voltage reached over 130 V. The application of the parallel VDR causes the electric arc voltage to limit up to about 49 V (about 62%), the peak value of the TRV is also limited (from 848 V to 19 V, thus over 44 times). Connecting the VDR in parallel to the operated switch causes the frequency of the TRV oscillations to decrease. This could be achieved, because the energy stored in the inductive load can be discharged through the conducting VDR, which limits the TRV. The arcing time is shorter in the situation, when the VDR is connected to the operated switch (the decrease from 1080 μ s to 413 μ s).

In order to determine the influence of the connection of the VDR in parallel to the operated switch on the limitation of the electric arc, the following waveforms were calculated: the electric arc power $p_{A_VDR_90^\circ}$, the electric arc energy $e_{A_VDR_90^\circ}$, the power generated at the VDR $p_{B_VDR_90^\circ}$, as well as, the energy absorbed by the VDR $e_{B_VDR_90^\circ}$. The waveforms of the above-mentioned magnitudes are presented in Figure 7.14. The calculations were performed according to the description presented in the section 6.1.2.

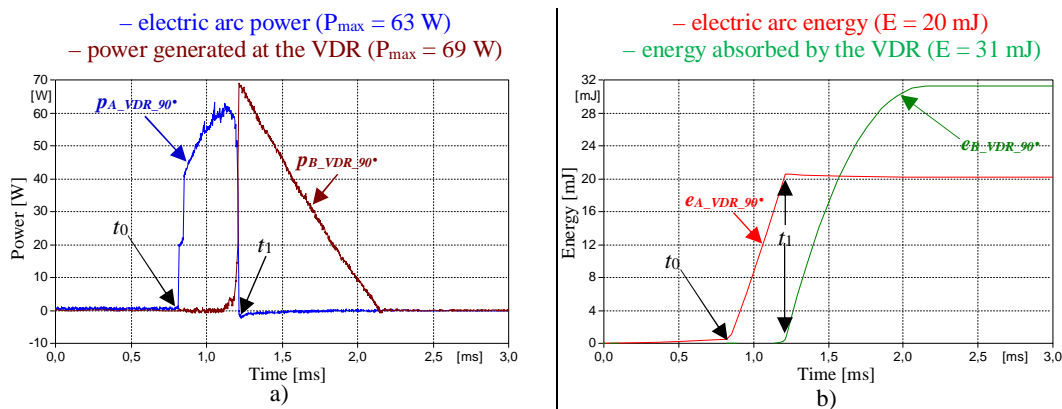


Figure 7.14. The calculated waveforms of the electric arc power, and the power generated at the VDR (a), the calculated waveforms of the arc energy and the energy absorbed by the VDR (b) during the current interruption process

As shown in Figure 7.14, connecting the VDR to the operated switch does not influence on peak of the electric arc power (in the base case it is also 64 W). However, the application of the VDR impacts the increase of the steepness of the electric arc power that tends fast to its zero-crossing. When the arcing voltage exceeds the minimal operating voltage of the VDR, the current of the operated switch $i_{S_VDR_90^\circ}$ rapidly starts to commute into the VDR branch, which can be observed in the waveforms presented in Figure 7.14a. The peak value of the power generated at the VDR branch $p_{B_VDR_90^\circ}$ exceeds the peak value of the electric arc power $p_{A_VDR_90^\circ}$. The application of the considered method impacts the limitation of the electric arc energy (the reduction from 51 mJ to 20 mJ, about 61%).

7.2.3 Transient Voltage Suppressor (TVS)

Another examined method to passive limitation of the electric arc is the connection of the Transient Voltage Suppressor (TVS) in parallel in the operated switch according to Figure presented in Table 6.1 (row 3). The parameters of the applied TVS are also listed in Table 6.1.

A waveform of the current flowing through the operated switch $i_{S_TVS_90^\circ}$, a waveform of the current commuted into the parallel TVS $i_{B_TVS_90^\circ}$, as well as, a waveform of the measured voltage across the operated switch during the current interruption $u_{S_VDR_90^\circ}$ are presented in Figure 7.15.

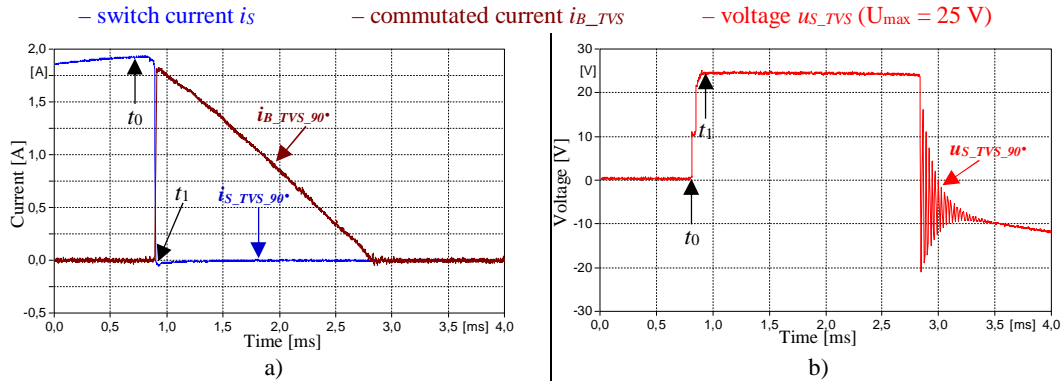


Figure 7.15. The measured currents (a), the measured voltage across the operated switch (b). The TVS is connected in parallel to the operated switch

As shown in Figure 7.15, the application of the Transient Voltage Suppressor (TVS) limits the arcing voltage, the arcing time, as well as, the overvoltages of the TRV in comparison to the situation, when the current $i_{S_90^\circ}$ was interrupted by the standalone switch (Figure 7.7). The measured differences in the waveforms can be observed in Figure 7.16, where the waveforms of the currents and the voltages are presented for the both analyzed cases.

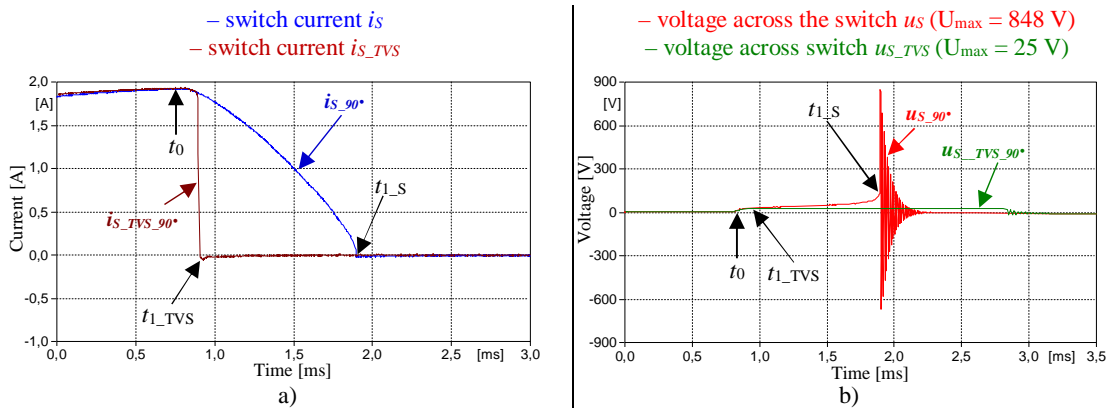


Figure 7.16. The measured current waveforms (a) and measured voltages across the operated switch (b) when the operated switch interrupts current as standalone one, as well as, when the TVS is connected in parallel to the operated switch

As shown in Figure 7.16a, the connection of the TVS in parallel to the operated switch changes the shape of the current waveform $i_{S_TVS_90^\circ}$ significantly. As it can be visible in the current waveform, the current of the operated switch $i_{S_TVS_90^\circ}$ reaches its zero-crossing almost immediately after the contact separation. When the operated switch interrupts the current $i_{S_90^\circ}$ as the standalone one, the arcing voltage reaches over 130 V. The application of the parallel TVS causes to limit the electric arc voltage up to about 25 V (about 80%), the peak value of the TRV is also limited (from 848 V to 21 V, thus over 40 times). Connecting the TVS in parallel to the operated switch causes the frequency of the TRV oscillations to decrease. This could be achieved, because the energy stored in the inductive load can be discharged through the conducting TVS, which limits the TRV. The arcing time is shorter in the situation, when the TVS is connected to the operated switch (the decrease from 1080 μ s to 89 μ s).

In order to determine an influence of the connection of the TVS in parallel to the operated switch on the limitation of the electric arc, the following waveforms were calculated: the electric arc power $p_{A_TVS_90^\circ}$, the electric arc energy $e_{A_TVS_90^\circ}$, the power generated at the TVS $p_{B_TVS_90^\circ}$, as well as, the energy absorbed by the TVS $e_{B_TVS_90^\circ}$. The waveforms of the above-mentioned magnitudes are presented in Figure 7.17. The calculations were performed according to the description presented in the section 6.1.2.

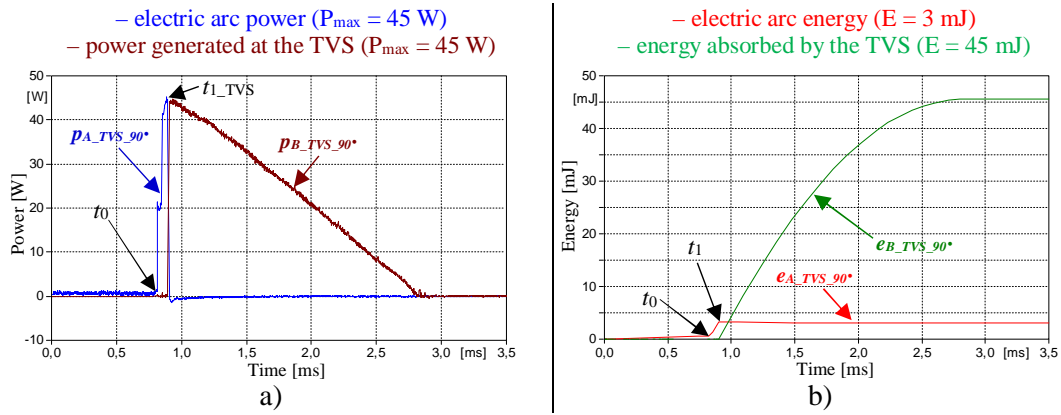


Figure 7.17. The calculated waveforms of the electric arc power, and the power generated at the TVS (a), the calculated waveforms of the arc energy and the energy absorbed by the TVS (b) during the current interruption process

As shown in Figure 7.17, the application of the VDR impacts the increase of the steepness of the electric arc power $p_{A_TVS_90^\circ}$ that tends almost immediately to its zero-crossing after the contact separation. When the arcing voltage exceeds the minimal operating voltage of the TVS, the current of the operated switch rapidly starts to commute into the TVS branch, which can be observed in the waveforms presented in Figure 7.17a. The peak value of the power generated at the TVS branch $p_{B_TVS_90^\circ}$ is at the same level in comparison to the electric arc power $p_{A_TVS_90^\circ}$. The application of the considered method impacts the limitation of the electric arc energy (the reduction from 51 mJ to 3 mJ, so about 94%).

7.2.4 Zener Voltage Limiter (ZVL)

Another examined method to limit the electric arc is the connection of the Zener Voltage Limiter (ZVL) in parallel to the operated switch. The applied branch consists of two ZVLs connected in series, according to Figure presented in Table 6.1 (row 4). The parameters of the applied ZVLs are also listed in Table 6.1.

A waveform of the current flowing through the operated switch, $i_{S_ZVL_90^\circ}$ a waveform of the current commuted into the parallel ZVL $i_{B_ZVL_90^\circ}$, as well as, a waveform of the measured voltage across the operated switch during the current interruption $u_{S_ZVL_90^\circ}$ are presented in Figure 7.18.

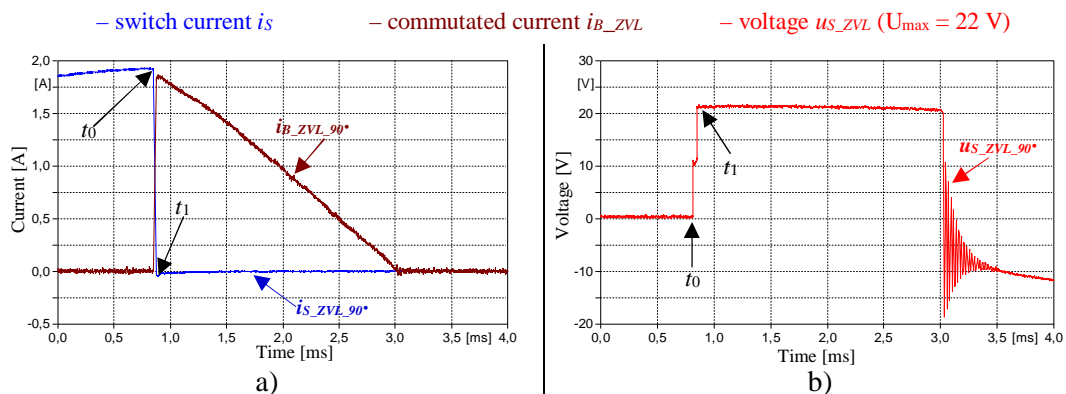


Figure 7.18. The measured currents (a), the measured voltage across the operated switch (b). The ZVL is connected in parallel to the operated switch

As shown in Figure 7.18, the application of the Zener Voltage Limiter (ZVL) limits the arcing voltage, the arcing time, as well as, the overvoltages of the TRV in comparison to the situation, when the current $i_{S_90^\circ}$ was interrupted by the standalone switch (Figure 7.7). The measured

differences in the waveforms can be observed in Figure 7.19, where the waveforms of the currents and the voltages are presented for the both analyzed cases.

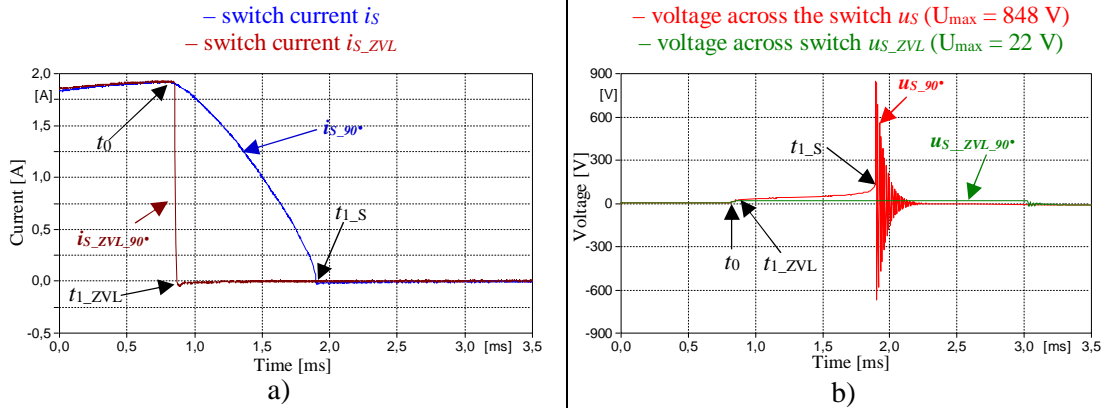


Figure 7.19. The measured current waveforms (a) and measured voltages across the operated switch (b) when the operated switch interrupts current as the standalone one, as well as, when the ZVL is connected in parallel to the operated switch

As shown in Figure 7.19a, the connection of the ZVL in parallel to the operated switch changes the shape of the current waveform $i_{s_ZVL_90^\circ}$ significantly. As it can be visible in the current waveform, the current of the operated switch $i_{s_ZVL_90^\circ}$ reaches its zero-crossing almost immediately after the contact separation. When the operated switch interrupts the current $i_{s_90^\circ}$ as the standalone one, the arcing voltage reaches over 130 V. The application of the parallel ZVL causes the limitation of the electric arc voltage up to about 22 V (about 83%), the peak value of the TRV is also limited (from 848 V to 19 V, thus over 44 times). Connecting the ZVL in parallel to the operated switch causes the frequency of the TRV oscillations to decrease. This could be achieved, because the energy stored in the inductive load can be discharged through the conducting ZVL, which limits the TRV. The arcing time is shorter in the situation, when the ZVL is connected to the operated switch (the decrease from 1080 μ s to 55 μ s).

In order to determine the influence of the connection of the ZVL in parallel to the operated switch on the limitation of the electric arc, the following waveforms were calculated: the electric arc power $p_{A_ZVL_90^\circ}$, the electric arc energy $e_{A_ZVL_90^\circ}$, the power generated at the ZVL $p_{B_ZVL_90^\circ}$, as well as, the energy absorbed by the ZVL $e_{B_ZVL_90^\circ}$. The waveforms of the above-mentioned magnitudes are presented in Figure 7.18. The calculations were performed according to the description presented in the section 6.1.2.

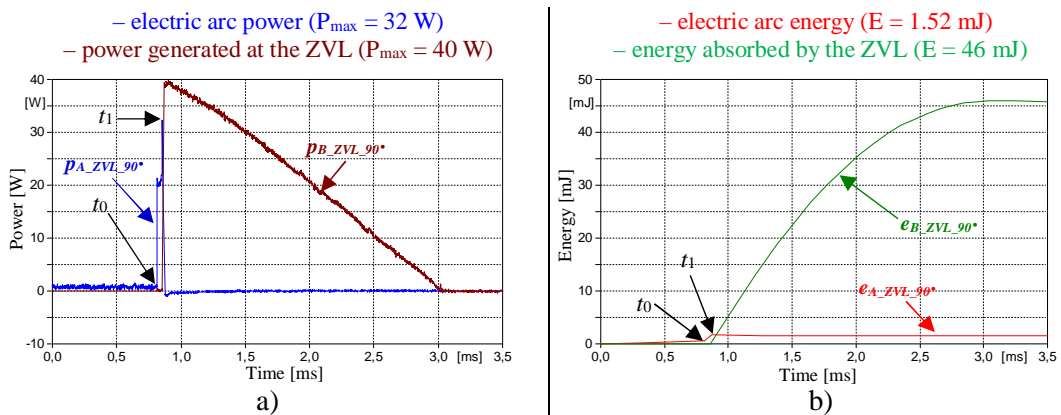


Figure 7.20. The calculated waveforms of the electric arc power, and the power generated at the ZVL (a), the calculated waveforms of the arc energy and the energy absorbed by the ZVL (b) during the current interruption process

As shown in Figure 7.20, the application of the ZVL impacts the increase of the steepness of the electric arc power $p_{A_ZVL_90^\circ}$ that tends almost immediately to its zero-crossing after the contact separation. When the arcing voltage exceeds the minimal operating voltage of the ZVL, the current of the operated switch $i_{S_ZVL_90^\circ}$ rapidly starts to commute into the ZVL branch, which can be observed in the waveforms presented in Figure 7.20a. The peak value of the electric arc power $p_{A_ZVL_90^\circ}$ is limited in this case (from 64 W for standalone switch to 32 W in here). The application of the considered method impacts the limitation of the electric arc energy (the reduction from 51 mJ to about 1.5 mJ, so about 97%).

7.3 Hybrid Switching

According to the description presented in the section 6.1.2, the researches on the limitation of the electric arc were performed for the hybrid switching. This method is based on the connection of the semiconductor branch in parallel to the operated switch. The semiconductor branch is fully controlled by the microcontroller system. The detailed description of the hybrid switching is presented in the section 6.4. The measurements results for researches performed within this method in the tested circuit supply by the 12 V voltage source are presented in this section.

A waveform of the current flowing through the operated switch $i_{S_HS_90^\circ}$, a waveform of the current commuted into the semiconductor branch $i_{B_HS_90^\circ}$, as well as, a waveform of the measured voltage across the entire operated switch $u_{S_HS_90^\circ}$ with connected the semiconductor branch during the current interruption are presented in Figure 7.21.

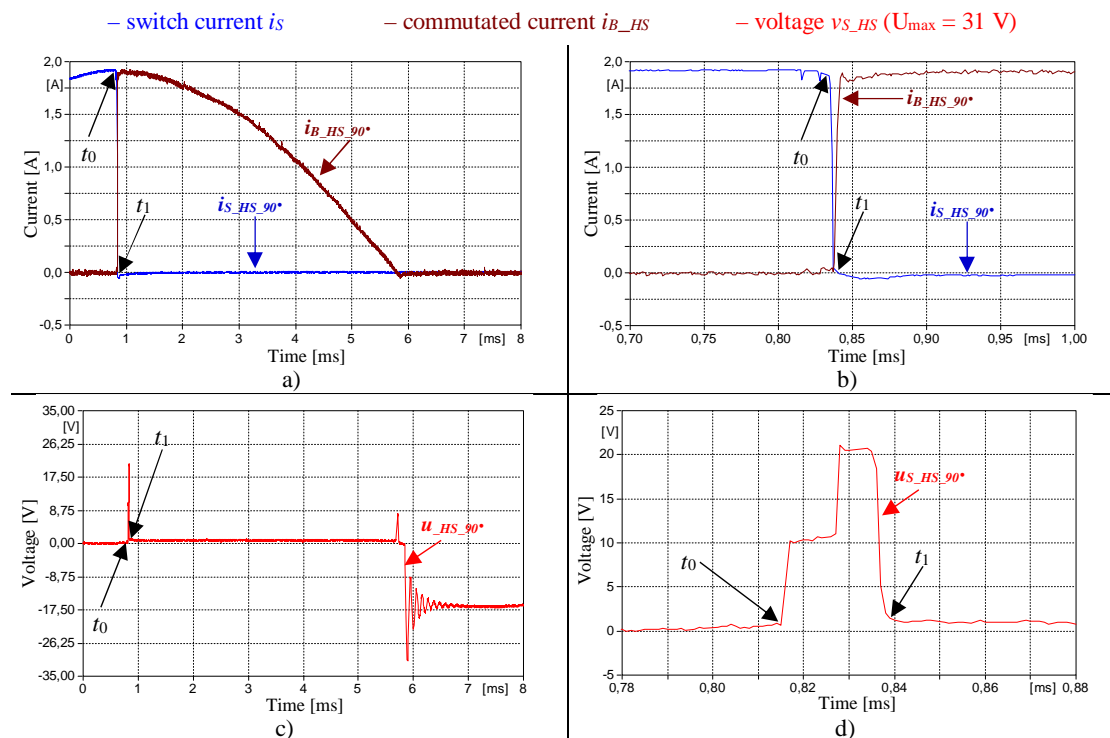


Figure 7.21. The measured currents (a), the measured voltage across the operated switch (b) during the hybrid switching

As shown in Figure 7.21, the application of the hybrid switching limits the arcing voltage, the arcing time, as well as, the overvoltages of the TRV in comparison to the situation, when the current $i_{S_90^\circ}$ was interrupted by the standalone switch (Figure 7.7). The measured differences in the waveforms can be observed in Figure 7.22, where the waveforms of the currents and the voltages are presented for the both analyzed cases.

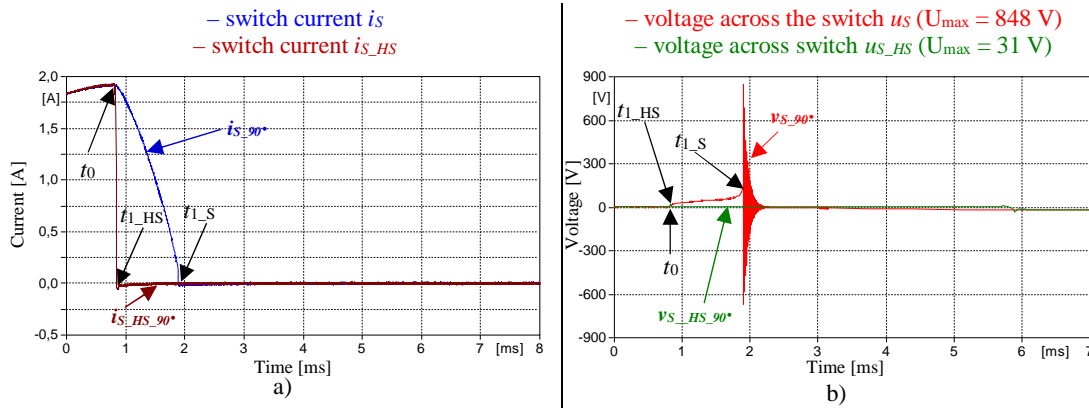


Figure 7.22. The measured current waveforms (a) and measured voltages across the operated switch (b) when the operated switch interrupts current as standalone one, and during the hybrid switching

As shown in Figure 7.22a, the application of the hybrid switching changes the shape of the current waveform $i_{S_HS_90^\circ}$ significantly. As it can be visible in the current waveform, the current of the operated switch $i_{S_HS_90^\circ}$ reaches its zero-crossing practically immediately after the contact separation. When the operated switch interrupts the current $i_{S_90^\circ}$ as the standalone one, the arcing voltage reaches over 130 V. The application of the hybrid switching causes the electric arc voltage to limit up to about 22 V (about 83%), the peak value of the TRV is also limited (from 848 V to 31 V, thus over 27 times). The application of the SSR in parallel to the operated switch causes also the frequency of the TRV oscillations to decrease. This could be achieved, because the energy stored in the inductive load can be discharged through the components integrated inside of the SSR applied to the hybrid switching (see the section 6.4 for details). The arcing time is also shorter during the hybrid switching (the decrease from 1080 μ s to 35 μ s was observed).

In order to determine the influence of the application of the hybrid switching on the limitation of the electric arc, the following waveforms were calculated: the electric arc power $p_{A_HS_90^\circ}$, the electric arc energy $e_{A_HS_90^\circ}$, the power generated at the semiconductor branch $p_{B_HS_90^\circ}$, as well as, the energy absorbed by the semiconductor branch $e_{B_HS_90^\circ}$. The waveforms of the above-mentioned magnitudes are presented in Figure 7.23. The calculations were performed according to the description presented in the section 6.1.2.

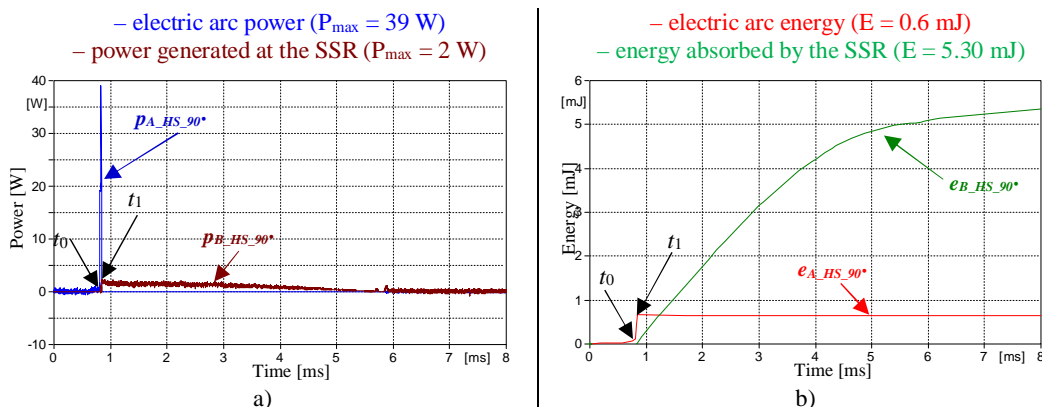


Figure 7.23. The calculated waveforms of the electric arc power, and the power generated at the SSR (a), the calculated waveforms of the arc energy and the energy absorbed by the SSR (b) during the current interruption process

As shown in Figure 7.23, the application of the hybrid switching impacts the increase of the steepness of the electric arc power $p_{A_HS_90^\circ}$ that tends almost immediately to its zero-crossing after the contact separation. When the arcing voltage exceeds the minimal operating voltage

of the SSR, the current of the operated switch $i_{S_HS_90^\circ}$ rapidly starts to commute into the SSR branch, which can be observed in the waveforms presented in Figure 7.23a. The peak value of the electric arc power $p_{A_HS_90^\circ}$ is also limited in this case (from 64 W for standalone switch to 38 W in here). It is observed, because the current $i_{S_HS_90^\circ}$ commutates almost immediately into the parallel branch, and the electric arc power is not able to achieve significant values. The application of the considered method impacts the limitation of the electric arc energy (the reduction from 51 mJ to about 0.6 mJ, so about 99%).

7.4 Summary of Measurement Results

In this section, the summary of measurement results for the limitation of the electric arc performed in the tested circuit supplied by the 12 V voltage source for the different considered methods were presented, when the contacts of the operated switch was separated at 90° of the current period. In order to compare the measurement results, the following magnitudes were collected in Table 7.2 for the performed researches:

- the maximum peak value of the voltage measured across the operated switch (U_{\max}),
- the maximum value of the arcing voltage ($U_{\text{arc_max}}$),
- the arcing time measured from the time of the contact separation to the time, when the TRV starts to appear across the operated switch (t_{arc}),
- the maximum electric arc power (P_{arc}),
- the power generated at the external branch connected in parallel to the operated switch (P_{snuubber}),
- the electric arc energy (E_{arc}),
- the energy absorbed by the external branch connected in the parallel to the operated switch (E_{snuubber}),
- the calculated differences of the arcing times (Δt_{arc}) and the electric arc energies (ΔE_{arc}) between the base case and the analyzed method expressed as a percentage.

Table 7.2. Measurement results for the considered methods limiting the electric arc at 12 V

Type	U_{\max}	$U_{\text{arc_max}}$	t_{arc}	P_{arc}	P_{snuubber}	E_{arc}	E_{snuubber}	Δt_{arc}	ΔE_{arc}
	[V]	[V]	[μs]	[W]	[W]	[mJ]	[mJ]	[%]	[%]
The Base case	848	130	1080	64	-	51	-	-	-
The RC arc suppressor	184	75	912	64	42	44	0.5	16	14
The Voltage-Dependent Resistor (VDR)	49	49	413	63	69	20	31	62	61
The Transient Voltage Suppressor (TVS)	25	25	55	45	45	3	45	95	94
The Zener Voltage Limiter (ZVL)	22	22	89	32	40	1.52	46	92	97
The Hybrid Switching	31	22	25	39	2	0.6	5.3	98	99

As shown in Table 7.2, the electric arc energy is limited in the different way in dependence of the application of the considered method. Thus, it can be concluded, that in the tested circuit the least effective method to limit the electric arc is the connection of the RC arc suppressor in parallel to the operated switch (in this situation, the electric arc energy is limited only about 7 mJ, thus, it is only 14% lower in reference to the base case). In contrast to this case, the

method giving the best results for the limitation of the electric arc is the hybrid switching (in this situation, the electric arc energy is reduced from 50 mJ up to 0.6 mJ, which is about 99% in reference to the base case).

The measured arcing times show also similar trend with the calculated arc energies – the least effective method for the limitation of the electric arc due to the reduction of the arcing time is the connection of the RC arc suppressor in parallel to the operated switch (it provides the limitation of the arcing time from 1080 μ s to 912 μ s, so only about 16%), whereas the method giving the best results is the hybrid switching (this solution provides the limitation of the arcing time from 1080 μ s to 25 μ s, so about 99%).

Thus, it can be concluded that the hybrid switching is the most effective method giving the best results for the limitation both of the electric arc energy, as well as, the electric arcing time in the tested circuit supplied by the 12 V voltage source.

In order to compare the shapes and the values of the analyzed magnitudes for the different considered methods, the waveforms of the measured currents, the measured voltage across switch, the calculated powers and energies, as well as, the calculated resistances for the different considered methods applied to limit the electric arc are presented in Figure 7.24- Figure 7.30.

The comparison of the voltage waveforms measured across the operated switch u_s for the considered methods is shown in Figure 7.24. The voltage measured across the operated switch interrupted the current as the standalone one is not presented in here for the clarity of the figure, due to the significant values of registered overvoltages (over 800 V).

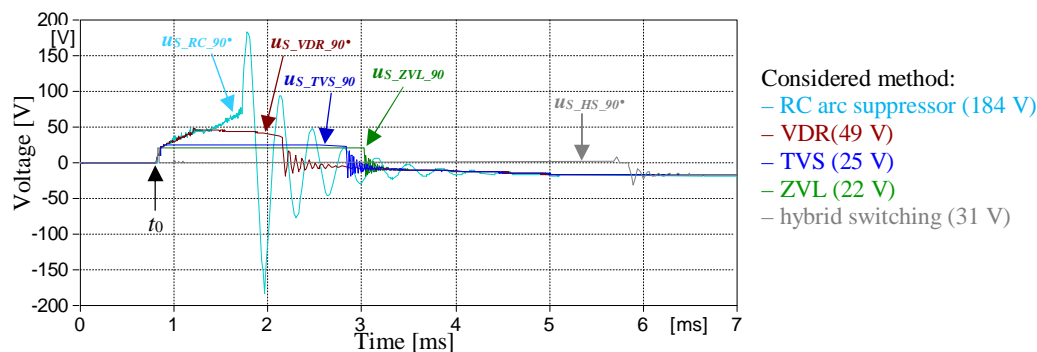


Figure 7.24. The waveforms of the measured voltage across the operated switch for the different methods limiting the electric arc

As shown in Figure 7.24, all measured arcing voltages start to increase in the same time, when the contacts start to separate. At the beginning, the shape of the arcing voltage has the same character for the all considered methods. The arcing voltages increase up to the different maximum values in dependence of the applied method to limit the electric arc.

In case of the application of the RC arc suppressor, the arcing voltage increases up to 75 V, and just after that, the significant oscillations in the TRV can be noticeable (the maximum overvoltage in the TRV exceeds 180 V).

The application of the VDR, the TVS, and the ZVL causes to the limitation of the arcing voltage at the level related to the minimal operating voltage of each applied nonlinear voltage component (the arcing voltage is limited respectively: up to 49 V for the VDR, up to 25 V for the TVS, and up to 22 V for the ZVL).

During the hybrid switching, the arcing voltage achieves maximally 22 V until the arcing voltage value exceeds the minimal operating voltage of the applied SSR (it takes about 35 μ s). At this time, the entire current commutes into the semiconductor branch, so as a consequence,

the measured voltage across the operated switch achieves the on-state voltage of the applied SSR, until the value of the commuted current does not reach the minimal holding current of the SSR. From this moment, the current stops flowing in the entire analyzed circuit, and the TRV appears between the contacts of the operated switch.

The frequency of the TRV oscillations depends on the considered method and it is related to the conditions for discharging the energy stored in the inductive coil after the current interruption.

The comparison of the measured current waveforms of the operated switch i_S for the all considered methods applied to limit the electric arc are presented in Figure 7.25.

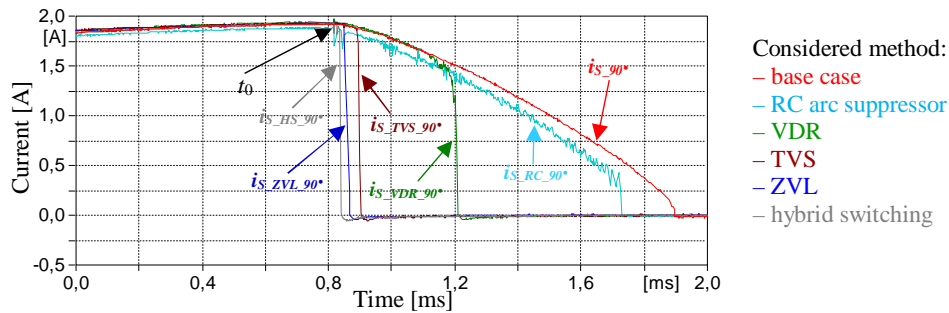


Figure 7.25. The waveforms of the measured currents of the operated switch for the different methods limiting the electric arc

As shown in Figure 7.25, the application of the all considered methods limiting the electric arc causes the reduction of the arcing times in comparison to situation, when the operated switch interrupts the current $i_{S_90^\circ}$ as the standalone one. In dependence on the effectiveness of the considered method, the current tends to its zero-crossing faster or longer from the time of the contact separation. Thus, the considered methods are mentioned in the following order from the worst case considering the effectiveness of the limitation of the arcing time: the base case, the RC arc suppressor, the VDR, the TVS, the ZVL, the hybrid switching. During the hybrid switching, the current of the operated switch reaches its zero-crossing with the highest steepness.

The comparison of the waveforms of the commuted currents into the external branches i_B for the different considered methods applied to limit the electric arc are shown in Figure 7.26. The presented waveforms were measured during the current interruption.

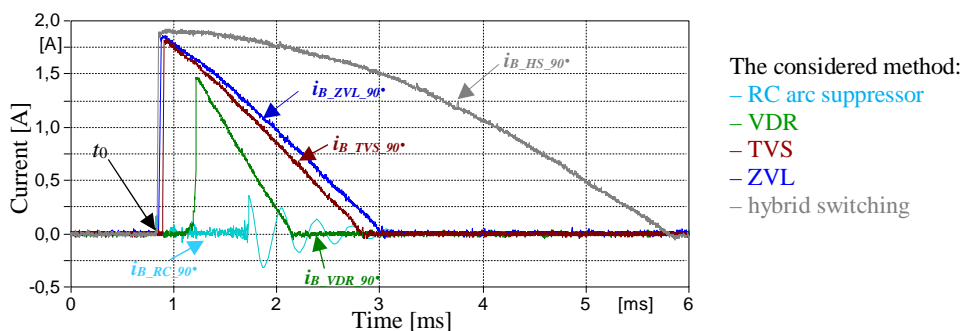


Figure 7.26. The waveforms of the measured currents commutated into the external branch for the different methods limiting the electric arc

As shown in Figure 7.26, the effectiveness of the analyzed method depends on the time, when the commutation process starts, as well as, on the value of the initial peak of the commuted current. The considered method is more effective, when the current is able to commute into

external branch as soon as possible after the contact separation time, with the peak value comparable to the instantaneous value of the current flowing by the operated switch.

Thus, as it can be observed in Figure 7.26, in case of the application of the TVS, the ZVL and the hybrid switching, the current starts to commute almost immediately after the time of the contact separation, and the value of the commuted peak current is similar to the instantaneous value of the current of the operated switch when its contacts start to separate.

During the hybrid switching, the zero-crossing of the commuted current $i_{B_HS_90^\circ}$ is reached much later in comparison to the other considered methods. This is observed, because the resistance of the p-n junction of the SSR is significantly lower in comparison to the other considered methods. The current $i_{S_VDR_90^\circ}$ starts to commute into the VDR branch later in comparison to the current $i_{S_TVS_90^\circ}$, the current $i_{S_ZVL_90^\circ}$ and the current $i_{S_HS_90^\circ}$, due to its higher value of the minimal operating voltage. The application of the RC arc suppressor allows to commute only the single current peaks just after the time of the contact separation, which as a consequence makes it possible to limit the electric arc energy only slightly. Moreover, the application of the RC arc suppressor causes the current oscillations after the electric arc quenching to appear, which is caused by discharging the capacitance connected between the contacts of the operated switch.

The comparison of the calculated waveforms of the electric arc power, as well as, the comparison of the calculated waveforms of the external branches power are presented respectively in Figure 7.27 and in Figure 7.28. The presented waveforms were calculated based on the measured currents and the measured voltages, according to the description presented in the section 6.1.2.

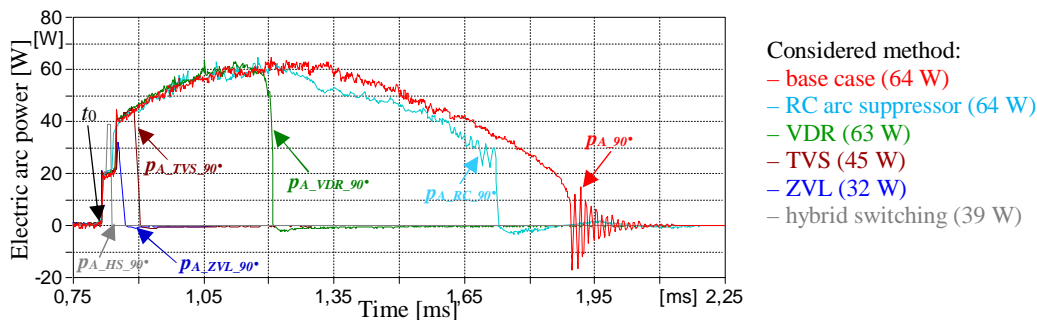


Figure 7.27. The waveforms of the calculated powers of the electric arc for the different methods limiting the electric arc

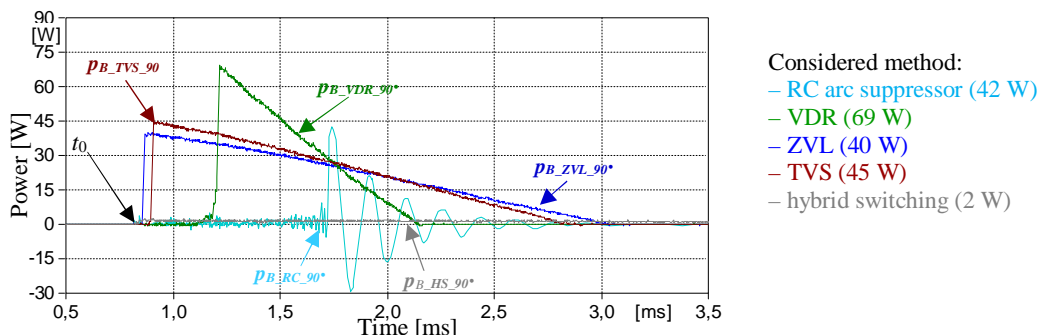


Figure 7.28. The waveforms of the calculated powers generated at the external branch for the different methods limiting the electric arc

The waveforms of the calculated powers p_B illustrated in Figure 7.27 – Figure 7.28 shows the similar trend with conclusions for the effectiveness of the considered methods that could be

also visible in Figure 7.25 – Figure 7.26. For this reason, the detailed analysis of the waveforms of the electric powers is omitted in this section.

The waveforms of the electric arc energies e_A , as well as, the waveforms of the energies generated at the external branches e_B were calculated and presented respectively in Figure 7.29 – Figure 7.30. The calculations were performed based on data presented in Figure 7.27 – Figure 7.28 according to the description presented in the section 6.1.2.

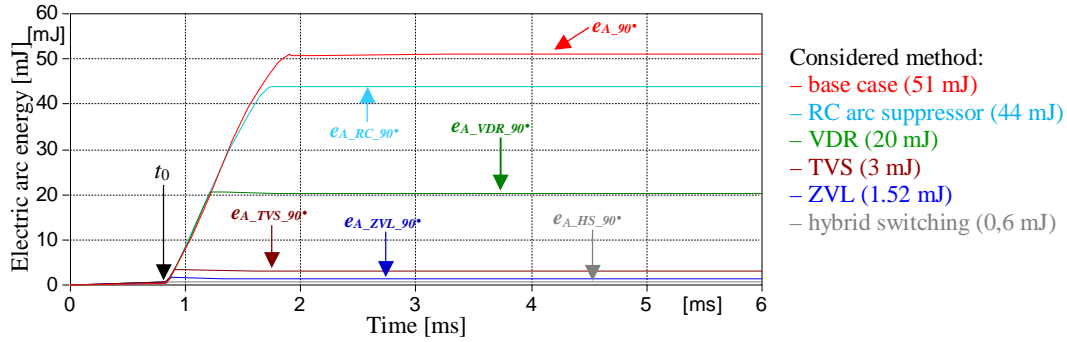


Figure 7.29. The waveforms of the calculated energies of the electric arc for the different methods limiting the electric arc

As shown in Figure 7.29, the conclusions from the previous part of this section can be confirmed. The considered methods can be classified due to the effectiveness of the limitation of the electric arc in the following order from the most to the worst effective method due to the limitation of the electric arc: the hybrid switching, the ZVL, the TVS, the VDR, the RC arc suppressor.

The comparison of the waveforms of the energies generated at the external branches connected in parallel to the operated switch e_B is presented in Figure 7.30.

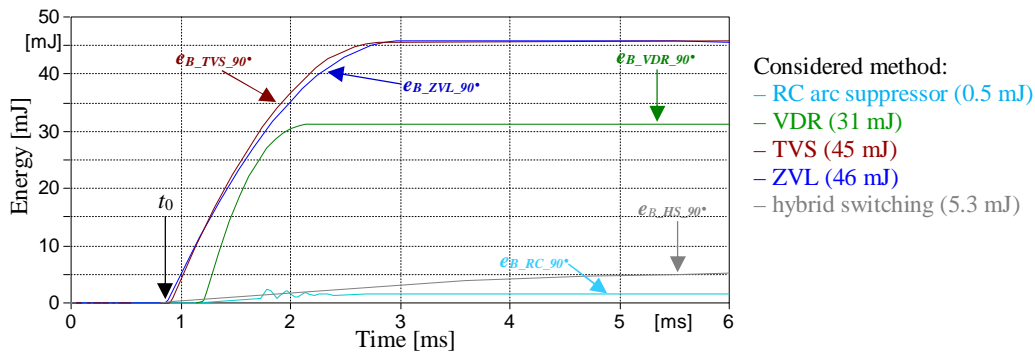


Figure 7.30. The waveforms of the calculated energies absorbed by the external branch for the different methods limiting the electric arc

As shown in Figure 7.30, the largest values of the energies absorbed by the external passive branches can be observed for the situations, when the TVS and the ZVL were connected to the operated switch. This is caused by faster time of the current commutation into the external branch in comparison to the VDR application, which is caused by lower values of the minimal operating voltages of the TVS and the ZVL. Therefore, the TVS and the ZVL can start to commute the current earlier.

During the hybrid switching, the time needed to the start of the current commutation is the shortest, and the value of the resistance of the p-n junction is also significantly lower than for the other considered methods. For this reason, the application of the hybrid switching allows to limit the electric arc with the very small amount of the absorbed energy by the

semiconductor branch. The waveforms of calculated resistances of the external branches r_B connected to the operated switch during the current interruption are presented in Figure 7.31.

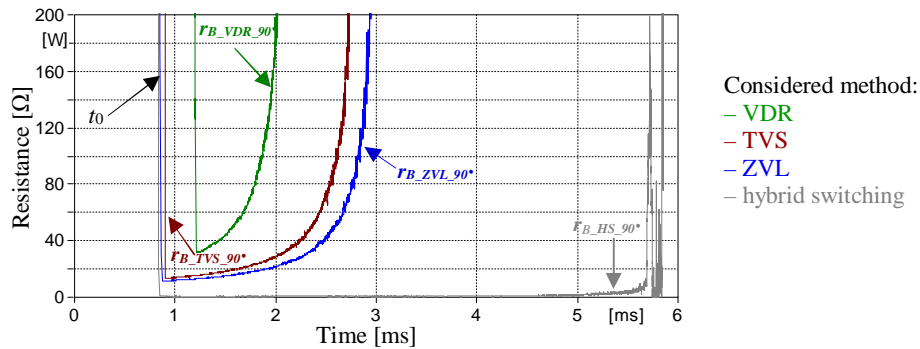


Figure 7.31. The waveforms of the calculated resistances of the external branches for the different methods limiting the electric arc

The waveforms of the calculated arc resistances r_A for the all considered methods to limit the electric arc energy are presented in Figure 7.32.

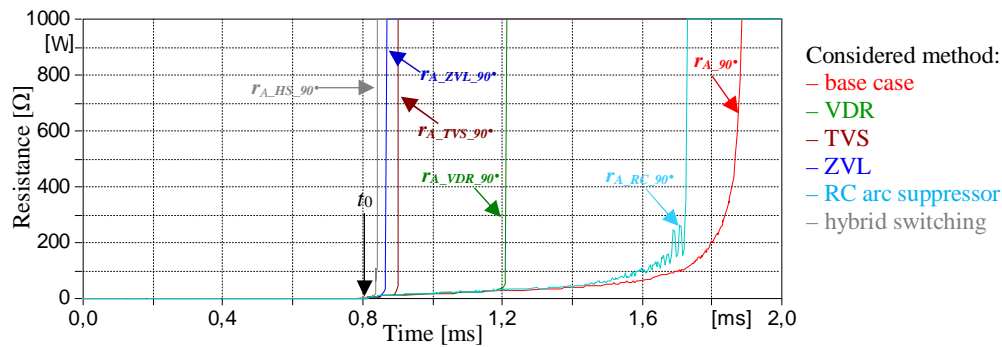


Figure 7.32. The waveforms of the calculated resistances of the electric arc for the different methods limiting the electric arc

The zoomed resistance waveforms presented in Figure 7.32 are also shown in Figure 7.33.

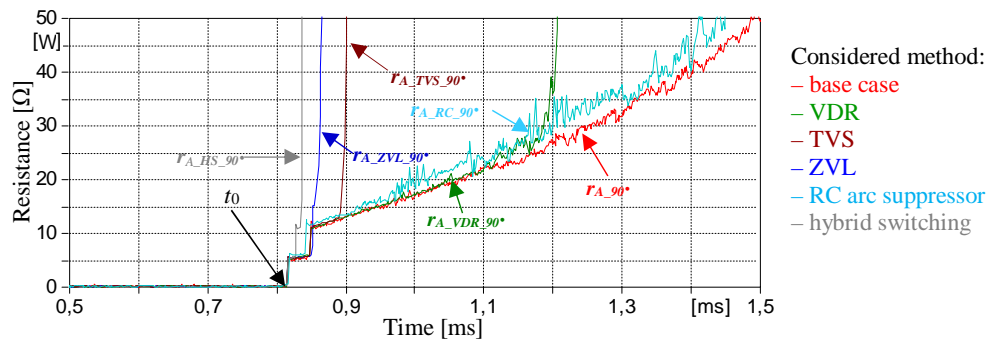


Figure 7.33. The zoomed waveforms of the calculated resistances of the electric arc for the different methods limiting the electric arc

In reference to Figure 7.32-Figure 7.33, it can be concluded, that the steepness of increasing the arc resistance is strongly related to the effectiveness of the considered method applied to the mitigation of the electric arc. The arc resistance tends faster to the infinity, when the electric arc energy is efficiently limited. Thus, the largest calculated steepness of the electric arc resistance can be observed during the application of the hybrid switching, whereas, the electric arc resistance tends to the infinity the slowest, when the methods for the limitation of the electric arc are not applied.

8 Measurement Results for the Limitation of the Electric Arc at 230 V

This chapter presents the measurement results for the researches on the limitation of the electric arc. The experiments were performed in the tested circuit supplied by the 230 V voltage source. The measurements presented inhere were performed according to the detailed description presented in the section 6, for the following scenarios of the researches:

- performing the contact separation of the operated switch at the defined angle of the current period (the detailed description is presented in the section 6.2),
- the connection of the external passive branches in parallel to the operated switch (the detailed description is presented in the section 6.3),
- the application of the hybrid switching (the detailed description is presented in the section 6.4).

The measurement results for the above-mentioned cases are presented respectively in the sections 8.1-8.3. The waveforms of the following magnitudes are presented in this chapter: the measured currents, the measured voltage across switch, the calculated electric arc powers, the calculated electric arc energies, the calculated powers generated at external branches connected in parallel to the operated switch, as well as, the calculated energies absorbed by the external branches. The calculations of the electric powers and the energies were performed according to the description presented in the section 6.1.2. The key instants were marked in waveforms:

- t_0 – the time, when the contacts of the operated switch start to separate,
- t_1 – the time, when the electric arc was quenched,
- t_2 – the time, when the steady state voltage appears between the contacts of operated switch after the end of the TRV.

8.1 Time-Controlled Contact Separation at the Precise Time Slot of the Current Period

The results of the researches on the limitation of the electric arc energy performed by the application of the time-controlled contact separation are presented in this section. The measurements were conducted according to the description presented in the section 6.2. In order to perform the researches, the contact separation was performed at four different angles of the current period, respectively: at 35° , at 90° and at 145° , as well as, just before the current zero-crossing (as close as possible due to the dispersion of the mechanical inertia of the switch drive – in practice, the contacts of the operated switch were separated tens of microseconds before the expected current zero-crossing).

The following magnitudes summarizing the measurements are listed in Table 7.1:

- the electric arc times t_{arc} ,
- the maximum observed value of the TRV during the current interruption U_{TRV_max} ,
- the maximum arcing voltage value U_{arc_max} ,
- the maximum value of the power of the electric arc P_{max} (calculated according to the description presented in the section 6.1),
- the maximum value of the electric arc energy E_{arc} (calculated according to the description presented in the section 6.1).

Table 8.1. The measurement results for the considered times of the contact separation – the tested circuit supplied by the 230 V voltage source

The time of the contact separation	t_{arc}	U_{TRV_max}	U_{arc_max}	P_{max}	E_{arc}
[degrees]	[ms]	[V]	[V]	[W]	[mJ]
Just before 0	0.223	731	40	48	<0.01
35	7.218	502	120	1560	7.97
90	5.047	651	120	1262	4.62
145	1.943	510	120	647	0.73

As shown in Table 8.1, the electric arc energy is the smallest (less than 10 mJ) when the contacts of the operated switch open just before the current zero-crossing, whereas the highest value of the electric arc energy (almost 8 J) is observed when the contacts start to separate at 35° of the current period. During the contact separation at 90° and at 145° of the current period, the electric arc energy was calculated respectively as 4.62 J and as 0.73 J. Thus, it can be concluded, that the electric arc energy is the smallest, when the contacts start to separate after the current extreme, while the current tends to its natural zero-crossing.

The compatible trend is observed for the measured arcing times that are also listed in Table 8.1. The shortest arcing time is observed when the contacts of the operated switch start to separate just before the natural current zero-crossing, whereas, the longest arcing time is noticeable in the situation, when the contacts open during the current extreme.

The measured voltages across the operated switch u_s during the contact separation performed at the considered times are presented in Figure 8.1. The zoomed waveforms of the arcing voltage are presented respectively in Figure 8.6a – Figure 8.8a.

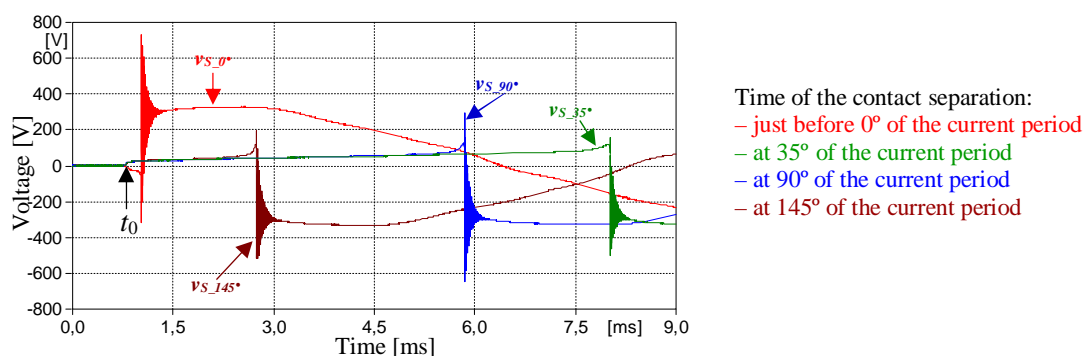


Figure 8.1. The voltages measured across the operated switch for the different times of the contact separation (t_0 – the contact separation time)

As shown in Figure 8.1, as well as, in the zoomed waveforms presented respectively in Figure 8.5a – Figure 8.8a, the maximum values of the arcing voltage can be limited by performing the contact separation in the specific time (see also Figure 8.1 for details).

In the case, when the contacts of the operated switch are separated just before the natural current zero-crossing, the arcing voltage achieves 40 V. However, when the contacts are separated at other considered times (respectively: at 35°, 90° and at 145° of the current period), the arcing voltage reaches maximally about 120 V.

Thus, the maximum observed arcing voltage does not exceed even the half of the voltage peak of the supply voltage at the steady state ($U_{PS_peak} \approx 325$ V). This is an important difference in comparison to the observed arcing voltages in the tested circuit supplied by the 12 V voltage source, where the arcing voltage achieves over 10 times in comparison to the voltage peak of the supply voltage at the steady state (see the chapter 7.1 for details).

In this case, the maximum observed TRV overvoltage exceeds 730 V, and this value is over twice greater in comparison to the maximum peak voltage of the supply source at the steady state. Thus, in this case, the relative overvoltage in the TRV is also smaller in comparison to the situation presented in the section 7.1, where the TRV peak archives even 50 times of the maximum peak voltage of the supply voltage at the steady state. The frequency of the TRV oscillations is related only to the electrical parameters of the tested circuit, thus the time of the contact separation does not influence these oscillations.

The measured waveforms of the interrupted current i_S during the contact separation performed at the considered times are presented in Figure 8.2. The zoomed current waveforms are presented respectively in Figure 8.5b – Figure 8.8b.

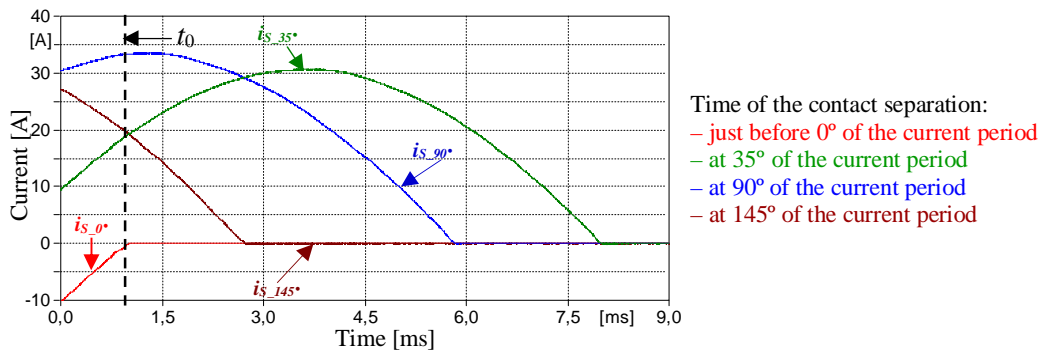


Figure 8.2. The measured currents of the operated switch for the different times of the contact separation (t_0 – the contact separation time)

As shown in Figure 8.2, after the time of the contact separation, the all measured current curves tend to the zero-crossing as the sinusoidal-shape with a slight deformation (the current zero-crossing is achieved faster than in the case, when the current flows through the contacts of the closed switch). This phenomenon is related to the appearance of the arc resistance in the tested circuit that influences on the deformation of the current curve, similarly to measurement results presented in the section 7.1. However, the electric arc resistance is significantly lower in comparison to the measurement results presented in the section 7.1. For this reason, the deformation of the current presented in Figure 8.2 is only slight in comparison to the measurement results presented in the section 7.1 (Figure 7.2).

As it can be observed in Figure 8.2, the electric arc quenches almost immediately when the contacts start to separate just before the current zero-crossing $i_{S_0^\circ}$ (shorter than 0.3 ms). In contrast, the arcing time takes the longest (over 7.2 ms) when the contacts start to open at time while the current $i_{S_{35^\circ}}$ increases (at 35° of the current period). This is an important difference in comparison to the situation presented in the section 7.1, where the greater value of the electric arc energy was observed at the time when the contacts started to separate at the current extreme (see the current $i_{S_{90^\circ}}$ in Figure 7.2 for the details). This difference is observed, because better conditions for the ionization of the gas localized between the separated contacts of the operated switch occur in this situation: both the greater value of the electric field, as well as, the greater instantaneous value of the interrupting current in comparison to the situation presented in the section 7.1. These differences help to achieve greater temperature rise between the contacts, which is necessary to gain the more intensive gas ionization (according to the description presented in chapter 3). As a consequence, it leads to creation of smaller electric arc resistance. This also influences smaller arcing voltage, which is also observed in Figure 8.1. Moreover, the most intensive ionization causes that the value of the arc resistance increases longer after the contact separation in comparison to the measurement results presented in the section 7.1. For this reason, in this case, the electric arc energy and the arcing time are the greater, when the contacts start to separate at 35° of the current period (see Figure 8.4). In this situation, the electric arc can burn longer, because the arc resistance

increases longer, which causes that the current reaches its zero-crossing later (so as a consequence, also the arcing time takes longer) in comparison to the analogous test in the tested circuit supplied by the 12 V voltage source. A detailed analysis of the electric arc resistance for the considered case is presented in the section 8.4.

As shown in Figure 8.2, the differences in the arcing times between the contact separation performed at 90° and 145° of the current period is over 3 ms (it takes respectively over 5 ms and almost 2 ms). Thus, it can be concluded, that the arcing time is shorter when the contacts of the operated switch open during the current tending to its natural zero-crossing, similarly to the measurement result presented in the section 7.1.

The waveforms of the electric arc power p_A calculated for the considered times of the contact separation are presented in Figure 8.3. The calculations were performed according to the description presented in the section 6.1.2. The zoomed waveforms of the electric arc power are presented respectively in Figure 8.5c – Figure 8.8c.

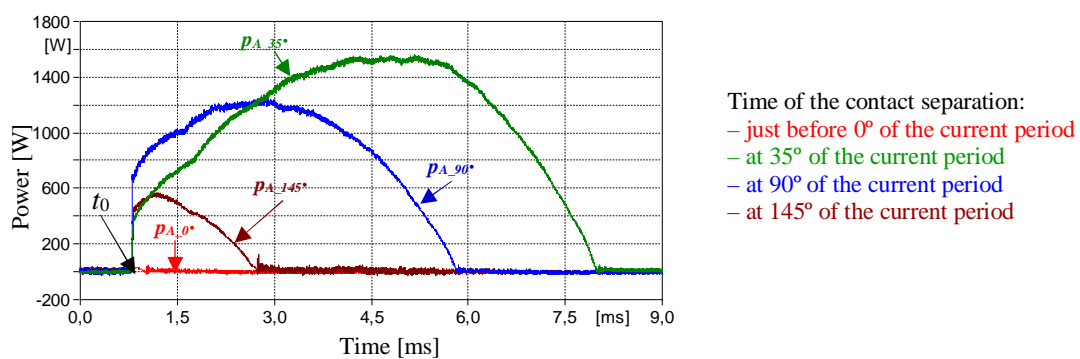


Figure 8.3. The calculated electric arc powers for the different times of the contact separation (t_0 – the contact separation time)

As shown in Figure 8.3, when the contacts of the operated switch start to separate just before the natural current zero-crossing, the electric arc power $p_{A_0^\circ}$ is observed only for a short time (shorter than 250 μ s). In this case, the power curve is similar in the double-stepped shape with the 30 W peak value (see Figure 8.5c for details). For other considered cases, the waveforms of the power curves are very similar in the half-sinusoidal shapes. The considered times of the contact separations are mentioned in the order from the worst case considering the effectiveness of the limitation of the arcing time, respectively: 35°, 90°, 145° of the current period, and the time just before the natural current zero-crossing.

The waveforms of the electric arc energy calculated e_A for the considered times of the contact separation are presented in Figure 8.4. The calculations were performed according to the description presented in the section 6.1.2. The zoomed waveforms of the electric arc energy are presented respectively in Figure 8.5d – Figure 8.8d.

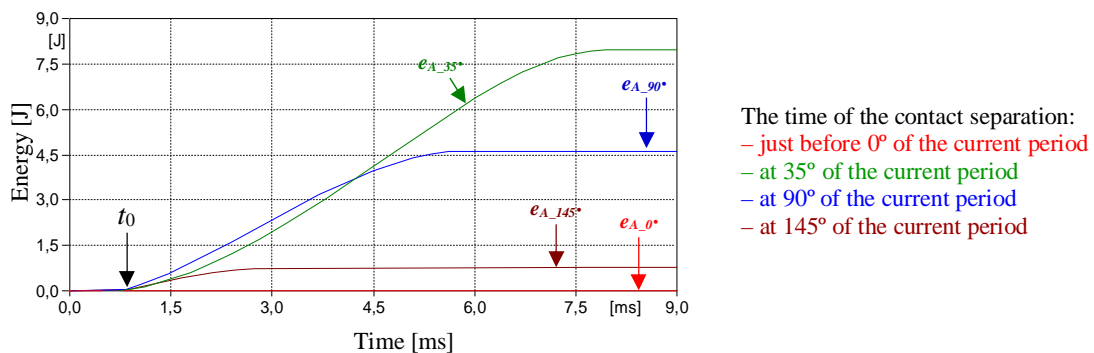


Figure 8.4. The electric arc energies calculated for the different times of the contact separation

As shown in Figure 8.4, as well as, in the zoomed waveforms of the electric arc energy presented respectively in Figure 8.5d – Figure 8.8d, the greatest values of electric arc energies e_A were calculated for the situations when the contacts were separated respectively at 35° , at 90° , at 145° of the current period and just before the zero-crossing of the current period, which is consistent with the trend observed for the calculated electric arc powers.

Thus, similarly to the measurement results presented in the section 7.1, it can be concluded that the most favorable conditions for the current interruption occur in the tested circuit supplied by the 230 V voltage source, when the contacts of the operated switch start to separate just before the current zero-crossing. Only in this situation, the electric arc energy is effectively limited, which can have slight influence on creating the arc erosion in the contact surfaces of the operated switch. The best conditions for the current interruption are precisely at the current zero-crossing. However, due to the dispersion of the mechanical inertia of the operated switch, this situation is very difficult to achieve in the practice. The electric arc energy is the greatest, when the contacts of the operated switch open at 35° of the current period. In this situation, the electric arc energy is observed in the considerable amount, which can influence creation of the electric arc erosion significantly.

The zoomed waveforms of the voltage measured across the switch u_S , the interrupted current i_S , the electric arc power p_A and the electric arc energy e_A are presented respectively in the sections 8.1.1 – 8.1.4 for the considered times of the contact separation.

8.1.1 Separation of the Contacts just before the Natural Zero-Crossing of the Current Period

In this section, the waveforms are presented for the situation, when the contacts of the operated switch start to separate just before the natural zero-crossing. The measured voltage across the operated switch $u_{S_0^\circ}$, the interrupted current $i_{S_0^\circ}$, the electric arc power $p_{A_0^\circ}$, as well as, the electric arc energy $e_{A_0^\circ}$ during the current interruption are presented in Figure 8.5.

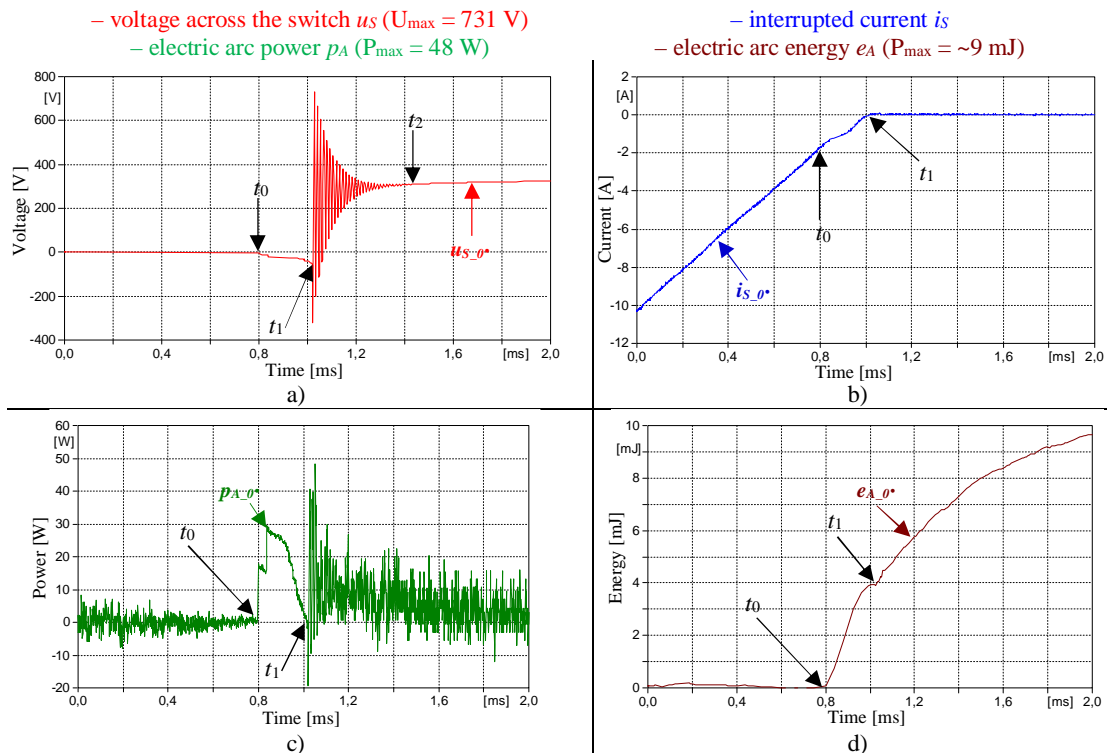


Figure 8.5. Contact separation just before the natural current zero-crossing : the measured voltage across the operated switch (a), the current of the operated switch (b), the calculated electric arc power (c), the electric arc energy (d)

8.1.2 Separation of the Contacts at 35° of the Current Period

In this section, the detailed waveforms are presented for the situation, when the contacts of the operated switch start to separate at 35° of the current period. The detailed waveforms of the measured voltage across the operated switch $u_{S_{35^\circ}}$, the interrupted current $i_{S_{35^\circ}}$, the electric arc power $p_{A_{35^\circ}}$, as well as, the electric arc energy $e_{A_{35^\circ}}$ during the current interruption are presented in Figure 8.6.

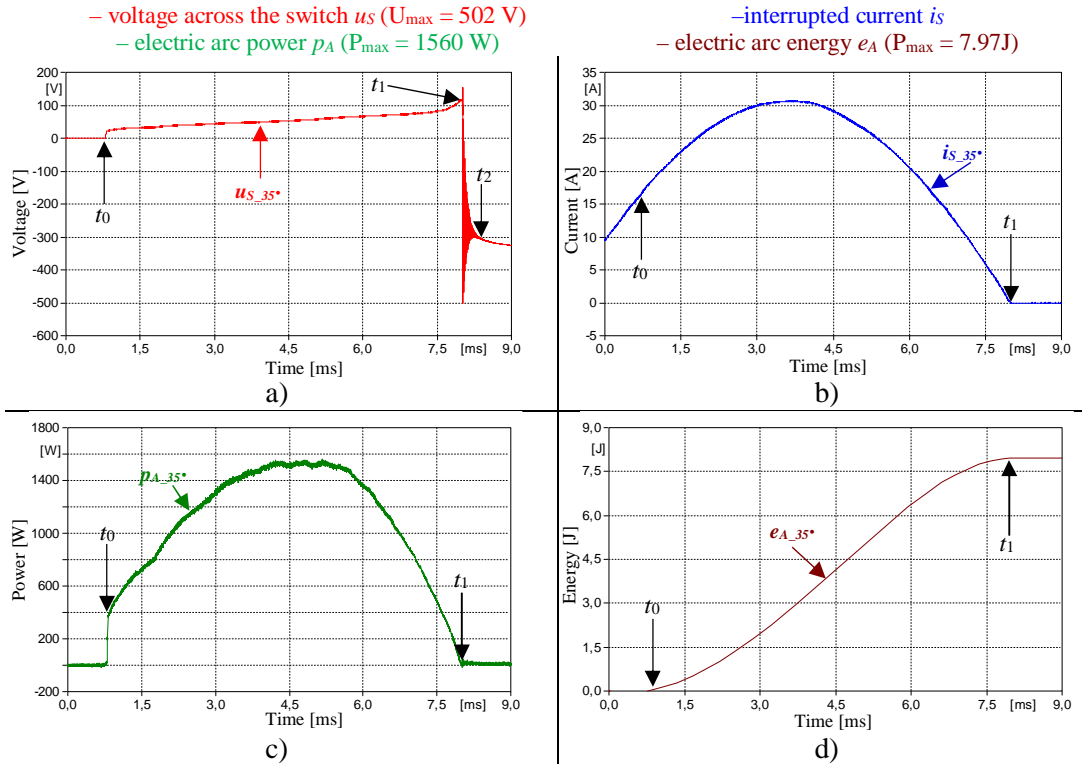
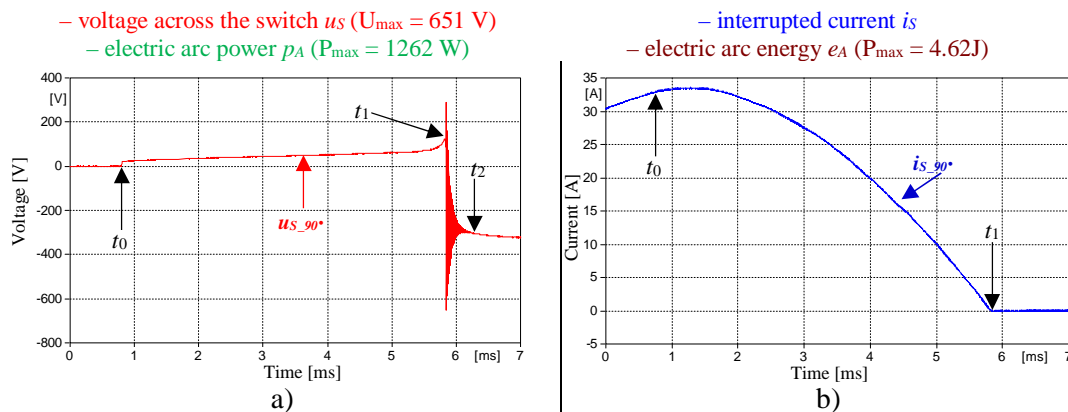


Figure 8.6. Contact separation at 35° of the current period. The measured voltage across the operated switch (a), the current of the operated switch (b), the calculated electric arc power (c), the electric arc energy (d)

8.1.3 Separation of the Contacts at 90° of the Current Period

In this section, the detailed waveforms are presented for the situation, when the contacts of the operated switch start to separate at 90° of the current period. The detailed waveforms of the measured voltage across the operated switch $u_{S_{90^\circ}}$, the interrupted current $i_{S_{90^\circ}}$, the electric arc power $p_{A_{90^\circ}}$, and the electric arc energy $e_{A_{90^\circ}}$ during the current interruption are presented in Figure 8.7.



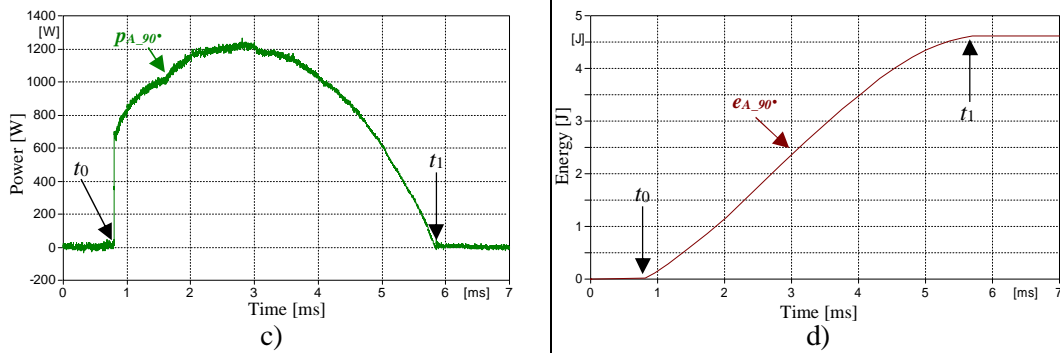


Figure 8.7. Contact separation at 90° of the current period: the measured voltage across the operated switch (a), the current of the operated switch (b), the calculated electric arc power (c), the electric arc energy (d)

8.1.4 Separation of the Contacts at 145° of the Current Period

In this section, the detailed waveforms are presented for the situation, when the contacts of the operated switch start to separate at 145° of the current period. The detailed waveforms of the measured voltage across the operated switch $u_{S_145^\circ}$, the interrupted current $i_{S_145^\circ}$, the electric arc power $p_{A_145^\circ}$, and the electric arc energy $e_{A_145^\circ}$ during the current interruption are presented in Figure 8.8.

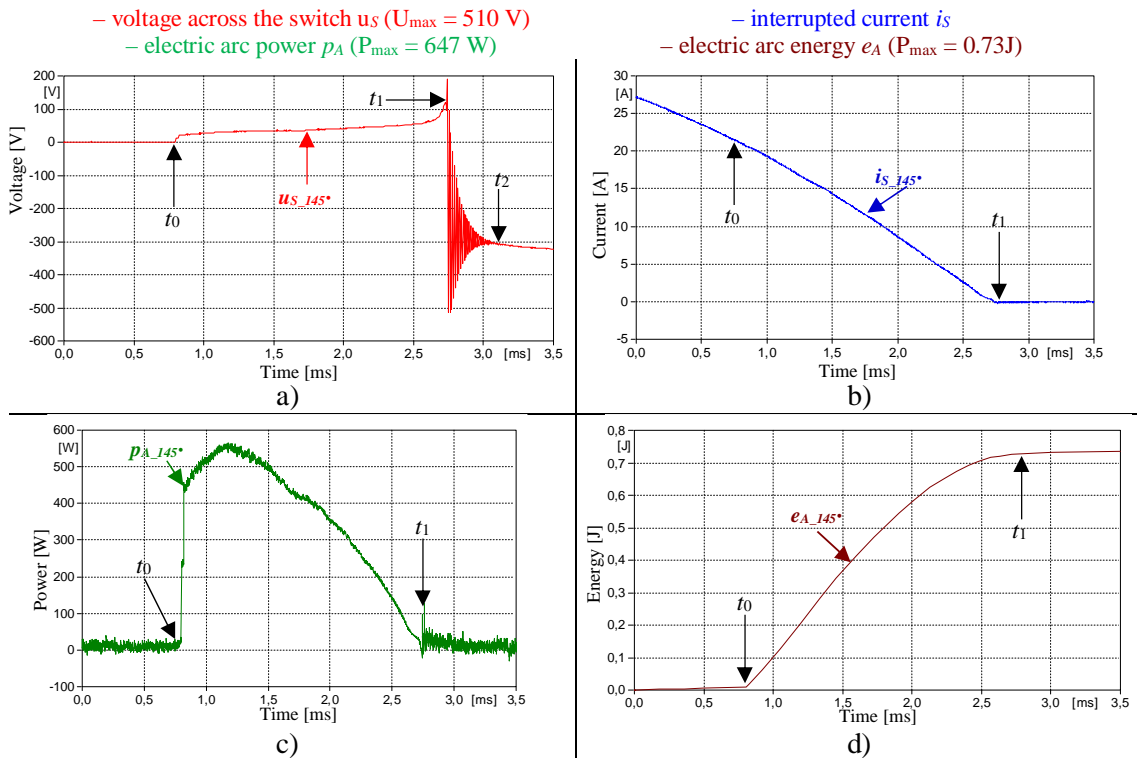


Figure 8.8. Contact separation at 145° of the current period: the measured voltage across the operated switch (a), the current of the operated switch (b), the calculated electric arc power (c), the electric arc energy (d)

8.2 Connection of the Passive Branches in Parallel to the Operated Switch

In this section, the measurement results are presented for limiting the electric arc energy by means of the connection of the different passive branches in parallel to the operated switch. The following branches were connected in parallel to the operated switch:

- RC arc suppressor,
- Voltage-Dependent Resistor (VDR),
- Transient Voltage Suppressor (TVS),
- Zener Voltage Limiter (ZVL).

The researches were performed in the tested circuit supplied by the 230 V voltage source for the situation, when the contacts of the operated switch start to separate at 35° of the current period. This case was chosen to the researches due to greater value of the electric arc energy, based on the measurement results presented in the section 8.1.

Thus, the effectiveness of the limitation of the electric arc was investigated in the tested circuit for the different external branches connected in parallel to the operated switch. The detailed description of the research plan was presented in the section 6.2.

In the course of the researches, the following magnitudes were measured: the voltage across the operated switch u_S , the current of the operated switch i_S and the current commuted into the external branch i_B during the current interruption. Based on these magnitudes, the following waveforms were calculated and presented in this section: the electric arc power p_A , the electric arc energy e_A , the power generated at the parallel branches p_B and the energy absorbed by the parallel branches e_B . The above-mentioned waveforms are presented in this section for each of the considered method limiting the electric arc.

8.2.1 RC Arc Suppressor

In order to determine the influence of the RC suppressor connected in parallel to the operated switch on the electric arc energy, the researches were performed. For this purpose, the RC suppressor was connected in parallel to the operated switch according to the figure presented in Table 6.1 (row 1). The parameters of the RC suppressor are also listed in Table 6.1 (row 1).

A waveform of the current flowing through the operated switch $i_{S_RC_35^\circ}$, a waveform of the current commuted into the parallel branch $i_{B_RC_35^\circ}$ with the RC suppressor, a waveform of the measured voltage across the operated switch $u_{S_RC_35^\circ}$ during the current interruption, as well as, a waveform of the measured voltage across the operated switch $u_{S_35^\circ}$ during the current interruption performed by the standalone switch are presented in Figure 8.9.

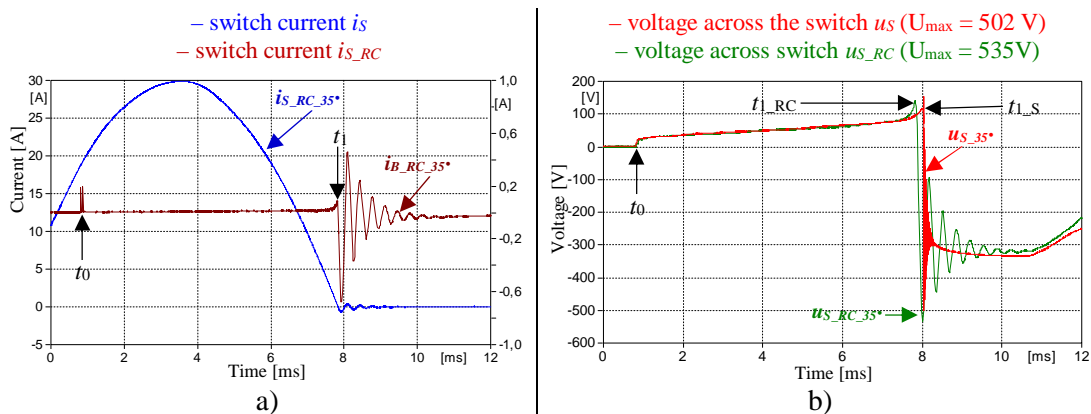


Figure 8.9. The measured current waveforms (a) and measured voltages across the operated switch (b) when the operated switch interrupts the current as the standalone one, and when the RC suppressor is connected in parallel to the operated switch

As shown in Figure 8.9a, the current $i_{B_RC_35^\circ}$ starts to flow into the parallel branch only for a short moment just after the time of the contact separation, which does not impact apparently on the shape of the current of the operated switch $i_{S_RC_35^\circ}$. The commutation of the small amount of the current $i_{S_RC_35^\circ}$ just after the contact separation is possible due to a sudden

increase in the arcing voltage at the time t_0 , when the contacts open, which makes to the energization of the capacitance being the part of the RC suppressor possible.

As shown in Figure 8.9b, the arcing voltage reaches maximally about 130 V. In this case, the maximum arcing voltage is even greater (about 8%) in comparison to the arcing voltage observed, when the current $i_{S_35^\circ}$ is interrupted by the standalone switch (120 V). This slight difference is caused by a specified repeatability of the processes taking the part in the formulation of the electric arc during the current interruption. Thus, it can be assumed that the both observed values of the arcing voltage are comparable, so the connection of the RC suppressor in parallel to the operated switch does not influence on the arcing voltage.

Just after quenching the electric arc, when the TRV starts to appear between the contacts of the operated switch, the current $i_{B_RC_35^\circ}$ starts to oscillate in the parallel branch with small peaks (lower than 0.5 A). This phenomenon is related to de-energizing the energy stored in the inductive load through the capacitance connected in the parallel to the operated switch. This process causes also reduction of the frequency of the TRV oscillations, which can be visible in Figure 8.9b. However, in this case, the TRV peak achieves slightly greater value (about 33 V, so about 6%) in comparison to the situation, in which the current was interrupted by the standalone switch (Figure 8.6).

The application of the RC suppressor also does not influence the arcing time noticeably (it takes about 144 μs shorter, so only 2% in comparison to the situation when the current is interrupted by the standalone switch). A comparison of the measurement results is summarized in Table 8.2.

In order to determine the influence of the connection of the RC suppressor in parallel to the operated switch on the limitation of the electric arc, the following waveforms were calculated: the electric arc power $p_{A_RC_35^\circ}$, the electric arc energy $e_{A_RC_35^\circ}$, the power generated at the RC suppressor $p_{B_RC_35^\circ}$, as well as, the energy absorbed by the RC suppressor $e_{B_RC_35^\circ}$. The waveforms of the above-mentioned magnitudes are presented in Figure 8.10. The calculations were performed according to the description presented in the section 6.1.2.

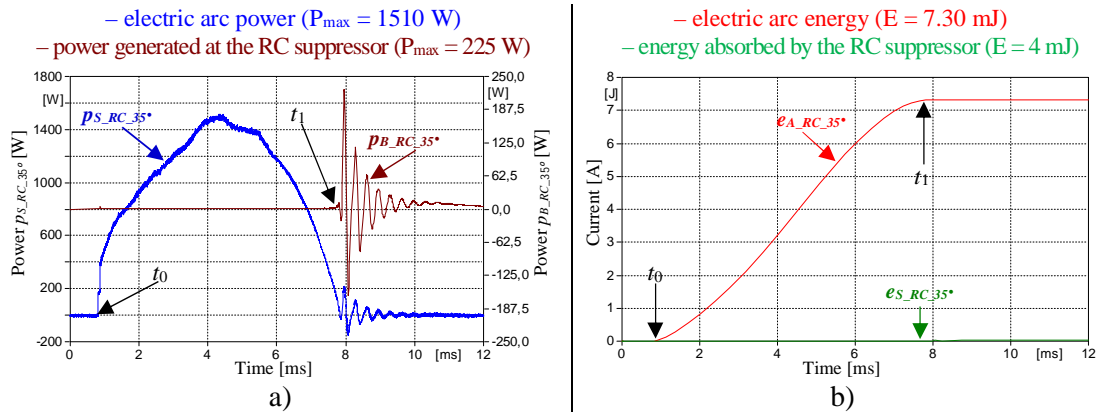


Figure 8.10. The calculated waveforms of the electric arc power, and the power generated at the RC suppressor (a), the calculated waveforms of the arc energy and the energy absorbed by the RC suppressor (b) during the current interruption process

As shown in Figure 8.10a, the connection of the RC suppressor in parallel to the operated switch limits the peak value of the electric arc power only slightly (in the situation, when the current was interrupted by the standalone switch, the maximum electric arc power $p_{A_35^\circ}$ was 1560 W, so the difference is only about 3%). This small difference is caused by the small amount of the current $p_{B_RC_35^\circ}$ that is able to commute into the RC suppressor, only just after the contact separation of the operated switch (see Figure 8.9a). Thus, in this case, it was

possible to limit the electric arc energy from 7.97 J to 7.30 mJ, so about 8%. According to Figure 8.10b, the energy absorbed by the RC suppressor is also slight (only about 4 mJ).

8.2.2 Voltage-Dependent Resistor (VDR)

The next examined method applied to the passive limitation of the electric arc is based on the connection of the Voltage-Dependent Resistor (VDR) in parallel to the operated switch, according to the figure presented in Table 6.1 (row 2). The parameters of the applied VDR are also listed in Table 6.1.

A waveform of the current flowing through the operated switch $i_{S_VDR_35^\circ}$, a waveform of the current commuted into the parallel VDR $i_{B_VDR_35^\circ}$, a waveform of the measured voltages across the operated switch $u_{S_VDR_35^\circ}$ during the current interruption, as well as, a waveform of the measured voltage across the operated switch $u_{S_35^\circ}$ during the current interruption performed by the standalone switch are presented in Figure 8.11.

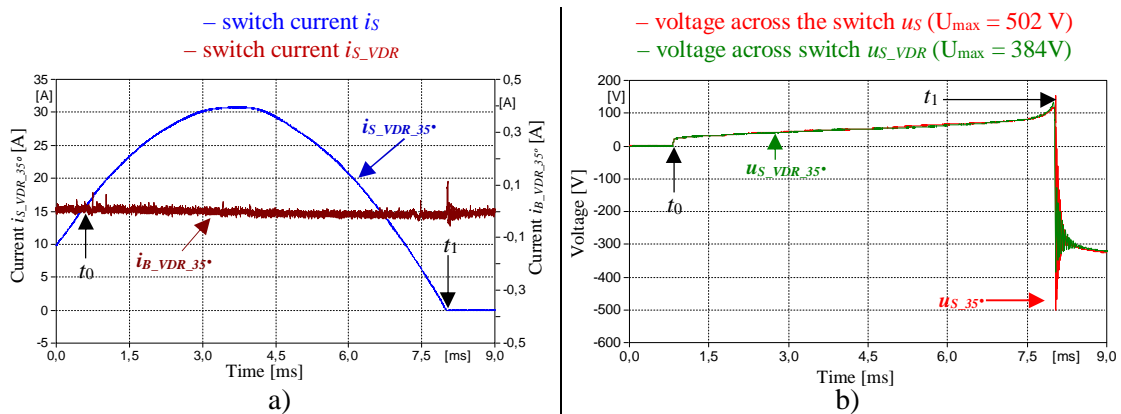


Figure 8.11. The measured current waveforms (a) and measured voltages across the operated switch (b) when the operated switch interrupts the current as the standalone one, and when the VDR is connected in parallel to the operated switch

As shown in Figure 8.11a, the current $i_{B_VDR_35^\circ}$ starts to flow in the parallel branch only for a short moment, when the current of the operated switch $i_{S_VDR_35^\circ}$ is already interrupted. During the current interruption, the arcing voltage is significantly below the minimal operating voltage of the VDR, so the current cannot commutate into the VDR branch. The VDR starts to conduct only, when the electric arc is already quenched, and the TRV appears between the contacts of the operated switch. Thus, it can be noticeable, that the TRV application does not limit the electric arc energy, but only limits the peak of the TRV from 502 V to 384 V (so almost 24%). For this reason, the frequency of the TRV oscillations decreases – when the VDR starts to conduct during the TRV, the energy stored in the inductive load can be discharged by the VDR. As shown in Figure 8.11b, the arcing voltage increases up to 130 V similarly to the previous analyzed cases. Also difference in the arcing times after the application of the VDR is slight (the observed difference about 17 μ s is caused by the specified repeatability of the processes taking the part in the formulation of the electric arc during the current interruption).

In order to confirm above conclusions, the following waveforms were calculated: the electric arc power $p_{A_VDR_35^\circ}$, the electric arc energy $e_{A_VDR_35^\circ}$, the power generated at the VDR branch $p_{B_VDR_35^\circ}$, as well as, the energy absorbed by the VDR branch $e_{B_VDR_35^\circ}$. The waveforms of the above-mentioned magnitudes are presented in Figure 8.12. The calculations were performed according to the description presented in the section 6.1.2.

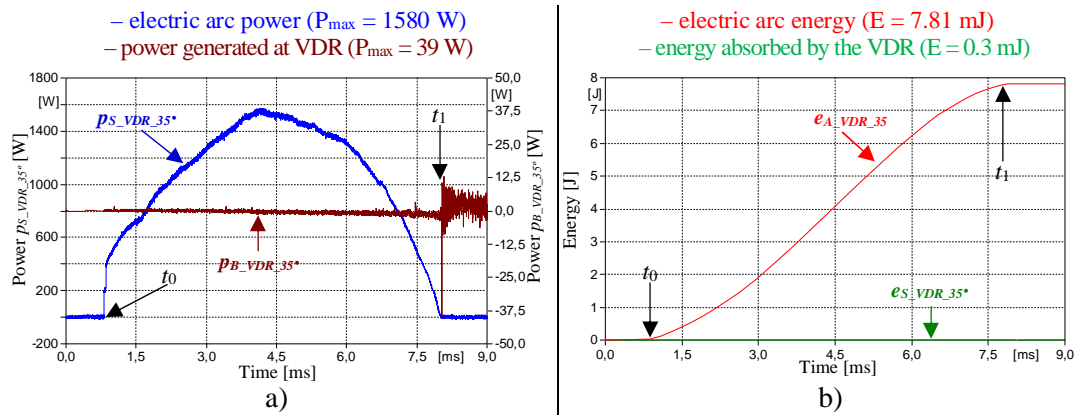


Figure 8.12. The calculated waveforms of the electric arc power, and the power generated at the VDR (a), the calculated waveforms of the arc energy and the energy absorbed by the VDR (b) during the current interruption process

As shown in Figure 8.12a, the connection of the VDR branch to the operated switch does not influence the peak of the electric arc power $p_{A_VDR_35^\circ}$. In the situation, the peak power is even greater about 20 W in comparison to the case, when the current $i_{S_35^\circ}$ is interrupted by the standalone switch. This slight difference is caused by the specified repeatability of the processes taking the part in the formulation of the electric arc during the current interruption. The power generated at the VDR branch $p_{B_VDR_35^\circ}$ starts to be observed, only just after the current zero-crossing, when the VDR starts to conduct due to the significant value of the TRV, which is greater than the voltage threshold of the VDR. Thus, in analyzed case, the calculated electric arc energy is 7.81 J, and the difference in comparison to the situation with the standalone switch (where the value of the electric arc energy is 7.97 J) is caused only by the specified repeatability of the processes taking part in the formulation of the electric arc during the current interruption. Thus, the VDR branch does not participate in the limitation of the electric arc energy during the current interruption process in the analyzed case.

8.2.3 Transient Voltage Suppressor (TVS)

Another examined method to passive limitation of the electric arc is the connection of the Transient Voltage Suppressor (TVS) in parallel in the operated switch according to the figure presented in Table 6.1 (row 3). The parameters of the applied TVS are also listed in Table 6.1. A waveform of the current flowing through the operated switch $i_{S_TVS_35^\circ}$, a waveform of the current commuted into the parallel TVS $i_{B_TVS_35^\circ}$, a waveform of the measured voltages across the operated switch $u_{S_TVS_35^\circ}$, as well as, a waveform of the measured voltage across the standalone switch $u_{S_35^\circ}$ during the current interruption are presented in Figure 8.13.

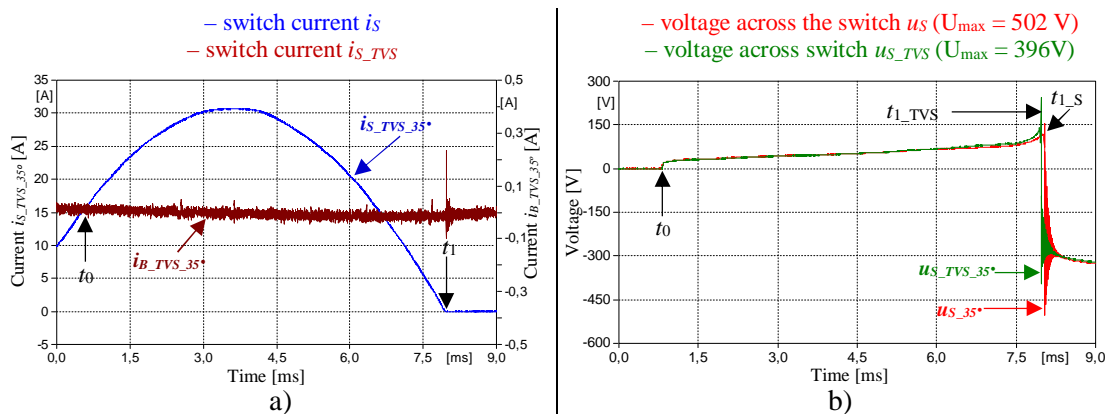


Figure 8.13. The measured current waveforms (a) and measured voltages across the operated switch (b) when the operated switch interrupts the current as the standalone one, and the TVS is connected in parallel to the operated switch

As shown in Figure 8.13a, similarly to the situation presented in the section 8.2.2, the arcing voltage during the current interruption is significantly below the minimal operating voltage of the TVS, so the current $i_{S_TVS_35^\circ}$ cannot commutate into the TVS branch. The TVS starts to conduct only, when the electric arc is already quenched, and the TRV appears between the contacts of the operated switch. Thus, it can be noticeable, that the TRV application does not limit the electric arc energy, but only limits the peak of TRV from 502 V to 396 V (so about 21%). For this reason, the frequency of the TRV oscillations decreases – when the TVS starts to conduct during the TRV, the energy stored in the inductive load can be discharged by the TVS. As shown in Figure 8.13b, the arcing voltage increases up to 135 V similarly to the previous analyzed cases. Also the difference in the arcing times after the application of the TVS practically does not exist (the observed difference about 64 μ s is caused by the specified repeatability of the processes taking the part in the formulation of the electric arc during the current interruption).

In order to confirm above conclusions, the following waveforms were calculated: the electric arc power $p_{A_TVS_35^\circ}$, the electric arc energy $e_{A_TVS_35^\circ}$, the power generated at the TVS branch $p_{B_TVS_35^\circ}$, as well as, the energy absorbed by the TVS branch $e_{B_TVS_35^\circ}$. The waveforms of the above-mentioned magnitudes are presented in Figure 8.14. The calculations were performed according to the description presented in the section 6.1.2.

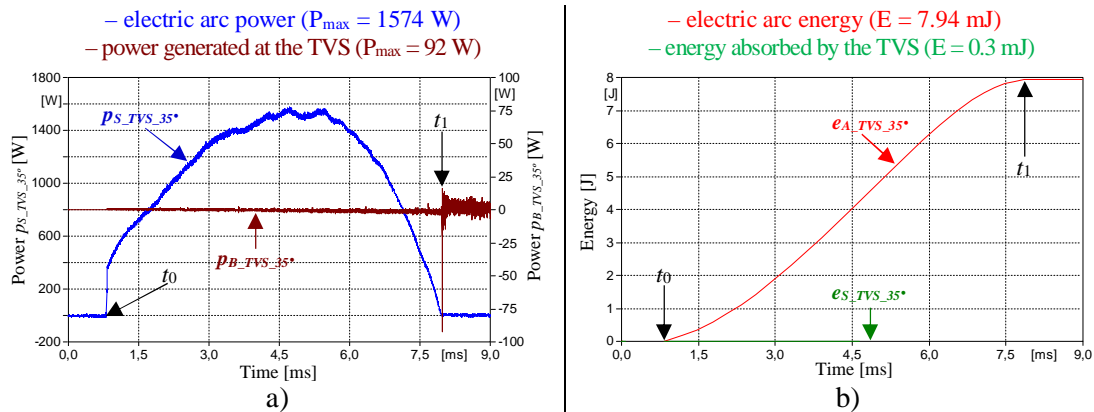


Figure 8.14. The calculated waveforms of the electric arc power, and the power generated at the TVS (a), the calculated waveforms of the arc energy and the energy absorbed by the TVS (b) during the current interruption process

As shown in Figure 8.14a, similarly to the situation presented in the section 8.2.2, the connection of the TVS branch to the operated switch does not influence on the peak of the electric arc power. In the analyzed case, the peak power $p_{A_TVS_35^\circ}$ is even greater about 14 W in comparison to the case, when the current $i_{S_35^\circ}$ is interrupted by the standalone switch. This slight difference is caused by the specified repeatability of the processes taking the part in the formulation of the electric arc during the current interruption. The power generated at the TVS branch starts to be observed, only just after the current zero-crossing, when the TVS starts to conduct due to the significant value of the TRV. Thus, in analyzed case, the calculated electric arc energy is 7.94 J, and the difference in comparison to the situation with the standalone switch (where the value of the electric arc energy is 7.97 J) is caused by the specified repeatability of the processes taking the part in the formulation of the electric arc during the current interruption. Thus, the TVS branch does not participate in the limitation of the electric arc energy during the current interruption process in the analyzed case.

8.2.4 Zener Voltage Limiter (ZVL)

Another examined method to limit the electric arc is the connection of the Zener Voltage Limiter (ZVL) in parallel to the operated switch. The applied branch consists of two ZVLs

connected in series, according to Figure 6.7. The parameters of the applied ZVLs are listed in Table 6.1.

A waveform of the current flowing through the operated switch $i_{S_ZVL_35^\circ}$, a waveform of the current commuted into the parallel ZVL $i_{B_ZVL_35^\circ}$, a waveform of the measured voltage across the operated switch $u_{S_ZVL_35^\circ}$ during the current interruption, as well as, a waveform of the measured voltage across the operated switch $u_{S_35^\circ}$ during the current interruption performed by the standalone switch are presented in Figure 8.15.

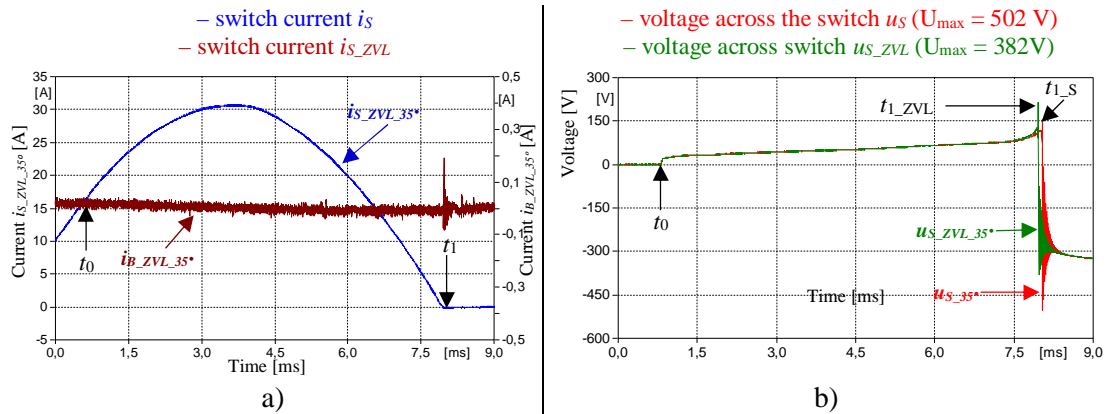


Figure 8.15. The measured current waveforms (a) and measured voltages across the operated switch (b) when the operated switch interrupts the current as the standalone one, and when the ZVL is connected in parallel to the operated switch

As shown in Figure 8.15a, similarly to the situations presented in the sections 8.2.2 – 8.2.3, the arcing voltage during the current interruption is significantly below the minimal operating voltage of the ZVL, so the current $i_{S_ZVL_35^\circ}$ cannot commutate into the ZVL branch. The ZVL starts to conduct only, when the electric arc is already quenched, and the ZVL appears between the contacts of the operated switch. Thus, it can be noticeable, that the ZVL application does not limit the electric arc energy, but only limits the peak of TRV from 502 V to 382 V (so about 24%). For this reason, the frequency of the TRV oscillations decreases – when the ZVL starts to conduct during the TRV, the energy stored in the inductive load can be discharged by the ZVL. As shown in Figure 8.15b, the arcing voltage increases up to 130 V similarly to the previous analyzed cases. Also difference in the arcing times after the application of the ZVL practically does not exist (the observed difference about 67 μ s is caused by the specified repeatability of the processes taking the part in the formulation of the electric arc during the current interruption).

In order to confirm above conclusions, the following waveforms were calculated: the electric arc power $p_{A_ZVL_35^\circ}$, the electric arc energy $e_{A_ZVL_35^\circ}$, the power generated at the TVS branch $p_{B_ZVL_35^\circ}$, as well as, the energy absorbed by the ZVL branch $e_{B_ZVL_35^\circ}$. The waveforms of the above-mentioned magnitudes are presented in Figure 8.16. The calculations were performed according to the description presented in the section 6.1.2.

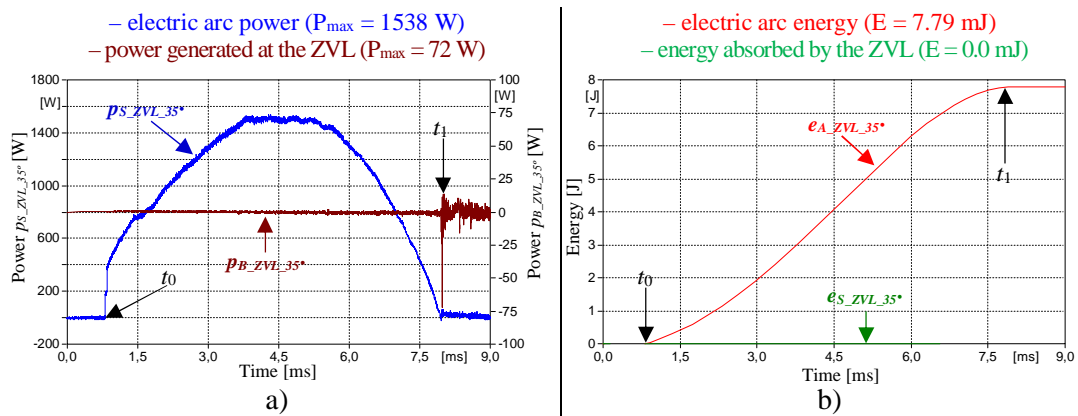


Figure 8.16. The calculated waveforms of the electric arc power, and the power generated at the ZVL (a), the calculated waveforms of the arc energy and the energy absorbed by the ZVL (b) during the current interruption process

As shown in Figure 8.16a, similarly to the situation presented in the sections 8.2.2 – 8.2.3, the connection of the ZVL branch to the operated switch does not influence the peak of the electric arc power $p_{A_ZVL_35^\circ}$. In the analyzed case, the peak power is lower about 22 W in comparison to the case, when the current is interrupted by the standalone switch. This slight difference is caused by the specified repeatability of the processes taking the part in the formulation of the electric arc during the current interruption. The power generated at the ZVL branch starts to be observed, only just after the current zero-crossing, when the ZVL starts to conduct due to the significant value of the TRV. Thus, in analyzed case, the calculated electric arc energy is 7.79 J, and the difference in comparison to the situation with the standalone switch (where the value of the electric arc energy is 7.97 J) is caused by the specified repeatability of the processes taking the part in the formulation of the electric arc during the current interruption. Thus, the ZVL branch does not participate in the limitation of the electric arc energy during the current interruption process in the analyzed case.

8.3 Hybrid Switching

According to the description presented in the section 6.1.2, the researches on the limitation of the electric arc were performed for the hybrid switching. This method is based on the connection of the semiconductor branch in parallel to the operated switch. The semiconductor branch is fully controlled by the microcontroller system, the detailed description of the hybrid switching is presented in the section 6.4. The measurements results for performed researches on this method in the tested circuit supply by 230 V are presented in this section.

A waveform of the current flowing through the operated switch $i_{S_HS_35^\circ}$, a waveform of the current commuted into the semiconductor branch $i_{B_HS_35^\circ}$, as well as, a waveform of the measured voltage across the entire operated switch $u_{S_HS_35^\circ}$ with connected the semiconductor branch during the current interruption are presented in Figure 8.17.

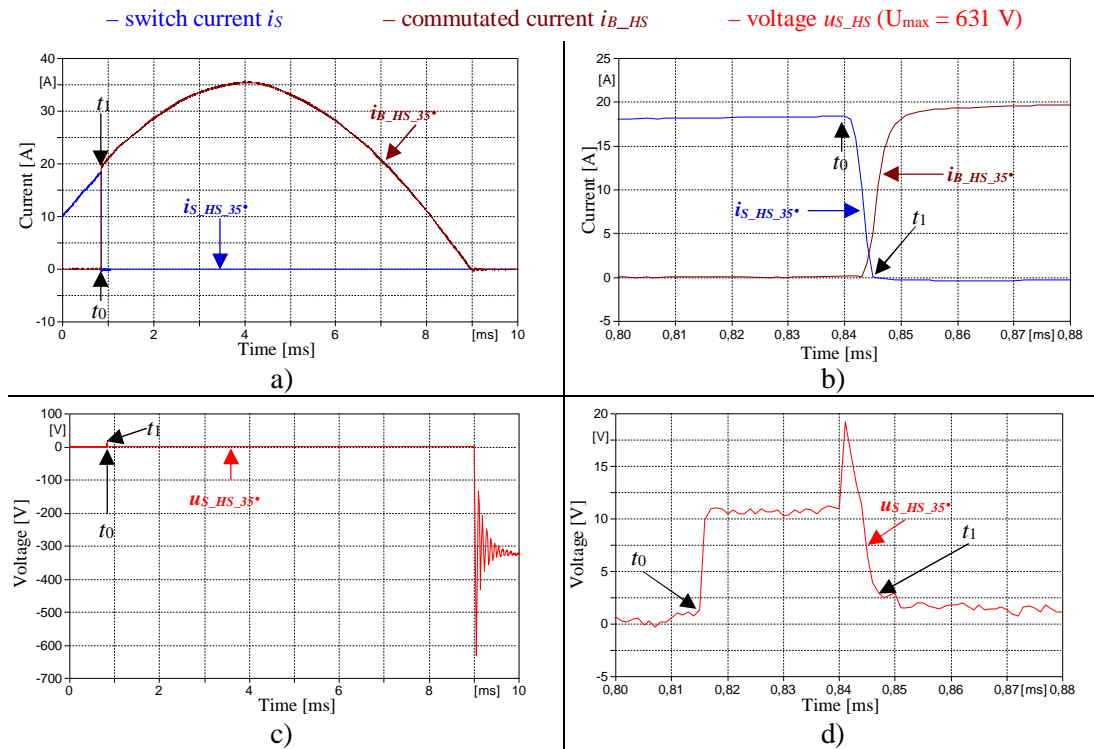


Figure 8.17. The measured currents (a), the measured voltage across the operated switch (b) during the hybrid switching

As shown in Figure 8.17, the application of the hybrid switching limits the arcing voltage, the arcing time, as well as, the overvoltages of the TRV in comparison to the situation, when the current $i_{S_{35^\circ}}$ was interrupted by the standalone switch (Figure 8.6). The measured differences in the waveforms can be observed in Figure 8.18, where the waveforms of the currents and the voltages are presented for both analyzed cases.

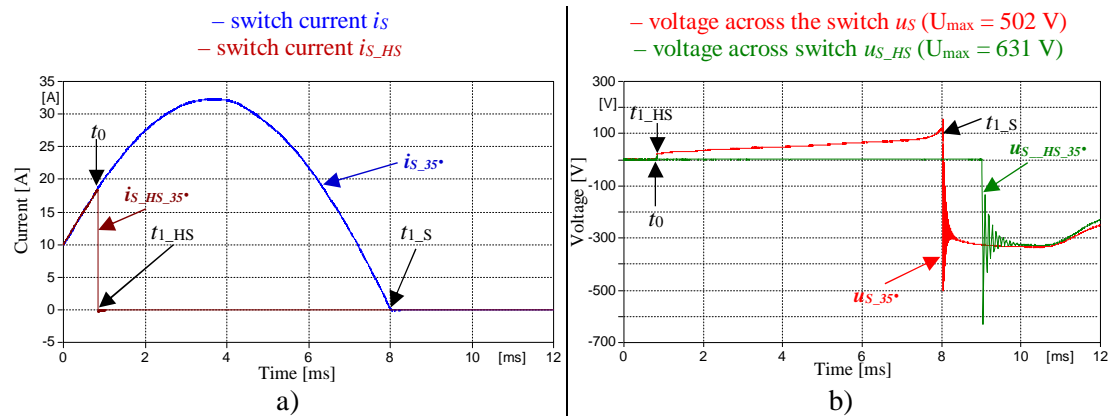


Figure 8.18. The measured current waveforms (a) and measured voltages across the operated switch (b) when the operated switch interrupts the current as the standalone one, and during the hybrid switching

As shown in Figure 8.18a, the application of the hybrid switching changes the shape of the current waveform $i_{S_{HS_{35^\circ}}}$ significantly. As it can be visible in the current waveform, the current of the operated switch $i_{S_{HS_{35^\circ}}}$ reaches its zero-crossing practically immediately after the contact separation. When the operated switch interrupts the current $i_{S_{35^\circ}}$ as the standalone one, the arcing voltage reached about 120 V. The application of the hybrid switching causes limitation of the electric arc voltage up to about 20 V (about 83%), but in this case, the TRV peak value has the larger value in comparison to the situation when the current is interrupted by the standalone switch (631 V instead of 502 V, thus about 26% greater). However, in both

analyzed cases, the absolute value of the first peak of the TRV is comparable (about 620-630 V). The application of the SSR in parallel to the operated switch causes the frequency of the TRV oscillations to decrease. This could be achieved, because the energy stored in the inductive load can be discharged through the components integrated inside of the SSR applied to the hybrid switching (see the section 6.4 for details), which limits the TRV. The arcing time is shorter in the situation, during the hybrid switching (the decrease from 7.222 ms to 35 μ s, so over 99%).

In order to determine the influence of the application of the hybrid switching on the limitation of the electric arc, the following waveforms were calculated: the electric arc power $p_{A_HS_35^\circ}$, the electric arc energy $e_{A_HS_35^\circ}$, the power generated at the semiconductor branch $p_{B_HS_35^\circ}$, as well as, the energy absorbed by the semiconductor branch $e_{B_HS_35^\circ}$. The waveforms of the above-mentioned magnitudes are presented in Figure 8.19. The calculations were performed according to the description presented in the section 6.1.2.

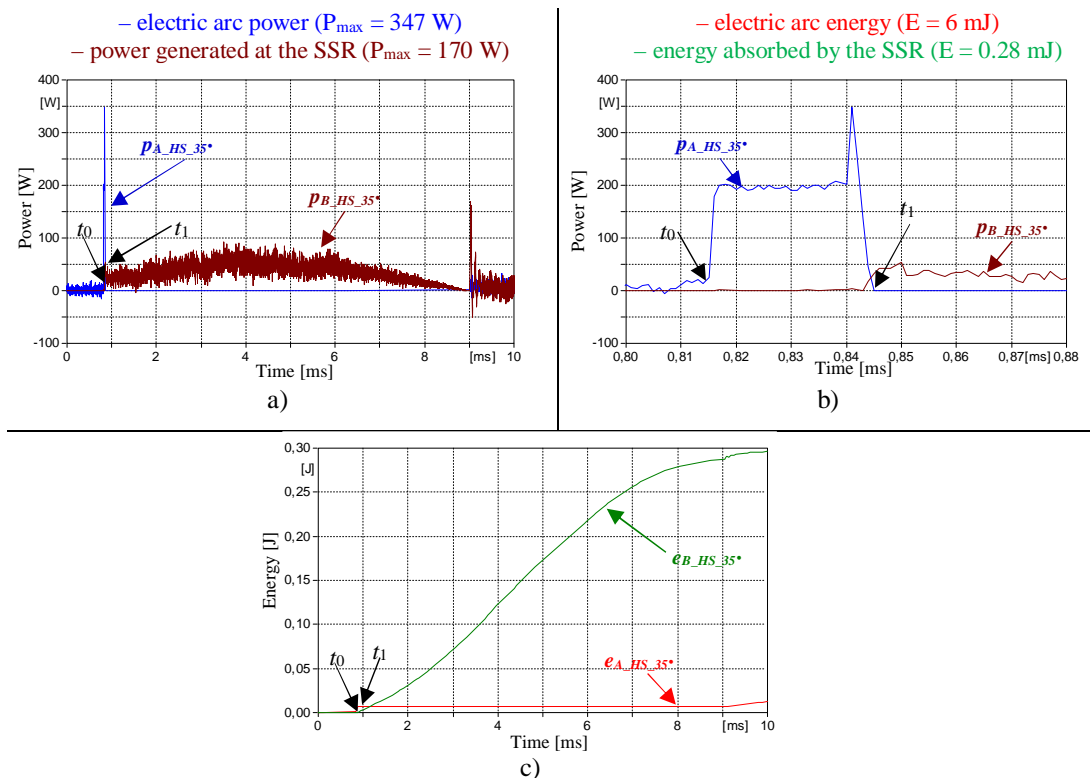


Figure 8.19. The calculated waveforms of the electric arc power, and the power generated at the SSR (a), the calculated waveforms of the arc energy and the energy absorbed by the SSR (b) during the current interruption process

As shown in Figure 8.19, the application of the hybrid switching impacts the increase of the steepness of the electric arc power $p_{A_HS_35^\circ}$ that tends almost immediately to its zero-crossing after the contact separation. When the arcing voltage exceeds the minimal operating voltage of the SSR, the current of the operated switch $i_{S_HS_35^\circ}$ rapidly starts to commute into the SSR branch, which can be observed in the waveforms presented in Figure 8.18a. The peak value of the electric arc power $p_{A_HS_35^\circ}$ is also limited in this case (from 1560 W for standalone switch to 39 W in here). It can be observed, because the current $i_{S_HS_35^\circ}$ commutates almost immediately into the parallel branch, and the electric arc power is not able to achieve significant values. The application of the considered method impacts significantly the limitation of the electric arc energy (the reduction from 7.97 J to about 6 mJ, so about over 99%).

8.4 Summary of the Measurement Results

In this section, the summary measurement results for the limitation of the electric arc energy performed in the tested circuit supplied by the 230 V the voltage source for the different considered methods were presented. In order to compare the measurement results, the following magnitudes for the performed researches were collected in Table 8.2:

- the maximum peak value of the voltage measured across the operated switch (U_{\max}),
- the maximum value of the arcing voltage ($U_{\text{arc_max}}$),
- the arcing time measured from the time of the contact separation to the time, when the TRV starts to appear across the operated switch (t_{arc}),
- the maximum electric arc power (P_{arc}),
- the power generated at the external branch connected in parallel to the operated switch (P_{snuubber}),
- the electric arc energy (E_{arc}),
- the energy generated at the external branch connected in the parallel to the operated switch (E_{snuubber}),
- the calculated differences of the arcing times (Δt_{arc}) and the electric arc energies (ΔE_{arc}) between the base case and the analyzed method expressed as a percentage.

Table 8.2. Measurement results for the considered methods limiting the electric arc at 230 V

Type	U_{\max}	$U_{\text{arc_max}}$	t_{arc}	P_{arc}	P_{snuubber}	E_{arc}	E_{snuubber}	Δt_{arc}	ΔE_{arc}
	[V]	[V]	[μs]	[W]	[W]	[J]	[J]	[%]	[%]
The Base case	502	120	7.222	1560	-	7.97	-	-	-
The RC arc suppressor	535	130	7.078	1510	225	7.30	0.004	1.99	8.41
The Voltage-Dependent Resistor (VDR)	384	130	7.205	1580	38	7.81	0.0003	0.24	2.01
The Transient Voltage Suppressor (TVS)	382	135	7.155	1538	72	7.79	0.0002	0.93	2.26
The Zener Voltage Limiter (ZVL)	396	130	7.158	1574	92	7.94	0.0003	0.89	0.38
The Hybrid Switching	631	20	0.035	347	170	0.006	0.28	99.52	99.92

As shown in Table 8.2, the electric arc energy is limited in the different way in dependence of the considered method. It can be concluded, that the application of the RC arc suppressor limits the electric arc energy only slightly (about 680 mJ, so over 8%). The connection of the VDR, the TVS and the ZVL in parallel to the operated switch does not limit electric arc energy even slightly. The small differences in the presented values of the measured magnitudes for the following cases: the base case, the VDR, the TVS and the ZVL are caused only by the specified repeatability of the processes taking part in the formulation of the electric arc during the current interruption. The only method providing the satisfactory results for the limitation of the electric arc is the hybrid switching (for this method, the electric arc energy is reduced from 7.97 J up to 6 mJ, which is about 99.9% in reference to the base case).

The similar trend can be observed for the measured arcing times. The connection of the RC arc suppressor in parallel to the operated switch limits the arcing times slightly (it provides the reduction of the arcing time from 7.222 ms to 7.078 ms, so about 2%), whereas the only method providing the significant limitation of the acing time is the application of the hybrid

switching (this solution provides limitation of the arcing time from 7.222 ms to 35 μ s, so about 99.5%).

Thus, based on the data listed in Table 8.2, it can be concluded that the application of the hybrid switching is the most effective method providing the best results for the limitation of both of the electric arc energy, as well as, the electric arcing time in the tested circuit supplied by the 230 V voltage source.

In order to compare shapes and values of the analyzed magnitudes for the different considered methods, the measured waveforms were presented in the same figures, which are presented in Figure 8.20 – Figure 8.27.

The comparison of the voltage waveforms measured across the operated switch u_s for the considered methods is shown in Figure 8.20.

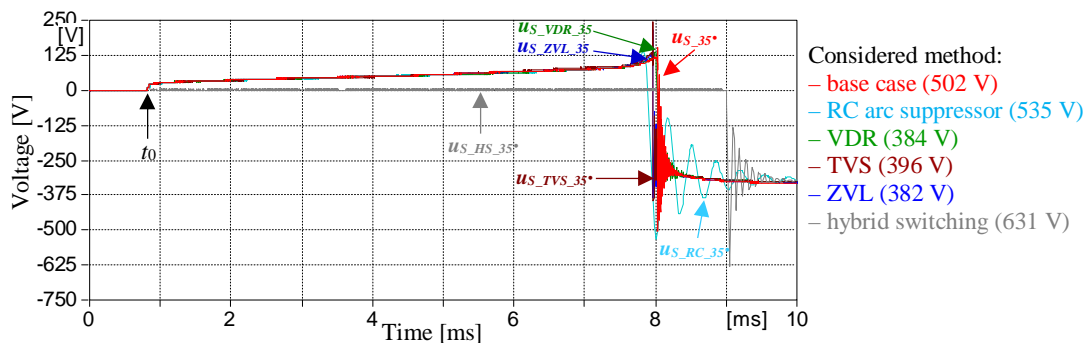


Figure 8.20. The waveforms of the measured voltage across the operated switch for the different methods limiting the electric arc

As shown in Figure 8.20, all measured voltages start to increase at the same time, when the contacts of the operated switch start to separate. At the beginning, the shape of the arcing voltage is the same for all of the considered methods. All measured arcing voltages (except for the voltage measured during the hybrid switching) increase up to about 120-135 V. The differences are caused only by the specified repeatability of the processes taking part in the formulation of the electric arc during the current interruption.

As it is shown in Figure 8.20, only the application of the hybrid switching causes the noticeable limitation of the arcing voltage – from about 120 V up to about 20 V. During the hybrid switching, the arcing voltage takes only about 35 μ s until its value exceeds the minimal operating voltage of the applied SSR (in practice about 20 V). At this time, the entire current commutes into the semiconductor branch, so as a consequence, the voltage measured across the operated switch achieves the on-state voltage of the applied SSR. This state takes until the value of the commuted current decreases up the minimal holding current of the applied SSR. From this moment, the current stops flowing in the tested circuit, and the TRV appears between the contacts of the operated switch. The application of the hybrid switching causes limitation of the electric arc voltage up to about 20 V (about 83%), but the TRV peak value has larger value in comparison to the situation when the current is interrupted by the standalone switch (631 V instead of 502 V, thus about 26% greater). However, in both analyzed cases, the absolute value of the TRV is comparable (about 620-630 V). The application of the SSR in parallel to the operated switch causes also the frequency of the TRV oscillations to decrease.

The voltage waveforms of the measured voltages across the operated switch with the zoomed TRV for the different considered methods are presented in Figure 8.21.

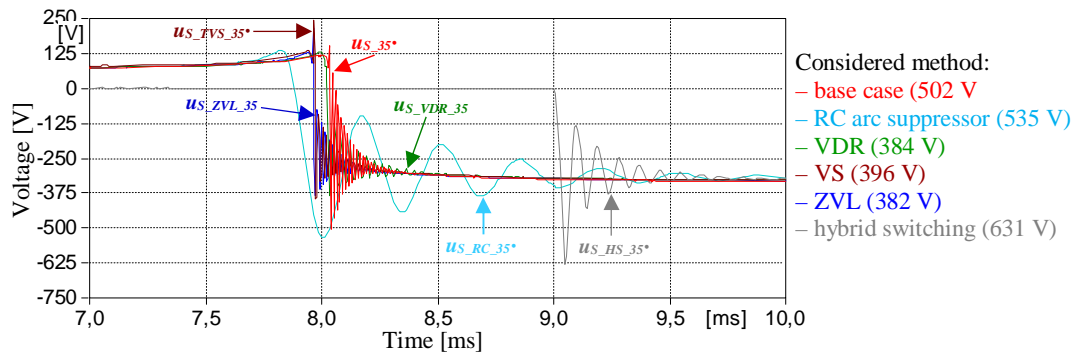


Figure 8.21. The waveforms of the measured voltage across the operated switch for the different methods limiting the electric arc

As shown in Figure 8.21, the frequency of the TRV oscillations depends on the application of the considered method to limit the electric arc energy. In the case, when the parallel branch connected to the operated switch starts to commutate during the current interruption, the energy stored in the inductive load of the tested circuit can be de-energized through the parallel branch, which as a consequence causes the TRV oscillations to limit. The significantly smaller frequency of the TRV oscillations can be observed especially during the application of the RC arc suppressor and the application of the hybrid switching.

The comparison of the measured current waveforms i_S of the operated switch for the all considered methods applied to limit the electric arc are presented in Figure 8.22.

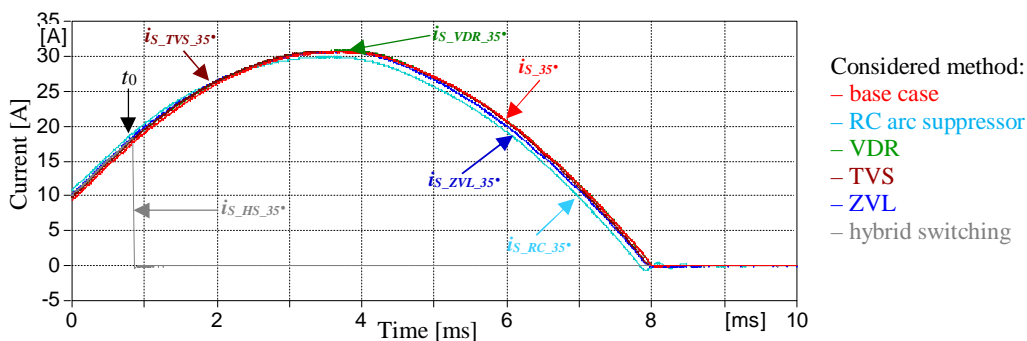


Figure 8.22. The waveforms of the measured currents of the operated switch for the different methods limiting the electric arc

As shown in Figure 8.22, the all measured current waveforms are very similar in the shape (except for the current measured during the hybrid switching). The current measured for the situation, when the RC suppressor is connected in parallel to the operated switch achieves the zero-crossing slightly earlier in comparison to other waveforms. It can be visible, that the current waveforms measured for the base case, the VDR, the ZVL, the TVS practically overlap with each other.

On the other hand, during the hybrid switching, the current of the operated switch reaches the zero-crossing almost immediately after the contact separation of the operated switch. Thus, the presented waveforms correspond to the measured arcing times listed in Table 8.2

The waveforms of the commuted currents into the external branches i_B for the different considered methods applied to limit the electric arc are shown in Figure 8.23. The presented waveforms were measured during the current interruption.

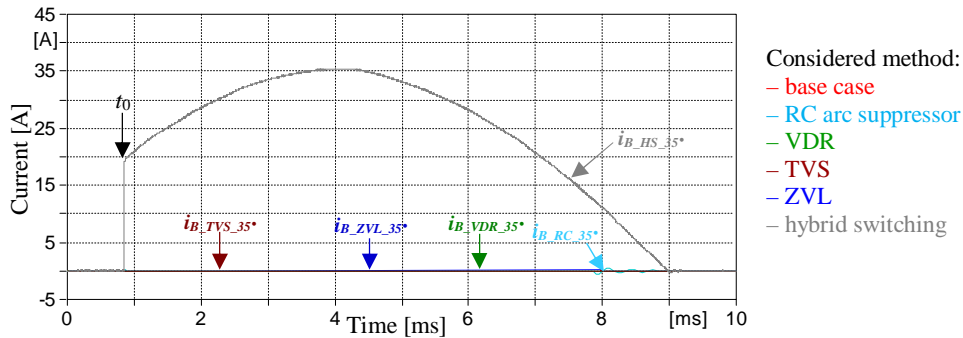


Figure 8.23. The waveforms of the measured currents commutated into the external branch for the different methods limiting the electric arc

As shown in Figure 8.23, the current of the operated switch commutes into the external branch only in two cases: when the RC suppressor is connected in parallel to the operated switch, as well as, during the hybrid switching. The current does not commute during the connection of the ZVL, the VDR, and the TVS in parallel to the operated switch during burning the electric arc. The application of the RC arc suppressor allows to commute only the single current peaks just after the contact separation, which as a consequence limits the electric arc energy only slightly. Moreover, the application of the RC arc suppressor causes appearance of the current oscillations after quenching the electric arc. The application of the RC suppressor makes the de-energization of the energy stored in the inductive load through the parallel branch possible. On the other hand, the current starts to commute into the semiconductor branch almost immediately after the time of the contact separation while the hybrid switching.

The calculated waveforms of the electric arc power p_A , as well as, the comparison of the calculated waveforms of the external branches power p_B are presented respectively in Figure 8.24 and in Figure 8.25. The presented waveforms were calculated, according to the description presented in the section 6.1.2.

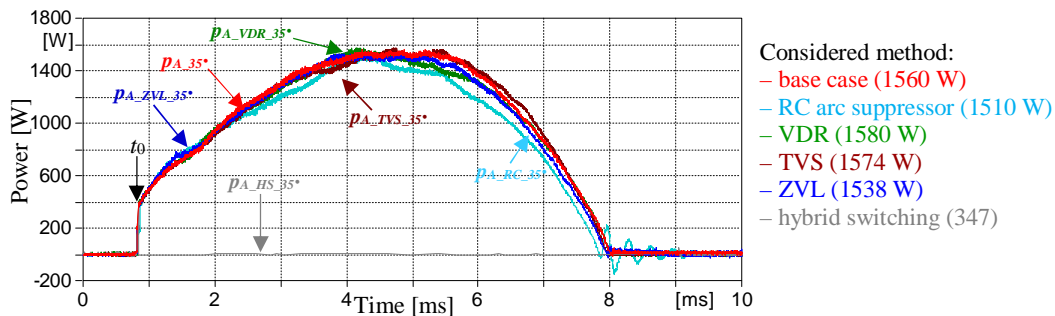


Figure 8.24. The waveforms of the calculated powers of the electric arc for the different methods limiting the electric arc

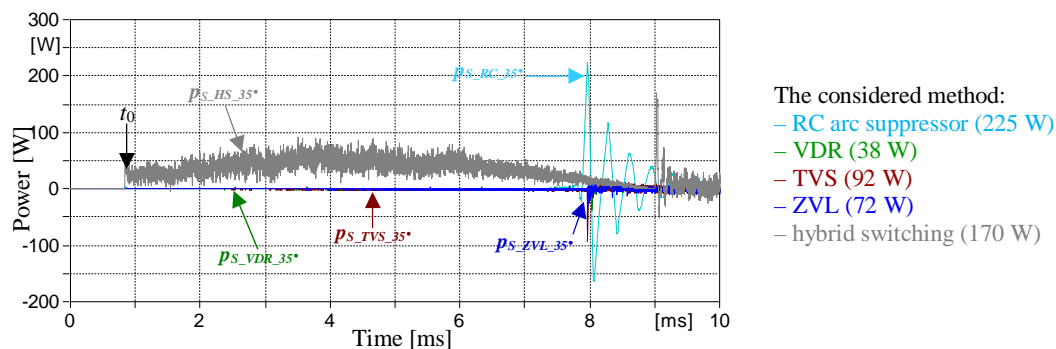


Figure 8.25. The waveforms of the calculated powers generated at the external branch for the different methods limiting the electric arc

The waveforms of the calculated powers presented in Figure 8.24 – Figure 8.25 show the similar trend with conclusions for the effectiveness of the considered methods that could be also visible in Figure 8.23 – Figure 8.24. For this reason, the detailed analysis of the waveforms of the electric powers is omitted in this section.

The waveforms of the electric arc energies e_A , as well as, the waveforms of the energies generated at the external branches e_B were calculated and presented respectively in Figure 8.24 – Figure 8.25. The calculations were performed based on data presented in Figure 8.26, and in Figure 8.27 according to the description presented in the section 6.1.2.

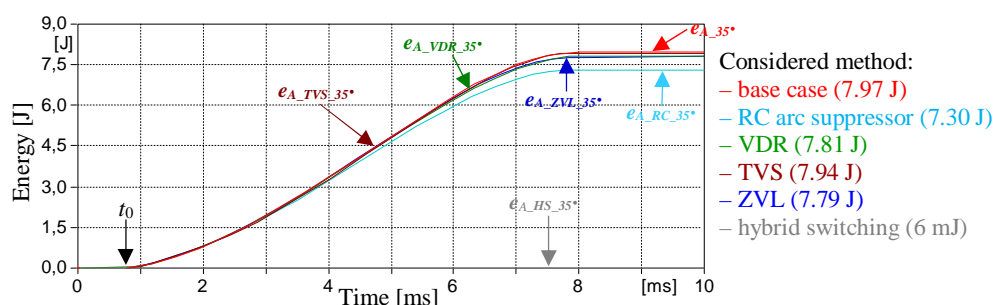


Figure 8.26. The waveforms of the calculated energies of the electric arc for the different methods limiting the electric arc

As shown in Figure 8.26, the conclusions from the previous part of this section can be confirmed. The application of the RC suppressor provides the limitation of the electric arc only slightly. The only method providing the effective limitation of the electric arc energy is the hybrid switching.

The comparison of the waveforms of the energies generated at the external branches e_B connected in parallel to the operated switch is presented in Figure 8.27.

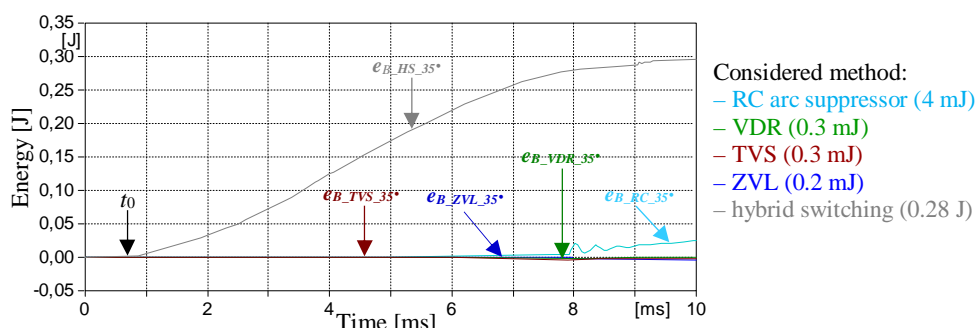


Figure 8.27. The waveforms of the calculated energies absorbed by the external branch for the different methods limiting the electric arc

As shown in Figure 8.27, the largest amount of the electric arc energy was absorbed by the SSR during the hybrid switching. In the situation, when the RC suppressor is connected in parallel to the operated switch, only the small amount of the energy is dissipated across the RC suppressor. Another considered branches, such as: the VDR, the ZVL, and the TVS do not absorb the energy during the entire current interruption. On the other hand, during the hybrid switching, the interrupting current $i_{S_HS_35^\circ}$ commutes into the parallel branch almost immediately after the contact separation, and the p-n junction resistance of the SSR is significantly lower than the resistance of the electric arc. For this reason, the application of the hybrid switching allows to limit significantly the electric arc energy, simultaneously with the very small energy absorbed by the semiconductor branch connected in parallel to the operated switch.

The waveforms illustrating the calculated electric arc resistance $r_{A_35^\circ}$ and the current of the operated switch $i_{S_35^\circ}$, when the standalone switch interrupts the current in the tested circuit are presented in Figure 8.28.

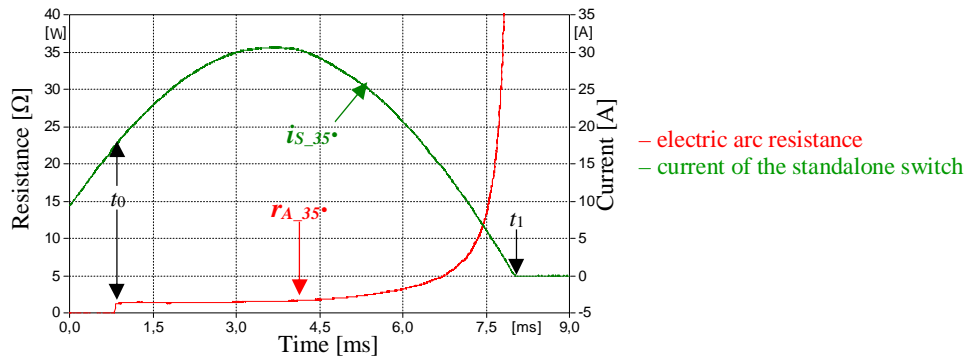


Figure 8.28. The calculated electric arc resistance and the measured current of the standalone switch during the current interruption

As illustrated in Figure 8.28, the contacts of the operated switch start to open just before 1st ms. At this time, the electric arc resistance achieves rapidly about 1 Ω. For next 5 ms, the electric arc resistance increases slightly up to about 3 Ω. Then, since 6th ms, the electric arc resistance $r_{A_35^\circ}$ rapidly increases, which causes the current $i_{S_35^\circ}$ at 8 ms to interrupt.

The character of the electric arc resistance is significantly different during the hybrid switching. Waveforms of the electric arc resistance $r_{A_HS_35^\circ}$, the semiconductor resistance $r_{B_HS_35^\circ}$ and the measured currents $i_{S_HS_35^\circ}$ and $i_{B_HS_35^\circ}$ during the hybrid switching are presented in Figure 8.29.

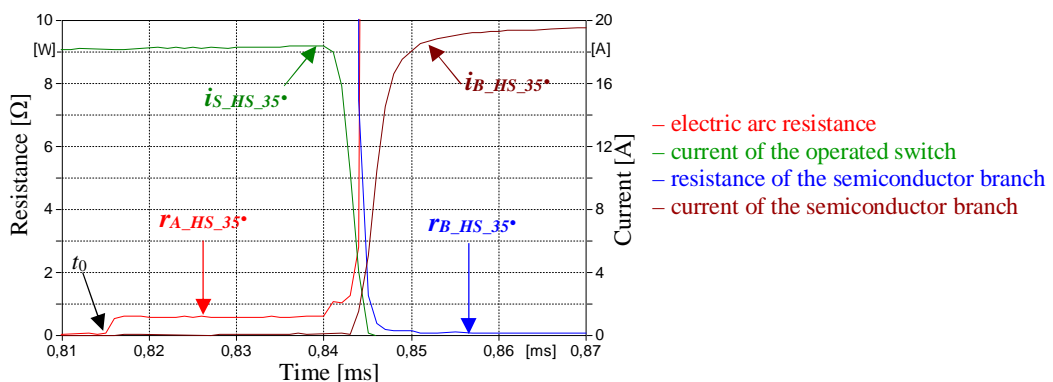


Figure 8.29. Waveforms of calculated resistances measured currents during hybrid switching

As shown in Figure 8.29, the electric arc resistance $r_{A_HS_35^\circ}$ reaches about 0.6 Ω just after the contacts separation and after next 30 μs, the resistance $r_{A_HS_35^\circ}$ starts to rapidly increase up. At the same time, the resistance of the semiconductor branch $r_{B_HS_35^\circ}$ rapidly decreases, and the current $i_{S_HS_35^\circ}$ starts to commute into the semiconductor branch. Finally, the resistance of the semiconductor branch $r_{B_HS_35^\circ}$ is significantly lower in comparison to the electric arc resistance $r_{A_HS_35^\circ}$ during the current interruption, and the semiconductor branch takes over the entire interrupted current. Just before the expected current zero-crossing $i_{B_HS_35^\circ}$ (above the minimal holding current of the applied SSR), the resistance of the semiconductor $r_{B_HS_35^\circ}$ rapidly increases, and as a consequence, the current stops flowing in the tested circuit.

9 Analysis of the Effects of Electric Arc Limitation

This chapter presents an analysis and a discussion on the effects of the considered methods for the limitation of the electric arc. In order to indicate direct differences in the effectiveness of the limitation of the electric arc for the different considered methods, the following features of the electric arc are compared in this section:

- the measured arcing times,
- the calculated electric arc energy,
- the calculated dynamic V-I characteristics of the electric arc,

Thus, the Voltage-Current characteristics of the electric arc, the comparison of the measured arcing times, as well as, the comparison of the calculated electric arc energies are presented in this section for all of the considered methods to compare the effectiveness of the limitation of the electric arc. Whereby, it was possible to indicate the influence of the application of the analyzed method on the effectiveness of the limitation electric arc. The analyses were performed for both voltage levels of the voltage source supplied the tested circuit (12 V and 230 V) to distinguish the effectiveness of the considered methods in both tested cases.

In this section, only the summary analysis is performed for selected, above-mentioned features of the electric arc to highlight the summary conclusions. The comparison of the measured and calculated waveforms of other analyzed magnitudes (such as: the measured currents, the measured voltage across the operated switch, the electric arc power, the power generated at external branch, the electric arc absorbed by external branch, the electric arc resistance, the resistance of external branch) were presented in the section 7.4 for the tested circuit supplied by the 12 V voltage source, as well as, in the section 8.4 for the tested circuit supplied by the 230 V voltage source. The analyses of the other magnitudes presented in these sections also confirm results of the analysis shown inhere.

9.1 Measurement Results Performed at 12 V

This section presents the analysis of the effects of the limitation of the electric arc for the considered methods applied to limit the electric arc energy in the tested circuit supplied by the 12 V supply voltage.

The analysis was conducted both for the time-controlled contact separation performed at the precise angle of the current period, as well as, for the connection of the external parallel branches into the operated switch, including also the hybrid switching method. The obtained measurement results were analyzed and discussed in details in the next part of this section.

9.1.1 Time-Controlled Contact Separation performed at Precise Time Slot of the Current Period

According to the description presented in the previous part of the thesis, performing the contact separation at the defined angle of the current period influences meaningfully on the arcing time and the electric arc energy in the tested circuit. Thus, performing the contact separation in controlled way due to the most appropriate time for the contact separation can lead to significant limitation of the electric arc. In order to compare the values of the electric arc times and the calculated electric arc energies for the different times of the contact

separation, data from Table 7.1 were taken and presented in the form of the column charts in Figure 9.1.

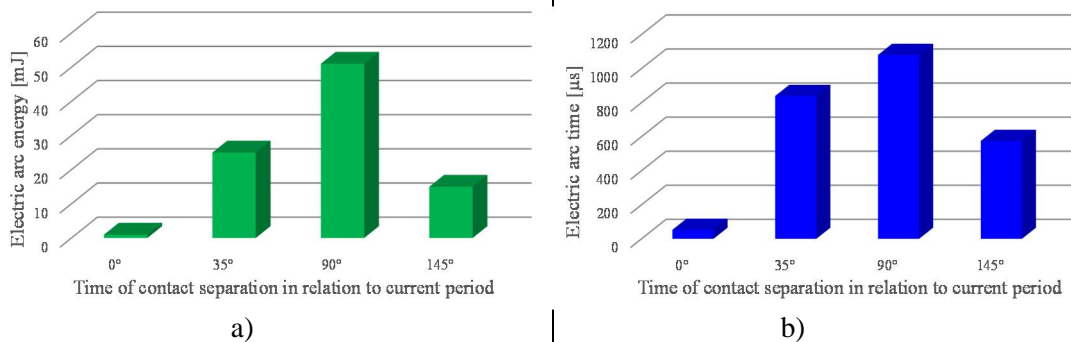


Figure 9.1. The column chart illustrating electric arc energies (a) and the electric arc times (b) for the contact separation performed in various times of the current period at 12 V

As shown in Figure 9.1.a, the electric arc energy is the smallest (less than 1 mJ) during the current interruption performed just before the current zero-crossing, whereas the highest value of the electric arc energy (51 mJ) occurs during the current interruption at the current extreme. The values of the electric arc energy during the contact separation at 35° and at 145° are comparable (respectively 25 mJ and 15 mJ). The same trend can be observed for the arcing times duration, which can be also visible in Figure 9.1b. Thus, when the contacts of the operated switch are separated just before the current zero-crossing, the current can be interrupted in the very short time.

In order to perform the detailed analysis of phenomena taking the part during creation of the electric arc at the time of the current interruption process, the dynamic voltage-current characteristics of the electric arc were calculated based on the waveforms of the interrupted current and the arcing voltage presented in the section 7.1. The calculated dynamic voltage-current characteristics for the time-controlled contact separation performed at the precise time slot of the current period are presented in Figure 9.2.

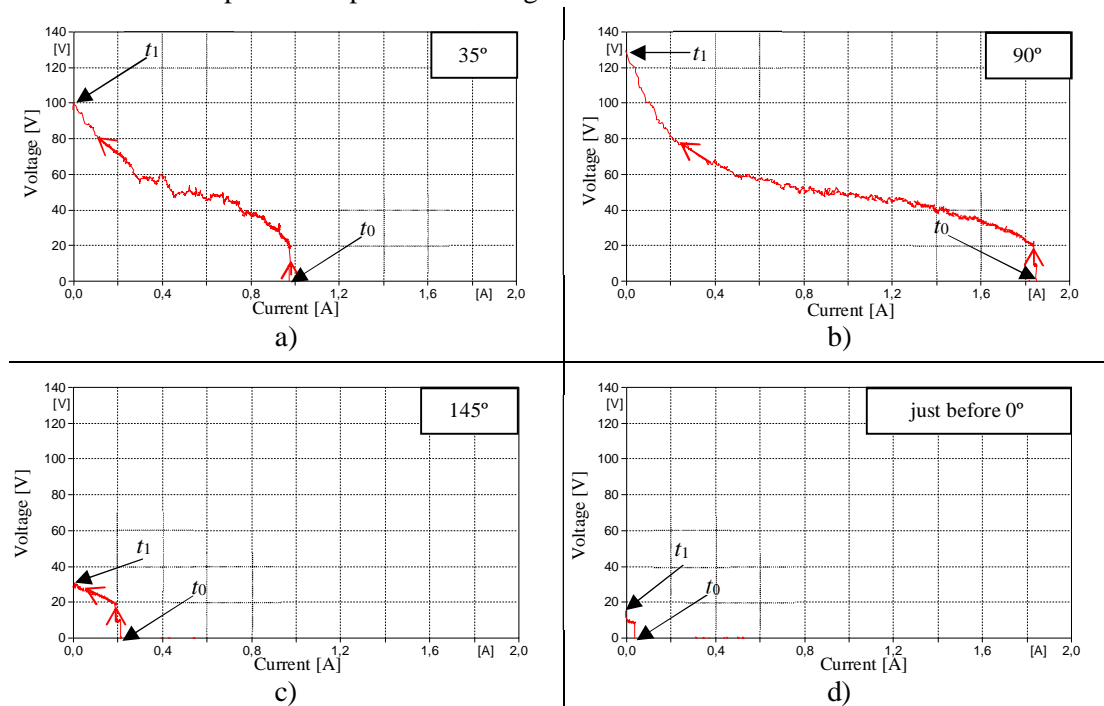


Figure 9.2. The V-I characteristics of the electric arc, the contact separation was performed at 12 V supply voltage at the angle of the current period: a) 35°, b) 90°, c) 145°, d) just before 0°

The direction of the development of the arcing voltage (from the time of the contact separation to time, when the electric arc quenches) is marked by means of the red arrows in each of the presented characteristic in Figure 9.2.

As shown in Figure 9.2, when the contacts of the operated switch start to separate just before the current zero-crossing, the arcing voltage does not exceed 20 V, however, when the contacts are separated at the current extreme, the arcing voltage can achieve even 130 V. When contacts are open at 35° and 145° of the current period, the arcing voltage achieves respectively 100 V and 30 V. Thus, the similar trend (in the comparison to Figure 9.1) can be also observed at the arcing voltage.

As shown in Figure 9.2, the arcing voltage can achieve significant values in the comparison to the maximum voltage peak value at 12 V of the supply voltage (about 17 V_{peak}). Figure 9.2b shows the worst case, when the arcing voltage achieves 130 V just before the current zero-crossing. The arcing voltages impacts significantly on the deformation of the current curve (according to the description presented in the section 3.3.2). For this reason, the current tends to the zero-crossing with the high steepness, independently of the time of the contact separation. This phenomenon is related to weak ionization conditions of the gas localized between the separated contacts of the operated switch: the relatively small value of the electric field, as well as, the small instantaneous value of the interrupting current, insufficient to achieve the significant temperature rise between the contact surface, which is necessary to obtain the powerful gas ionization (according to the description presented in chapter 3). The design of the operated switch to interrupt current has also the influence on the shape of the V-I arc characteristics – the electric arc is divided into two shorter arcs in both quenching chambers, which improves the cooling down parameters of the electric arc (see Figure 6.3). The averaged velocity of the contact separation is about 1 m/s, which also makes the good conditions for quick lengthening and cooling down the electric arc, which is reflected in the high resistance of the electric arc. These reasons impact the V-I electric arc characteristics through increasing the electric arc resistance rapidly that is a source of the significant arcing voltage and undesirable switching overvoltages in the tested circuit. This phenomenon can be especially observed in the TRV peaks (see Table 7.1). The values of overvoltages in the tested circuit exceed even 50 times (848 V) in the comparison to the voltage peak value at the steady state (about 17 V). The creation of significant overvoltages in arcing voltage is caused by the high value of the di/dt steepness (caused by the rapidly increasing high resistance of the electric arc) that is observed just after the contact separation. The creation of the significant overvoltages in the TRV is related to the energy stored in the inductive coil, which tends to discharge as soon as possible after the contact separation of the operated switch.

Thus, it can be concluded, that the control of the contact separation time in the reference to the instantaneous value of the interrupted current has the significant influence on the arcing time and the electric arc energy during the current interruption process. The application of the time-controlled contact separation can almost totally limit the electric arc energy (in the performed researches, this method allows to limit the electric arc energy from 51 mJ to 0.1 mJ for the two extreme cases, thus more than 99%). This method is also very helpful to limit the switching overvoltages, which can be also observed in the reduction of the TRV peak (from 848 V to 293 V for the two considered extreme cases).

However, in the practical implementation of the considered method, there could be a problem related to dispersion of the inertial delay time of the electromechanical drive of the operated switch. All of the researches presented in this thesis were performed at the similar environmental conditions. Therefore, the dispersion value of the inertial delay time of the electromechanical drive was always shorter than 1 ms. For this reason, it can be concluded that the implementation of this method at the constant environment conditions can limit the

energy arc significantly with the good reproducibility, when the inertial delay time of the electromechanical drive of the operated switch is known and repeatable. In order to perform the effective limitation of the electric arc energy, the contact separation should be always realized at least 1 ms before the expected zero-crossing of the interrupted current. In the practical maintenance of the operated switch, when the environment conditions can be variable, the presented method can provide different results due to the dispersion of the inertial delay time of the electromechanical drive of the operated switch. For this reason, the analysis of methods providing the limitation of the electric arc independently of the external factors is presented in the section 9.1.2.

9.1.2 Connection of the External Parallel Branches into the Operated Switch

According to the measurement results presented in the section 7.2, the connection of the different considered parallel branches into the operated switch can influence meaningfully on the arcing time, as well as, the electric arc energy. The electric arc energies and the arcing times for considered methods of the limitation of the electric arc (such as: the RC arc suppressor, the Voltage-Dependent Resistor, the Transient Voltage Suppressor, the Zener Voltage Limiter, as well as, the hybrid switching) are presented in Figure 9.3-Figure 9.4 based on the data taken from Table 7.2.

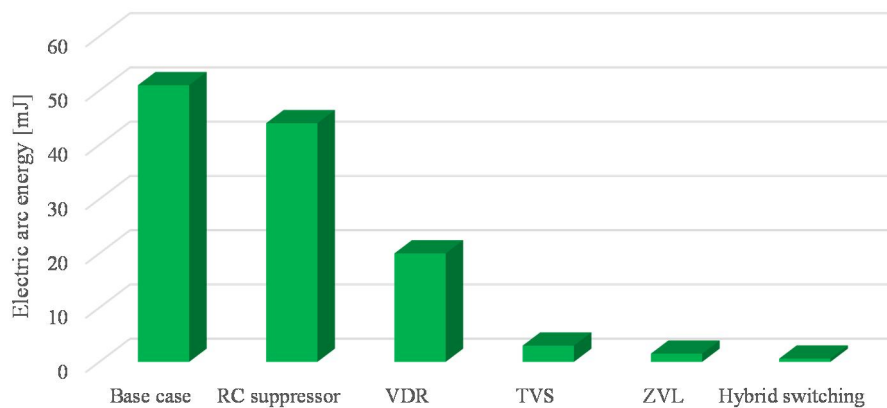


Figure 9.3. The calculated values of the electric arc energy for the different methods of the electric arc limitation, the data are taken from Table 7.2

As shown in Figure 9.3, the electric arc energy is limited in the different way depending on the selected method applied for this purpose. It can be concluded, that the least effective method for limiting the electric arc is the connection of the RC arc suppressor in parallel to the contacts of the operated switch (in this situation, the electric arc energy is limited only about 7 mJ, thus, it is only about 14% in comparison to the situation, when the operated switch interrupts the current as the standalone one).

The limitation of the electric arc energy through the application of the nonlinear voltage component in parallel to the operated switch is possible in this case, due to the significant value of the arcing voltage during the current interruption, greater than the value of the voltage supply source at the steady state. Thus, the current commutation is possible in this situation, because the nonlinear components start to conduct when arcing voltage exceeds the minimal operating voltage that has to be greater than the voltage peak of the voltage source at the steady state. The application of the nonlinear voltage components such as the Voltage-Dependent Resistor (VDR), the Transient Voltage Suppressor (TVS), and the Zener Voltage Limiter (ZVL) allows to limit the electric arc in the different way, better than the application of the RC arc suppressor. The differences in the level of the limited electric arc energy are related to the different parameters of the applied nonlinear voltage components (according to

the description presented in the section 6.3). In practice, the considered nonlinear voltage components start to conduct at the different voltage levels, with the different resistance level, and for this reason, the total amount of the absorbed energy is different for each of the considered components. The electric arc energy was limited in the smaller way, when the VDR was connected to the contacts of the operated switch. On the other hand, the application of the ZVL proved to be the most effective passive method to limit the electric arc energy among the all analyzed nonlinear voltage components. However, the method giving the best results for the limitation of the electric arc among all of the analyzed methods in the thesis proved to be the application of the hybrid switching.

The application of the hybrid switching in the tested circuit supplied by the 12 V voltage source allows to limit the electric arc energy from 50 mJ up to 0.6 mJ, which is about 99% in reference to the situation, when the operated switch interrupts the current as the standalone one. These good results are caused by the connection of the semiconductor branch with the small on-state resistance in parallel to the operated switch, which is fully-controlled by the microprocessor system. For this reason, the current commutation into external branch can be performed incomparably faster in reference to other considered methods, which causes significant limitation of the electric arc energy, and absorption of the small amount of the energy by the semiconductor branch. Thus, it can be concluded that the hybrid switching is the method providing the best results for the limitation of the electric arc in this situation.

The electric arcing times measured for the different method applied to limit the electric arc, are presented in Figure 9.4, according to the data listed in Table 7.2.

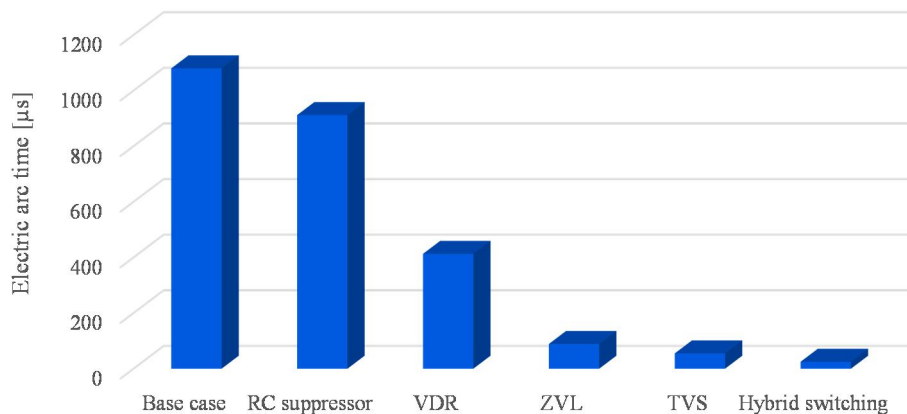


Figure 9.4. The electric arcing times presented for the different methods of the electric arc limitation, the data are taken from Table 7.2

As shown in Figure 9.4, similar trend with Figure 9.3 can be also observed in here. The least effective method for the limitation of the electric arc is the connection of the RC arc suppressor in parallel to the operated switch (it provides the reduction of the arcing time from 1080 μs to 912 μs, so only about 16% in comparison to the situation, when the operated switch interrupts the current as the standalone one). On the other hand, the method providing the best results is the hybrid switching (this solution provides limitation of the arcing time from 1080 μs to 35 μs, so about 99%).

In order to perform a detailed analysis of the electric arc phenomena during the current interruption process for the considered methods applied to limit the electric arc, the dynamic voltage-current characteristics of the electric arc were calculated. For this purpose, data taken from the waveforms presented in the section 7.2 were used. The dynamic voltage-current characteristics calculated for the connection of the different parallel branches in parallel to the operated switch are presented in Figure 9.5. The level of the peak voltage, which appears at the steady state between the contacts of the operated switch is marked as the blue line in

Figure 9.5a. The direction of the development of the arcing voltage (from the time of the contact separation to time, when the electric arc quenches) is marked by means of the red arrows in each of the presented characteristic.

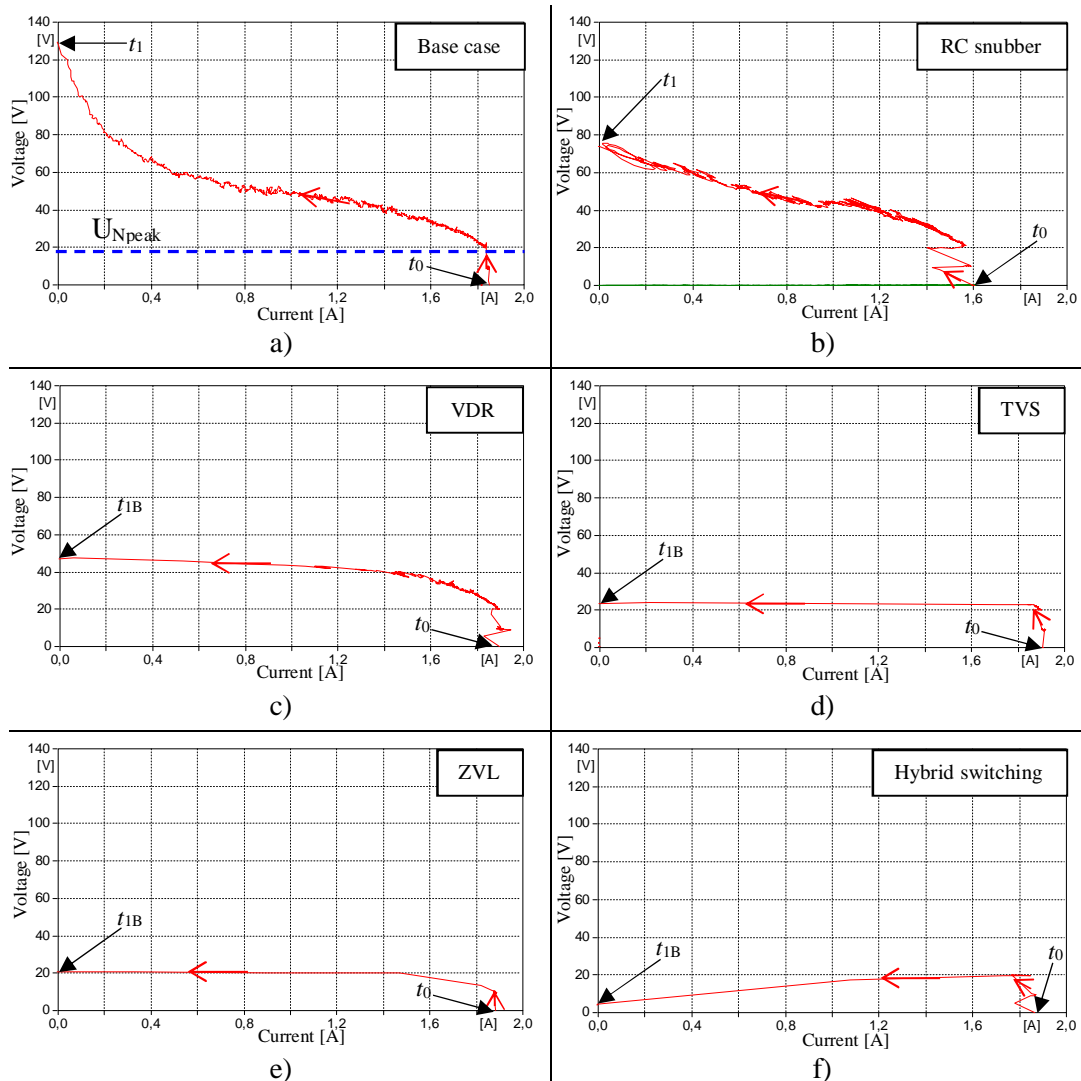


Figure 9.5. The dynamic V-I characteristics of the electric arc, the contact separation was performed at 90° of the current period, the characteristics were calculated for the following considered cases: a) the base case, b) the RC suppressor, c) the Voltage-Dependent Resistor, d) the Transient Voltage Suppressor, e) the Zener Voltage Limiter, f) the hybrid switching

As shown in Figure 9.5, the arcing voltage can be limited differently, in the dependence of the chosen considered method. The all calculated characteristics presented in Figure 9.5 show the case, when the contacts of the operated switch start to separate during the current extreme, due to the expected greater electric arc energy in comparison to other considered cases (according to the description presented in the previous part of the thesis). Figure 9.5a presents the base case, when the current is interrupted by the standalone switch. The value of the peak voltage at the steady state was marked by blue line ($U_{Npeak} \approx 17$ V). The arcing voltage in this case reaches about 130 V, thus over 7 times more than the voltage peak of the supply source at the steady state.

As illustrated in Figure 9.5b, the connection of the RC arc suppressor in parallel to the operated switch can limit the arcing voltage only partially (the maximum arcing voltage is limited up to about 75 V, thus about 42%). The current commutates into the RC branch only,

when the arcing voltage reaches the high steepness dU/dt , which can be also observed in Figure 7.9b. Based on data listed in Table 7.2, the application of this method can limit the arcing time in the analyzed case by about 16%, and the electric arc energy by about 14%. Thus, it can be concluded that this method can influence limitation of the electric arc only slightly. However, in some cases, the connection of the RC arc suppressor in parallel to the operated switch can be worth considering due to its application simplicity, as well as, the low cost of this method.

Figure 9.5c-Figure 9.5e show the situation, when the nonlinear-voltage component is connected in parallel into the operated switch. In dependence on the minimal operating voltage of the applied component, the considered parallel branch starts to commute the current at the various voltage levels, providing different influence on the limitation of the electric arc. Among all of the considered methods, the method providing the most satisfactory results is the connection of the Zener Voltage Limiter in parallel to the operated switch. In this case, the arcing voltage is limited up to about 22 V (about 83%), which also provides limitation of the arcing time by about 92% and limitation of the electric arc energy by about 97%. In contrast to this situation, the connection of the Voltage-Dependent Resistor into the operated switch causes limitation of the arcing voltage only to about 49 V (by about 62%), and provides limitation of the arcing time by about 62%, and the limitation of the electric arc energy by about 61%.

Figure 9.5b-Figure 9.5e present the V-I characteristics of the electric arc calculated for the passive methods limiting the electric arc (which do not require the external power supply). However, among all analyzed approaches, the most effective proved to be the hybrid switching providing the most satisfactory results. Figure 9.2f presents the V-I characteristic of the electric arc calculated for the hybrid switching. In this case, the current starts to commutate into the external branch, when the arcing voltage exceeds the minimal operated voltage of the applied Solid State Relay (for this reason, the arcing voltage is limited up to 22 V, so about 83%). This provides the limitation of the arcing times by about 98% and the electric arc energy by about 99%.

9.2 Measurement Results Performed at 230 V

This section presents the analysis of the effects of the limitation of the electric arc for the considered methods applied to limit the electric arc energy in the tested circuit supplied by the 230 V supply voltage.

The analysis was conducted both for the time-controlled contact separation performed at the precise angle of the current period, as well as, for the connection of the external parallel branches into the operated switch, including also the hybrid switching method. The obtained measurement results were analyzed and discussed in details in the next part of this section.

9.2.1 Time-Controlled Contact Separation performed at Precise Time Slot of the Current Period

According to the description presented in the previous part of the thesis, performing the contact separation at the defined angle of the current period influences on the arcing time and the electric arc energy meaningfully. Thus, performing the contact separation in controlled way due to the most appropriate time for the contact separation can lead to significant limitation of the electric arc.

In order to compare the measured values of the electric arc times and the calculated electric arc energies for the different contact separation times, data were taken from Table 8.1 and presented in the form of the column charts in Figure 9.6.

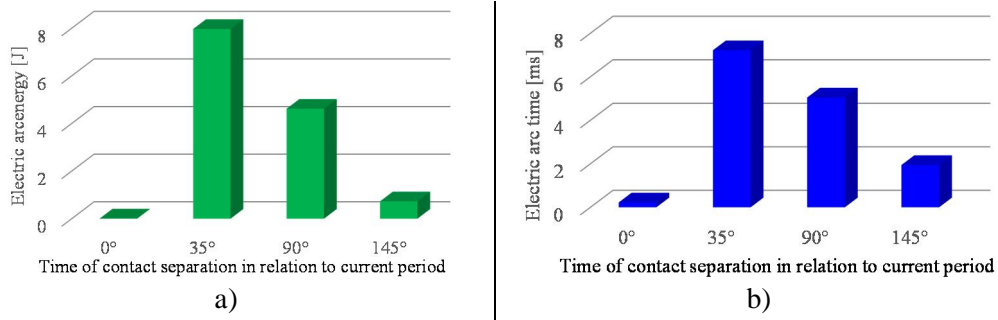


Figure 9.6. The column chart illustrating electric arc energies (a) and the electric arc times (b) for the contact separation performed in various times of the current period at 230 V

As shown in Figure 9.6a, the electric arc energy is the smallest (less than 10 mJ) during the contact separation performed just before the current zero-crossing, whereas the higher value of the electric arc energy (almost 8 J) can be noticeable during the contact separation performed at 35° of the current period. The values of the electric arc energy for the contact separation performed at 90° and at 145° of the current period were calculated respectively as 4.62 J and 0.73 J. Thus, it can be concluded, that the electric arc energy is the smallest, when the contacts are separated after the current extreme, while the current tends to its natural zero-crossing. The same trend can be observed in case of the analysis of the arcing times duration, which can be visible in Figure 9.6b. The character of the column charts presented in Figure 9.6a-Figure 9.6b is very similar.

In order to perform the detailed analysis of electric arc phenomena during the current interruption process, the dynamic voltage-current characteristics of the electric arc were calculated based on the waveforms of the interrupted current and the arcing voltage presented in the section 8.1. The calculated voltage-current characteristics for the time-controlled current interruption at the precise time slot of the current period are presented in Figure 9.7.

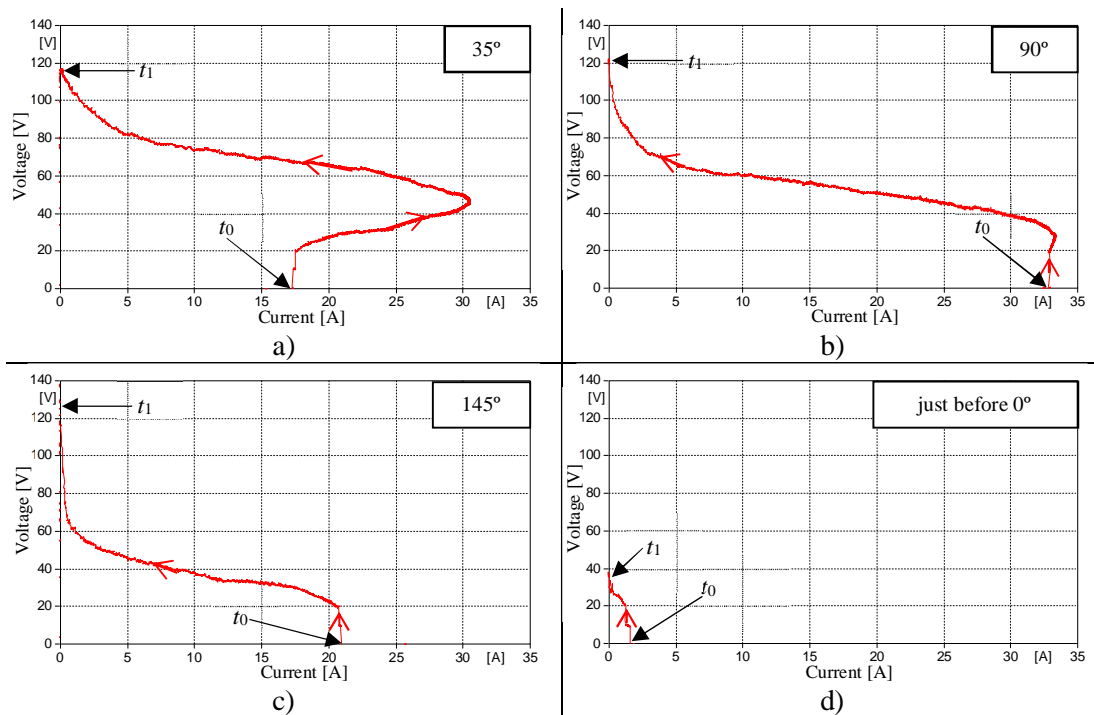


Figure 9.7. The dynamic V-I characteristics of the electric arc, the contact separation was performed at 230 V supply voltage at the angle of the current period: a) 35°, b) 90°, c) 145°, d) just before 0°

The development of the creation of the arcing voltage (from the time of the contact separation to time, when the electric arc quenches) is marked by means of red arrows in each of the presented characteristic in Figure 9.7.

As shown in Figure 9.7a-Figure 9.7c, the arcing voltage achieves the maximum value about 120 V in analyzed cases, when the contacts are separated at 35°, 90° and at 145° of the current period. In opposite to these situations, the maximum observed arcing voltage is significantly lower (about 40 V), when the contacts of the operated switch start to separate just before the natural current zero-crossing (Figure 9.7d). Thus, it can be concluded that the shape of the observed V-I characteristics depends on the time of the contact separation of the operated switch.

When the contacts of the operated switch start to separate at 35° of the current period, while the instantaneous value of the current increases after the contact separation, the current still increases up to about 30 A together with the arcing voltage (50 V) up to time of the expected current extreme. In the analyzed circuit during the steady state, when the contacts of the operated switch are closed and the current flows thorough the inductive load, the current peak value is about 35 A. The difference 5 A between both peak values is caused by the presence of the resistance of the electric arc during the current interruption. Just after the current extreme, the current starts to tend to its zero-crossing. During this process, the arcing voltage still increases up to about 120 V, up to the time, when the current achieves its zero-crossing. This phenomenon is related to more intensive (in comparison to the situation presented in the section 9.1.1) ionization conditions of the gas located between contacts in the arc column: the relatively greater value of the electric field, as well as, the greater instantaneous value of the interrupting current, resulted in achieving the higher rise of the temperature around the contact surface, which is necessary to obtain the more intense gas ionization (according to the description presented in the chapter 3). In this case, the electric arc burns more intensively and stably, which influences the electric arc resistance that is much lower in comparison to situation, when the operated switch interrupts current in the tested circuit supplied by the 12 V voltage source. Smaller arc resistance also caused a situation when the observed di/dt steepness after the contact separation is significantly lower in comparison to the situation, when the current interruption is performed in the tested circuit supplied by the 12 V voltage source. In this considered case, the electric arc resistance increases more slight after the contact separation. For this reason, the longest arcing time and the greatest electric arc energy can be noticeable, when the contacts of the operated switch are separated at 35° of the current period in the analyzed circuit (according to Table 8.1). Thus, during the most intensive ionization of gas, the value of the electric arc resistance is smaller, and the electric arc burns longer, and the observed current curve after the contact separation is not deformed significantly in comparison to measurement results presented in chapter 7. The smaller arc resistance also influences smaller arcing voltage. Thus, the maximum observed arcing voltage does not exceed even the half of the voltage peak of the supply voltage at the steady state ($U_{S_peak} \approx 325$ V). This is the important difference in comparison to the observed arcing voltages in the tested circuit supplied by the 12 V voltage source, when the arcing voltage achieves over 10 times in comparison to the voltage peak of the supply voltage at the steady state.

The V-I characteristics of the electric arc presented in Figure 9.7b and Figure 9.7c are very similar in the shape. Thus, when the contacts of the operated switch open, while the instantaneous value of the interrupting current decreases, the arcing voltage also increases similarly. In this case, the steepness of the increasing arcing voltage depends on the value of the interrupted current, when the contacts of the operated switch start to separate.

Thus, it can be concluded, that the time of the contact separation performed in reference to the instantaneous value of the interrupted current has the significant influence on the arcing time and the electric arc energy during the current interruption process. The application of this method can limit the electric arc energy almost totally (in the performed researches, this method allows to limit the electric arc energy from 7.97 J to about 0.10 J for the two extreme cases, thus about 99%). Thus, it can be concluded, that in this situation, the most favorable time for the contact separation is observed just before the natural current zero-crossing. This can be also noticeable in Figure 9.7d, where the arcing voltage does not exceed even 40 V.

However, according to the description presented in the section 9.2.1, the application of the considered method in practical implementation with the recurrent effectiveness could be problematic. For this reason, the analysis of methods providing the limitation of the electric arc independently of external factors is presented in the section 9.2.2.

9.2.2 Connection of the External Parallel Branches into the Operated Switch

Similarly to the analysis presented in the section 9.1.2, which was performed for the measurement results for 12 V of the supply voltage in the tested circuit, the influence of the connection of the different parallel branches in parallel to the operated switch (according to the measurement results presented in the section 8.2.) was investigated inhere for the tests performed in the circuit supplied by the 230 V the supply voltage.

The electric arc energies and the arcing times for the considered methods of the limitation of the electric arc were presented in Figure 9.8-Figure 9.9 respectively, based on the data taken from Table 8.2.

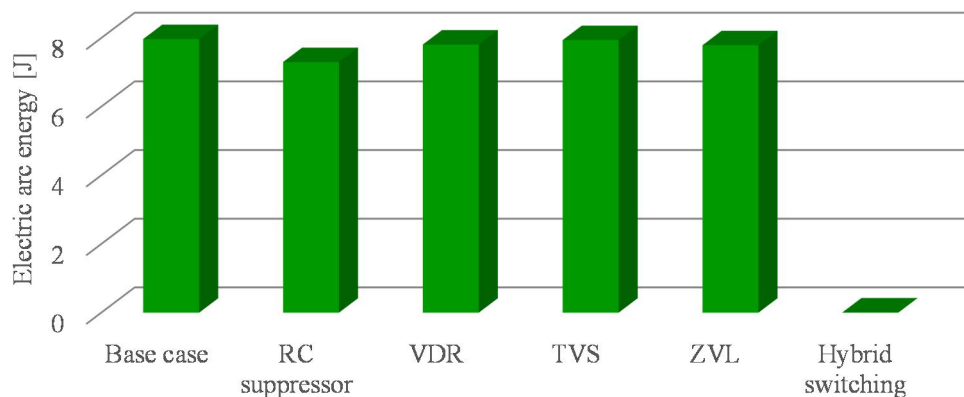


Figure 9.8. The calculated values of the electric arc energy for the different methods of the electric arc limitation, the data are taken from Table 8.2

As shown in Figure 9.8, the electric arc energy is comparable for the following cases: base case, the RC suppressor, the VDR, the TVS, the ZVL. As it can be noticeable, the application of the RC arc suppressor allows to limit the electric arc energy only slightly (about 680 mJ, so over 8%) in comparison to the situation, when the current was interrupted in the analyzed circuit by the standalone switch. Only a small amount of the current is commuted into the RC suppressor branch just after the contact separation of the operated switch.

The connection of the VDR, the TVS and the ZVL in parallel to the operated switch does not limit the electric arc energy even slightly. This is observed, because the arcing voltage is significantly below their minimal operating voltages. For this reason, the commutation process is not possible at time, when the electric arc burns between the contacts of the operated switch. Thus, the VDR, the TVS, as well as, the ZVL connected in parallel to the operated switch start to conduct in the tested circuit only after the current zero-crossing, when the TRV exceeds their minimal operating voltages. The noticeable small differences in the calculated electric arc energies for the following cases: the base case, and the connection of the VDR,

the TVS and the ZVL in parallel to the operated switch are caused only by the random phenomena taking the part in the physical process of the formation of electric arc between the contacts of the operated switch.

The method providing the satisfactory results for the limitation of the electric arc is the hybrid switching (in this situation, the electric arc energy is reduced from 7.97 J up to 6 mJ, which is about 99.9% in reference to the base case). These good results are caused by the connection of the semiconductor branch in parallel to the operated switch, which is fully-controlled by the microprocessor system. Thus, it can be concluded that the hybrid switching is the only method providing satisfactory results for the limitation of the electric arc.

The electric arcing times for the considered methods of the limitation of the electric arc are presented in Figure 9.9 based on data listed in Table 8.2.

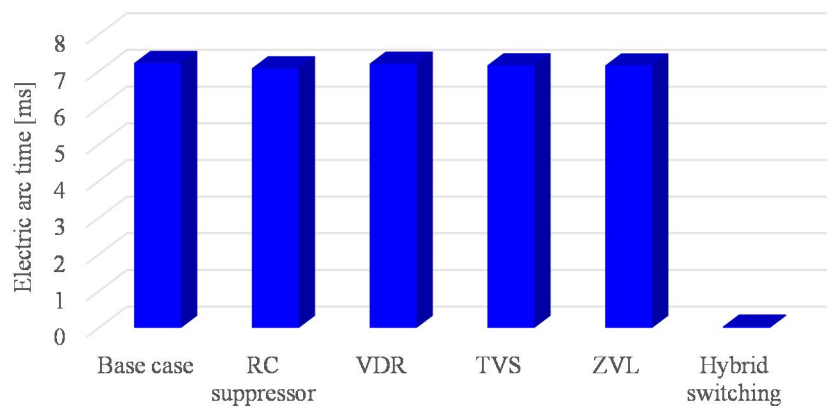


Figure 9.9. The calculated values of the electric arcing times for the different methods of the electric arc limitation, the data are taken from Table 8.2

As shown in Figure 9.9, the similar trend with Figure 9.8 can be also observed. The connection of the RC arc suppressor in parallel to the operated switch limits the arcing times only slightly (it provides the reduction of the arcing time from 7.222 ms to 7.078 ms, so about 2%). The method providing the significant limitation of the arcing time is the hybrid switching (this method provides limitation of the arcing time from 7.222 ms to 35 μ s, so about 99.5%).

Based on the data presented in Figure 9.8-Figure 9.9, it can be concluded that the hybrid switching is the most effective method providing the best results for the limitation both of electric arc energy, as well as, the electric arcing time in the tested circuit supplied by the 230 V voltage source.

In order to perform a detailed analysis of the electric arc phenomena during the current interruption process for the considered methods applied to limit the electric arc, the voltage-current characteristics of the electric arc were calculated. For this purpose, data taken from the waveforms presented in the section 8.2 were used. The calculated dynamic voltage-current characteristics for the connection of the different parallel branches in parallel to the operated switch are presented in Figure 9.10. The level of the peak voltage, which appears at the steady state between the contacts of the operated switch is marked as the blue line in Figure 9.10a. The direction of the development of the arcing voltage (from the time of the contact separation to time, when the electric arc quenches) is marked by means of the red arrows in each of the presented characteristic.

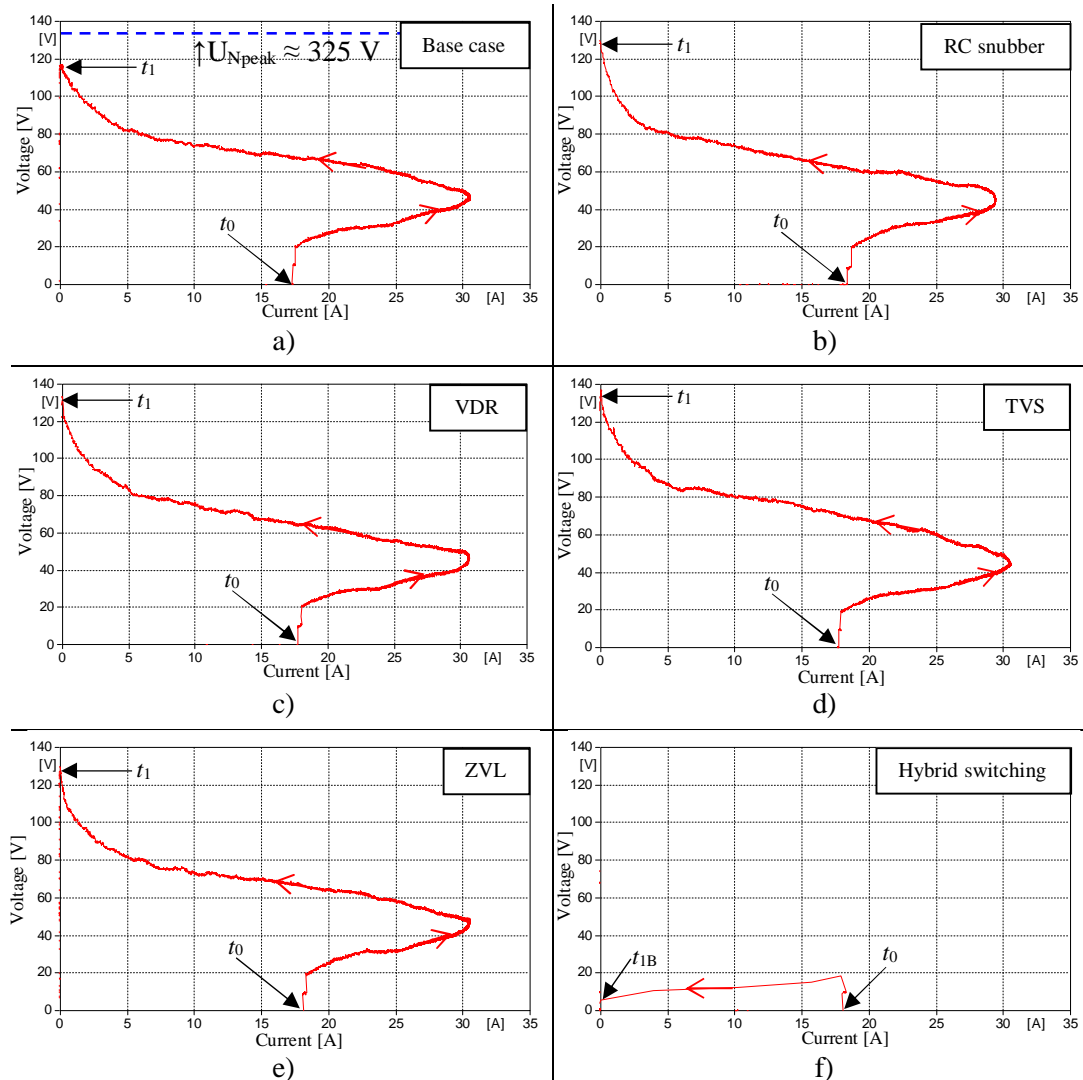


Figure 9.10. The dynamic V-I characteristics of the electric arc, the contact separation was performed at 230 V supply voltage at 35° of the current period, the characteristics were calculated for the following considered cases: a) the base case, b) the RC suppressor, c) the Voltage-Dependent Resistor, d) the Transient Voltage Suppressor, e) the Zener Voltage Limiter, f) the hybrid switching

As shown in Figure 9.10a - Figure 9.10e, the V-I characteristics of the electric arc are characterized by the similar shape, the arcing voltage increases up to about 120-130 V. The voltage peak value in the tested circuit during the steady state, when the contacts of the operated switch is about 325 V, which was illustrated in Figure 9.10a.

The connection of the RC suppressor in parallel to the operated switch practically does not influence on the V-I characteristic of the electric arc, which can be observed in Figure 9.10b. The small amount of the current is commutated into the external branch, which is not reflected in the shape of V-I characteristic of the electric arc.

The connection of the nonlinear voltage components, such as: the VDR, the TVS, and the ZVL in parallel to the operated switch does not impact on the V-I characteristics of the electric arc in any way. Each of these voltage-dependent components start to conduct the current, when the voltage across the operated switch achieves the overvoltage greater than their minimal operating voltages which have to be greater than the peak voltage of the supply voltage source during the steady state. On the other hand, in this case, the arcing voltage does not exceed even the half of the peak voltage of the voltage source during the steady state. For

this reason, the considered nonlinear voltage components do not take part in the commutation process. The considered nonlinear components start to conduct only for short time just after quenching the electric arc, when the TRV value exceeds their minimal operating voltages. Therefore, in the analyzed circuit supplied by the 230 V voltage source, the application of the VDR, the TVS, and the ZVL in parallel to the operated switch does not influence on the V-I characteristics, as well as, the limitation of the electric arc energy during the current interruption process. The slight differences in the observed V-I characteristics for these cases are caused only by random phenomena taking part in a physical process of the electric arc formulation. Thus, it can be concluded, that in this case, the nonlinear voltage components only perform the function of the overvoltage protection.

Thus, the only method that is able to limit the electric arc energy effectively in this situation is the application of the hybrid switching. As shown in Figure 9.10f, the V-I characteristic of the electric arc is completely different in comparison to the characteristics presented in Figure 9.10a-Figure 9.10e. During the hybrid switching, the interrupting current starts to commute into the external branch when the arcing voltage exceeds the minimal operated voltage of the applied Solid State Relay (thus, in practice, the arcing voltage does not exceed about 20 V, so it is limited about 84%). The application of the hybrid switching method provides limitation of the arcing times about 99.5% and the electric arc energy about 99.9%.

10 Observations of the Limitation of the Electric Arc Performed by the High Speed Camera

In order to investigate the formulation of the electric arc between the contacts of the operated switch, the researches were performed by means of the High Speed Camera. This device allows to register the movies in the slow motion.

According to the detailed plan presented in the section 6.5, the observations of the formulation of the electric arc between the contacts of the operated switch were performed for the two cases:

- the current was interrupted in the tested circuit by means of the standalone operated switch,
- the current was interrupted in the tested circuit by means of the operated switch with implemented hybrid switching system (see the section 6.4 for details).

The observations were performed for the contact system of the operated switch during the current interruption. The simplified diagram of the single-pole contact system of the operated switch is presented in Figure 6.3. The different stages of the contact movement can be visible in the registered frames. The observations were performed for the time, when the contacts of the operated switch start to separate, up to the time, when the contacts of the operated switch become to be fully opened.

The observations were performed in the tested circuit supplied at 230 V, when the contacts of the operated switch start to separate at 35° of the current period. These conditions were selected to the observations of the contact system due to the greater value of the energy arc during the current interruption process among the all analyzed cases (see the section 7.4 and the section 8.4 for the more details). For this reason, the registered differences for the two compared situations can be highlighted.

The key features of the High Speed Camera (AOS Technologies, type AG Q-MIZE) [9] used to the observations, as well as, the description of the modification of the operated switch (a sidewall of the relay housing were removed, whereby the contact system of the operated switch could be visible to perform the observations, see Figure 6.11 for the details) were also presented in the section 6.5.

In this chapter, the pictures presented as the single frames from the registered movies in slow-motion are shown. The registered movies are placed in the Compact Disc, which is attached to the thesis.

10.1 Registration of the Formulation of the Electric Arc in the Standalone Switch

Figure 10.1 presents the frames registered during the current interruption performed by the standalone switch. The presented inhere frames illustrate the contact system of the standalone operated switch at the different stages of the movement of the contacts.

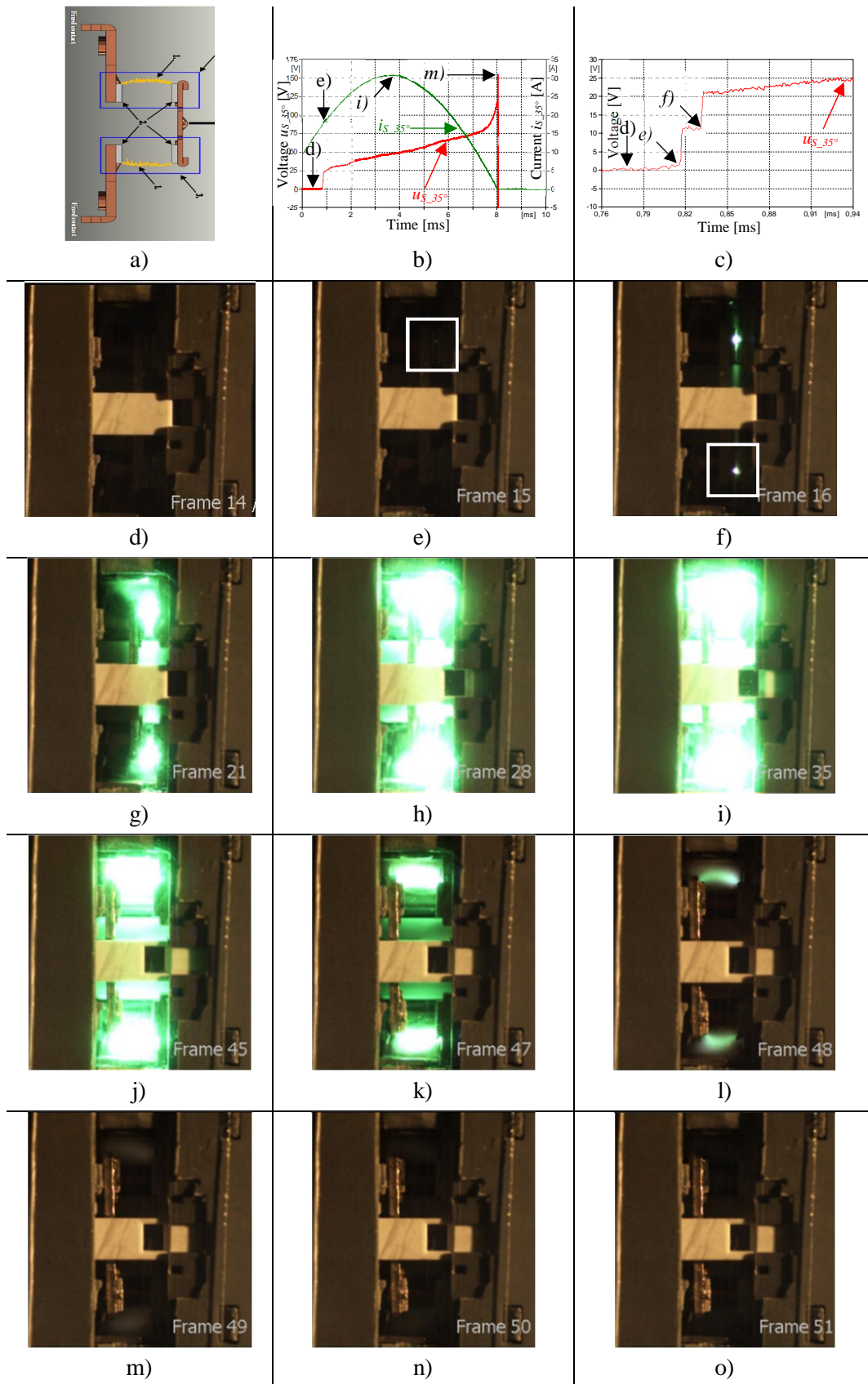


Figure 10.1. The contact system (a); waveforms of the current i_s and the voltage u_s with marked number of frames (b), (c); the contact system registered by the High Speed Camera at the different stages of the contact movement (d)-(o). Frames registered for the standalone switch, the contacts start to separate at 35° of the current period at 230 V

Figure 10.1a shows the contact system of the operated switch (according to Figure 6.13). Figure 10.1b presents measured current (green) and arcing voltage (red) during current interruption together with marked reference to registered frames. Zoomed waveform of arcing voltage at the time when the electric arc starts to burn and the bridge explodes is presented in Figure 10.1c.

Figure 10.1d presents the closed contacts of the operated switch just before the time, when the contacts start to separate (the entire current of the tested circuit flows through the closed contacts).

Figure 10.1e illustrates the situation, when the contacts start to separate. The moveable contact (see Figure 6.3) starts to move not simultaneously, so as a consequence, the bridge explodes and the electric arc burns firstly in the one of the two quenching chambers, which was marked as the white frame in Figure 10.1e. Time of burning the electric arc between contacts that were placed in first chamber takes about 35 μ s.

Just after that, the contacts continue its movement, and second bridge explodes (white frame in Figure 10.1f), which as a consequence leads to burning the electric arc in the second quenching chamber. This phenomenon causes the stair-shape of the arcing voltage at the beginning of the all measured voltage waveforms across the operated switch for the all performed measurements presented in the thesis.

Figure 10.1g-Figure 10.1i show how the electric arc starts to burn more intensely (which can be observed as a form of expanding arc column), up to the time, when the interrupting current achieves its extreme value. When the current is maximal (Figure 10.1i), strong process of evaporation of electrodes can be observed. Moreover, formation of the intense plasma channel that is created from connected anode flux and cathode flux can be observed. At this time, diameter of plasma channel is even greater than surface of contacts. Metal vapors of electrodes influence also the color of discharge [25]. When the current starts to decrease the electric arc quenches, which can be observed in Figure 10.1i-Figure 10.1l, where the diameter of plasma channel decreases.

Figure 10.1m-Figure 10.1n present hot remnants of drops and vapors of contact material. At this time, the current already does not flow in the tested circuit anymore. Figure 10.1o shows the opened contacts of the operated switch just after the current interruption.

Based on observed intensity of the electric arc it can be stated that temperature of metal drops leaving the area of the electric arc increases with a rise of the current intensity. A much bigger number of metal drops can be observed around column of the electric arc that are dissipated into surroundings, and sizes of metal drops that were emitted outside of the electric arc column decrease significantly.

10.2 Registration of the Formation of the Electric Arc during the Hybrid Switching

In order to indicate the difference in the intensity of the burning electric arc during the hybrid switching, the registration of the contact system was performed while the current was interrupted with the application of the hybrid method.

Figure 10.2 presents the frames registered during hybrid switching, illustrating the contact system of the operated switch for the different stages of the movement of the moveable contact.

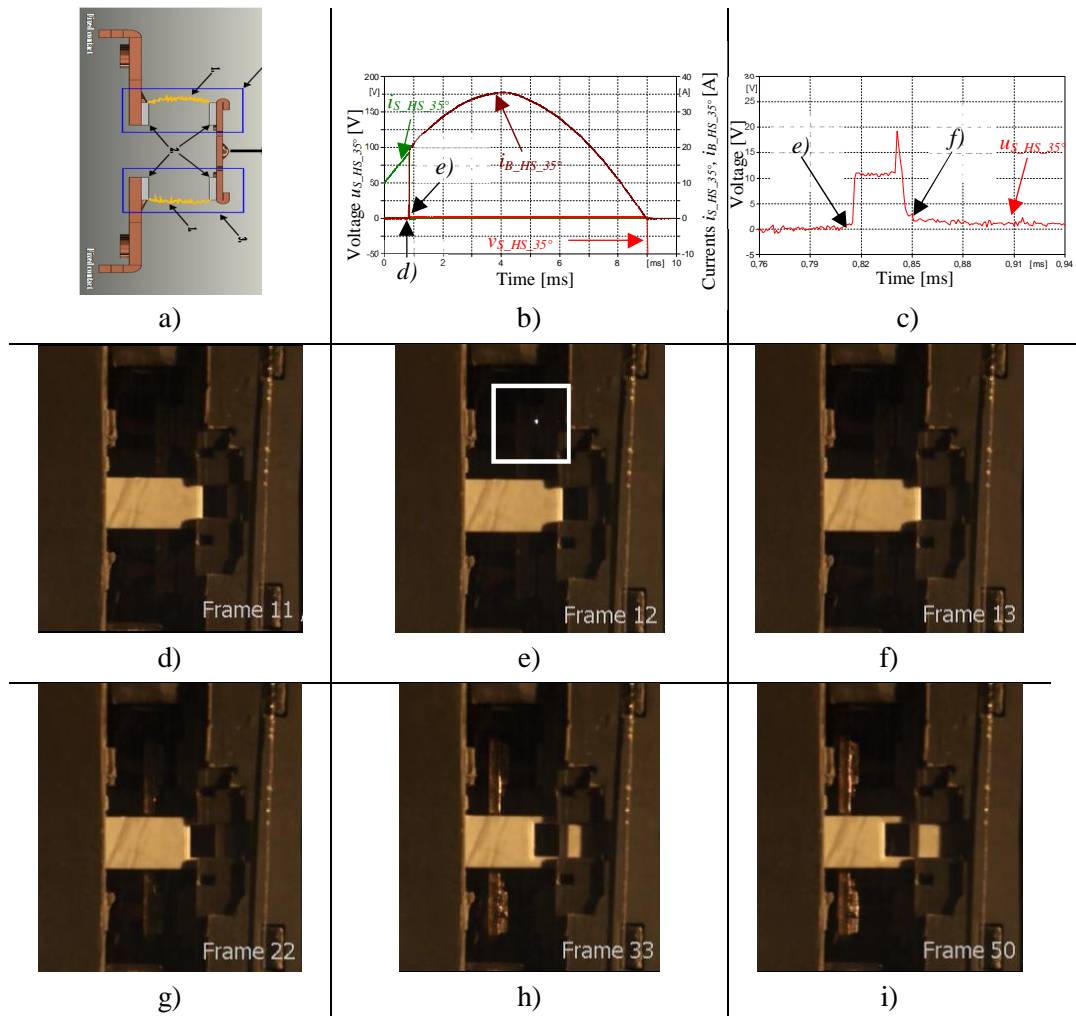


Figure 10.2. The contact system (a); waveforms of the current i_s and the voltage u_s with marked number of frames (b), (c); The contact system registered by the High Speed Camera at the different stages of the contact movement (d)-(i). Frames registered for the hybrid switching, the contacts start to separate at 35° of the current period at 230 V

Similarly to the description presented in section 10.1, Figure 10.2a shows the contact system of the operated switch (according to Figure 6.13). Figure 10.2b presents measured current (green) and arcing voltage (red) during current interruption together with marked reference to registered frames. Zoomed waveform of arcing voltage at the time when the electric arc starts to burn and the bridge explodes is presented in Figure 10.2.

As shown in Figure 10.2d, the contacts are closed and the entire current of the tested circuit flows through the contacts of the operated switch.

Figure 10.2e shows the time, when the contacts start to separate. Similarly to the situation presented in section 10.1, the analyzed inhere contacts also start to move not simultaneously, so as a consequence, the bridge explodes and the electric arc burns firstly in the one of the two quenching chambers, which is marked as the blue frame in Figure 10.2e. This state takes about 35 μ s.

Just after that, the bridge starts to explode between contacts in second chamber and the electric arc starts to burn, so as a consequence the arcing voltage achieves the value of the minimal operating voltage of the Solid State Relay. At this time, the entire interrupted current is able to commute into the semiconductor branch, so as a consequence, the electric arc quenches which can be observed in Figure 10.2f.

In the next sequence, the contacts open already without the electric arc, which was illustrated in Figure 10.2g-Figure 10.2i. In the meantime, the commuted current into the semiconductor branch exceeds the minimal holding current of the Solid State Relay, whereby the current stops flowing in the entire tested circuit.

Figure 10.2f shows the situation, when the contacts are opened fully, and the current already does not flow in the tested circuit anymore.

10.3 Comparison of the Results

In order to indicate differences in the intensity of the burning electric arc for the both analyzed cases (when the current was interrupted by the standalone switch, as well as, during the hybrid switching). The two frames taken from the registered movies were compared and presented in Figure 10.3 at the time, when the electric arc was registered as the most intensive.

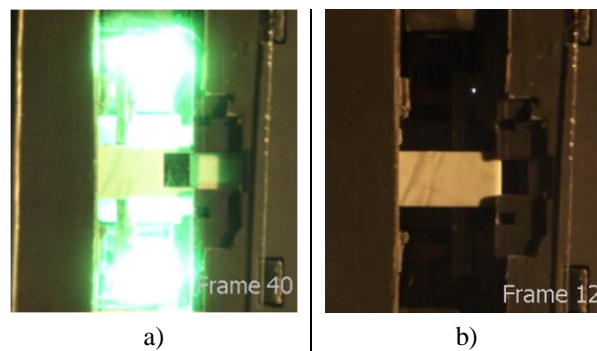


Figure 10.3. The comparison of electric arc intensity. The time, when the electric arc is the most intensive: a) the current interrupted by the standalone switch; b) the hybrid switching

As shown in Figure 10.3, the electric arc is incomparably more intensive, when the current is interrupted by the standalone switch. This significantly influences on the level of the created electric arc erosion in the contact surfaces during the standard maintenance of the switch.

The read out values of the arcing time from the measured waveforms (based on the chapter 8) and from registered movies were listed and compared in Table 10.1.

Table 10.1. The comparison of the read out values of the arcing times

The experiment scenario	The digital oscilloscope	The High Speed Camera
The standalone switch	About 7.2 ms	32 frames (about 8ms)
The hybrid switching	35 μ s	1 frame (250 μ s)

As shown in Table 10.1, the read out values of the arcing times are comparable for the both measurement approaches, when the current is interrupted by the standalone switch. The High Speed Camera was able to register only the 1 frame illustrating the electric arc during the hybrid switching, due to the low registration resolution (the 1 frame per each 250 μ s). In this case, the measurements performed by the digital oscilloscope were more accurate.

11 Evaluation of the Electric Arc Erosion of the Electrical Contacts in the Tested Switches

In this chapter, the morphology analysis performed for the investigated contacts is presented. In order to perform the researches on the limitation of the electric arc erosion, 200 000 cycles of current interruptions were conducted in the tested circuit totally. The overall research plan is presented in the section 6.1.3, and the detailed description of the experiments is presented in the section 6.5.

In order to compare the condition of the surfaces of the contacts taken from the analyzed switches, the following methods were applied: photographs of the analyzed contacts, the measurements of the roughness profiles of the analyzed contact surfaces, the optical microscope observations and the Scanning Electron Microscopy (SEM) method coupled with the Energy Dispersion Spectroscopy (EDS). The areas of the contacts localized as closely possible to the inner edge were chosen for the analysis, due to expected greatest degree of the arc erosion in this area. The examined areas of the analyzed contacts are presented in Figure 6.15 (marked as the white circle). The measurements performed by the roughness tester were conducted across the coaxial line on the contact surfaces (see Figure 6.16 for the details).

11.1 Condition of the Surfaces of the Contacts

According to the research plan, the contacts taken from the all tested switches were photographed, and their photos are presented in this section. Also the contact taken from the new switch was photographed to compare the impact of the arc erosion. Figure 11.1 presents a comparison of the surfaces of the all fixed contacts (the contacts #2 according to the notations presented in Figure 6.13).

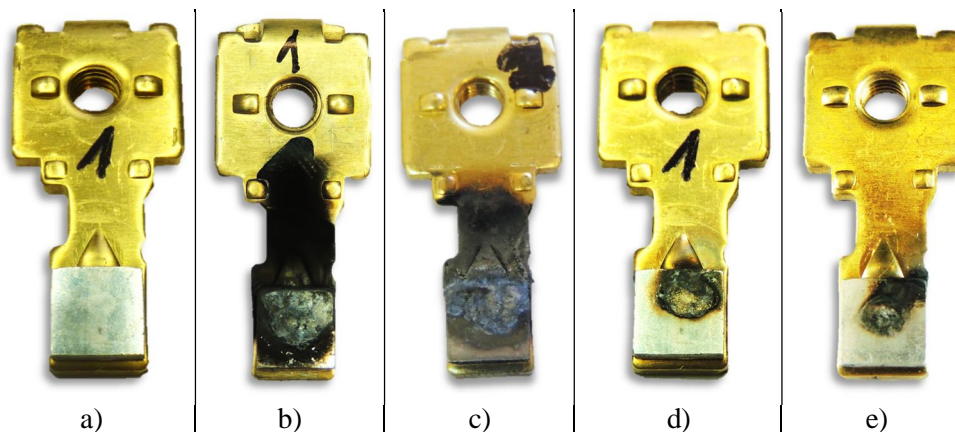


Figure 11.1. Comparison of fixed contacts #2: a) new contact; b), c) contacts taken from standalone switches; d), e) contacts after hybrid switching tests

As shown in Figure 11.1, differences in the surface condition of the analyzed contacts are significant. The surface areas shown in Figure 11.1b and Figure 11.1c are definitely much more damaged in comparison to the surfaces shown in Figure 11.1d and in Figure 11.1e. Moreover, it should be pointed out, that almost the entire surfaces of the contacts presented in Figure 11.1b and Figure 11.1c were destroyed, whereby the part of the metal terminal was covered with the burned layer. As show in Figure 11.1d and in Figure 11.1e, only the part of the silver contact was damaged, and the burned layer was not created. Thus, the thermal

influence of the electric arc can be clearly noticeable as the surface destruction of the contacts, in the case, when the electric arc energy is not limited.

Figure 11.2 presents a comparison of the surfaces of the all fixed contacts taken from the tested switch (the contact #3 according to the notations presented in Figure 6.13).

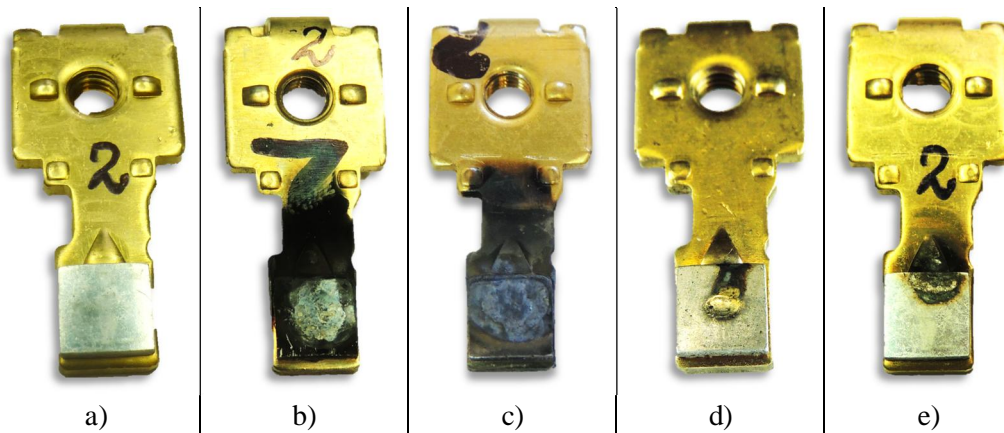


Figure 11.2. Comparison of fixed contacts #3: a) new contact; b), c) contacts taken from standalone switches; d), e) contacts after hybrid switching tests

As shown in Figure 11.2, the condition of the presented surfaces is similar in the damages in comparison to the surfaces of the contacts #1 presented in Figure 11.1. However, the destructions of the contacts illustrated in Figure 11.2d and in Figure 11.2e are significantly smaller in comparison to the contacts shown in Figure 11.1d and in Figure 11.1e. These differences are caused by the not simultaneous movement of the moveable contact in both arc-quenching chambers, according to the description presented in the section 6.5, and in the section 10.1. Apart from this difference, other significant differences are not observed in the surface condition in comparison to the contacts presented in Figure 11.2.

Figure 11.3 presents the comparison in the surface condition of the moveable contacts taken from the tested switches (the contact #1 according to the notations presented in Figure 6.13).

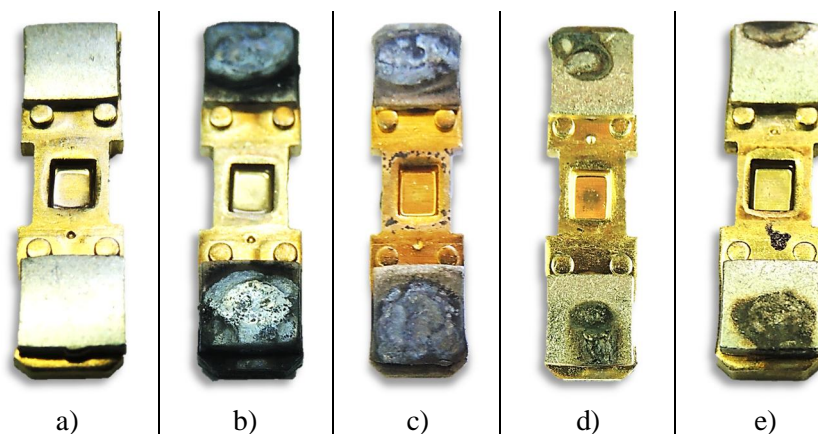


Figure 11.3. Comparison of contacts #1: a) new contact; b), c) contact after tests without supporting method to quench arc; d) contact after tests hybrid switching; e) contact after tests hybrid switching with no current making operation

As shown in Figure 11.3, the surface condition of the analyzed contacts is similar in the damages in comparison to the surfaces of the contacts shown in Figure 11.1 - Figure 11.2. However, the destructions of the contacts illustrated in the above part of Figure 11.3d and Figure 11.3e are significantly smaller in reference to the contacts presented in the below part of these Figures. These differences confirm the observations from Figure 11.2 related to the not simultaneous movement of the moveable contact in the both arc-quenching chambers of

the operated switch. Apart from this distinction, other significant differences are not observed in the surface condition in comparison to the contacts presented in Figure 11.2.

11.2 Observations Performed by means of the Optical Microscope

In order to perform the more accurate observations of the contact surfaces, the observation of the microstructure of the contact surfaces was performed by means of the optical microscope (to show cracking microstructure, deformations, and discoloration of surfaces). For this purpose, the areas presented in Figure 6.15 were selected to the analysis. In this section, the microscope observations of the reference contact, the contact taken from the standalone switch after the 50 000 cycles of the current interruptions, and the contact taken from the hybrid switch after the 50 000 cycles of the current interruptions were presented. Due to similar condition of the observed surfaces (according to the description presented in the section 11.1), the observations presented inhere were performed only for the one of the analyzed contact #1 (respectively Figure 11.1a, Figure 11.1b, Figure 11.1d).

11.2.1 Reference Contact

The microscope observations of the reference contact (taken from the new switch) are presented in Figure 11.4a – Figure 11.4d. The observations presented inhere were performed for the area indicated in Figure 6.15 (marked as the white circle) in neighboring areas.

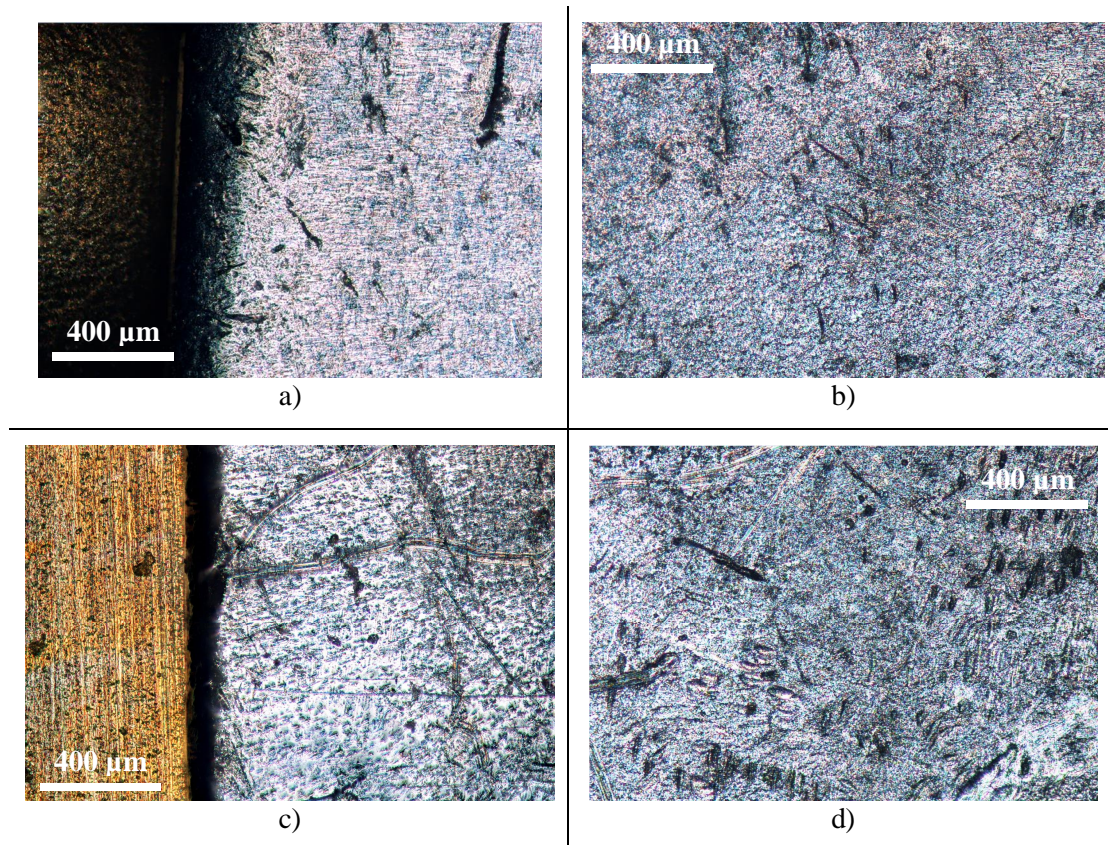


Figure 11.4. The microscope observations of the contact taken from the new switch

As shown in Figure 11.4a – Figure 11.4d, the observed surfaces are slightly rough, however, substantial deformations in the microstructure of the contact surface are not noticeable. The entire surface of the new contact is characterized by the similar microstructure presented in Figure 11.4a – Figure 11.4d.

11.2.2 Contact Taken from Standalone Switch after 50 000 the Current Interruptions

The microscope observations of the contact taken from the standalone switch after the 50 000 cycles of the current interruptions are presented in Figure 11.5a – Figure 11.5d. The observations presented inhere were performed for the area indicated in Figure 6.15 (marked as the white circle) in neighboring areas.

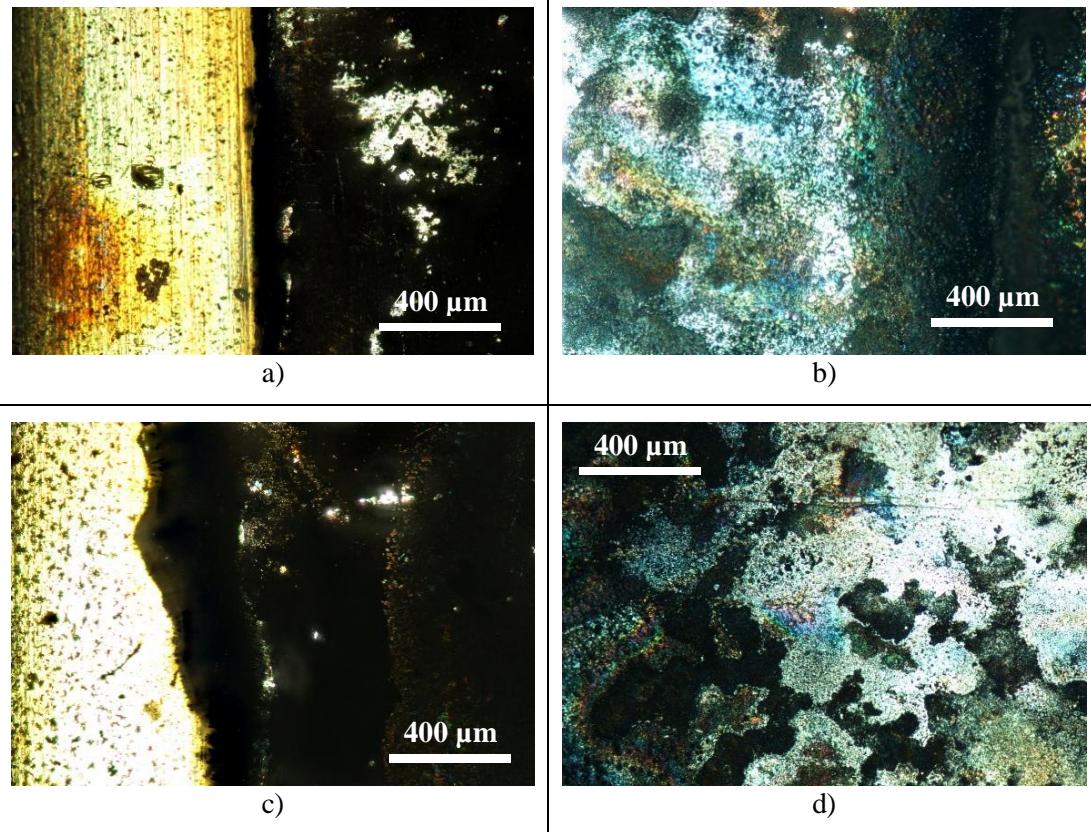


Figure 11.5. The microscope observations of the contact taken from the switch interrupting the current as the standalone one after the 50 000 cycles of the current interruption

As shown in Figure 11.5a – Figure 11.5d, the observed surfaces are heavily distorted in comparison to the intact microstructures presented in Figure 11.4a – Figure 11.4d, where the entire observed surface is homogeneously smooth. In Figure 11.5a – Figure 11.5d, the many undulations and the discolorations of the surface caused by the thermal influence of the electric arc can be visible in the observed contact surfaces. The significantly burning layer can be noticeable especially in Figure 11.5a – Figure 11.5b, very close to the left edge of the contact.

11.2.3 Contact Taken from the Hybrid Switch after 50 000 the Current Interruptions

The microscope observations of the contact taken from the switch with the implemented hybrid switching sequence one after the 50 000 cycles of the current interruptions are presented in Figure 11.6a – Figure 11.6d. The observations presented inhere were performed for the area indicated in Figure 6.15 (marked as the white circle) in neighboring areas.

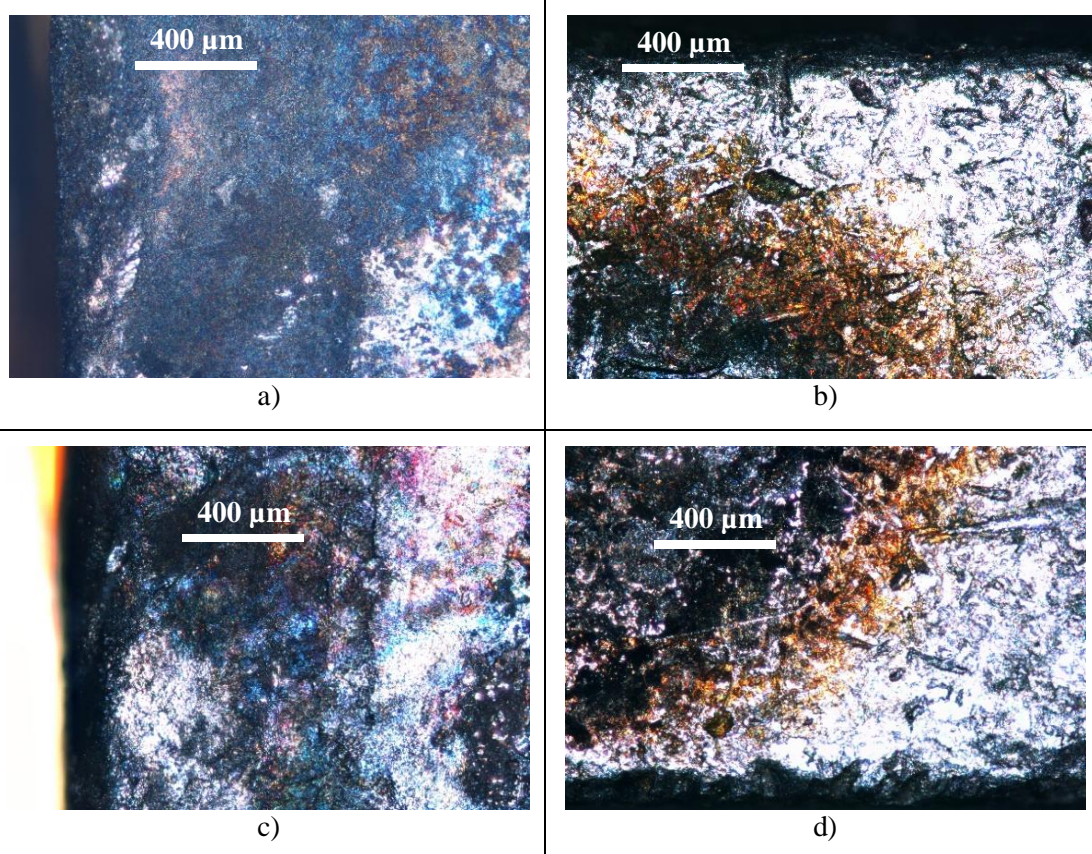


Figure 11.6. The microscope observations of the contact taken from the switch interrupting the current as the hybrid one after the 50 000 cycles of the current interruption

As shown in Figure 11.6a – Figure 11.6d, the observed surfaces are only partially distorted in comparison to the highly damaged microstructures shown in Figure 11.5a-Figure 11.5d. The analyzed inhere areas are characterized by the deformations of the surface layer, however, their level is noticeably lower in comparison to the damages presented in Figure 11.5a-Figure 11.5d. Moreover, in contrast to the contact taken from the standalone switch, the deformations observed in the area of the contact presented here are noticeable only in the part of the observed area – in Figure 11.5b and in Figure 11.5d a boundary between the deformed and intact areas is visible.

11.3 Roughness Profiles of the Analyzed Contacts

In order to compare the degree of the electric arc erosion, the roughness profiles of the surface of analyzed contacts were measured. The investigations were performed according to the description presented in the section 6.6. The researches were conducted for the all tested contacts, however, only three selected roughness profiles were presented in this section, due to the good repeatability of the measurement results. Selected parameters describing the measured roughness profile (the average roughness R_a , the ten point average roughness R_z , and the maximum roughness height within a sample length R_{max}) were presented and compared to indicate the differences in degree of the damaged surfaces.

The detailed description of the analyzed roughness parameters is presented in the section 5. The measurements were performed by means of the ESA RUGOSURF Roughness Tester 90G [144]. The key features of the Roughness Tester used are presented in the section 6.6.

The measurements of roughness profiles were performed for the analyzed contact #1 taken from the analyzed switches (presented respectively in Figure 11.1a, Figure 11.1b, Figure

11.1d). The roughness profiles were measured across the coaxial line of the entire contacts, with initial point as close as possible to the contact edge, according to Figure 6.15b. The measured roughness profiles of the analyzed contacts are presented in Figure 11.7.

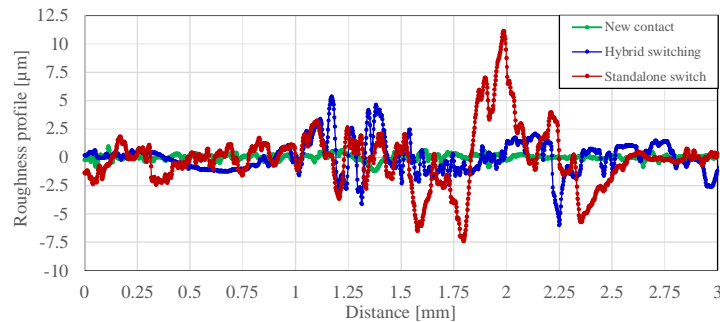


Figure 11.7. *The measured roughness profiles of the analyzed contacts*

As shown in Figure 11.7, the measured roughness profiles of the analyzed contacts are quite different in the shape, as well as, in the peak values.

The measured roughness profile of the new contact is characterized by the small roughness peaks (about 1 μm) in the analyzed surface. These micro-deformations are caused by the imperfections of the production cycle (that can be also visible in the photographs presented in the section 11.2.1).

In contrast to this situation, the most rugged surface was measured for the contact taken from the standalone switch. In this case, the significant peaks in the surface roughness can be observed. Many micro-cracks, and micro-deformations caused by melting the contact material can be noticeable in the measured roughness profile.

A smoother roughness profile was measured for the contact taken from the hybrid switch. As it can be visible in Figure 11.7, the peaks in the surface roughness are smaller for this case in comparison to the contact taken from the standalone switch. However, some micro-deformations can be also visible here in comparison to the measured profile roughness of the new contact.

Both for the measured profiles for the standalone switch, as well as, for the hybrid switch, the deformations can be visible about 1 mm from the left edge. These changes in the surfaces are caused by the mechanical abrasion of the surface created from the close-open cycles realized by the switches. About 2 mm from the left edge of the analyzed contact, the significant amplitudes in the surface roughness are noticeable in the measured roughness profile of the contact taken from the standalone switch. These strong deformations are related to melting of the contact material, caused by the thermal influence of the electric arc. These deformations are not visible in the measured roughness profile of the contact taken from the hybrid switch, which also proves the effectiveness of the application of the hybrid switching to limit the electric arc erosion.

In order to compare the condition of the contact surfaces, the selected roughness parameters of the analyzed surfaces were compared. The following roughness parameters were selected to the analysis: the average roughness R_a , the ten point average roughness R_z , the maximum roughness height within a sample length R_{max} . Table 11.1 presented the comparison of the analyzed roughness parameters. The detailed description of the parameters is presented in the section 5.

Table 11.1. Measured surface profile parameters: the average roughness R_a , the ten point average roughness R_z , the maximum roughness height within a sample length R_{max}

	R_a	R_z	R_{max}
	[μm]		
New contact	0.18	1.62	1.87
Standalone switch	1.66	9.39	18.56
Hybrid switching	1.03	5.90	9.50

As shown in Table 11.1, the smallest values of the analyzed parameters were measured for the contact taken from the new switch. In contrast to this situation, the greatest values of analyzed parameters are observed for the contact taken from standalone switch (respectively: the R_a is greater over 9 times, the R_z is greater almost 6 times, and the R_{max} is greater almost 10 times), which indicates the significant deformations in the analyzed surfaces.

The parameters of the roughness profile measured for the contact taken from the hybrid switch are in the middle between the parameters of the new and standalone contact. Thus, based on the measured roughness profiles, as well as, the analyzed parameters, it can be concluded, that the condition of the contact surface taken from the standalone switch is more damaged in comparison to the condition of the contact surface taken from the hybrid switch.

11.4 Morphological Analysis

In order to evaluate the quantitative and qualitative degree of the arc erosion in the surface of the analyzed contacts, the Scanning Electron Microscope (SEM) technique coupled with the Energy Dispersion Spectroscopy (EDS) were applied. The SEM method was applied with the greater magnification in comparison to the microscope observations presented in the section 11.3 to perform the more accurate researches on the condition of the analyzed surfaces. The EDS technique is able to provide the information about the quantitative atomic concentration in analyzed metal parts. To perform an analysis of the arc erosion degree in the analyzed samples, a percentage content of chemical elements was measured in the examined samples.

The measurement results presented in this section, were carried out according to the research plan described in the section 6.6. The parameters of the performed observations were also presented in the section 6.6.

The EDS measurements were performed for the all tested contacts, however, only a single set of selected points was presented in this section, due to the good repeatability of the measurement results. The SEM observations were performed for the area indicated in Figure 6.15. The observations presented inhere were presented for the one of the analyzed contact #1 (respectively Figure 11.1a, Figure 11.1b, Figure 11.1d).

11.4.1 Reference Contact

The SEM images of the intact surface of the contact taken from the new switch are shown in Figure 11.8a-Figure 11.8d. The observations presented inhere were performed for the area indicated in Figure 6.15 (marked as the white circle).

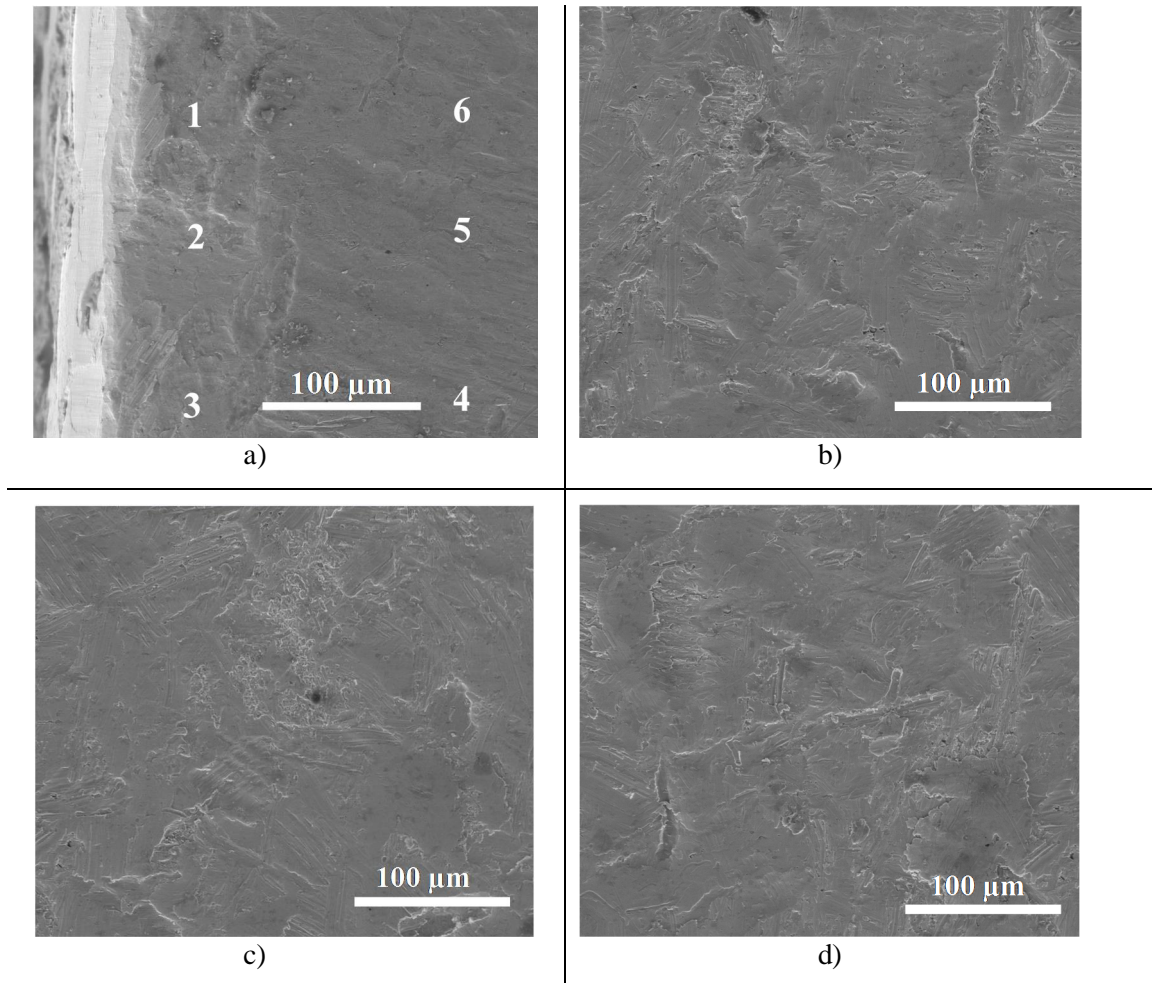


Figure 11.8. The selected SEM images of the intact contact surface.
The contact edge is visible on the left side (a)

As shown in Figure 11.8a – Figure 11.8d, observed surfaces are slightly rough (which also confirms the microscope observations presented in the section 11.3.1, and roughness measurements presented in the section 11.3). The substantial deformations in the observed microstructure of the contact surface are not noticeable.

The analysis results of the EDS spectrum performed for the point 1 marked in the Figure 11.8a are presented in Figure 11.9.

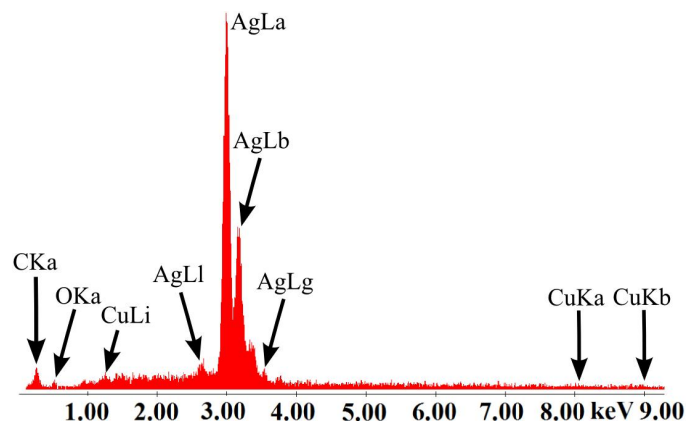


Figure 11.9. The EDS spectrum measured for the point 1 marked in Figure 11.8a

As illustrated in Figure 11.9, the significant peaks related to the presence of silver can be observed in the analyzed spectrum, whereas the content of the other chemical elements is at

the low level. The similar spectra were obtained for all of the 6 points presented in Figure 11.8a, and the calculated averages for each of the elements are listed in Table 11.2.

Table 11.2. *The results of the EDS analysis for points indicated in Figure 11.8a*

Element	Number of point, percentage content [wt.%]						Average [wt.%]
	1	2	3	4	5	6	
Ag	92.37	90.46	92.01	95.35	90.04	91.43	91.94
C	3.98	3.61	3.55	2.62	5.7	3.75	3.87
O	1.97	3.83	2.19	0.99	3.02	2.01	2.34
Cu	1.68	2.10	2.26	1.04	1.25	2.81	1.86

As shown in Table 11.2, the percentage content of the silver in the analyzed area (over 90 wt.% in the all analyzed points) is dominant. In addition to this, the minor amounts of the carbon, the oxide and the copper are located in the examined surface layer of the contact surface as an admixture.

11.4.2 Contact Taken from the Standalone Switch after 50 000 Cycles of the Current Interruption

The SEM images of the contact surface of the contact taken from the standalone switch after the 50 000 cycles of the current interruption are shown in Figure 11.10a-Figure 11.10d.

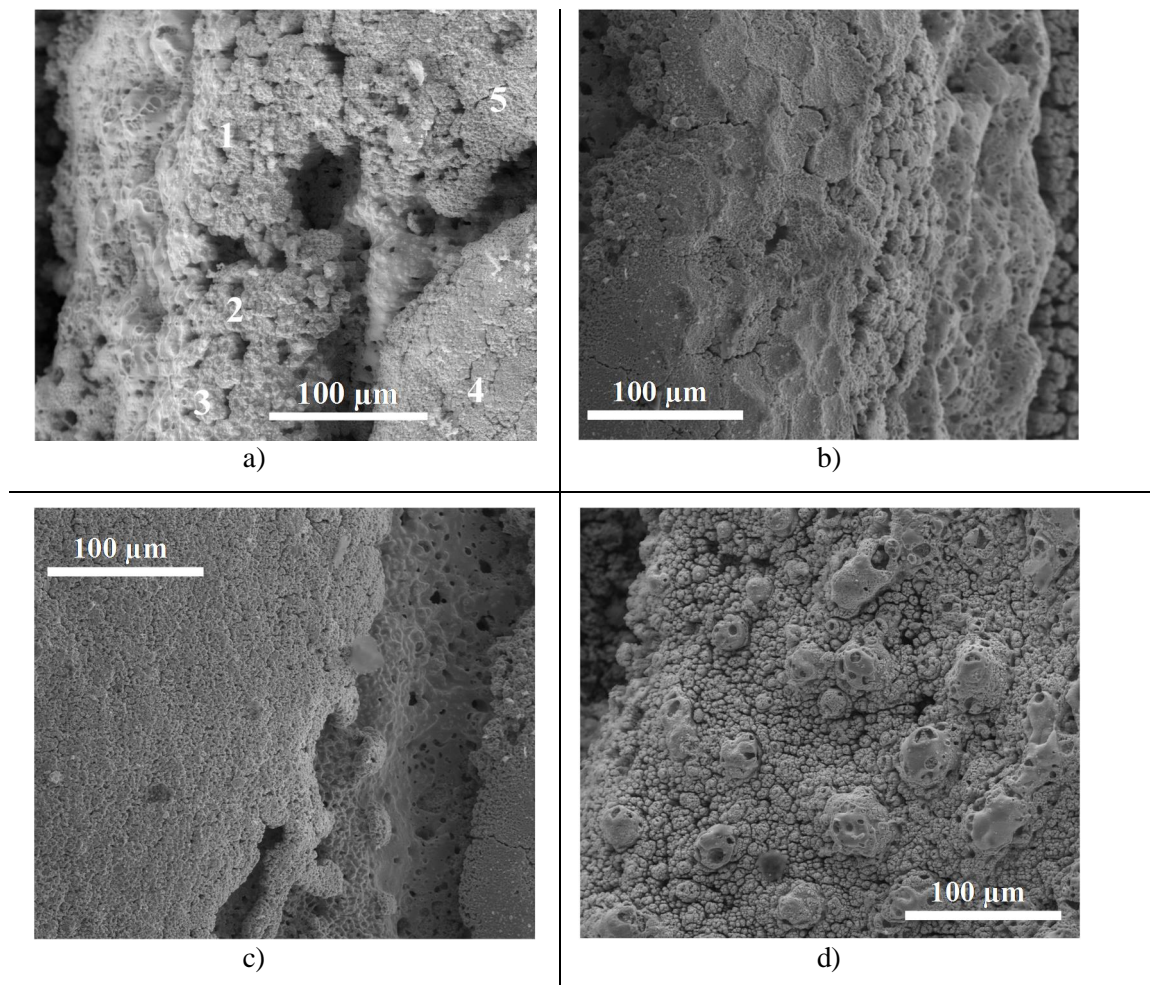


Figure 11.10. *The selected SEM images of the contact taken from the standalone switch after the 50 000 cycles of the current interruption. The contact edge is visible on the left side (a)*

The observations presented in Figure 11.10a – Figure 11.10d were performed for the area indicated in Figure 6.15 (marked as the white circle).

As shown in Figure 11.10a – Figure 11.10d, the observed surfaces are heavily distorted in comparison to the intact microstructures presented in Figure 11.8a – Figure 11.8d, where the entire observed surface is homogeneously smooth. In Figure 11.10a, the significant cracks can be observed especially between the line of the points 1-3 and the points 4 and 5. Moreover, a lot of damages in the microstructure caused by melting the contacts material during the electric arc formation can be also observed in the analyzed area in form of the microcracks (visible especially in Figure 11.10b) and in form of the deformations of the surface layer, which can be well visible in Figure 11.10c – Figure 11.10d.

The analysis results of the EDS spectrum performed for the point 1 marked in the Figure 11.10a is presented in Figure 11.11.

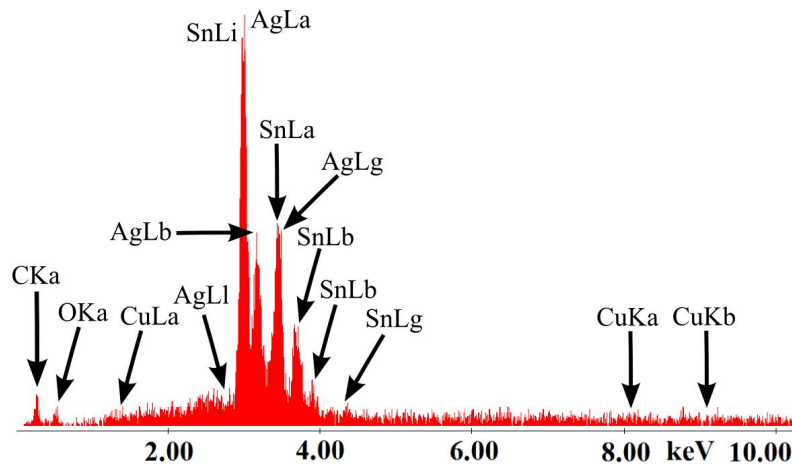


Figure 11.11. The EDS spectrum measured for the point 1 marked in Figure 11.10a

As shown in Figure 11.11, the significant peaks created by the presence of silver can be observed in the spectrum, similarly to the measurement results for the reference sample presented in Figure 11.9. In this case, the strong signal was also detected for the tin. This material is being applied in the analyzed electrical contacts to connect the silver part of the electric contact with the electrical terminal. For this reason, tin presence in the analyzed surface layer might be caused through deeply burnt silver layer, which causes these elements to mix with the materials coming from deeper layers. These observations prove the high level of the arc erosion in the contact surface. The EDS analysis was performed for all points marked in Figure 11.10a. The measurement results and the calculated averages for each of the elements are collected in Table 11.3.

Table 11.3. The results of the EDS analysis for points indicated in Figure 11.10a

Element	Number of point, percentage content [wt.%]					Average [wt.%]
	1	2	3	4	5	
Ag	53.55	63.35	53.87	38.78	48.09	51.53
Sn	38.37	22.38	29.36	53.03	45.10	37.65
C	3.12	6.01	8.48	4.37	2.35	4.87
O	2.46	5.75	6.72	3.02	2.37	4.06
Cu	2.50	2.50	1.56	0.81	2.09	1.89

As illustrated in Table 11.3, the percentage content of silver in the analyzed points is significant. The content of tin also becomes visible in the analyzed surfaces as expected (in the point 4, the content of tin is even greater than the amount of silver). The percent of the carbon composition and the oxide composition is also elevated in comparison to the

measurement results obtained for the new contact surface, instead the copper contribution is comparable to data measured for the new contact surface. The percent composition of carbon, oxide and copper does not exceed 5% similarly to data listed in Table 11.2.

Thus, it can be concluded, that the percentage composition of silver and the tin can be determinant for the degree of the arc erosion created in the observed surfaces of the electrical contacts.

11.4.3 Contact Taken from the Hybrid Switch after 50 000 Cycles of the Current Interruption

The SEM images of the contact surface of the contact taken from the hybrid switch after the 50 000 cycles of the current interruption are shown in Figure 11.12a – Figure 11.12d. The observations presented inhere were performed for the area indicated in Figure 6.15 (marked as the white circle).

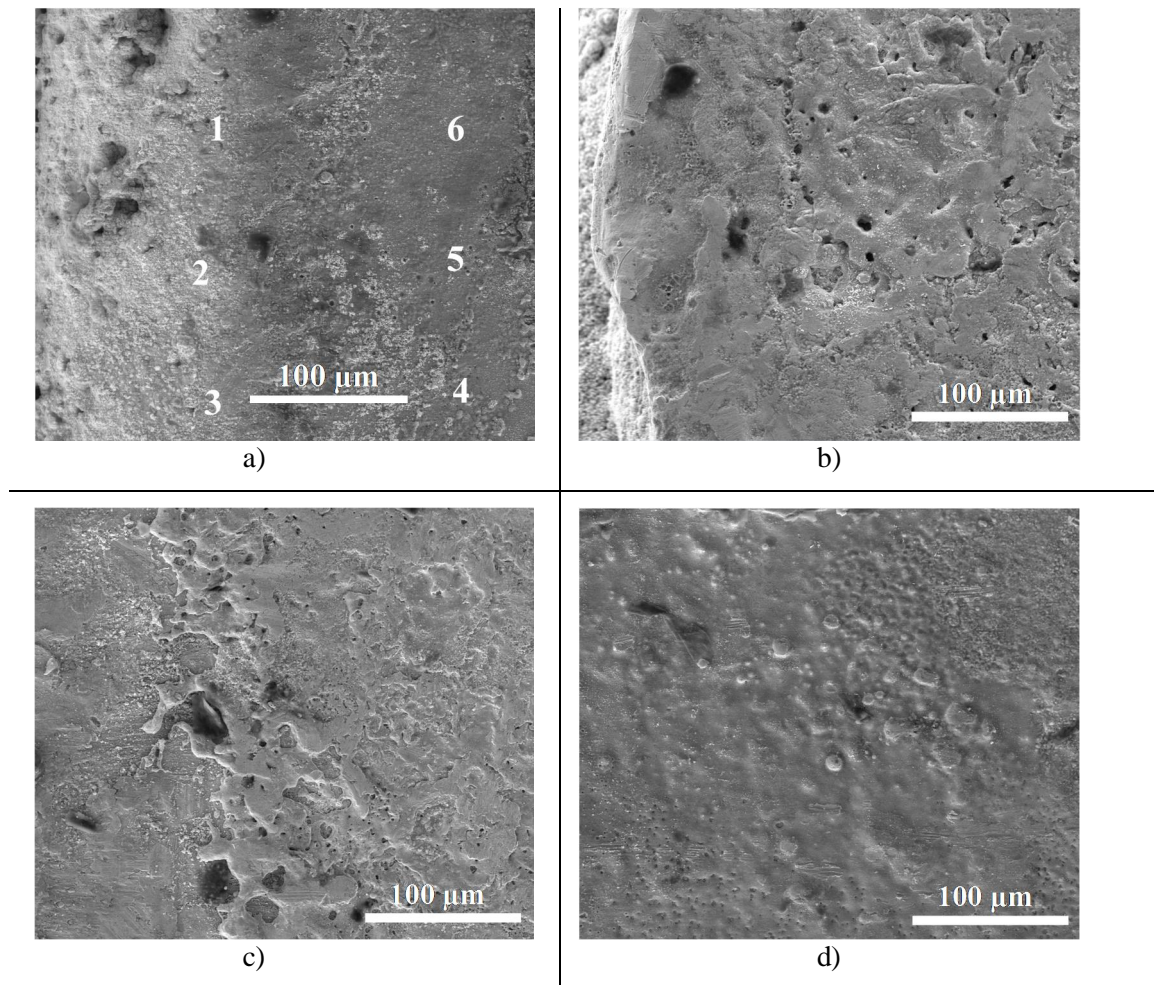


Figure 11.12. The selected SEM images of contact surface taken from hybrid switch after 50 000 operations. Contact edge is visible on the left side (a)

As shown in Figure 11.12a – Figure 11.12d, similarly to the microscope observations presented in the section 11.3.3, the observed surface is only slightly distorted in comparison to the highly damaged microstructure shown in Figure 11.10a – Figure 11.10d. The analyzed surfaces of the contacts presented in Figure 11.12a – Figure 11.12d are characterized by many small deformations of the outer layer as the domed surfaces. However, in this case, the heavily distorted areas (similar to damage presented in Figure 11.10a – Figure 11.10d) with significant cracks and deformations are not visible. The EDS analysis was performed for the

all points marked in Figure 11.12a. The results of the EDS analysis performed for the point 1 marked in Figure 11.12a are presented in Figure 11.13.

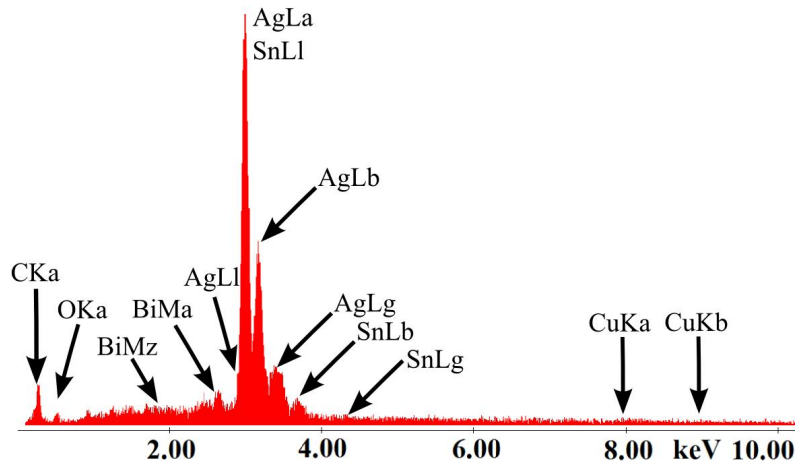


Figure 11.13. The EDS spectrum measured for the point 1 marked in Figure 11.12a

As shown in Figure 11.13, the significant peaks of the silver can be observed in the spectrum similarly to the situations presented in Figure 11.9, and in Figure 11.11. However, in this case, the amount of tin is less noticeable in comparison to the spectrum presented in Figure 11.9. Also the content of the other chemical elements is at the low level, similarly to the measured spectrums illustrated in Figure 11.9 and Figure 11.11. The bismuth presence in a small amount in the analyzed points is a result of the contamination of the analyzed contact surface. The elemental analysis was performed by means of EDS for the all points marked in Figure 11.12a. The measurement results and the calculated averages for each of the elements are collected in Table 11.4.

Table 11.4. The results of the EDS analysis for points indicated in Figure 11.12a

Element	Number of point, percentage content [wt.%]						Average [wt.%]
	1	2	3	4	5	6	
Ag	74.54	86.39	87.86	75.84	75.97	74.08	79.11
Sn	11.89	4.60	3.71	11.05	11.54	10.78	8.93
C	6.25	2.74	2.46	3.84	4.93	6.77	4.50
Bi	2.73	2.24	2.68	4.08	3.27	3.23	3.04
O	2.04	1.27	0.71	2.40	2.20	2.44	1.84
Cu	1.95	2.01	1.54	1.15	1.20	1.68	1.59

As shown in Table 11.4, the percentage composition of silver in the analyzed points is significant, and its level in the analyzed points is located between the values presented in Table 11.2 and Table 11.3. Also, the content of tin is lower in comparison to data listed in Table 11.3. Similarly to the previous measurement results, the averaged composition percentage of other elements does not exceed 5%, instead the lower oxidation of the contact surfaces can be clearly noticeable in this case in comparison to the measurement results presented in the section 11.4.2.

11.4.4 Summary of the Measurement Results

The averaged values of the percentage composition calculated for the chemical elements based on the measurement results presented in the sections 11.4.1-11.4.3 are collected in Table 11.5 (the data were taken from Table 11.2 – Table 11.4).

Table 11.5. *The averaged percentage composition of the chemical elements in the analyzed areas*

Element	Number of point, percentage content [wt.%]		
	The new contact	The standalone switch	The hybrid switching
Ag	91.94	51.53	79.11
Sn	-	37.65	8.93
C	3.87	4.87	4.50
O	2.34	4.06	1.84
Cu	1.86	1.89	1.59
Bi	-	-	3.04
Cl	-	-	0.99

According to data listed in Table 11.5, the averaged percentage composition of the silver is the lowest for the situation, when the current was interrupted in the analyzed circuit by the standalone switch. Averaged percentage of the composition of tin is also smaller for the situation, when the hybrid switching was applied in comparison to the situation, when the current was interrupted by the standalone switch. The averaged percentage composition of the tin is the greatest in the contacts of the standalone switch, and the smallest in the contacts of the hybrid switch. Tin does not exist in the analyzed surfaces of the new contacts. The averaged percentage composition of the other elements in analyzed samples values is below 5%, and their level is comparable in each of the analyzed cases (except for the measurements of the oxide in the contact surfaces of the standalone switch, its value is twice larger in comparison to two other cases).

Thus, it can be concluded, that the percentage composition of the silver and tin can be determinant for the degree of the arc erosion created in the observed surfaces of the electrical contacts.

12 Analysis of the Limitation of the Electric Arc Erosion

This chapter presents an analysis and a discussion on the effects of the electric arc erosion limitation. In order to indicate direct differences in the effectiveness of the limitation of electric arc erosion for the considered methods, the following features of the analyzed contact surfaces were discussed:

- the visual conditions of the contact surface,
- the results obtained from the measurement performed by the roughness tester,
- the observation performed by the optical microscope,
- the results obtained from the SEM method coupled with the EDS method.

The most important conclusions from researches performed on arc erosion are discussed in this chapter. For this purpose, measurement results presented in chapter 11 are presented in the form of the bar graphs. The values of the measured parameters of the surface profiles taken from Table 11.1 are presented in Figure 12.1.

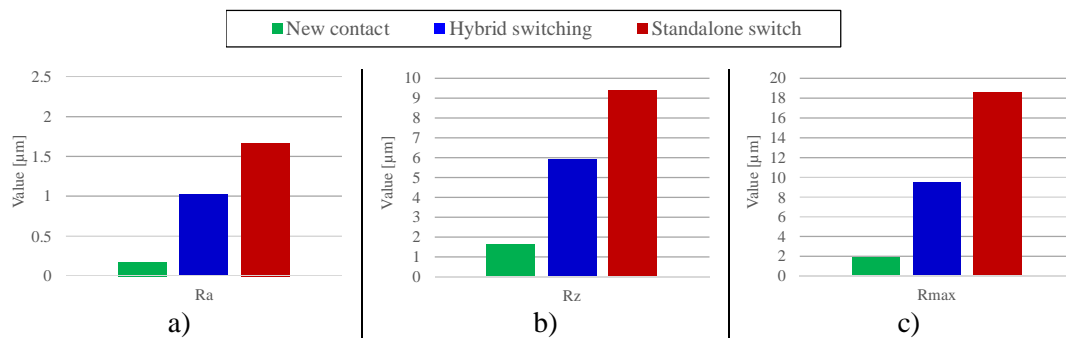


Figure 12.1. The parameters of measured surface profiles: the average roughness R_a (a); the ten point average roughness R_z (b); the maximum roughness height within a sample length R_{max} (c)

As shown in Figure 12.1, the smallest values of the analyzed parameters were measured for the surfaces of the new contact.

In contrast to this situation, the greatest values of the analyzed parameters are noticed for the contact taken from the standalone switch (respectively: the average roughness R_a is greater over 9 times, the ten point average roughness R_z is greater almost 6 times, and the maximum roughness height within a sample length R_{max} is greater almost 10 times), which indicates the significant deformations in the analyzed surfaces in comparison to other analyzed contacts.

The parameters of the surface profile measured for the contact taken from the hybrid switch are in the middle. Thus, based on the analyzed parameters it can be concluded that the surface of the contact taken from the standalone switch is the most damaged in comparison to the condition of the surface of the contact taken from the hybrid switch.

In order to compare the percentage composition of the contact material in the analyzed surfaces, the calculated averaged values of the percentage composition for the considered chemical elements are collected and presented in Figure 12.2 as a bar graphs. For this purpose, the data were taken from Table 11.2 – Table 11.4.

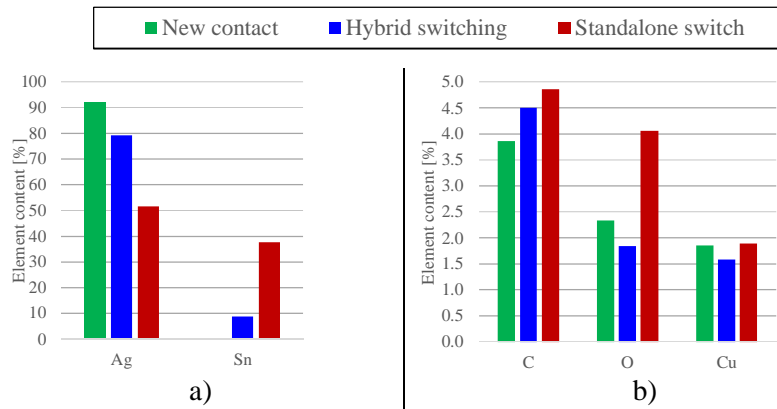


Figure 12.2. The averaged percent composition of the chemical elements of the analyzed contact surface

As illustrated in Figure 12.2a, the averaged percentage composition of the silver is the lowest for the situation, when the current was interrupted in the analyzed circuit by the standalone switch. The averaged percentage composition of the tin is also smaller for the case, when the hybrid switching was applied in comparison to the situation, when the current was interrupted by the standalone switch. Figure 12.2b shows the averaged percentage composition of other elements in the analyzed contact surface. The averaged percentage composition of other the elements in analyzed samples is below 5%, and their level is comparable in the each analyzed case (except from the measurements of oxide in the contact surfaces of the standalone switch, its value is twice larger in comparison to two other cases).

Thus, the following important conclusions and the observations from performed researches on arc erosion can be pointed out:

1. the obtained measurement results of the arc erosion are repeatable in the analysis of the all contacts installed in tested switches interrupting the current in the tested circuit,
2. damages in surfaces of contacts #2 and contacts #3 (respectively the anode and the cathode) are similar, which proves that in the analyzed circuit the contact material is transferred in comparable amounts in both directions (between the anode and the cathode) during the metallic and gaseous phases (see Figure 5.8),
3. the hybrid switching application allows to protect the surfaces of the electric contacts against the damage (such as: burning of the outer layer, the creation of the micro-cracks and melting of the contact layers) created from the influence of the electric arc,
4. the conclusion 1 was confirmed in the following work through the observations of the surfaces of the electrical contacts performed by the following methods: the photo camera, the optical microscope, the roughness tester, as well as, the Scanning Electron Microscope (SEM) coupled with the Energy Dispersive Spectroscopy (EDS),
5. the application of the hybrid switching impacts on the roughness profiles of the analyzed contacts. The surfaces of the contacts taken from the hybrid switch after the 50 000 cycles of the current interruptions is characterized by the smaller roughness in comparison to the surfaces of the contacts taken from the standalone switch after the 50 000 cycles of the current interruptions. The roughness parameters of the analyzed surfaces (the average roughness R_a , the ten point average roughness R_z , the maximum roughness height within a sample length R_{max}) are significantly reduced for the contacts taken from the hybrid switch in comparison to the contacts taken from the standalone switch (respectively, the R_a is lower by about 38%, the R_z is less about 37%, and the R_{max} is lower by about 49%).
6. the average percentage of the composition of silver in the surface of the contact taken from the hybrid switch after the 50 000 cycles of the current interruption is only 13% lower in comparison to the surface of the new contact, instead the average percentage

composition of the silver in the surface of the contact taken from the standalone switch after 50 000 cycles of the current interruption is 40% lower in comparison to the surface of the new contact. Thus, in this analysis, the application of the hybrid switching causes the situation to improve by about 27%,

7. the application of the hybrid switching was able to reduce the averaged level of the tin in the analyzed areas from 38% to 9%. Thus, the application of the hybrid switching causes to improve the situation about 29%,
8. the average percentage composition of the carbon, oxide, and copper is below 5% in the surfaces of the new contacts, as well as, the contact taken from the hybrid switch. The higher content of the carbon and the oxide is observed in the contacts taken from the standalone switch in comparison to the surfaces of the contacts taken from the hybrid switch. Thus, it can be concluded, that the higher electric arc energy influenced higher content of carbon and oxide in the analyzed contact surfaces,
9. based on the measurement results, it can be concluded that the percentage composition of silver and tin can be the determinant for the degree of the arc erosion created in the observed surfaces of the electrical contacts,
10. the electric arc erosion has a negative influence on ensuring the reliability of the operated switch and its lifespan. The damage of the electrical contacts caused by the arc erosion may even lead to lacks in the power supply in the electrical circuit with the operated switches installed. For this reason, the limitation of the arc erosion is the important issue in order to increase the reliability of the entire electrical circuit with the installed switch. The effective limitation of the electric arc erosion can be achieved by limiting the electric arc energy through the application of the hybrid switching. This method leads to the significant mitigation of the arc erosion.

13 Discussion and Conclusions

13.1 Summary

The motivation for the work presented in this thesis was to extend the knowledge related to the methods that could be used to limit the electric arc energy, so as a consequence, also to reduce the electric arc erosion in the LV switches. The character of this thesis is multidisciplinary which includes both the electrical experiments, as well as, the material researches. The researches on the mitigation of the electric arc energy and the electric arc erosion were performed in the inductive circuit to create the challenging conditions for quenching the electric arc.

Thus, the researches presented in this thesis could be used to develop the improved switches with the increased level of the reliability. Increasing the reliability of the operated switch positively influences its lifespan, which increases as a consequence also the reliability of the entire electrical circuit, where the switch is installed. This aim could be achieved through the application of the hybrid switching determined in this thesis as the most effective way to limit the electric arc energy among all the considered methods independently of the V-I characteristic of the electric arc.

The work comprised of several steps. At first, the scope of the thesis and the research plan were defined. Based on this data, the functionality of the laboratory stand was determined, and the parameters of the components used to the researches were selected. At this stage, the hybrid switching sequence was defined precisely. The above-mentioned assumptions were used to design the laboratory stand. For this purpose, the special microcontroller system was designed, which was used to the control of the entire laboratory stand. The laboratory stand was also equipped with the High Speed Camera.

Secondly, different considered methods applied to limit the electric arc energy were investigated in the tested circuit supplied by the 12 V voltage source. In the course of the researches, the following methods were applied to determine their effectiveness on the limitation of the electric arc energy: the contact separation of the operated switch performed at defined angle of the current period, the connection of the various passive branches in parallel to the operated switch, as well as, the application of the hybrid switching. The analyzed methods give the diverse level of the electric arc mitigation in the tested circuit supply by 12 V. A summary description for this case is presented in the section 13.2.

The next step of the performed researches was to use the analogical approach to limit the electric arc energy in the tested circuit with the increased supply voltage up to 230 V. In this case, the contact separation performed at defined angle of the current period gives comparable results to the measurement results performed in the tested circuit supplied by the 12 V voltage source. However, together with increasing the supply voltage in the tested circuit, the V-I characteristic of the electric arc changes, which caused the arcing voltage to decrease below the voltage peak of the supplied voltage source at the steady state. For this reason, the considered passive branches connected in parallel to the operated switch do not limit the electric arc energy in the tested circuit supplied by the 230 V voltage source, because their minimal operating voltage has to be greater than the voltage peak of the supplied voltage source at the steady state. Among all of the considered passive methods, only the application of the RC suppressor is able to reduce the electric arc energy by about just a few percent. Thus, the connection of the passive branch in parallel to the operated switch ceased to be the effective method to limit the electric arc energy. In this case, only the application of the hybrid

switching allows to limit the electric arc energy effectively. A summary description for this case is presented in the section 13.3.

The electrical tests presented in this thesis were performed in this same tested circuit supplied by the two different levels of the supply voltage (12 V and 230 V). This approach was applied to indicate the differences in voltage-current characteristics of the electric arc, that strongly influence on the effectiveness of considered passive methods applied to limit the electric arc.

The next step of the performed researches, was to investigate the effectiveness of the application of the hybrid switching for limiting the electric arc erosion. For this purpose, the 200 000 cycles of the current interruption were performed in the tested circuit by the four different switches. The each analyzed switch performed the 50 000 cycles of the current interruptions in total. Two analyzed switches interrupted the current in the tested circuit as the standalone switches, and two switches performed the 50 000 cycles of the current interruptions during the hybrid switching. The conditions of the electrical contact surfaces taken from the all analyzed switches were investigated and compared. It can be concluded that the application of the hybrid switching allows to reduce the arc erosion significantly. A summary description for this case is presented in the section 13.4.

The final step of the following thesis was to analyze the measurement results (from the electrical tests, as well as, from the material researches), which was presented respectively in the section 9 and in the section 12.

A summary of the actives performed in frame of the thesis is presented in Table 13.1.

Table 13.1. Summary of the actives performed in frame of the thesis

	Step of the work	Section
Step 1	Development of the laboratory stand	
	Definition of the laboratory stand functionality	6.1 6.7.1
	Selection of the parameters of the components used to the researches	6.1.4 6.3
	Definition of the hybrid switching sequence	6.4
	Design of the laboratory stand	6.7.1
	Design of the microcontroller system used to the control of the entire laboratory stand	6.7.2
	Installation of the High Speed Camera	6.5
Step 2	Electrical tests performed in the tested circuit supplied by 12 V	
	Performing measurements for time-controlled contact separation at the precise time slot of the current period	7.1
	Performing measurements for connection of passive components connected in parallel to the operated switch	7.2
	Performing measurements for the hybrid switching	7.3
Step 3	Electrical tests performed in the tested circuit supplied by 230 V	
	Performing measurements for time-controlled contact separation at the precise time slot of the current period	8.1
	Performing measurements for connection of passive components connected in parallel to the operated switch	8.2
	Performing measurements for the hybrid switching	8.3
	Performing the observations of the limitation of the electric arc by means of the High Speed Camera	10

Step of the work		Section
Step 4	Material researches	
	Performing 200 000 current interruptions in total by 4 tested switches at the AGH University	–
	Performing observations of the electric arc erosion by means of the camera	11.1
	Performing observations of the electric arc erosion by means of the optical microscope	11.2
	Performing measurements of the contact surfaces performed by the roughness tester	11.3
	Performing SEM and EDS measurements at the AGH University	11.4
Step 5	Analyses of the measurement results	
	Analysis of the electrical measurement results performed at 12 V	9.1
	Analysis of the electrical measurement results performed at 230 V	9.2
	Analysis of the material measurement results	12

13.2 Analysis of the Effects of the Limitation of the Electric Arc Energy in the Tested Circuit Supplied by the 12 V Voltage Source

In this part of the thesis, an analysis of the effects of the limitation of the electric arc performed in the tested circuit supplied by the 12 V voltage source is presented. For this purpose, the following methods were discussed to indicate the most effective method limiting the electric arc: the contact separation performed at the defined angle of the current period, the connection of the various passive parallel branches into the operated switch, as well as, the application of the hybrid switching.

Based on the performed researches, it can be concluded, that the control of the contact separation time of the operated switch in reference to the instantaneous value of interrupted current has the significant influence on the arcing time, as well as, on the electric arc energy during the current interruption. The application of this method makes it possible to limit almost totally the electric arc energy (in the performed researches, this method allows to limit the electric arc energy from 51 mJ and 0.1 mJ for two the extreme cases, thus more than 99%). This method is also very helpful for the limitation of the switching overvoltages, which can be observed in the reduction of the TRV peak (from 848 V to 293 V for the two considered extreme cases analyzed inhere).

However, for the practical implementation purpose of the considered method, there could be the problem related to the dispersion of the inertial delay time of the operated switch drive. All of the researches presented in this thesis were performed in the similar environmental conditions. Thus, the dispersion of the inertial delay time of the switch drive was always shorter than 1 ms. This provides possibility for performing the repeatable contact separation at the precise time. For this reason, it can be concluded that the implementation of this method in the constant environment conditions can limit the energy arc significantly with the good reproducibility, when the inertial delay time of the drive of the operated switch is known and repeatable. For this purpose, the contact separation should be always realized at least 1 ms before the expected current zero-crossing in the tested circuit. In the practical maintenance of the operated switch, when environment conditions can be variable, the considered method can give different results due to the greater dispersion of the inertial delay time of the switch drive. For this reason, the analysis of the methods providing the limitation of the electric arc independently of the dispersion of the inertial delay time of the switch drive was the subject

of the further researches presented in the following thesis. For this purpose, the connection of the different parallel branches connected in parallel to the operated switch that could limit the arcing time and the electric arc energy was investigated.

Thus, the second investigated approach applied to limit the electric arc energy was to the connection of the different parallel branches into operated switch. The arcing voltage in the tested circuit achieves the significant values (over 10 times greater) in comparison to the peak voltage of the voltage source during steady state. Therefore, it was possible to apply the passive components (the RC snubber, the VDR, the TVS, the ZVL) connected in parallel to the operated switch to make the possibility of the current commutation into the parallel branch during the current interruption. The application of the considered passive parallel components changes differently the V-I characteristic of the electric arc in the tested circuit. For this reason, the application of this method is able to limit the electric arc energy with different levels of the effectiveness.

However, the most effective method to limit the electric arc energy proved to be the application of the hybrid switching. This method is based on the connection of the semiconductor branch in parallel to the operated switch. The semiconductor branch is fully controlled by the microcontroller system. This method allows to limit the arcing voltage up to 22 V, so about 83%. Also, the application of this method provides limitation of the arcing times by about 98% and the electric arc energy by about 99%. Therefore, based on the research results, the application of the hybrid switching is recommended to limit the electric arc in the considered circuit.

13.3 Analysis of the Effects of the Limitation of the Electric Arc Energy in the Tested Circuit Supplied by the 230 V Voltage Source

In this part of the work, an analysis of the experiment results performed in the tested circuit supplied by the 230 V voltage source is discussed. The measurements were performed to verify the effectiveness of the considered methods for the higher level of the voltage source in the tested circuit. Thus, similarly to the previous researches, the following methods were discussed to indicate the most effective method limiting the electric arc: the contact separation performed at the defined angle of the current period, the connection of the various passive parallel branches into the operated switch, as well as, the application of the hybrid switching.

Similarly to the measurement results obtained in the tested circuit supplied by the 12 V voltage source, also in this case the control of the contact separation time in reference to the instantaneous value of the interrupted current has the significant influence on the arcing time and the electric arc energy during the current interruption process. The application of this method can almost totally limit the electric arc energy (in performed researches, this method allows to limit the electric arc energy from 7.97 J to about 0.10 J for the two extreme cases, thus about 99%).

The next step was to perform the tests for the connection of the passive components (such as: the RC snubber, the VDR, the TVS, the ZVL) in parallel to the operated switch. The application of this method does not impact on the V-I characteristics of the electric arc in the tested circuit. Only the connection of the RC suppressor in parallel to the operated switch allows to limit the electric arc energy slightly. Other passive parallel components start to conduct only, when the voltage across the operated switch achieves the voltage greater than the minimal operating voltage of the applied nonlinear voltage components. For this reason, these components do not take part in the commutation process. The current starts to flow through the external branch only for the short time, just after quenching the electric arc, when the TRV exceeds their minimal operating voltage. This situation is presented in Figure 13.1,

where the waveforms of the voltage across the operated switch are presented for the tested circuit supplied by the 12 V voltage source, as well as, by the 230 V voltage source.

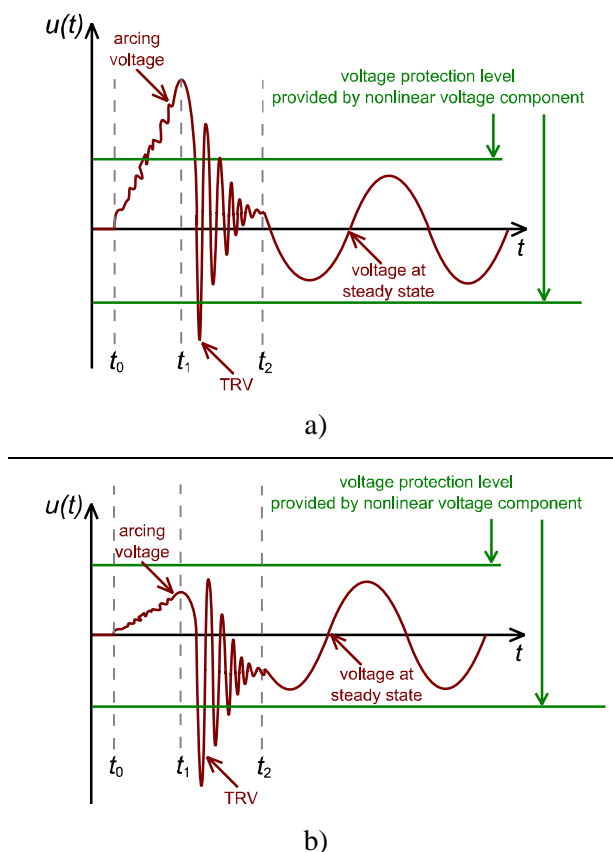


Figure 13.1. The waveforms of the voltage across the operated switch; a) the tested circuit is supplied by the 12 V voltage source; b) the tested circuit is supplied by the 230 V voltage source t_0 – the time, when the contacts start to separate, and the arc starts to burn, t_1 – the time, when the electric arc quenches, and the TRV appears at the terminals of the operated switch, t_2 – the time, when the TRV disappears, the voltage achieves steady state

As shown in Figure 13.1, in the tested circuit supplied by the 230 V voltage source, the application of the passive components connected in parallel to the operated switch does not influence the V-I characteristics, so as a consequence, the electric arc is also not limited during the current interruption.

Thus, the most effective method, which is able to effectively limit the electric arc energy is the application of the hybrid switching. In this case, the current starts to commute into the external branch, when the arcing voltage exceeds the minimal operated voltage of the applied Solid State Relay (thus, the arcing voltage is limited up to about 20 V, so about 84%). This approach provides limitation of the arcing times by about 99.5% and the electric arc energy about 99.9%. The effectiveness of this method was also confirmed through the observations of the contact system of the operated switch performed by means of the High Speed Camera for the two considered cases: when the current was interrupted by the standalone switch, as well as, when the current was interrupted during the hybrid switching.

13.4 Analysis of the Effects of the Limitation of the Electric Arc Erosion

Based on the measurement results obtained from the electrical tests, it can be concluded that the recommended method giving the satisfactory results for the mitigation of the electric arc

energy independently of the circuit parameters is the hybrid switching. For this reason, this method was chosen to perform the measurements of the arc erosion mitigation in the switches installed in the tested circuit.

In order to perform the researches on the mitigation of the arc erosion, the 200 000 cycles of the current interruptions were performed in the tested circuit by means of the four switches in total. Each analyzed switch performed the 50 000 cycles of the current interruptions. In order to determine the repeatability of phenomenon, the experiments were performed twice. For this purpose, the two analyzed switches performed the current interruptions in the tested circuit as the standalone switches, and another two switches performed the 50 000 cycles of the current interruptions with implementation of the hybrid switching. The conditions of the surfaces of the electrical contacts taken from all analyzed switches were investigated and compared. It can be concluded, that the application of the hybrid switching allows to reduce significantly the arc erosion. This conclusion was confirmed through observations of the surfaces of the electric contacts performed by the photo camera, the optical microscope, the roughness tester, as well as, the SEM method coupled with the EDS method.

In general, the average percentage of the silver composition in the surface of the contact taken from the hybrid switch after the 50 000 cycles of the current interruption is only 13% lower in comparison to the surface of the new contact, instead the average percentage composition of silver in the surface of the contacts taken from the standalone switch after 50 000 cycles of the current interruption is 40% lower in comparison to the surface of the new contact. Thus, in this analysis, the application of the hybrid switching causes the situation to improve by about 27%. The application of the hybrid switching was also able to reduce the average level of tin in the analyzed areas from 38% to 9%.

13.5 Reference to the Main Thesis

The results of the laboratory measurements allow to state that it is possible to limit effectively the electric arc energy, as well as, the electric arc erosion through the application of the hybrid switching. Also, performing the contact separation at the precise angle of the current period may effectively limit the electric arc energy and the electric arcing time.

The outcome of this thesis is the analyses of the various considered methods that could be applied to limit the electric arc energy in the tested circuit. The considered methods are commonly used in the electrical circuits, most often without a detailed analysis of their real influence on the limitation of the electric arc and the electric arc erosion. For this reason, to indicate the effectiveness of considered methods applied in the tested circuit, the quantitative and the qualitative influence of the considered methods on the mitigation of the electric arc energy was presented in this thesis. The researches on the limitation of the arc erosion were performed for the determined hybrid switching method limiting effectively the electric arc energy, which gives the best results.

13.6 Future Recommendations Related to the Studies on the Limitation of the Electric Arc in the LV switches

The measurement results obtained for the limitation of the electric arc energy, as well as, for the limitation of the electric arc erosion performed in the tested circuit can be a motivation to start the work on the redesigning of the operated switch.

The application of the hybrid switching allows to limit significantly the electric arc energy, so an integration of the hybrid module inside of the switch can be considered. For this purpose, the design of the quenching chambers, the contact system, and the drive of the operated switch

could be changed. Currently, the design of switch is predicted to quench the electric arc featured by significant electric arc energy. After application of the hybrid module connected to the contacts of the switch, the electric arc energy inside of the quenching chamber decreases significantly. Thus, proposed modifications of the switch could be related to minimize the switch dimensions, and to redesign the shape of and dimension of the contact system. Another approach to develop the switch with the integrated hybrid module is a proposal to design the switch with the comparable dimensions, however with the significantly wider current and voltage ratings.

Another interesting issue for research could be behavior of the hybrid module during performing the current interruption under defined short-circuit conditions. For this purpose, the semiconductor branch of the hybrid module might be redesigned. The application of the components with the higher current ratings could be considered.

Design of the hybrid switch including the semiconductor branch with increasing voltage withstand could be also the next path to continue activities performed in frame of the following thesis.

In order to achieve the functionality of the developed hybrid switch comparable with the electromechanical switches, the application of an additional switch providing a full galvanic separation in an operated circuit could be considered. This additional switch could be also controlled through the existing microcontroller system for the defined switching sequence. It could be closing before the making operation of the hybrid switch, and opening after the breaking operation of the hybrid switch.

The previous measurement results could be also extended with an increased number of the switching operations. The electric contacts taken from the switch, which performed significantly greater the current interruptions (e.g. over 500 000 cycles) could be also investigated in differences of contact resistances, as well as, mass losses. These measurement result could predict an expected real lifespan of the switch in the tested circuit.

Another way for the further activities could be extended morphology measurements with increased ratings of the current and the voltage to indicate the differences in the deformation of the contact surfaces for worst switching parameters.

14 Bibliography

- [1] ABB Application Note 5SYA 2020-02: Design of RC snubbers for phase control applications, www.abb.com
- [2] ABB Buyer's and Application Guide: Controlled Switching
- [3] ABB materials, Mike de Swardt: *Circuit Breaker Technology made easy HV and MV distribution*, ABB Cape Technology, 2014
- [4] Agilent Technologies Application note 1399: Maximizing the Life Span of Your Relays, www.agilent.com
- [5] Ainetter J., Brauner G., Hauer H., Strof T., Kalinintchenko A.: *Thyristor aided diverter switch "TADS" – a progressive concept for the prolongation of maintenance-free intervals of on-load tap-changers of transformers*, CIRED, 1999
- [6] Aio A. I.: *Modelization and analysis of the electric arc in low voltage circuit breakers*, PhD Thesis, Universidad Del Pais Vasco Euskal Herriko Unibertsitatea, 2013
- [7] Ala G., Inzerillo M.: *An Improved Circuit-Breaker Model in MODELS Language for ATP-EMTP Code*, IPST '99 International Conference on Power Systems Transients, Budapest, Hungary, pp. 493-498, 1999
- [8] Ala, G.& Inzerillo, M.: *An improved circuit-breaker model in MODELS language for ATP-EMTP code*, IPST Proceedings, 1999
- [9] AOS Technologies AG Brochure: Q-MIZE EM High Speed Camera, www.aostechnologies.com
- [10] Au A., Ciok Z.: *Aparaty elektryczne*, Wydawnictwo Politechniki Warszawskiej, Warszawa 1982
- [11] Au A., Maksymiuk J., Pochanke Z.: *Podstawy obliczeń aparatów elektroenergetycznych*, Wydawnictwa Naukowo-Techniczne, Warszawa, 1976
- [12] Au A., Maksymiuk J., Podgórski A.: *Badania łączników elektroenergetycznych prądu zmiennego*, Wydawnictwa Naukowo-Techniczne, Warszawa, 1968
- [13] Balestrero A., Ghezzi L., Popov M., Tribulato G., Lou van der Sluis: *Black Box Modeling of Low-Voltage Circuit Breakers*, IEEE Transactions on Power Delivery, Vol. 25, No. 4, pp. 2481-2488, 2010
- [14] Bartosik M., Lasota R., Wójcik F.: *Modern dc circuit breakers*, Technika Transportu Szynowego, Technika Transportu Szynowego Nr 9, pp. 25-32, 2006
- [15] Bartosik M., Lasota R., Wójcik F.: *Nowa rodzina synchronizowanych wyłączników próżniowych SWT do systemów trakcji kolejowej zasilanych wysokimi napięciami przemiennymi*, Technika Transportu Szynowego 10/2007, pp. 41-52
- [16] Bartosik M., Lasota R., Wójcik F.: *Synchronizowany wyłącznik próżniowy SWT dla kolei dużych szybkości*, Czasopismo Techniczne z. 1-E/2007, Wydawnictwo Politechniki Krakowskiej
- [17] Bartosik M., Lasota R., Wójcik F.: *Wyłącznik hybrydowy DCH 0,8/400 dla trakcji miejskiej*, Technika Transportu Szynowego, Technika Transportu Szynowego Nr 6, pp. 30-37, 1999
- [18] Bartosik M.: *Wylączenie synchroniczne obwodów niskonapięciowych*, Redakcja Wydawnictw Naukowych Politechniki Łódzkiej, Zeszyty Naukowe - Politechnika Łódzka. Rozprawy Naukowe, z. 37, 1981

- [19] Bień A., Borkowski D., Wetula A.: *Estimation of power system parameters based on load variance observations - laboratory studies*, 9th International Conference on Electrical Power Quality and Utilisation, 2007
- [20] Bizjak, G., Zunko, P. and Povh, D.: *Circuit Breaker Model for Digital Simulation Based on Mayr's and Cassie's Differential Arc Equations*, 1995
- [21] Boghiu E., Maricel A., Andrușcă M., Micu M.: *Aspects Regarding the Controlled Switching of the Shunt Reactors*, International Conference and Exposition on Electrical and Power Engineering EPE, Iasi, Romania, pp. 119-122, 2016
- [22] Bolkowski S.: *Teoria obwodów elektrycznych*, Wydawnictwa Naukowo-Techniczne, Warszawa, 2008
- [23] Borkowski P.: *Arc erosion of contacts on switching high currents*, Archives of Electrical Engineering Vol. LIII No. 3, pp. 259-298, 2004
- [24] Borkowski P.: *Erozja łukowa styków łączników elektrycznych*, Wydawnictwo Politechniki Łódzkiej, Łódź, 2013
- [25] Borkowski P.: *Nowoczesne metody badań zestyków elektrycznych*, Akademicka Oficyna Wydawnicza EXIT, Warszawa, 2013
- [26] Brice C. W., Dougal R. A., Hudgins J. L.: *Review of technologies for current-limiting low-voltage circuit breakers*, IEEE Trans. Ind. Appl., Vol. 32, No. 5, pp. 1005–1010, 1996.
- [27] Bujłow A.: *Zasady budowy aparatów elektrycznych*, Państwowe Wydawnictwa Techniczne, Warszawa, 1951
- [28] Casado E., Colomer V., Sicilia R., Munoz-Serrano E.: *An Experimental Study of the Dependence on the Current Intensity of the erosion of Thoriated Tungsten Cathodes in Plasma Arcs*, IEEE Transactions on Plasma Science, Vol. 29, Issue 6, pp. 888-894, 2001
- [29] Cassie A. M.: *Arc rupture and circuit severity: a new theory*, Proceeding of Conference Internationale des Grands Reseaux Electriques a Haute Tension, Paris, France, pp. 1-14, 1932
- [30] Chandrasena W., Jacobson D., Wang P.: *Controlled Switching of a 1200 MVA Transformer in Manitoba*, IEEE Transactions on Power Delivery, Vol. 31, No. 5, 2016
- [31] Chen Z.-K., Sawa K.: *Effect of Arc Behavior on Material Transfer: A Review*, IEEE Transactions on Components, Packaging, and Manufacturing Technology - Part A, Vol. 21, No. 2, pp. 310-322, 1998
- [32] Chmielak W.: *Internal pressure diagnostic of vacuum circuit breaker based on the phenomenon of chopping current*, Selected Problems of Electrical Engineering and Electronics (WZEE), 2015
- [33] Chmielewski T., Oramus P., Florowski M.: *Modelowanie łuku elektrycznego w analizach przepięć łączeniowych podczas przerywania prądu przy użyciu niskonapięciowych przekaźników elektromechanicznych*, Przegląd Elektrotechniczny No. 2, pp. 202-206, 2016
- [34] Chmielewski T., Oramus P., Szewczyk M., Kuczek T., Piasecki W.: *Circuit breaker models for simulations of short-circuit current breaking and slow-front overvoltages in HV systems*, Electric Power Systems Research, Elsevier Science Publishers Ltd., No. 2, pp. 174-181, 2017
- [35] Czucha J., Lipski T., Zyborski J.: *Hybrid current limiting interrupting device for 3-phase 400 V AC applications*, in Proc. IET Int. Conf. Trends Distrib. Switchgear, pp. 161–166, 1998
- [36] Diotec Semiconductor datasheet: Silicon-Power-Zener Diodes, www.tme.eu

- [37] Domitrovich P. E. T., White K.: *Implementation of an arc flash reduction maintenance switch* — A case study, Electrical Safety Workshop (ESW), IEEE IAS, 2012
- [38] Dzierzbicki S.: *Aparaty elektroenergetyczne*, Wydawnictwo Naukowo-Techniczne, 1977
- [39] Faranda R., Giussani M., Testin G.: *RC filter to protect industrial arc furnace transformers during switching-off*, EE'07 Proceedings of the 2nd IASME/WSEAS international conference on Energy and environment, Portoroz, Slovenia, pp. 146-152, 2007
- [40] Fleszyński J., Beroual A., Rottenberg W.: *Wpływ modyfikacji powierzchni międzyfazowej na zjawiska elektryzacji statycznej olejów transformatorowych*, Przegląd Elektrotechniczny, nr 6/2009 pp. 182-187
- [41] Fleszyński J., Lutyński B.: *Macroparticle-initiated breakdown of insulating oil*, 8th International Conference on Conduction and Breakdown in Dielectric Liquids, Pavia, Italy, pp. 275-279, 1984
- [42] Flisowski Z.: *Technika Wysokich Napięć*, Wydawnictwa Naukowo-Techniczne, Warszawa, 1999
- [43] Florkowska B., Florkowski M., Furgał J., Pająk P., Roehrich J.: *Wpływ szybkich zjawisk łączeniowych na układy izolacji elektrycznej*, Przegląd Elektrotechniczny, R. 86 nr 4, pp. 158–161, 2010
- [44] Furgał J., Kuniewski M., Pająk P.: *Badania i symulacje przepięć łączeniowych przenoszonych przez uzwojenia transformatorów*, Przegląd Elektrotechniczny, R. 88 nr 11b, pp. 130–133, 2012
- [45] Genji T., Nakamura O., Isozaki M., Yamada M., Morita T., Kaneda M.: *400 V class high-speed current limiting circuit breaker for electric power system*, IEEE Transactions on Power Delivery, Vol. 9, No. 3, pp. 1428–1435, 1994
- [46] Greitzke S., Lindmayer M.: *Commutation and Erosion in Hybrid Contactor Systems*, IEEE Transactions on components, hybrids, and manufacturing technology, Vol. CHMT-8, No. 1, pp. 34-39, 1985
- [47] Guilin Z., Xi Ch.: *A Novel Synchronous Switch Method Based on Kalman Filter*, International Journal of Future Generation Communication and Networking Vol. 8, No. 2, pp. 33-44, 2015
- [48] Gurevich V.: *Electric Relays – Principles and Applications*, Israel Electric Corporation Haifa, Israel, CRC Press, 2006
- [49] Habedank U.: *Application of a New Arc Model for the Evaluation of Short-Circuit Breaking Tests*, IEEE Transactions on Power Delivery, Vol. 8, No. 4, 1993
- [50] Hansson T., Karlstrom P. O.: *PTC element*, U.S. Patent 5 382938, 1995
- [51] Hanzelka Z., Chmielowiec K., Firlit A., Świątek B.: *Nowe wyzwania w dziedzinie jakości dostawy energii elektrycznej*, Przegląd Elektrotechniczny, Nr 06, pp. 17-25, 2013
- [52] Hiquel Application Note Snubber: Circuits, www.hiquel.com
- [53] Honma H., Kimura S., Shoji K., Wakatsuki N.: *Arc discharge and surge suppression during a breaking operation of a magnetic relay*, Proceedings of the 53rd IEEE Holm Conference on Electrical Contacts, pp. 280-283, 2007
- [54] Horinouchi K., Tsukima M., Tohya N., Inoue T., Sasao H.: *Synchronous Controlled Switching by Vacuum Circuit Breaker (VCB) with Electromagnetic Operation Mechanism*, IEEE International Conference on Electric Utility Deregulation, Restructuring and Power Technologies, 2004
- [55] Idec General Application Guidelines: Contact Protection Circuit, www.idec.com

- [56] IEC 60947-4-1: Low-voltage switchgear and controlgear – Part 4-1: Contactors and motor-starters – Electromechanical contactors and motor-starters
- [57] Iturregi A., Torres E., Zamora I.: *Analysis of the Electric Arc in Low Voltage Circuit Breakers*, International Conference on Renewable Energies and Power Quality (ICREPQ'11) Las Palmas de Gran Canaria, Spain, 2011
- [58] Janiszewski J., Batura R.: *Badania modelowe stanu cieplnego zestyków elektrycznych*, Poznan University of Technology Academic Journals. Electrical Engineering Issue 83, pp. 253-260, 2015
- [59] Janiszewski J., Idziak P.: *The heating processes on anode surface in a high-current switching arc*, 6th IASME/WSEAS International Conference on HEAT TRANSFER, Thermal Engineerin and Environment (HTE'08) Rhodes, Greece, pp. 215-219, 2008
- [60] Janiszewski J., Książkiewicz A.: *Badania modelowe rezystancji zestykowej łączników próżniowych*, Poznan University of Technology Academic Journals. Electrical Engineering Issue 78, pp. 167-174, 2014
- [61] Janiszewski J., Książkiewicz A.: *Vacuum switches contact resistance*, Computer Applications in Electrical Engineering Vol. 12, pp. 227-236, 2014
- [62] Kacejko L.: *Aparaty elektryczne*, Wydawnictwa Szkolne i Pedagogiczne, Warszawa, 1974
- [63] Karady G. G., Heydt G. T.: *Novel concept for medium voltage circuit breakers using microswitches*, IEEE Trans. Power Del., Vol. 21, No. 1, pp. 536–537, 2006.
- [64] Kharin S.N., Sarsengeldin M., *Influence of Contact Materials on Phenomena in a Short Electrical Arc*, Key Engineering Materials, Vols. 510-511, pp. 321-329, 2012
- [65] Kiszło S.: *Nowe konstrukcje elektromechanicznych rozłączników napowietrznych średniego napięcia*, PhD Thesis, Lublin 2013
- [66] Klajn A.: *Właściwości dyfuzyjnego wyładowania lukowego w próżni w warunkach wymuszonego wyłączania prądu*, Oficyna Wydawnicza Politechniki Wrocławskiej, Wrocław, 2006
- [67] Komatsu H., Nomura J., and Souda M.: *Low frequency circuit breaker*, U.S. Patent Appl. 13/328,321, 2011
- [68] Królikowski Cz.: *Technika łączeniowa obwodów elektroenergetycznych*, Państwowe Wydawnictwa Naukowe, Warszawa, 1990
- [69] Krstic S., Theisen J. P.: *Push-Button Hybrid Switch*, IEEE Transactions on components, hybrids, and manufacturing technology, vol. CHMT-9, No. 1, pp. 101-105, 1986
- [70] Kuczek T., Florkowski M., Piasecki W.: *Transformer switching with vacuum circuit breaker: case study of PV inverter LC filters impact on transient overvoltages*, IEEE Transactions on Power Delivery, Vol. 31, Issue: 1, 2016
- [71] Kudo T., Wakatsuki N., Takatsu N.: *Transient Phenomena from Melting to Electric Discharge during Making and Breaking Operations of Electric Contacts*, IEEE 57th Holm Conference on Electrical Contacts (Holm), 2011
- [72] Kulas S. J.: *Capacitor Switching Techniques*, International Conference on Renewable Energies and Power Quality (ICREPQ'09), Valencia, Spain, 2009
- [73] Kulas S. J.: *Synchronous switching of power systems*, Proceedings of the 2nd IASME / WSEAS International Conference on Energy & Environment (EE'07), Portoroz, Slovenia, pp. 209-211, 2007
- [74] Kulas S.: *Tory prądowe i układy zestykowe*, Oficyna Wydawnicza Politechniki Warszawskiej, Warszawa, 2008

- [75] Kurioka H., Genji T., Isozaki M., Iwai H., Yamada M.: *Development of a high-speed current limiter for a 6 kV distribution system and evaluation of its effectiveness*, Elect. Eng. Jpn., Vol. 125, No. 3, pp. 11–20, 1998
- [76] Kutzner J.: *Przepływ plazmy w dyfuzyjnym wyladowaniu łukowym w próżni*, Wydawnictwo Politechniki Poznańskiej, 1993
- [77] Lehr F. M., and Kristiansen M.: *Electrode Erosion From High Current Moving Arcs*, IEEE Transactions on Plasma Science, Vol. 17, Issue 5, pp. 811-817, 1989
- [78] Lindmayer M., Mutzke A., Rütther T., Springstubbe M.: *Some aspects of arc behavior in low-voltage arc chutes*, XVIth Symp. on Physics of Switching Arc, Brno, Czech Republic, pp. 278-292, 2005
- [79] Littelfuse Varistor Design Examples, Application Notes, www.littelfuse.com
- [80] Littelfuse, Application Note: Inductive Load Arc Suppression, www.littelfuse.com
- [81] Liu L., Zhuang J., Wang Ch., Jiang Z., Wu J., Chen B.: *A Hybrid DC Vacuum Circuit breaker for Medium voltage: Principle and First Measurements*, IEEE Transactions on Power Delivery (Vol. 30, Issue 5, Oct. 2015), pp. 2096-2101
- [82] Liu P., Bahadur S., Verhoeven J. D., Gibson E. D., Kristiansen M., Donaldson A.: *Arc erosion of Cu-15%Nb and Cu-15%Cr in situ composites*, 11th International Conference on Wear of Materials, Vol. 203–204, pp. 36-45, 1997
- [83] Lou van der Sluis: *Transients in power systems*, John Wiley & sons, LTD, 2001
- [84] Ma H., Tian Y., Geng Y., Wang Z.: *Anode Erosion Pattern Caused by blowing Effect in Constricted Vacuum Arcs Subjected to Axial Magnetic Field*, IEEE Transactions on Plasma Science, Vol.: 43 Issue: 8, pp. 2329-2334, 2015
- [85] Maksić M., Matvoz D., Kosmač J., Papič I.: *Circuit Breaker Switching Transients at Arc Furnace Installation*, International Conference on Power Systems Transients (IPST2009) in Kyoto, Japan, pp. 1-6, 2009
- [86] Maksymiuk J., Pochanke Z.: *Obliczenia i badania diagnostyczne aparatury rozdzielczej*, Wydawnictwa Naukowo-Techniczne, Warszawa, 2001
- [87] Maksymiuk J.: *Aparaty elektryczne w pytaniach i odpowiedziach*, Wydawnictwa Naukowo-Techniczne, Warszawa, 1997
- [88] Maksymiuk J.: *Aparaty elektryczne*, Wydawnictwa Naukowo-Techniczne, Warszawa, 1995
- [89] Markevich N. V., Kiyatkin R. P., Maksimov O. P.: *Electric-Arc Erosion of Metal Plates of Arc Suppressors of Automatic Circuit Breaker for Extreme Commutation Currents*, Russian Electrical Engineering, Vol. 78, Issue 12, pp. 670–673, 2007
- [90] Mayr O.: *Beitrag zur theorie der statischen und der dynamischen lichtbogens*, Archiv fuer Elektrotechnik, Berlin, Germany, Vol. 37, pp. 588-608, 1943
- [91] Mecke H., Fischer W., Werter F.: *Soft switching inverter power source for arc welding*, EPE97 Conf., Trondheim. pp. 4333-4337, 1997
- [92] Meunier J.-L., Kandah M., Campbell M.: *Columnar Diamond Film Coverage of Vacuum Arc Erosion Canyons on Graphite*, IEEE Transactions on Plasma Science, Vol. 33, Issue 2, pp. 238-239, 2005
- [93] Mirkalaei S. A. M., Hashiesh F.: *Controlled Switching to Mitigate Power Transformers Inrush Current Phenomenon*, Power Engineering Conference (UPEC), 2015
- [94] Nikic D., Day A. C.: *Arc erosion of aluminum and titanium in presence of high currents*, 19th IEEE Pulsed Power Conference (PPC), 2013

- [95] Oramus P., Chmielewski T., Kuczek T., Florkowski M.: *Simulations of electric arc behavior in hybrid LV switches*, IEEE Conference Publications, Progress in Applied Electrical Engineering (PAEE), pp. 1-5, 2016
- [96] Oramus P., Chmielewski T., Kuczek T., Piasecki W., Szewczyk M.: *Transient Recovery Voltage analysis for various current breaking mathematical models: shunt reactor and capacitor bank de-energization study*, Archives of Electrical Engineering Vol. 64, Nr 3, pp. 441-458, 2015
- [97] Oramus P., Florkowski M., Rybak A., Sroka J.: *Investigation into Limitation of Arc Erosion in LV Switches through Application of Hybrid Switching*, IEEE Transactions on Plasma Science, Vol. 45, Issue 3, pp. 446-453, 2017
- [98] Oramus P., Florkowski M.: *Limitation of electric arc energy in LV switches during inductive current interruption*, IEEE Transactions on Power Delivery, Early Access, DOI: 10.1109/TPWRD.2016.2606518, 2017
- [99] Øyvang T., Fjeld E., Rondeel W., Hagen S. T.: *High current arc erosion on copper electrodes in air*, IEEE 57th Holm Conference on Electrical Contacts (Holm), 2011
- [100] Paktron Capacitors Application Note: Q/QRL Arc Suppressor Snubber Network, www.panconcorp.com
- [101] Pana S. K., H. J. Bahirat, M. Stanek: *Controlled Switching of Power Circuit Breakers*, IEEE International Conference on Power System Technology (POWERCON), 2016
- [102] Parakansky N., Boxman R. L., Goldsmith S., Rosenber Yu.: *Arc erosion reduction on electrical contacts using transverse current injection*, Proceedings XVIIth International Symposium on Discharges and Electrical Insulation in Vacuum, pp. 804-807, 1996
- [103] Phoenix Contact, Application Note 105396_en_00: Fundamentals of relay technology, www.phoenixcontact.com
- [104] Piróg S.: *Energoelektronika. Układy o komutacji sieciowej i o komutacji twardej*, Akademia Górniczo-Hutnicza. Uczelniane Wydawnictwa Naukowo-Dydaktyczne, Kraków, 2006
- [105] Piróg S.: *Układy o komutacji sieciowej i o komutacji twardej*, Uczelniane Wydawnictwa Naukowo-Dydaktyczne, Kraków, 2006
- [106] Pons F., Cherkaoui M.: *An electrical arc erosion model valid for high current: Vaporization and Splash Erosion*, Proceedings of the 54th IEEE Holm Conference on Electrical Contacts, pp. 9-14, 2008
- [107] Pons F.: *Electrical Contact Material Arc Erosion: Experiments and Modeling Towards the Design of An AgCdO Substitute*, PhD Thesis, Georgia Institute of Technology, 2010
- [108] Prousalidis J. M., Hatziaargyriou N.D, Papdias B.C.: *A Circuit Breaker Model for Small Inductive Current Interruption*, IPST '99 – International Conference on Power Systems Transients, Budapest - Hungary, pp. 499-504, 1999
- [109] Relpol Brochure: Przekazniki, Podstawowe Informacje, www.relpol.pl
- [110] Riddle K. A.: *Automatic synchronizing of mill power system circuit breakers*, Annual Pulp and Paper Industry Technical Conference, pp. 110-119, 1993
- [111] Sawicki A., Haltof M.: *Modelowanie wpływu zaburzeń zewnętrznych na charakterystyki dynamiczne łuku elektrycznego*, Przegląd Elektrotechniczny, R. 92, Nr 12, pp. 161-164, 2016
- [112] Sawicki A., Kruczynin A. M.: *Charakterystyki łuku plazmotronów spektrometrycznych*, Elektrotechnika i Elektronika Tom 24, Zeszyt 1, pp. 75-84, 2005
- [113] Sawicki A.: *Modelowanie łuku spawalniczego o zmiennej długości kolumny plazmowej*, Przegląd Spawalnictwa 6/2012, pp. 8-11, 2012

- [114] Schavemaker P. H., Lou van der Sluis: *An Improved Mayr-Type Arc Model Based on Current-Zero Measurements*, IEEE Transactions on Power Delivery, Vol. 15, No. 2, pp. 580-584, 2000
- [115] Schavemaker and P.H., L. van der Sluis, *The Arc Model Blockset*, Proceedings of the Second IASTED International Conference, Crete Greece, pp. 644-648, 2002
- [116] Schwarz J.: *Dynamisches Verhalten eines gasbeblasenen, turbulenzbestimmten schaltlichtbogens*, ETZ Arch., Vol. 92, pp. 389–391, 1971
- [117] Shea J.: *High Current AC Break Arc Contact Erosion*, Proceedings of the 54th IEEE Holm Conference on Electrical Contacts, 2008
- [118] Shujuan W., Yu T., Binrui Z., Guofu Z.: *Study of a New Hybrid Switch for the Application in the Railway*, IEEE Vehicle Power and Propulsion Conference, 2008
- [119] Shukla A., Demetriades D. G.: *A survey on Hybrid Circuit-Breaker Topologies*, IEEE Transactions on Power Delivery, Vol. 30, Issue 2, pp. 627-641, 2015
- [120] Siemens Cataloge: PSD01 Controlled Switching of High-Voltage Circuit-Breakers
- [121] Slade G. Paul: *The Vacuum Interrupter Theory, Design, and Application*, CRC Press Taylor & Francis Group, 2008, ISBN 0-84493-9091-5
- [122] Smugała D., Oramus P., Krysztofiak P., Bonk M., Piekarski P., Domurad Z., Kaczmarczyk T.: *Measurements of gas pressure into the MV arc plasma environment*, Plasma Physics and Technology, No. 2,1, pp. 78-82, 2015
- [123] Smugała D., Oramus P., Krysztofiak P., Bonk M., Piekarski P., Kaczmarczyk T.: *System for gas pressure measurements in the plasma arc environment*, Measurement, Elsevier Science Publishers Ltd., No. 08, pp. 199-207, 2016
- [124] STMicroelectronics datasheet: Transil 1.5KE, www.tme.eu
- [125] Swingler J., McBride J. W.: *Micro-Arcing and Arc Erosion Minimization Using a DC Hybrid Switching Device*, IEEE Transactions on components and packaging technologies, Vol. 31, No. 2, pp. 425-430, 2008
- [126] Szewczyk M., Kuczek T., Oramus P., Piasecki W.: *Modeling of repetitive ignitions in switching devices: case studies on Vacuum Circuit Breaker and GIS disconnecter*, Springer International Publishing: Lecture Notes in Electrical Engineering, Vol. 324, pp. 241-250, 2014
- [127] Tarczyński W., Daszkiewicz T.: *Switching arc simulation*, Przegląd Elektrotechniczny, Nr 07b, pp. 60-64, 2012
- [128] Tarczyński W., Hejman T., Smugała D.: *Computer-Controlled Testing System for Investigating the Dynamic Characteristics of Contactors with A.C. Electromagnet Drives*, Journal of the International Measurement Confederation Measurement 33, pp. 313-323, 2003
- [129] Tarociński Z.: *Wzrost odporności warstwy przykatodowej w czasie gaszenia łuku długiego prądu przemiennego*, Wydawnictwo Naukowe Politechniki Łódzkiej, Łódź 1969
- [130] TDK datasheet: SIOV metal oxide varistors, www.tme.eu
- [131] TE Connectivity Application Note: Relay Contact Life, www.te.com
- [132] Technical data: Surface Roughness, Excerpt from JIS B 0601 (1994) and JIS B 0031 (1994), https://us.misumi-ec.com/pdf/tech/mold/09_mo1517.pdf
- [133] Thinking Electronic Industrial Co., LT Application note: Metal Oxide Varistor: Application Note, www.thinking.com.tw
- [134] UchiiAffiliated T., Hoshina Y., Mori T., Kawano H., Nakamoto T., Mizoguchi H.: *Investigations on SF6-Free Gas Circuit Breaker Adopting CO2 Gas as an Alternative*

- Arc-Quenching and Insulating Medium, Gaseous Dielectrics X*, pp. 205-210, 2004
- [135] Wakatsuki N., Honnma H.: *Melting Phenomena and Arc Ignition of Breaking Relay Contacts*, Proceedings of the 54th IEEE Holm Conference on Electrical Contacts, 2008
- [136] Wakatsuki N., Yonezawa Y.: *Relay Contacts of Multi-Electrodes with Timely Controlled Operation for Arc Discharge Suppression*, Proceedings of the 50th IEEE Holm Conference on Electrical Contacts and the 22nd International Conference on Electrical Contacts Electrical Contacts, pp. 474-479, 2004
- [137] Walczuk E., Boczkowski D.: *Computer controlled investigations of the dynamic welding behavior of contact materials*, Proceedings of the Forty-Second IEEE Holm Conference on Electrical Contacts, 1996
- [138] Walczuk E., Borkowski P., Książek S., Missol W., Rdzawski Z., Durst K.: *Evaluation of Basic Electrical Parameters of Silver-Based Contact Materials of Different Chemical Composition and Manufacturing Technology*, Proceedings of the 56th IEEE Holm Conference on Electrical Contacts 56: pp. 1-8, 2010
- [139] Walczuk E., Lewandowski B.: *Commutation contact system with vacuum arc chamber of high-voltage earthing switches*. 9th Intern. Conference on Switching Arc Phenomena joint with Polish Grant Session on Switchgear and Arc Technology. Łódź, pp. 37-41, 2001
- [140] Walczuk E., Stolarz S., Wojtasik K.: *Experimental Study of Ag-W-Re Composite Materials Under High-Current Conditions*, IEEE Transactions on Components, Hybrids, and Manufacturing Technology, Vol. 10, Issue 2, 1987
- [141] Walczuk E.: *Arc erosion of high current contacts in the aspect of CAD of switching device*, Proceedings of the Thirty-Eighth IEEE Holm Conference on Electrical Contacts, pp. 1-16, 1992
- [142] Wańkowicz J., Bielecki J.: *Life estimation for long rod composite insulators subjected to accelerating ageing by combined static and cyclic loading*, IEEE Transactions on Dielectrics and Electrical Insulation, Vol.: 18, Issue: 1, pp. 106-113 2011
- [143] Wańkowicz J., Bielecki J.: *Models of the long-term mechanical strength of long rod composite insulators*, IEEE Transactions on Dielectrics and Electrical Insulation, Vol.: 17, Issue: 2, pp. 360-367, 2010
- [144] Willrich Precision Brochure: Surface Roughness Testing, www.willrich.com
- [145] Wolny A.: *Szporowskie korzenie Katedry Wysokich Napięć i Aparatów Elektrycznych Politechniki Gdańskiej*, Zeszyty Naukowe Wydziału Elektrotechniki i Automatyki Politechniki Gdańskiej nr 24, pp. 125-130, 2008
- [146] Wróblewski Z., Kornatka M.: *Analiza trwałości eksploatacyjnej i łączeniowej styczników elektromagnetycznych niskiego napięcia*, Wiadomości Elektrotechniczne, nr 5, pp. 217-219, 2003
- [147] Wróblewski Z.: *Symulacyjne modele cyfrowe niezawodności zestyków łączników elektroenergetycznych*. Przegląd Elektrotechniczny, R. 72, nr 9, pp. 230-234, 1996
- [148] Wróblewski Z.: *Wieloparametrowy symulacyjny model cyfrowy i metoda prognozowania trwałości zestyków styczników elektromagnetycznych z bieżącej produkcji*, Przegląd Elektrotechniczny, R. 80, nr 3, pp. 269-273, 2004
- [149] Yamamoto H.: *Circuit breaker and circuit breaking apparatus*, U.S. Patent 5 650 901, 1997
- [150] Zhao L., Li Z., Zhou Y.: *Arc Erosion Characteristics of Nanocrystalline CuCr Contact Material*, 1st International Conference on Electric Power Equipment – Switching Technology (ICEPE-ST), pp. 594-597, 2011

- [151] Zhou X., Cui X., Chen M., Zhai G.: *Evaporation Erosion of Contacts Under Static Arc by Gas Dynamics and Molten Pool Simulation*, IEEE Transactions on Plasma Science, Vol. 43, Issue 12, pp. 4149-4160, 2015
- [152] Żybowski J., Lipski T., Czucha J.: *Zabezpieczenia diod i tyrystorów*, Wydawnictwa Naukowo-Techniczne, Warszawa 1985